Covalently Anchored Polymerisation Initiator Monolayers for Polymer Brush Growth

---

A thesis submitted in partial fulfillment of

the requirements for the degree of

Master of Science in Chemistry

Ethan Robert Lankshear

University of Canterbury

Christchurch

New Zealand

2015

Acknowledgements

I would like to start by thanking my supervisor, Professor Alison Downard, for all the time, guidance, knowledge and support she has put into this work and myself. Without her encouragement and keeping me on track, I would surely never have come close to finishing this on time (or at all!). Dr Paula Brooksby and the rest of the Downard group have been amazingly supportive and helpful throughout my time at U.C.

I would like to especially thank those within the chemistry department who have helped me throughout my thesis, especially when it came down to chemical synthesis and proofreading. Robbie, Will, Dave and Rob have been an enormous help, and without them I would still be figuring out what solvent I need to use for my column or if I've made my compound or not. The support team at U.C. have been incredibly helpful. Specifically, Rob McGregor, for fixing all the electrodes and glassware I broke and for making custom reaction vessels for me. His work is a work of art and he is truly an asset to the university. I would like to thank Helen Devereux and Gary Turner at the Nanofabrication lab for allowing me to use the lab and for teaching me to use the AFM.

I would like to thank the MacDiarmid Institute for Advanced Materials and Nanotechnology for funding and travel costs, and Professor David Williams and Dr. Yiwen Pei at Auckland University for allowing me to visit, work in their lab and teaching me about polymerisation methods.

Thanks to my family and friends, you've always been there for me, supported my decisions and kept me from going astray.

Lastly, I thank Kirstyn, for being you.

Table of Contents

Abstract

This thesis describes the covalent modification of carbon electrodes with a monolayer of polymerisation initiators and the growth of polymer brushes by surface initiated atom transfer radical polymerisation (SI-ATRP). Monolayer modification was sought to preserve the underlying electrode properties and topography and to produce a well-organised layer from which the polymer brushes can be grown. This work investigated two approaches for immobilising a monolayer of polymerisation initiators. Firstly, the electrochemical grafting of protected aryl diazonium salts produced a covalently anchored monolayer of tether groups that can participate in subsequent amide coupling and click reactions, to covalently anchor the polymerisation initiator. Secondly, specific reactions between the electrode surface and appropriate polymerisation initiator derivatives have been used to covalently anchor the initiators.

For most systems, electro-active ferrocene (Fc) groups were reacted with modified surfaces as model reactants to enable the electrochemical estimation of the surface concentration of the polymer initiator groups. Film thickness measurements of the ethynylaryl (Ar-Eth) monolayer were carried out using atomic force microscopy confirming a monolayer. XPS analysis confirmed the presence of bromine on most of the polymerisation initiator modified samples.

Modification of surfaces with polymer brushes can introduce new surface properties, such as switchable wettability, while maintaining the underlying bulk substrate properties. This work focused on examining SI-ATRP at each of the polymerisation initiator monolayers, with the aim to identify the most promising system(s) for further investigation.

Polymer brushes of poly(3-(methacryloylamino)propyl)-*N,N*'-dimethyl(3-sulfopropyl)-ammonium hydroxide) (PMPDSAH) were grown from initiators tethered through the aryl

diazonium salts modification procedure. Redox probe voltammetry and XPS analysis indicated that the *grafting from* polymerisation by the copper catalysed SI-ATRP was successful.

Polymer brushes of poly(methyl methacrylate) PMMA were grown from the Ar-Eth modified monolayer by three SI-ATRP procedures: a standard procedure, an electrochemically mediated SI-ATRP method and a one-pot copper catalysed azide-alkyne click (CuAAC) reaction and SI-ATRP reaction from the Ar-Eth monolayer. Redox probe voltammetry and AFM images provided evidence for the growth of polymer brushes by these three methods. The successful one-pot CuAAC/SI-ATRP reaction for simultaneous coupling of the polymerisation initiator to the surface and polymerisation is a new approach for the production of polymer brushes and it minimises the number of surface modification steps needed. This method appears most promising for further development.

Abbreviations

Γ	Surface concentration (mol cm^{-2})
ABiA	α-Bromoisobutyric acid
ABiB	α-Bromoisobutyryl bromide
ABiC	α-Bromoisobutyryl chloride
ABiE	α-Bromoisobutyryl ester
ACN	Acetonitrile
AFM	Atomic force microscopy
APBiB	(3-Azidopropyl) bromoisobutyrate
Ar-COOH	Carboxyphenyl
Ar-Eth	Ethynylaryl
ATRP	Atom transfer radical polymerisation
Boc	*tert*-butyoxycarbonyl
CE	Calomel electrode
$(COCl)_2$	Oxalyl chloride
CuAAC	Copper catalysed azide-alkyne click reaction
CV	Cyclic voltammogram
DCM	Dichloromethane
DMSO	Dimethyl sulfoxide
DMF	Dimethylformamide
EtOH	Ethanol
ΔE_p	CV oxidation and reduction peak potential separation
$E_{p,a}$	CV anodic peak potential
$E_{p,c}$	CV cathodic peak potential

eSI-ATRP	Electrochemically mediated surface initiated atom transfer radical polymerisation
$E_{1/2}$	Half-wave potential
Fc	Ferrocene
Fc^{+}	Ferrocenium
FcCOCl	Ferrocenoyl chloride
FcCOOH	Ferrocene monocarboxylic acid
$Fe(CN)_6^{3-}$	Ferricyanide
Fm	9-Fluorenylmethyl
$FcMeN_3$	Azidomethylferrocene
GC	Glassy carbon
h	Hour(s)
LiCl	Lithium chloride
$LiClO_4$	Lithium perchlorate
mM	Millimol L^{-1}
MMA	Methyl methacrylate
MQ	Milli-Q
OCP	Open circuit potential
PBS	Phosphate buffered saline
PMMA	Poly(methyl methacrylate)
PMPDSAH	Poly(3-(methacryloylamido)propyl)-*N,N'*-dimethyl(3-sulfoprpyl) ammonium hydroxide)
PPF	Pyrolysed Photoresist Film
Q	Charge
s	Seconds

SCE	Saturated calomel electrode
SI-ATRP	Surface initiated atom transfer radical polymerisation
$TBABF_4$	Tetrabutylammonium tetrafluoroborate
TBAF	Tetra-n-butylammonium fluoride
THF	Tetrahydrofuran
TIPS	Triisopropylsilyl
ν	Scan rate
V	Volts
XPS	X-ray Photoelectron Spectroscopy

Chapter 1. Introduction

1.1. Graphitic Carbon Surfaces

Graphitic carbon materials are commonly used as electrodes. Low-cost, ease-of-handling, high mechanical stability, excellent electrical conductivity and wide potential windows are features of these materials.

Glassy carbon (GC) is a hard, conductive carbon material that is impermeable to solution.[1,2,3] Typically, GC is formed from a polymeric resin of polyacrylamide or phenol/formaldehyde polymers subjected to a series of pressurised heat treatments between 2000-3000 °C.

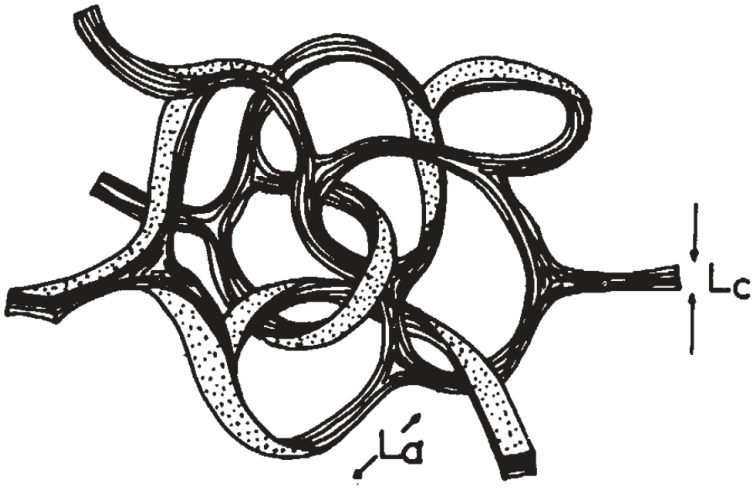

Figure 1.1. Structural model for the network of ribbon stacks in glassy carbon. Reproduced from reference 1.[1]

The structure of GC has been studied since initial production in the early 1960s. The commonly accepted model for the structure of GC is a disordered array of carbon containing sp^2 and sp^3 bonded carbon atoms with a complex network of interwoven graphitic ribbons as shown in Figure 1.1.[1,4]

GC typically has oxygen as ~ 2% of its surface atoms in a variety of oxide functionalities.[5] These oxygen-containing domains at the edge plane (Figure 1.2) can provide potential chemical reaction sites.

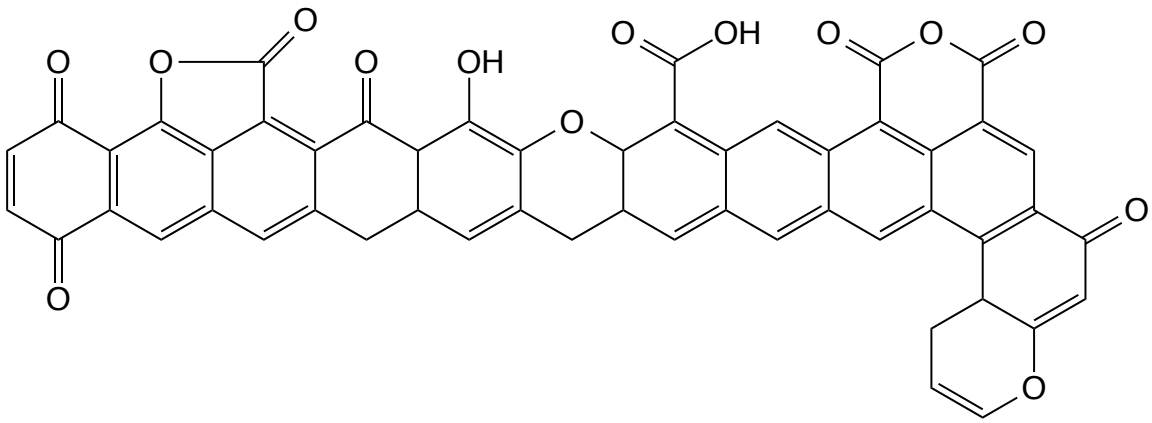

Figure 1.2. Edge plane sites of GC showing various oxygen-containing functional groups.

GC surfaces are usually pre-treated to obtain a reproducible electrode surface. Mechanical polishing or hand-polishing on a micro-fibre cloth with 1 micron alumina slurry or diamond paste, followed by ultrasonication in a solvent to remove the polishing compounds is the common pre-treatment method. Hand polishing was used in this thesis to prepare GC surfaces prior to modification.

Pyrolysed Photoresist Film (PPF) is a thin carbon film prepared by the pyrolysis of photoresists on silicon wafers at temperatures ranging from 600-1100 °C in an oxygen free environment.[6] When pyrolysed at ≥ 1000 °C, freshly prepared PPF surfaces typically have a surface O/C ratio of ~ 1%, and the electrochemical behaviour of PPF is comparable to GC. PPF surfaces are nearly atomically smooth with a typical root-mean-square roughness of 0.5 nm.[7] Due to the extremely low surface roughness, PPF is an excellent candidate for atomic force microscopy (AFM) imaging, including film thickness measurements through AFM tip scratching.[8] Compared to GC, PPF has a low background current and O/C atomic ratio, which indicates that the surfaces may be partially hydrogen terminated.

1.2. Surface Modification of Carbon Electrodes

The attachment of molecular species can be useful for altering the chemical and physical properties of a surface. Modification can lead to control over properties such as wettability, adhesion and resistance to chemical attack. Functionalising a surface can increase the reactivity of the surface and allows the tethering of complex molecules such as sensing or catalytic species.

Early carbon surface modification techniques involved the oxidation of the surface, leading to the generation of a variety of superficial carboxylic, quinonic, ketonic or hydroxylic groups.[9] Characterisation and control of these groups was difficult and the surface was often left rough and non-uniform.[10] In a more complex approach, pyrolytic carbon was pre-treated with radiofrequency oxygen plasma and subsequent lithium hydride reduction to increase the surface hydroxyl groups. The material was then reacted with cyanuric chloride followed by the reaction with nucleophiles.[11,12] Organosilanes have been shown to react with surface hydroxyls without pre-oxidation of graphitic carbon.[13]

Gallardo *et al*. have investigated the reaction between GC substrates and amines.[14] The mechanism has been assigned to a 'Michael-like' reaction between the amine acting as a nucleophile and the double bonds of the carbon structure. The proposed mechanism was more fully described by Lee and Downard.[15] Scheme 1.1 shows the attack of the amine derivative at the double bond of GC with electron delocalisation through the aromatic framework of GC. Using this reaction, Gallardo *et al.* attached 4-nitrobenzylamine, an electrochemically active compound, and calculated a surface coverage of $\sim 8 \times 10^{-10}$ mol cm^{-2}. The calculated surface coverage of a close-packed layer of nitrophenyl groups on a flat surface is $\sim 12 \times 10^{-10}$ mol cm^{-2}, and a typical GC surface roughness factor is 2, giving the experimental surface coverage of ~ 40% of a close packed monolayer.[16]

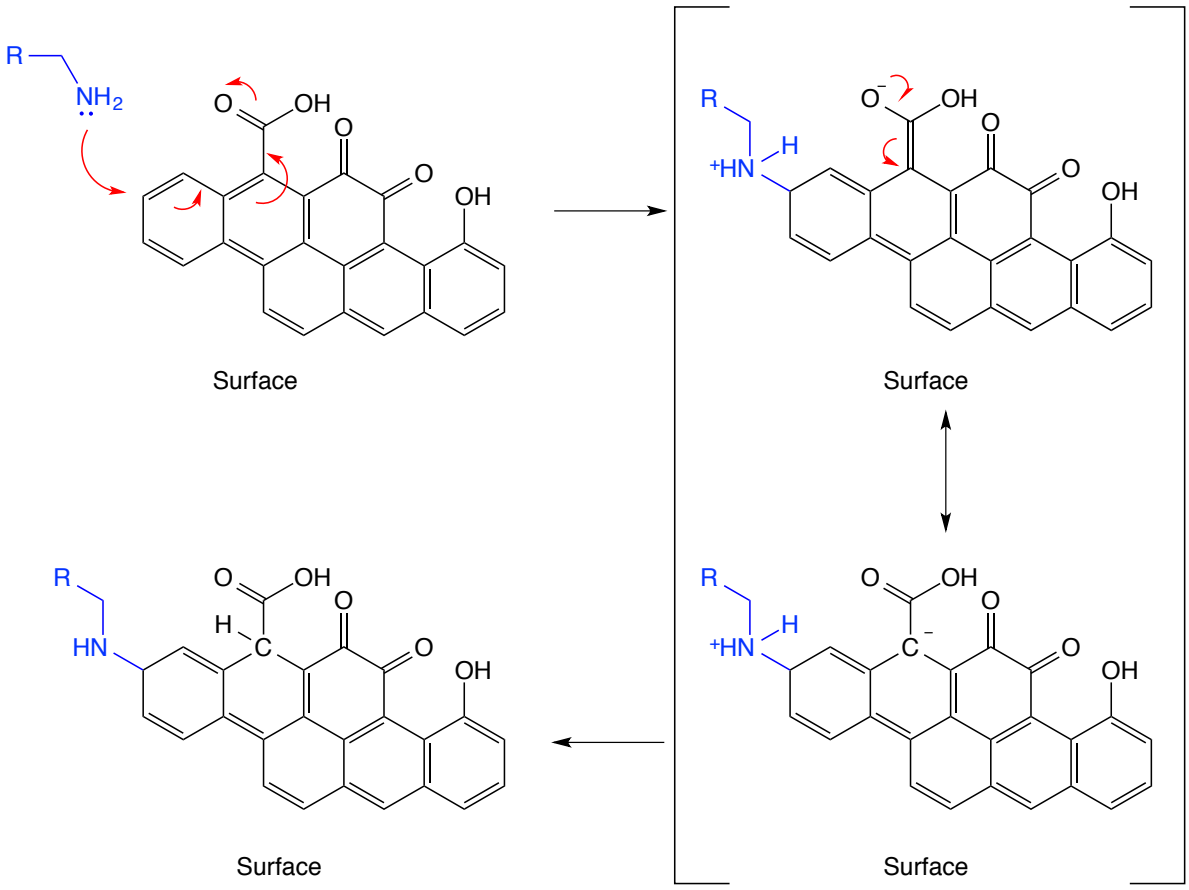

Scheme 1.1. Proposed mechanism for the reaction of an amine with GC surface via a Michael-like addition. Reproduced from reference 15.[15]

Ferrocene (Fc) derivatives have been immobilised on GC by Lee and Downard through similar methods.[15] $FcCH_2NH_2$ groups were reacted with polished GC in various solvents at open circuit potential (OCP) and with an applied potential. Reaction at OCP in acetonitrile (ACN) produced the highest surface coverage of Fc groups (~ 70% of a close-packed monolayer) when compared to other solvents (dimethylformamide (DMF) and dichloromethane (DCM)). The solvent dependency supports the proposed reaction mechanism as the more acidic ACN is expected to promote the Michael-like addition reaction for amines. When the reaction was undertaken at applied voltages of -0.8 and 0.2 V, the reaction yield decreased and increased respectively, compared with the yield at OCP. This is consistent with the requirement of electron delocalisation for the Michael-like mechanism.

Lee and Downard investigated amide coupling reactions of $FcCH_2NH_2$ with GC electrodes.[15] Treatment of the GC surface with oxalyl chloride ($(COCl)_2$) before reaction with $FcCH_2NH_2$ yielded higher surface concentrations of immobilised Fc compared to those obtained with traditional amide coupling agents. The proposed reaction mechanism is shown in Scheme 1.2. However, when $FcCH_2OH$ and FcCOOH were reacted under the same conditions, no or only trace amounts of immobilised Fc groups were detected, respectively. The lack of reaction of these derivatives at $(COCl)_2$-activated GC may be attributed to their poorer nucleophilicity than that of $FcCH_2NH_2$. Alternatively, it was suggested that a considerable amount of the coupling for $FcCH_2NH_2$ is actually through a Michael-like addition, and that surface carboxylic acid groups have low reactivity.

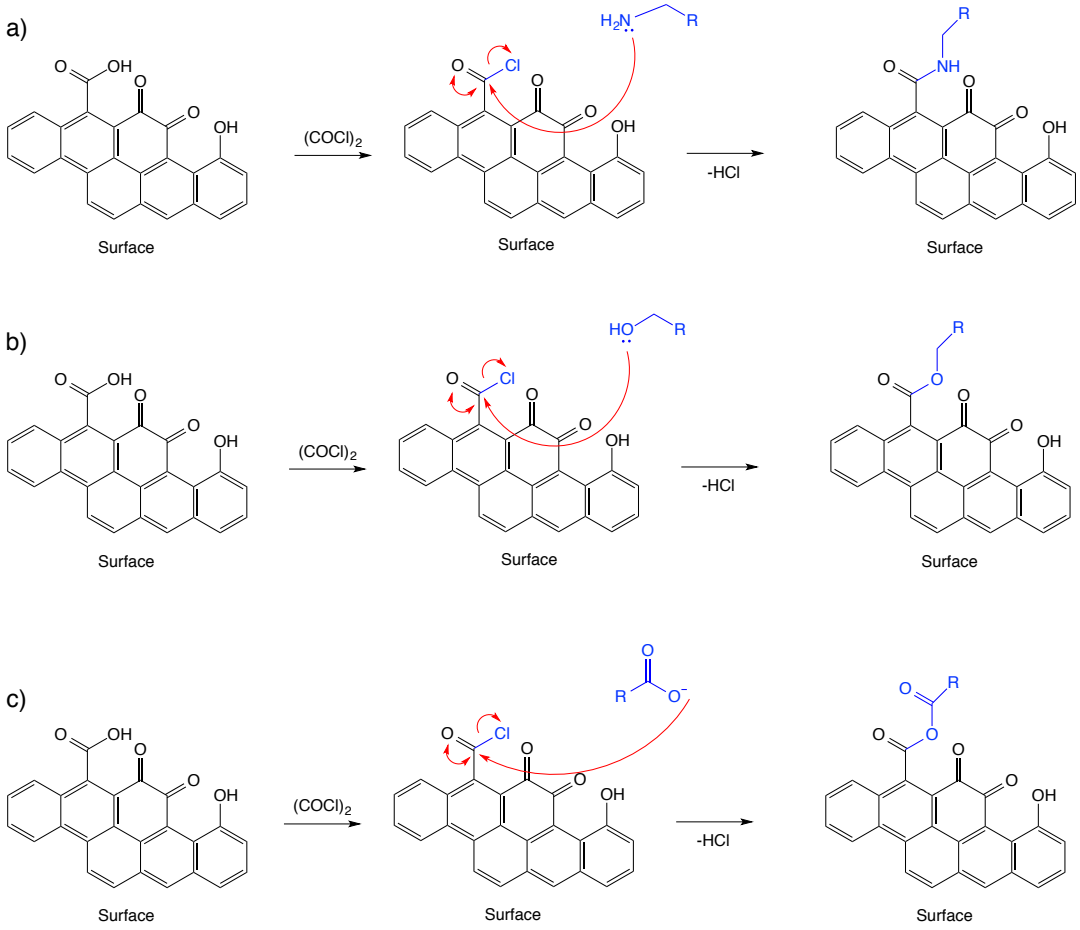

Scheme 1.2. Possible pathways for reaction of GC activated with $(COCl)_2$ with nucleophilic Fc derivatives a) $FcCH_2NH_2$, b) $FcCH_2OH$, and c) FcCOOH. Reproduced from reference 15.

In alternative experiments, polished GC surfaces were reacted with $(COCl)_2$-activated FcCOOH and $FcCH_2COOH$. Surface coverages of Fc groups were found to be (1.6 ± 0.2) and (2.4 ± 0.4) × 10^{-10} mol cm^{-2} for FcCOOH and $FcCH_2COOH$ respectively. The proposed reaction is shown in Scheme 1.3, with the formation of an ester linker through coupling to the surface hydroxyl group. The presence of ester linkages was tested by sonication of the $FcCH_2COOH$ modified surface in KOH. The surface coverage of Fc decreased by ~ 88%, which is consistent with the base hydrolysis of esters.

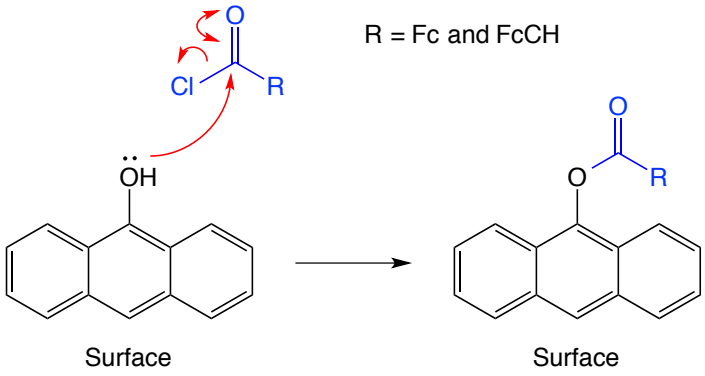

Scheme 1.3. The mechanism proposed for the reaction of GC with $(COCl_2)$-activated carboxylic acid derivatives. Reproduced from reference 15.[15]

The direct reaction between the modifying species and graphitic carbon has the advantages of being relatively simple, using common solvents and chemicals and mild reaction conditions. A disadvantage is that oxide functionalities are needed for some of these reactions to occur. Additionally, the formation of esters and anhydride linkages that can be hydrolysed in acidic or basic conditions is not appealing for applications that require robust tethering.

Other surface modification techniques are available, specifically those based on radial reactions. In 1990, Barbier *et al.* reported the electrochemical grafting of solution based radicals that coupled to the carbon surface, producing a covalent bond between the surface and radical species.[17] This has been developed to become a leading method for the attachment of organic films.

1.3. Aryl Diazonium Salts

Aryl diazonium salts are organic compounds with the formula of R-Ar-N_2^+ X^-, where X is an inorganic or organic anion such as Cl^- or BF_4^-. Diazotization, the process of forming aryl diazonium salts, is typically carried out in an acidic aqueous medium starting from an amine in the presence of $NaNO_2$.[9] Due to the range of aromatic amines commercially available, a large number of aryl diazonium salts can easily be prepared.[10]

Delamar *et al*. developed the method of forming a covalent bond between a carbon surface and an aryl radical produced in solution by the one electron electrochemical reduction of an aryl diazonium salt.[18] It was reported that the reduction of an aryl diazonium salt in the presence of a substrate leads to the grafting of the aryl group to the surface through the process shown in scheme 1.4. [19]

Aryl diazonium salts can be grafted onto a plethora of substrates. Through the electrochemical reduction of aryl diazonium salts, carbon-based substrates such as doped diamond,[20,21] highly oriented pyrolytic graphite (HOPG),[10,22,23,24] graphene, carbon nanotubes, pyrolysed photoresists (PPF), carbon black, carbon fibres and glassy carbon (GC) have been modified. A number of metals and semiconducting surfaces have also been modified.[9,25,26,27,28]

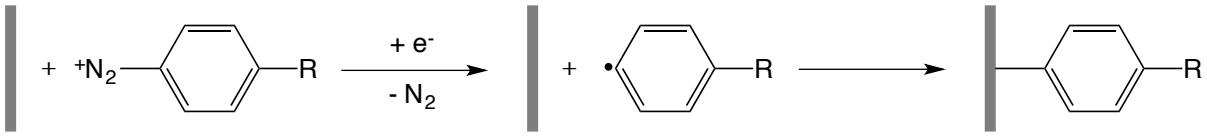

Scheme 1.4. Proposed pathway for the electrochemical reduction of an aryl diazonium salt and surface modification. Reproduced from reference 19.[19]

The formation of aryl films on conducting and non-conducting substrates from aryl diazonium salts in the absence of an applied potential is also possible. Grafting requires in-situ formation of aryl radicals through reduction by the substrate (so called spontaneous

grafting), or by use of a reducing agent such as hypophosphorous acid (H_3PO_2) or iron powder.[29,30]

The stability of aryl layers produced by the reduction of an aryl diazonium salt has been tested in many ways. Films on carbon and silicon were shown to be stable after six months under ambient conditions, and also after ultrasonication in harsh solvents.[10,31] Thermal gravimetric analysis and X-Ray photoelectron spectroscopy (XPS) analysis have shown *p*-nitrophenyl groups to be stable above 200°C in an inert atmosphere, with cleavage occurring in the 300-500°C range.[32] In regards to electrochemical stability, in a 0.1 M KCl solution, very negative (-2 V vs SCE) or very positive (1.8 V vs SCE) potentials are needed to restore the signal of the ferro/ferricyanide reversible redox system that is blocked by layers formed by aryl diazonium salt grafting.[33] Under these conditions, XPS analysis has indicated that the layer is not completely removed.[34]

A host of aryl diazonium salts have been synthesised.[10] Reactive R-group substituents are introduced to allow further reactions on the layer. For example, carboxylic acid[35] or amine[36,37] substituents can be used for amide coupling, while ethynylaryl groups can be reacted using click chemistry.[38,39]

Aryl radicals produced during grafting are highly reactive species that rapidly attack the substrate near where they are produced. They are also able to react with the already grafted aryl layer, forming a multilayer. Kariuki and McDermott described the nucleation and growth of aryl films, as depicted in Scheme 1.5.[23]

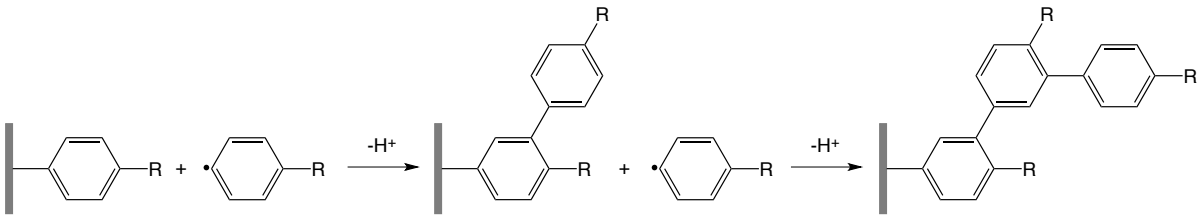

Scheme 1.5. Proposed scheme of attachment of free aryl radicals in solution to the aryl groups immobilised on the surface. Reproduced from reference 23.

Subsequently, the chemical structure of the layers was found to not only consist of aryl groups and the substituents, but also azo bonds (-N=N-). The formation of azo bonds was first proposed to account for N 1s peaks in the XPS spectra.[40] Dopplet *et al.* proposed a more complex mechanism of grafting (Scheme 1.6) and the incorporation of azo bonds in aryl layers based on Time-of-Flight Secondary Ion Mass Spectrometry (TOF-SIMS) experiments.[41]

The thickness of the grafted layer can range from a few to hundreds of nanometres.[9] Downard and co-workers have shown that the film thickness depends on the grafting potential.[8,42] More negative applied potentials result in a thicker film, indicating that film growth requires electron transfer from the electrode surface to the aryl diazonium cation in solution.[42]

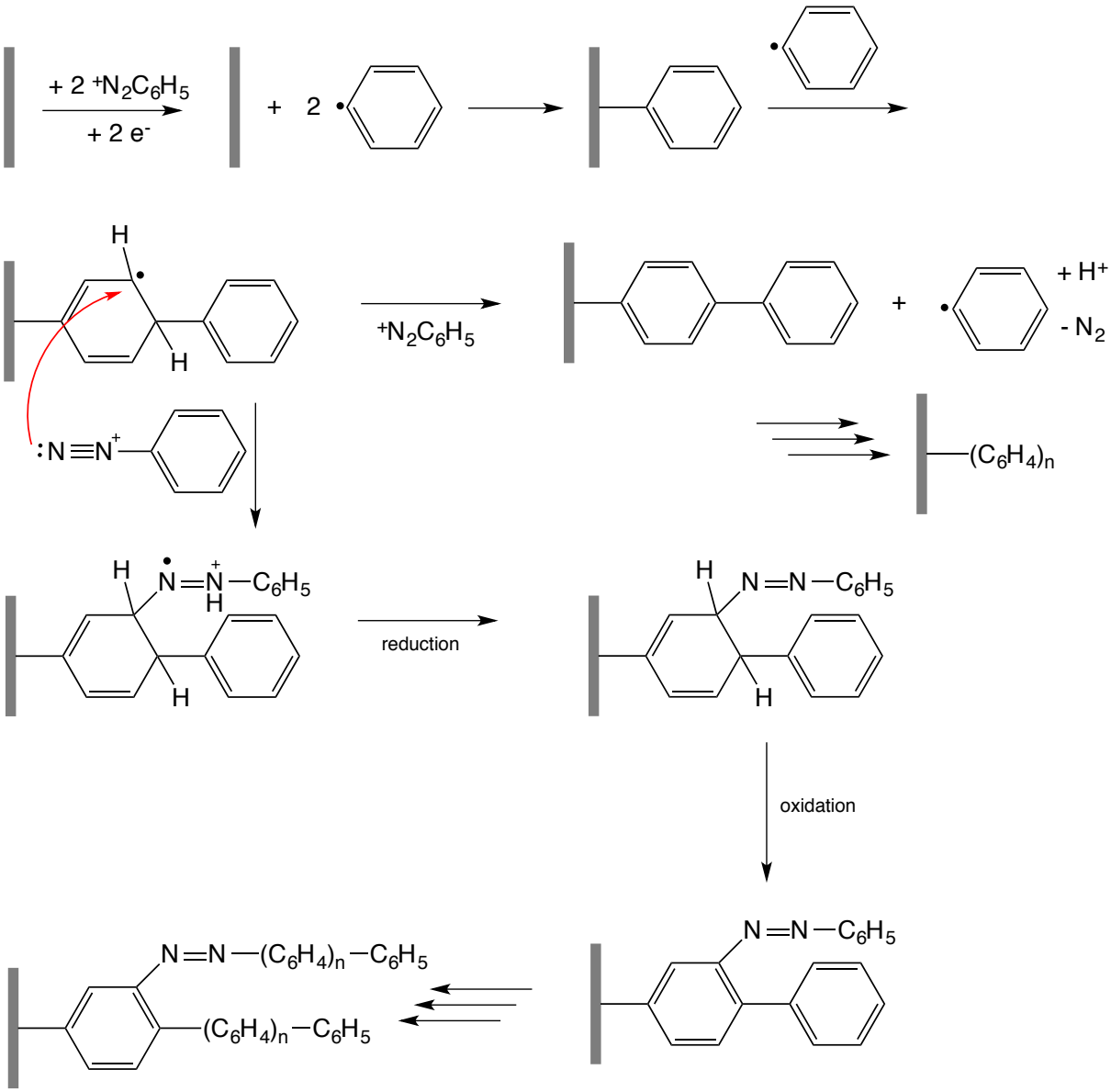

Scheme 1.6. Mechanism proposed by Dopplet *et al*. for the formation of multilayers and incorporation of azo bonds into the diazonium ion derived film. Reproduced from reference 41.

Measurements of film thickness can be made through scanning probe microscopy.[43] After the electrochemical grafting of an aryl layer on a flat PPF substrate, a section of the film can be mechanically scratched away using the tip of an AFM probe. Orthogonal scanning of the scratch produces a cross-sectional height profile as shown in Figure 1.3.

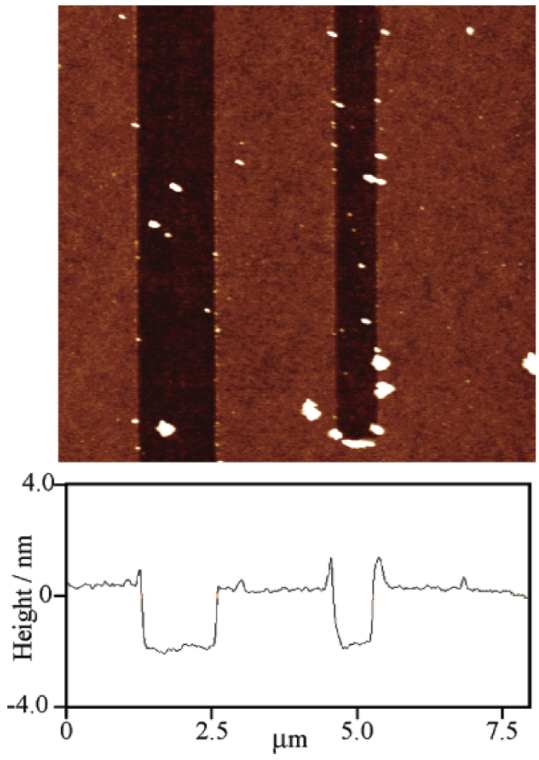

Figure 1.3. (Top) Topographical AFM image of a methylphenyl film on PPF with a section of film removed. (Bottom) A cross-sectional plot of the image in the top view showing the film height. Reproduced from reference 43.[43]

1.4. Monolayer Formation From Aryl Diazonium Salts

Although films grafted from aryl diazonium ions are usually disorganised multilayers, monolayers can be formed from aryl diazonium ions by various methods. Allongue *et al.* showed that limiting the charge during the electrografting step on a hydrogenated silicon substrate can limit the film to a monolayer.[44] Control over the concentration and reaction time for non-electrochemical grafting methods could potentially allow for only a monolayer to form.[45] However, in general conditions, the electrografting of aryl diazonium salts produces a multilayer. A leading method of obtaining a monolayer by electrochemical grafting of an aryl diazonium salt is through tuning the structure of the aryl diazonium salt. Combellas *et al.* investigated the effect on grafting when bulky sterically hindered aryl diazonium salts were

used.[46,47] Introducing a substituent (2-ethyl or 2,6-dimethyl) on either one or two *ortho* sites (*ortho* with respect to the diazonium functionality) on the aryl ring prevented any reaction with the surface. Two *meta* 2,5-*tert*-butyl groups with no *ortho* substituents limited the growth to a monolayer. The bulky substituents presumably prevent further attack on the grafted group by aryl radicals.

Mattiuzzi *et al.* electrografted calix[4]tetra-anilines by generating their corresponding diazonium cations *in situ.*[48] The 3D conical structure of the calix[4]arene core prevents the formation of multilayers and leads to densely packed monolayers. Post-functionalisation by coupling a ferrocene derivative through terminal carboxylic acid groups on the tails of the calixarene was used as proof of concept and to calculate the surface concentration, confirming monolayer coverage.

The introduction of a protecting group on the R moiety as a sacrificial group with a selectively cleavable bond is an extension of tuning the aryl diazonium salt. Nielsen *et al.* introduced a 'formation-degradation' approach where a purposely-formed multilayer is selectively degraded to give a 'near' monolayer.[49] As shown in Scheme 1.7, diaryl disulfide diazonium ions were grafted to a carbon surface, followed by the reductive cleavage of the disulfide bond to generate a layer containing one or two aryl groups. The authors showed that the immobilised ArS^- moieties could be reversibly oxidised to ArSSAr when in the presence of solution-based ArS^- groups, allowing the establishment of a relatively stable covalently attached ArSSAr/ArS^- redox pair. This gives electrochemical control over the surface properties. Repeating the formation/degradation procedure can eliminate pinholes and/or build up a surface layer by layer.

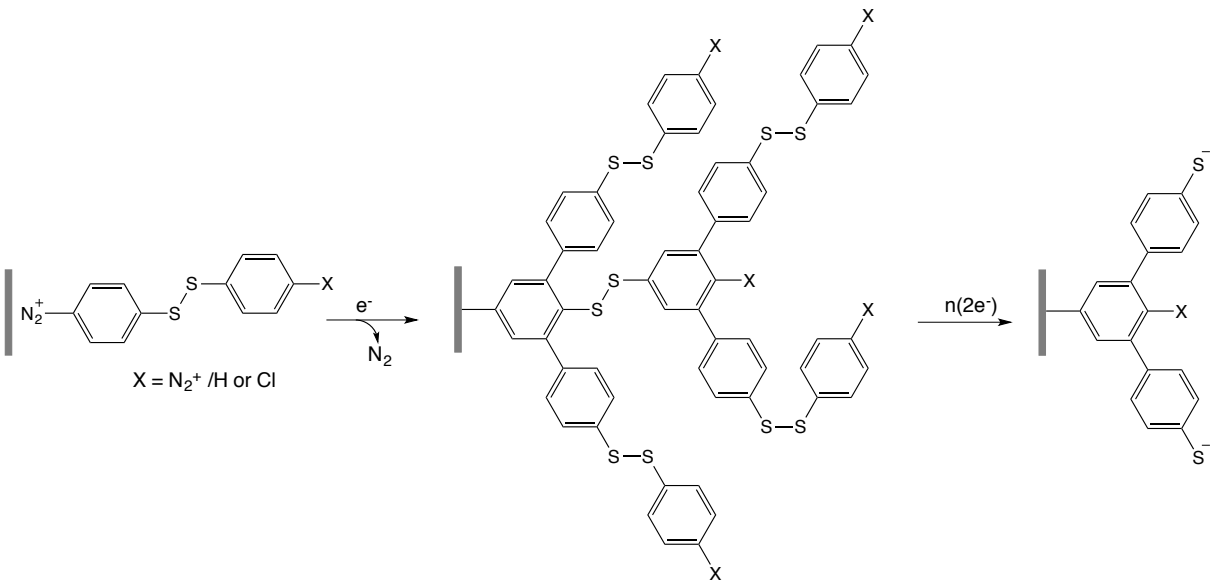

Scheme 1.7. Thiophenolate near monolayer by the formation-degradation method Adapted from reference 49.[49]

Leroux *et al.* further developed the formation-degradation approach by using bulky groups to protect grafted aryl rings from radical attack. They termed this strategy 'protection-deprotection'. They produced an ethynylaryl (Ar-Eth) monolayer by protecting the ethynyl benzenediazonium salt with triisopropylsilyl (TIPS), forming the molecule shown in Scheme 1.8.[39,50] The protecting group was shown to efficiently protect the functional group and the reactive *para* aryl position during the electrografting procedure. After TIPS deprotection by treatment with tetra-n-butylammonium fluoride/tetrahydrofuran, a resulting ethynylaryl monolayer was exposed. The reactivity of the monolayer was shown through a Cu^{I} catalysed Huisgen 1,3-dipolar cycloaddition reaction (a click reaction, see later for more details) with azidomethylferrocene ($FcCH_2N_3$) (Scheme 1.8). From the charge association with the redox reaction of the immobilised Fc group, the surface concentration of grafted Fc was 4.4×10^{-10} mol cm^{-2}. This is close to the maximum possible coverage when considering the size of a ferrocenyl group. The same experiment performed using the unprotected [N_2^+-Ar-Eth] BF_4 ion gave a surface concentration of immobilised Fc of 2.2×10^{-10} mol cm^{-2}. This suggested that although the latter film was thicker, the TIPS protecting group acts as an

organiser of the final film by spacing the Ar-Eth groups apart on the surface and thereby giving a higher yield for the click reaction with $FcCH_2N_3$.

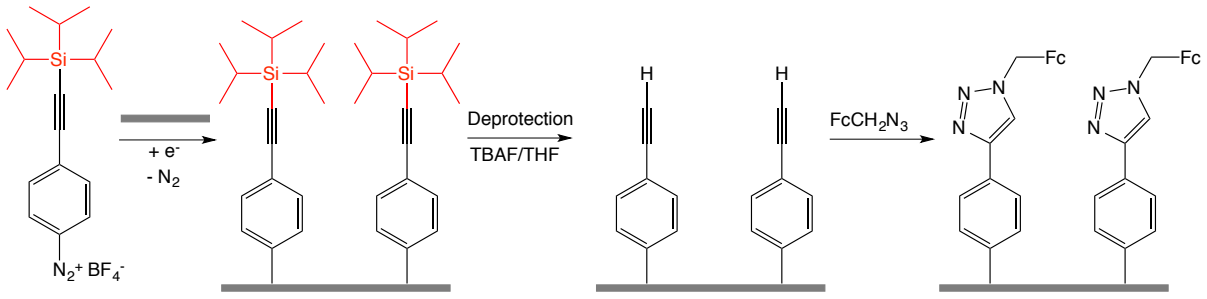

Scheme 1.8. Electrochemical grafting of TIPS protected ethynyl benzenediazonium salt followed by deprotection and the coupling of azidomethylferrocene *via* 'click' chemistry. Adapted from reference 50.[50b]

Leroux *et al.* extended the protection-deprotection strategy by synthesising ethynyl benzenediazonium salts with triethylsilyl (TES) and trimethylsilyl (TMS) protecting groups (scheme 1.9).[39] When electrografted, film thickness ranged from 0.8-2 nm, but regardless of the protecting group, once deprotected, films of ~ 0.6 nm were formed (the expected thickness of an ethynylaryl monolayer is ~ 0.66 nm). Concentrations of immobilised Fc were 3.3, 2.5, and 2.0 × 10^{-10} mol cm^{-2} for TMS, TES and TIPS protected diazonium ions respectively. This follows the expected trend as the increase in the size of the protecting group reduces the number of molecules grafted for a given area.

The Downard research group has used the TIPS protected ethynyl benzene diazonium salt for the preparation of mixed monolayers.[38] Using electrochemical grafting then deprotection of N_2^+-Ar-Eth-TIPS, followed by grafting N_2^+-Ar-NO_2 to fill the gaps, produced a mixed monolayer film with equal concentrations of modifiers.

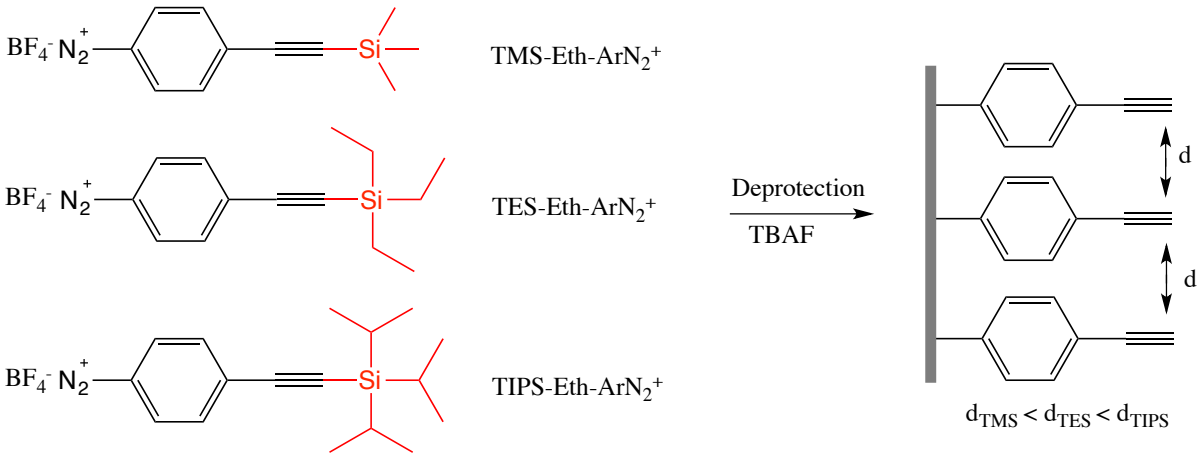

Scheme 1.9. Ethynylaryl monolayer formation from alkylsilyl-ethynyl aryl diazonium salts. Adapted from reference 39.

Ethynyl aryl layers are potentially of great use due to their facile reactivity towards azide groups. The ethynyl aryl monolayer has huge potential to tether functional molecules through click chemistry to any substrate that can be modified by aryl diazonium salt grafting.

The procedure of grafting a multilayer followed by selective cleavage has been utilised by the Downard group to produce carboxyphenyl films (Ar-COOH).[35] The 9-fluorenylmethyl (Fm)-protected carboxylate aryl diazonium salt (N_2^+-Ar-COO-Fm) was grafted to GC followed by removal of the Fm group by treating the surface with a solution of piperidine and DMF (scheme 1.10), giving a monolayer of Ar-COOH groups. The Ar-COOH monolayer was then reacted with primary amines in the presence of activating agents to produce an amide bond. Electrochemical detection of the tethered amine derivatives confirmed the reactivity of the monolayer for amide coupling and also allowed confirmation of monolayer coverage.

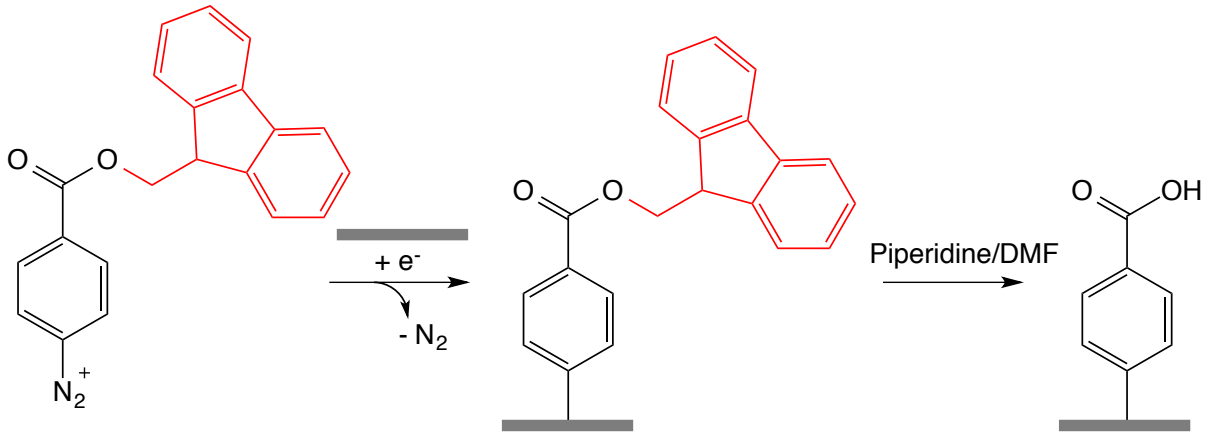

Scheme 1.10. Ar-COOH monolayer formation from protected carboxylate diazonium salt, N_2^+-Ar-COO-Fm. Reproduced from reference 35.

1.5. Click Chemistry

Click chemistry is a generic term applied to chemical syntheses tailored to generate substances by joining small units together with heteroatom links in a modular fashion. Click chemistry is not a single reaction, but are reactions that meet the criteria that Sharpless *et al.* defined in 2001;[51] "The conditions that the reaction must be *modular, wide in scope*, give *very high yields*, generate only *inoffensive by-products* that can be removed by non-chromatographic methods, and be *stereospecific* (but not necessarily enantioselective). The required process characteristics include *simple reaction conditions* (ideally, the process should be insensitive to oxygen and water), *readily available starting materials and reagents*, the use of *no solvent or a solvent that is benign* (such as water) *or easily removed*, and *simple product isolation*. Purification -if required- must be by non-chromatographic methods, such as crystallisation or distillation, and the product must be stable under physiological conditions."[51]

Click reactions achieve their required characteristics by having a high thermodynamic driving force, usually greater than 84 kJ mol^{-1}.[51] This allows the reactions to rapidly reach completion and be highly selective for a single product. Most click reactions involve carbon-heteroatom

bond formation, commonly cycloaddition of unsaturated species, nucleophilic substitution, and additions to carbon-carbon multiple bonds. Of these examples, cycloaddition reactions such as the Diels-Alder and the 1,3-dipolar cycloaddition, are leading click chemistry representations.

The Huisgen dipolar cycloaddition between an azide and alkyne giving a triazole is often regarded as the click chemistry 'cream of the crop'. Despite their safety concerns, azides are ideal for click chemistry as they have an extraordinary stability towards H_2O and O_2 and the majority of organic synthesis conditions.[52] The reaction of an azide and alkyne requires elevated temperatures and usually results in a mixture of the 1,4 and 1,5 regioisomers (Scheme 1.11).

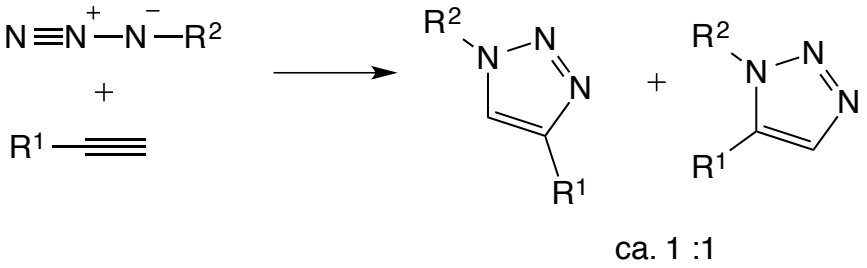

Scheme 1.11. Huisgen cycloaddition of an azide and alkyne. Reproduced from reference 52.

Two research groups reported the solution to the regioselectivity problem nearly simultaneously. Tornøe *et al.* outlined the use of Cu^{I} salts for the catalysis of the azide-alkyne cycloaddition (CuAAC) reaction for triazole synthesis on a solid support.[53] Reaction in a range of organic solvents gave full conversion and high purity of products. Rostovstev *at al.* reported that the reaction could be water based using Cu^{II} salts reduced *in situ* as a Cu^{I} source.[52]

Azide-alkyne coupling has rapidly risen in the field of polymer science.[54] It has been implemented as a method of polymerisation itself using molecules with both azide and alkyne

functionalities,[55] and also for polymerisation of hetero molecules containing either an azide or an alkyne,[56] for the formation of macrocyclic polymers,[57] and for the functionalisation of preformed polymers.[58]

1.6. Applications of Surfaces Modified With Aryl Diazonium Salts

As aryl diazonium salts are versatile coupling agents for the modification of surfaces, their potential applications are enormous. Aryl diazonium salts have been utilised as coupling agents for chemical and biological sensors,[59,60,61,62,63] where the functional species are required to have high selectivity towards the target analyte and to be stably immobilised on the electrode surface so to be robust and not affect the performance of the device. Modified surfaces have been used for molecular electronics applications, such as the incorporation of carbon nanotubes in microelectronic interconnectors[64] and molecular junctions.[65,66] A biomedical application of aryl diazonium ion modification is the coating of cardiovascular stents to increase the adhesion of a drug to the stent to prevent restenosis.[67] Macromolecules such as polymer chains have been attached to surfaces to alter the surface properties. These will be discussed in detail below. As polymers can be formed from a near endless number of monomers, so too can tethered polymer brushes. Polymer brushes allow for the introduction of functional groups all along the polymer backbone.[68]

1.7. Polymer Coated Materials

Polymer brushes are polymer chains with a single end covalently attached to a surface.[69,70,71] In the presence of a solvent, the extent to which polymer chains stretch away from the surface is determined by the delicate balance of forces between polymer chains and solvent molecules and the inter-chain forces. Grafting density plays an important role in determining the conformations available to surface-grafted polymers, with mushroom-, pancake- and brush-

like shapes being observed (Figure 1.4).[72] These three possible conformations are dependent on the distance between anchoring sites, polymer chain length, and the interactions between polymer chains. Typically, at low grafting density, polymer-surface interactions result in the polymer chain adopting a mushroom like conformation, where the neighbouring polymer chains do not interact with each other.[73,74] At higher grafting density, either the collapsed pancake or brush conformation will occur depending on the types and strength of interactions between polymer chains, solvent and salt molecules and the surface.

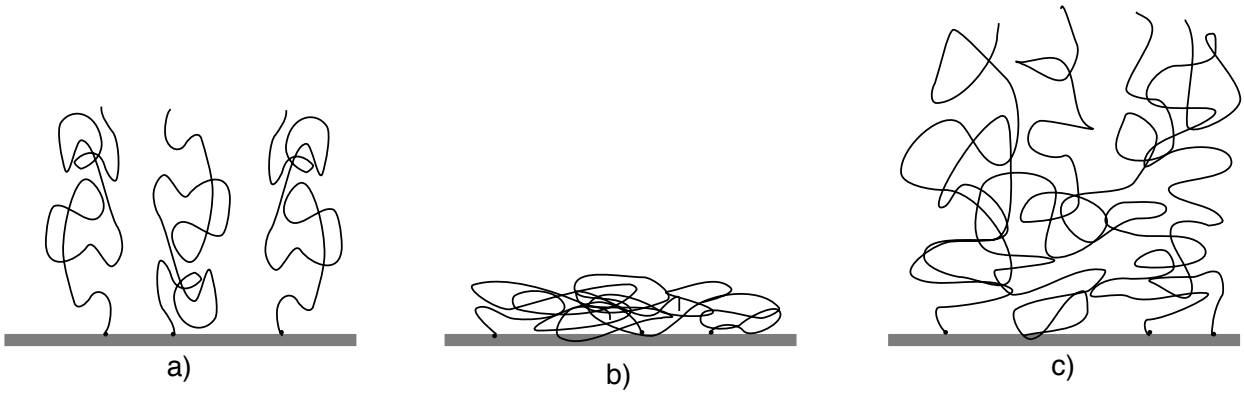

Figure 1.4. Possible conformations of a polymer brush on a flat surface: a) mushroom, b) pancake and c) brush. Adapted from reference 74.

1.8. Switchable Polymer Brushes

Switchable polymer brushes have the ability to respond to an environmental stimulus.[75] When induced by a trigger, switchable polymers undergo fast, reversible changes in microstructure that result in macroscopic changes (Figure 1.5). These macroscopic changes lead to alteration in the chemical and physical properties of a surface. The ability to control and change the conformation of a surface-attached polymer allows for manipulation of properties such as wettability, surface adhesion and surface dimensions. The method of switching is dependent upon the chemical composition of the polymer brush. A few examples of switching stimuli are described below.

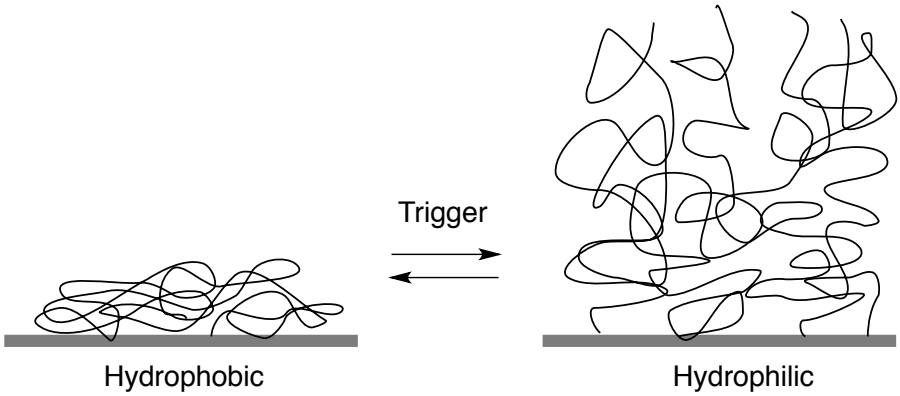

Figure 1.5. Reversible conformational switching of polymer brushes resulting in altered surface hydrophobicity.

Solvent and ionic strength can have a key role in dictating the conformational state of a polymer brush. In a 'good' solvent, the polymer chains will minimise contact with one another to maximise contact with the solvent molecules and will adopt the extended brush conformation.[70] In a 'poor' solvent, interactions between polymer chains will dominate, and the brush will collapse. Farhan *et al*. showed that switching between collapsed and extended conformational states for polymer brushes of poly[2-(methacryl-oyloxy)ethyl trimethylammonium chloride] (PMETAC) on gold is completely reversible by changing the solution from a methanol water solution to water only.[76]

The possibility of ionic strength to control polymer conformation is dependent on the charge composition of the polymer brush. Zhou *et al.* produced cationic brushes of poly[(dimethylamino)ethyl methacrylate] (Q-PDMAEMA).[77] They showed that some salts ($NaNO_3$) caused the brush to collapse due to charge screening, while more hydrophobic anions (ClO_4^-, PF_6^-, and $(CF_3SO_2)_2N^-$ (Tf_2N^-)) induced brush collapse because of ion-pairing leading to solubility changes. They investigated the charge transfer properties of the polymer brush through cyclic voltammetry and impedance spectroscopy. In the presence of $NaNO_3$, brushes exhibited a swollen state at low (1 mM) salt concentrations, and a collapsed state at high (1 M) concentrations. Fast electron transfer between the gold surface and the redox probe was shown for both salt concentrations. It was presumed that even at high salt

concentrations, significant amounts of water remain in the brush and the redox species are able to penetrate through the film. The polymer brushes became more hydrophobic in the presence of hydrophobic anions, leading to an increase in water contact angle measurements (NO_3 = 52 °, ClO_4^- = 73 °, PF_6^- = 87 °, and Tf_2N^- = 93 °). This wettability change is due to the conformational changes of the polymer chains and changes in hydration states resulting from the ion-pairing.

Thermally responsive polymers that operate within the biologically tolerable temperature range are of interest to researchers in tissue engineering and controlled drug delivery. Polymer brushes of poly(*N*-isopropylacrylamide) (PNIPAm) have well-known phase behaviour in aqueous solutions.[78] The lower critical solution temperature (LCST, the temperature that the polymer changes conformational state), is 32 °C for PNIPAm.[79] As depicted in Figure 1.6, below the LCST intermolecular hydrogen bonding between the polymer chains and water molecules give a hydrophilic brush conformation. Above the LCST, intramolecular interactions between the polymer strands cause the polymer brush to collapse and the surface to become hydrophobic.

Jones *et al.* produced PNIPAm chains on a mixed self assembled monolayer (SAM) layer of alkanethiols on silicon.[79] The chains displayed changes in topography, morphology, stiffness, and adhesion consistent with the reversible conformational surface changes from hydrophilic to hydrophobic. Sun *et al.* also used PNIPAm brushes on a silicon substrate and observed full conformational switching over the narrow temperature range of 15 °C.[80]

Electrochemical triggering of an underlying electrochemically active conducting polymer (ECP) substrate has been shown to trigger the conformational change of attached poly(sulfobetaine) polymers.[81] These polymers are polyzwitterionic, possessing permanent positive and negative charges on each monomer unit. Three types of interactions are found in

poly(sulfobetaine) chains (Figure 1.7): interactions between anionic sulfonate and cationic quaternary ammonium groups on the same monomer chain (intra-chain); stacking of opposite charges on the same polymer chain (intra-chain); and interactions between sulfonate and quaternary ammonium groups on neighbouring polymers (inter-chain).[74]

Due to this variety of charge interactions, poly(sulfobetaines) are able to switch between conformational states through ionic strength control. In the absence of added salts, all three of the above interactions occur leading to the collapse of the polymer brush. The addition of ions into the polymer matrix interrupts the intra and inter-molecular interactions by a charge screening effect, leading to an expanded brush conformational state.

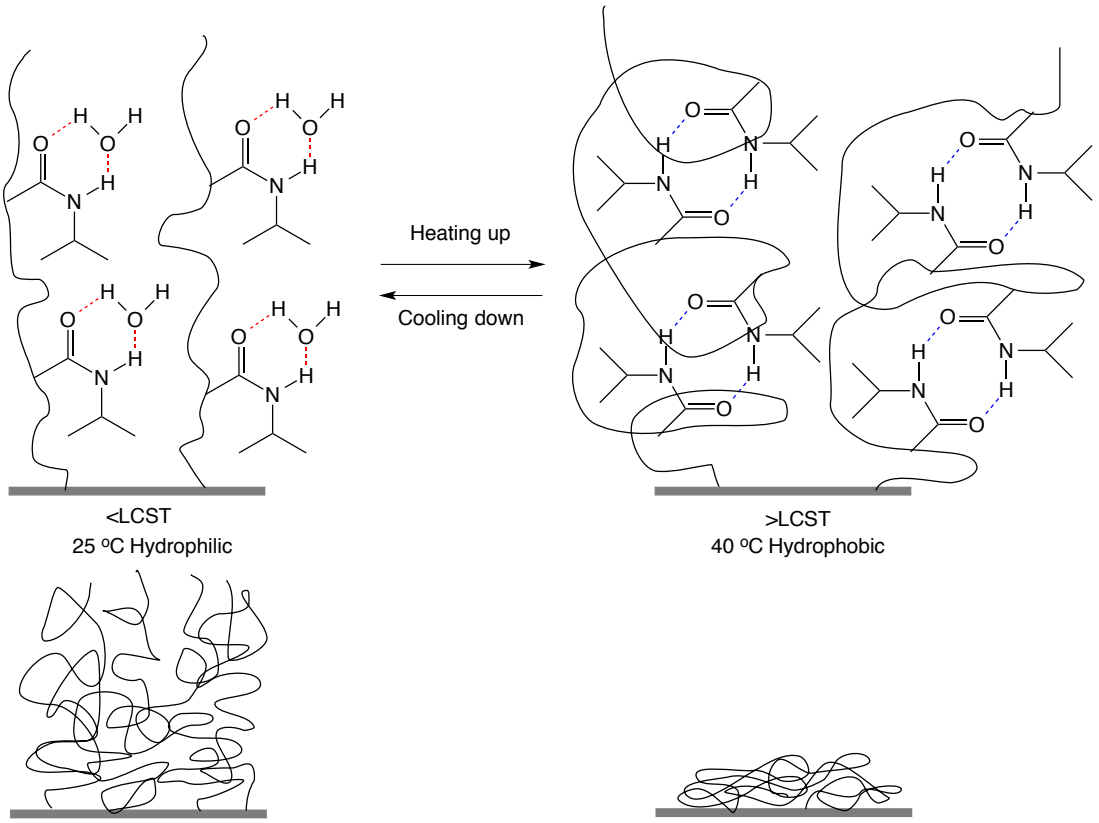

Figure 1.6. Reversible formation of intermolecular hydrogen bonding between (left) PNIPAm chains and water molecules at a temperature below the LCST and (right) intramolecular hydrogen bonding between C=O and N-H groups in PNIPAm chains above the LCST. Reproduced from reference 80.

Pei *et al.* grafted brushes of poly(3-(methacryloylamido)propyl)-*N,N'*-dimethyl(3-sulfopropyl)-ammonium hydroxide (PMPDSAH) onto an ECP and showed that changing the ionic strength by pumping ions using the underlying ECP gave conformational switching.[81] Secondary switching effects were also seen for the ionic strength of a droplet placed upon the modified surface and the temperature of the experiments conducted.

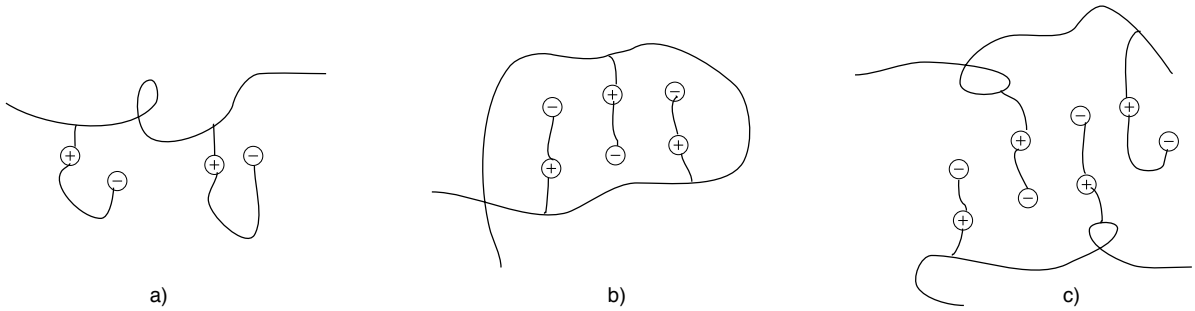

Figure 1.7. Associations of poly(sulfobetaines) a) intra-group, b) intra-chain and c) inter-chain. Reproduced from reference 74.[74]

In an extraordinary example of switchable polymer brushes, Xia *et al.* produced polymer brushes with sensitivity towards three triggers.[82] Temperature sensitive PNIPAm, and pH and glucose responsive poly(acrylamidophenylboronic acid) polymers were incorporated into poly(NIPAm-*co*acrylamidophenylboronic acid) brushes on flat and rough silicon substrates. The combination of polymers produced a surface that could reproducibly switch between superhydrophilicity and superhydrophobicity using temperature, pH and glucose triggers.

1.9. Synthesis of Polymers Brushes

Surface tethered polymer brushes can be formed by two methods: *grafting to*, where a preformed polymer chain is attached to a substrate, and *grafting from*, where the polymer chains is polymerised from a surface tethered initiator. These two methods will be compared after a brief introduction to polymerisation techniques.

1.9.1. Controlled Radical Polymerisation Techniques

Controlled or living radical polymerisations (CRP) are used to produce well-defined ionic polymers with excellent control over the polymer architecture. Though called 'living' radical polymerisation, these processes are not completely devoid of termination reactions, but do still allow for good control over the polymer structures. Atom transfer radical polymerisation (ATRP), nitroxide mediated polymerisation (NMP) and reversible addition fragmentation transfer (RAFT) are examples of CRP reactions, all of which enable the synthesis of polymers with well controlled molecular weight and narrow molecular weight distribution.

1.9.2. Atom Transfer Radical Polymerisation

ATRP is one of the leading polymerisation techniques for producing polymers with precise molar mass, composition and structure. ATRP was independently discovered by two research groups in 1995.[83,84,85] ATRP was developed from Atom Transfer Radical Addition (ATRA), which is an addition reaction of a halocarbon to an alkene or alkyne *via* a free radical mechanism. A simplified mechanism for reversible activation-deactivation of polymer chains during ATRP is shown in Figure 1.8. Radicals are generated through a reversible redox process catalysed by a transition metal complex, M_t^n-Y / Ligand (where Y may be another ligand or counter-ion), which undergoes a one-electron oxidation with concomitant abstraction of a (pseudo)halogen atom, X, from a dormant species R-X. Polymer chain growth occurs by the addition of intermediate radicals to monomers at a rate constant of activation k_{act} and k_{deact}.

ATRP remains the most investigated controlled radical polymerisation method for preparing polymer brushes.[86] It has been applied to a large set of reactive and functional homopolymers, block polymers and statistical polymers.[87]

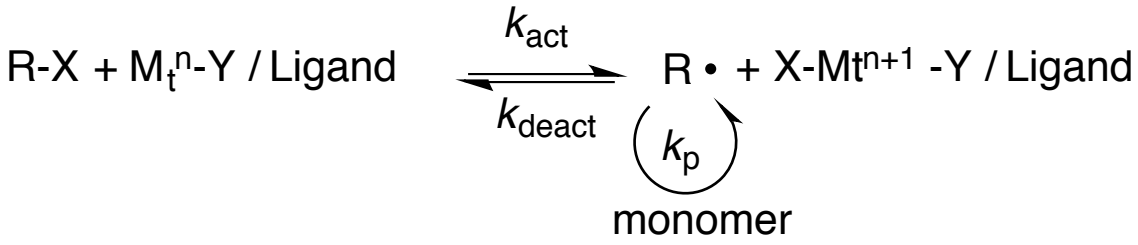

Figure 1.8. Simplified mechanism of transition metal-catalysed ATRP.[88]

While ATRP is the most widely used method for producing polymers, trace amounts of oxygen will oxidise Cu^{I} to the deactivating Cu^{II} species, and therefore, chain growth is usually carried out in an inert atmosphere. A high concentration of Cu^{II} will halt the polymerisation.[89]

Matyjaszewski *et al.* relaxed the stringent oxygen-free polymerisation conditions by introducing activators generated by electron transfer (ARGET), a catalytic technique that reduces air-stable deactivators to their respective activators in situ by means of a reducing agent. Reducing agents commonly used include ascorbic acid, tin^{II} 2-ethylhexanoate, and Cu^{0}. Having an excess of reducing agent in the system continuously regenerates the Cu^{I} activators from Cu^{II} deactivators.

The optimum amount of reducing agent is hard to estimate.[90] If too much reducing agent is added polymerisation control is lost as a relatively large concentration of Cu^{I} activators are produced. If too little is added, the concentration of Cu^{II} deactivator species is too large, leading to no polymerisation.

Further developments in the ATRP process to control the polymerisation have led to electrochemically mediated ATRP (eATRP).[91] The electrochemical regeneration of the activating Cu^{I} species by an applied potential decreases the oxygen sensitivity. If the potential applied is negative of $E_{1/2}$ of the Cu^{I}/Cu^{II} couple, then polymerisation rates are increased as

the Cu^{II} species is continually reduced to Cu^{I} (Figure 1.9). Magenau first demonstrated eATRP with the polymerisation of methyl methacrylate without extreme oxygen exclusion.[91]

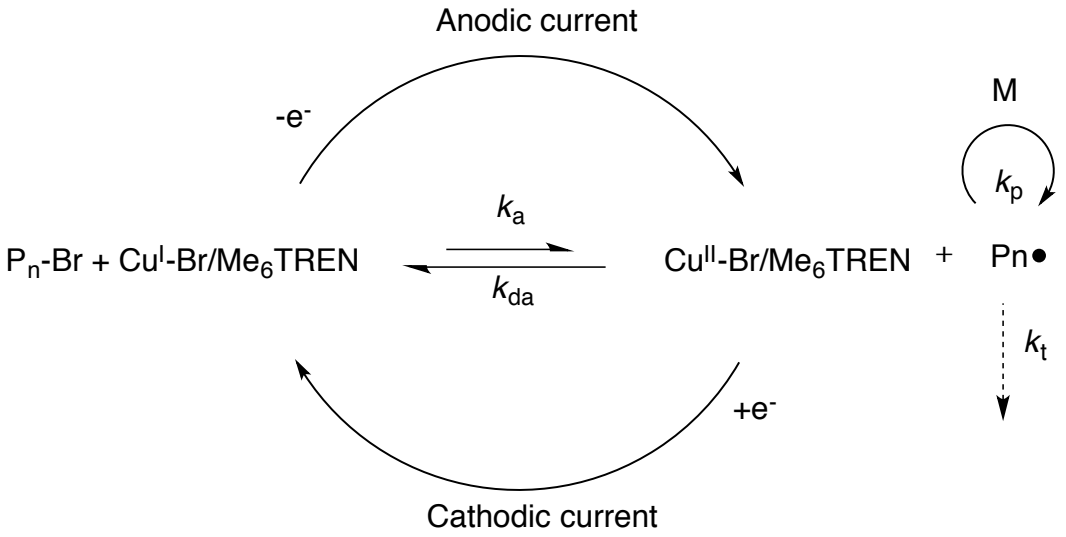

Figure 1.9. Mechanism of electrochemically mediated ATRP (eATRP) under cathodic current to (re)generate the $Cu^{I}Br_2/Me_6TREN$ complex and optional anodic current to revert to $Cu^{II}Br_2/Me_6TREN$ complex for termination of polymerisation. Reproduced from reference 91.[91]

1.9.3. *Grafting To* Approach For Preparation of Polymer Brushes

Grafting to takes a preformed, end-functionalised polymer and reacts it with a suitable surface under appropriate conditions to form a tethered polymer chain (Scheme 1.12). End-functionalised polymers can be synthesised by living anionic, cationic, radical, group transfer or any other means of polymerisation. As the polymer chains are in solution, narrow molecular weight distributions can be achieved through tight control over polymerisation conditions and through post synthetic work-up.

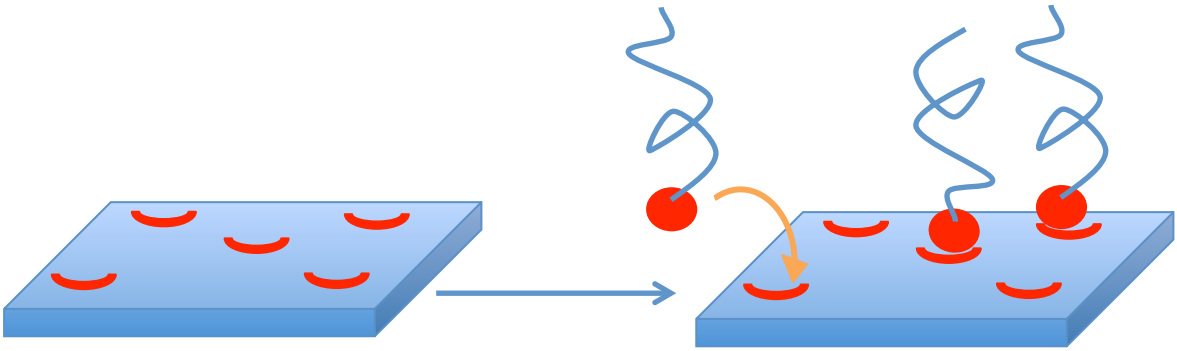

Scheme 1.12. *Grafting to* method for end-tethered polymer chains.

The method for covalently anchoring the polymer chain to the surface can be any conventional means of surface attachment. Thiol-terminated poly(styrene) chains have been assembled on gold surfaces.[92,93] Yang *et al.* also utilised self assembling monolayers, using a hydrosilylation reaction on silicon to covalently tether poly(methylhydrosiloxane) chains.[94] In another example, hydroxyl end functionalised random copolymers of styrene and methyl methacrylate synthesised by living radical polymerisation were reacted with silanol groups on silicon surfaces under vacuum at 140 °C, forming a polymer brush.[95] Bergbreiter *et al.* tethered terminally functionalised poly(*tert*-butyl acrylate) onto an oxidised polyethylene film.[96]

During the *grafting to* process, pre-formed polymer chains must diffuse through the existing polymer film to reach the active sites available on the surface. This diffusion barrier becomes more significant as more polymer chains are tethered. As a result, only small amounts of polymer can be immobilised and often result in a low graft density.

1.9.4. *Grafting From* Approach For Preparation of Polymer Brushes

The *grafting from* approach is the most promising method in the synthesis of polymer brushes with a higher grafting density compared to the *grafting to* approach. Polymerisation initiators are attached to a surface, followed by *in situ* surface initiated polymerisation (Scheme 1.13).

Through this method, the diffusion issues that plague *grafting to* are minimised as polymer growth, when using a well-controlled polymerisation technique, should be uniform from initiation points.

1.9.5. Surface Initiated-Atom Transfer Radical Polymerisation (SI-ATRP)

There have been many accounts of successful polymer chain growth at a surface by using SI-ATRP. An initiator molecule can be attached to a surface ensuring that in the absence of chain transfer or thermal self-initiation events, chains can be grown solely from that surface. This method of polymer chain growth is a *grafting from* process.

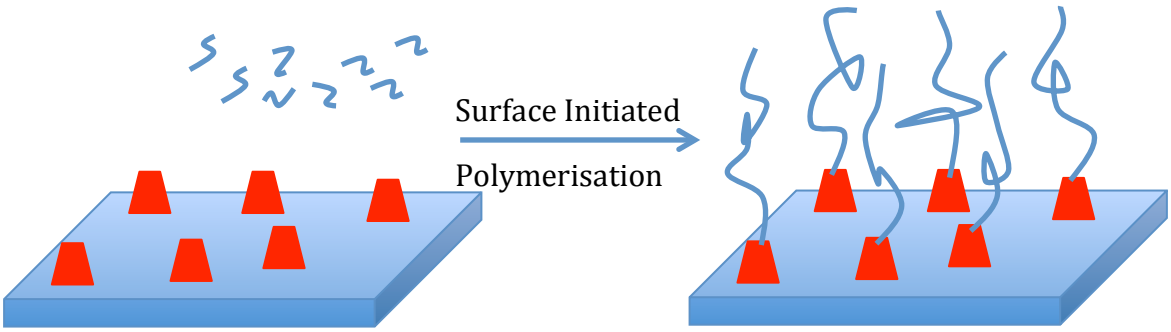

Scheme 1.13. *Grafting from* method for end-tethered polymer chains.

Polymerisation initiators can be immobilised on a substrate through a variety of methods. Pei *et al.* attached ABiB to an ECP surface through an esterification between the acid-bromide of the initiator and a terminal hydroxyl group of the ECP film, shown in Scheme 1.14.[81] Polymer brushes of PMPDSAH were then grown from this initiator-terminated film.

eATRP can be further applied to the formation of polymer brushes. Electrochemically induced SI-ATRP was demonstrated by Li *et al.* in 2012 for the production of polymer brushes.[89] A constant potential was applied to the system, facilitating the reduction of the $Cu^{II}Cl_2$/bipy complex to the catalytic $Cu^{I}Cl_2$/bipy complex. Using a gold electrode modified with an ATRP initiator terminated SAM, polymer brushes of poly(3-sulfopropyl

methacrylate) (PSPMA) and poly (hydroxyethylmethacrylate) (pHEMA) were grown in the presence of air. It has been shown that the polymerisation solution can be reused, with seven samples obtaining almost the same thickness after 1 h, all grown from the same stock solution. This can be particularly useful when producing polymer brushes from exotic or expensive monomers.

The same group explored the application of a square-wave potential during the polymerisation to better control brush growth. Applying a reducing potential will initiate polymerisation, while applying a reverse positive potential will deactivate it. Cycling between activation and deactivation of the catalyst increases the polymerisation control.[89]

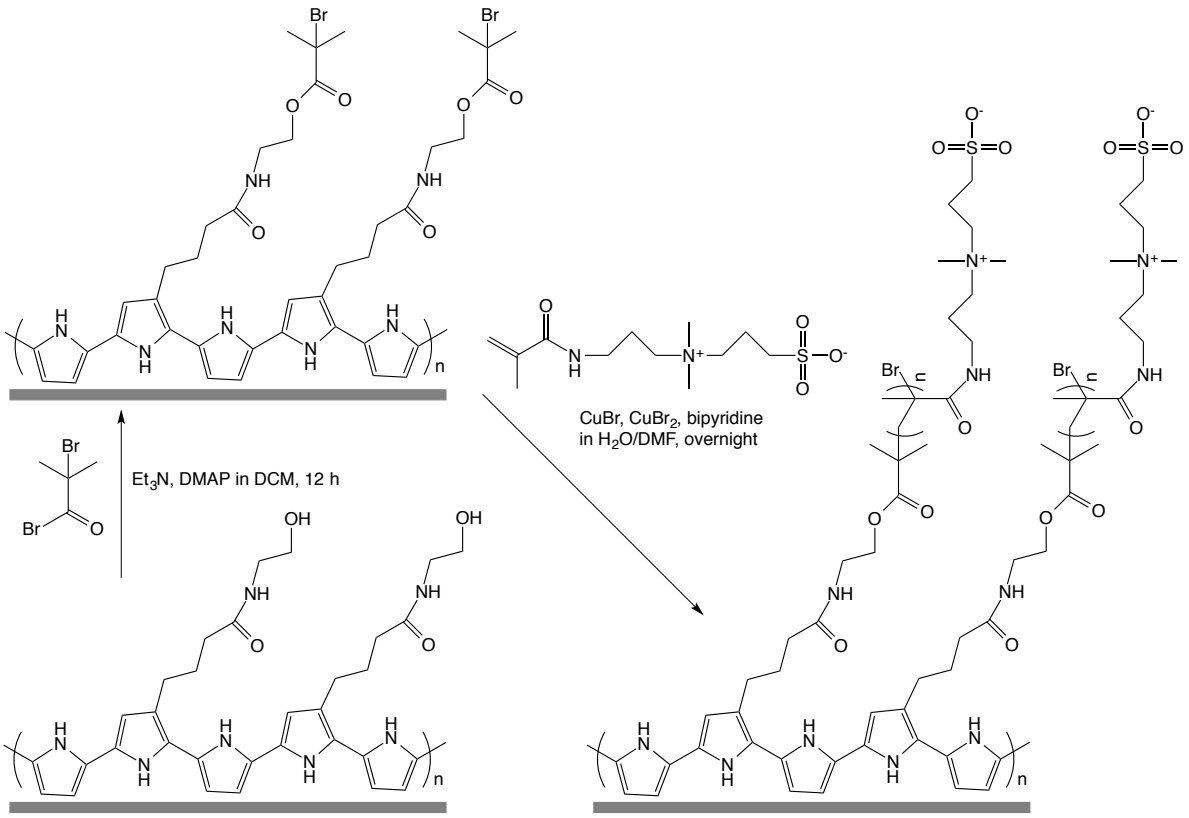

Scheme 1.14. Attachment of a polymer initiator, ABiB, to a modified ECP film followed by SI-ATRP polymerisation of PMPDSAH. Reproduced from reference 81.

1.9.6. ATRP Initiators

The primary role of an initiator is to define the number of growing polymer chains.[88] If initiation is fast and the number of transfer and termination events is negligible, the number of growing chains is constant and equal to the initial initiator concentration. Typical ATRP polymer initiators include halogenated alkanes, benzylic halides, α-haloesters, α-haloketones, α-halonitriles and sulfenyl halides. Chloride and bromide are the most commonly used halides, as the halogen radical must rapidly and selectively migrate between the growing chain and the transition metal complex.[97] Iodide has been used, but fluoride is not suitable, as the C-F bond is too strong to be homolytically cleaved. There are a sizable number of effective ATRP initiators, but only two specific molecules used in this work will be mentioned here.

α-Bromoisobutyrates are often used as ATRP initiators.[81,88,98] α-Bromoisobutyryl bromide, (ABiB) (Figure 1.10 (a)) is an acid-bromide capable of undergoing esterification or amide coupling reactions whilst retaining its initiating functions after reaction. (3-Azidopropyl) bromoisobutyrate (APBiB), Figure 1.10 (b), is an azide functionalised α-bromoisobutyrate capable of initiating polymerisation and undergoing click reactions through the azide functional group. It is synthesised by the esterification of azidopropanol and ABiB.

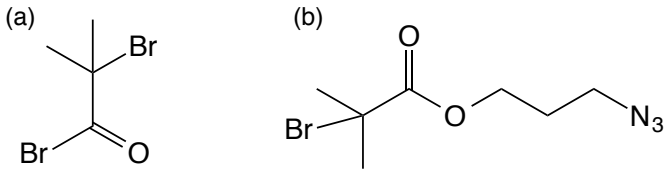

Figure 1.10. a) ABiB and b) APBiB, initiators for ATRP

There are few examples of polymer brushes being tethered to a surface through grafting of an aryl diazonium salt. Matrab *et al.* used a diazonium salt analogue (Figure 1.11 (a)) of a bulk

solution ATRP initiator, (1-bromoethyl)benzene (Figure 1.11 (b)) to attach the initiator to an iron surface.[99] Polymer brushes of methyl methacrylate, *n*-butyl acrylate and styrene were grown from the modified iron surface. AFM imaging of the initiator layer showed the maximum height of the electrografted film to be 50 nm. After polymerisation, the PMMA brushes displayed a maximum height of 150 nm. This indicates that the grafted layer was efficient at initiating polymerisation from the metal surface. When a solution-based sacrificial initiator was used to better control the growth of polymer chains, the polymer layer maximum height reached 200 nm.

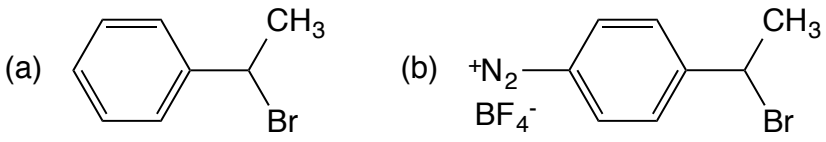

Figure 1.11. Comparison of the chemical structures of a bulk solution ATRP initiator and its diazonium salt analogue.[99]

In a two step procedure, Iruthayaraj *et al.* coupled ABiB to a hydroxyl terminated film produced *via* the electrochemical grafting of 4-(2-Hydroxyethyl)benzenediazonium tetrafluoroborate (Scheme 1.15 (a)).[100] Polymer brushes of MMA were then grown from the film using ATRP. The authors also attempted to polymerise methyl methacrylate (MMA) from a surface modified with the molecule shown in Scheme 1.15 (b), an aryl diazonium salt containing the α-bromoisobutyrate group,[100] but after electrochemical grafting XPS analysis showed no trace of bromine in the film and SI-ATRP attempts failed. It was speculated that aryl radicals abstracted the bromine atoms during the grafting process.

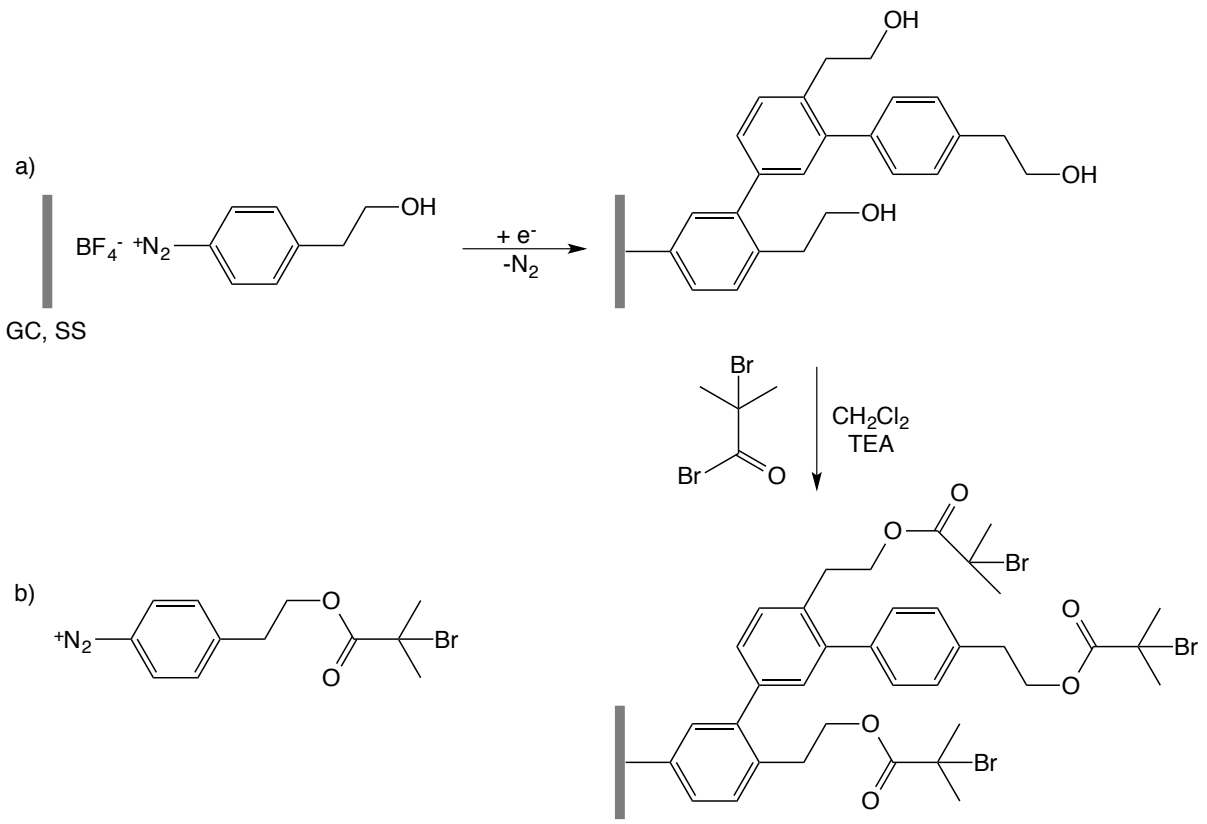

Scheme 1.15. a) Formation of a covalently attached initiator film *via* electrografting of an aryl diazonium salt followed by a chemical reaction with ABiB, and b) potential grafting agent incorporating an initiator group. Reproduced from reference 100.

According to literature, various research groups have used APBiB as a polymerisation initiator for the *grafting to* approach for synthesis of polymer brushes and in producing block copolymers. For example, Li *et al.* increased the water solubility of C_{60} fullerenes by attaching polymer chains of PNIPAm using a *grafting to* approach (Scheme 1.16).[101] APBiB was used to polymerise PNIPAm. The azide groups of APBiB were then reacted with the ethynyl modified C_{60} fullerenes. Jiang *et al*. produced biodegradable polymer brushes for gene delivery through clicking polymer chains of poly(2-(dimethylamino)ethyl methacrylate) (pDMAEMA) initiated by APBiB to a block co-polymer backbone functionalised with alkyne groups.[102] Glass and silicon surfaces have been modified by He *et al.* using poly(ionic liquid)s (PILs).[103] PILs were produced by the polymerisation of 1-(4-vinylbenzyl)-3-butylimidazolium bis(triflouromethylsulfonyl)imide using ATRP initiated from APBiB. The terminal azide

group was then clicked to alkyne functionalised glass and silicon surfaces. Cotton has been functionalised with polymer chains by click chemistry using a similar approach.[104]

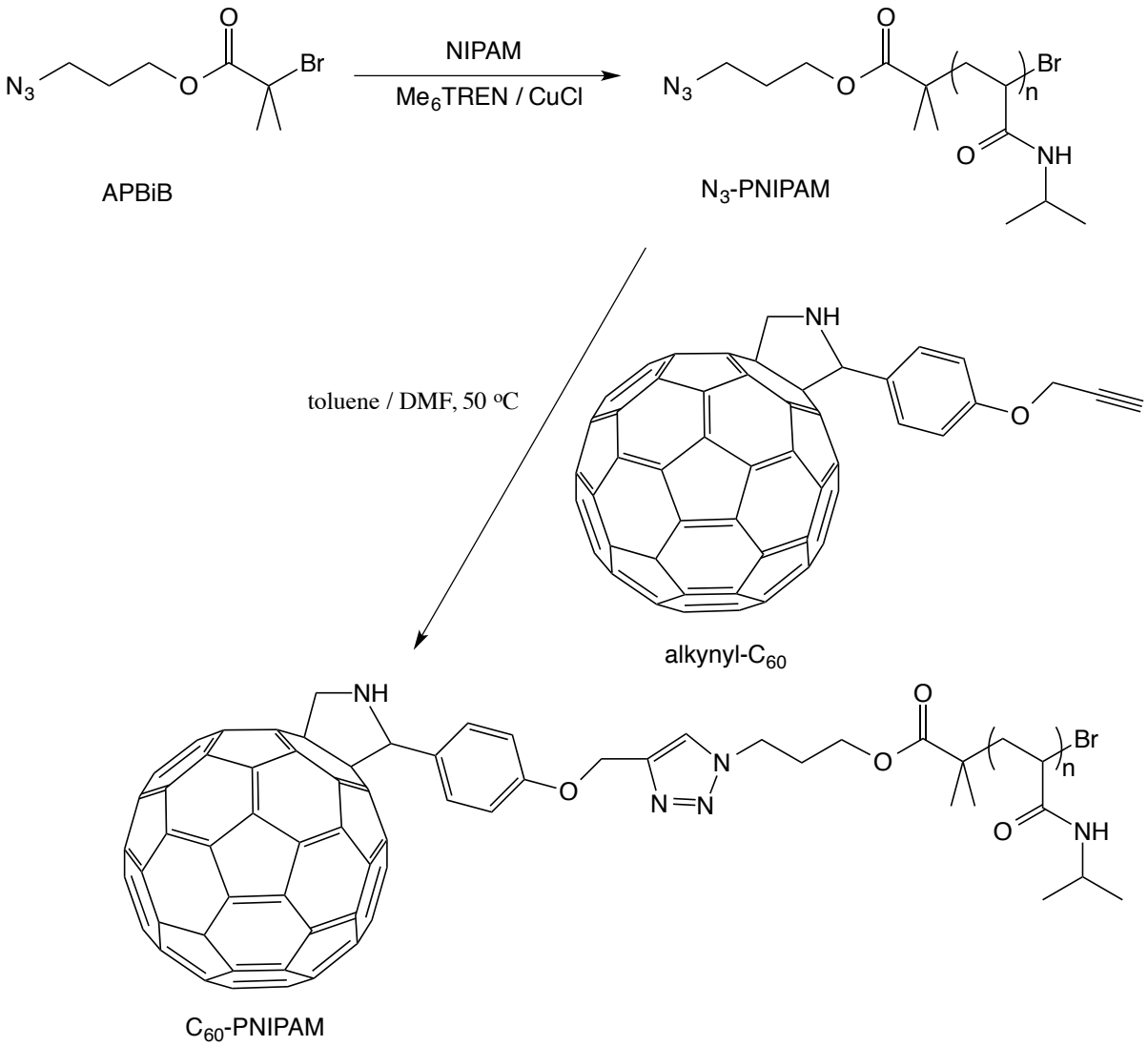

Scheme 1.16. Preparation of C_{60}-PNIPAM utilising APBiB as the ATRP initiator. Reproduced from reference 101.

Block copolymers of poly(3-hexylthiophene)-*b*-poly(styrene) were synthesised by Urien *et al.* using APBiB.[105] Scheme 1.17 shows the polymerisation of styrene from APBiB *via* ATRP, followed by the click of the azido-poly(styrene) molecules to ethynyl terminated poly(3-hexylthiophene) chains. The alkyl spacer between the ethynyl group and the conjugated

polymer was necessary to retain the electronic environment needed for the cycloaddition click reaction.

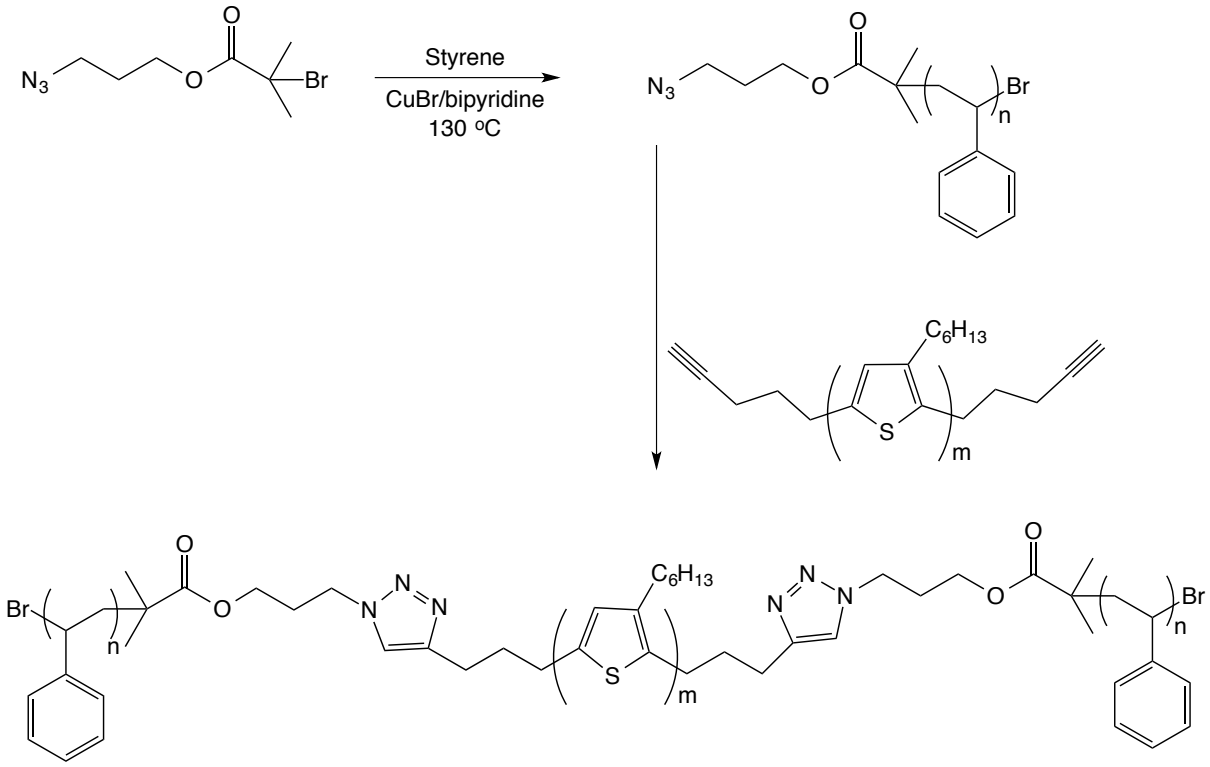

Scheme 1.17. Synthesis of poly(3-hexylthiophene)-*b*-poly(styrene) block polymers by click chemistry. Adapted from reference 105.

APBiB has been proven to initiate ATRP while having the capability of reaction with molecules containing an alkyne group. So far, there are no reports describing the use of APBiB as a polymerisation initiator from a surface for the *grafting from* approach of polymer brush synthesis. APBiB is also a prime candidate for use in a combined ATRP/CuAAC reaction.

1.9.7. One-Pot synthesis

The ATRP polymerisation reaction and the CuAAC reaction both rely on a Cu^{I} catalyst and are tolerant towards non-protected functional groups. The combination of these two techniques as a 'one-pot' process is an attractive approach for preparing functional materials.

Mantovani *et al.* reported the first example of a one-pot tandem Cu^{I} catalysed sequential living radical polymerisation (LRP)/CuAAC process.[106] The group synthesised azide functionalised PMMA polymer chains using a $Cu^{I}Br$/iminopyridine catalyst. Once clicked to alkyne containing dyes, the polymers fluoresced.

Further investigation by the group involved the simultaneous CuAAC reaction and LRP of an alkyne-containing monomer (propargyl methacrylate) and an ATRP initiator (APBiB) using a CuBr/*N*-ethyl pyridine-imine/triethylamine complex as a catalyst.[107] They tested a number of solvents including toluene, dimethyl sulfoxide (DMSO) and DMF. In toluene at 60°C, the reactions were found to be sequential (Path 1, Scheme 1.18). When azides 1 and 2 were used, the CuAAC reaction had reached near completion before the polymerisation began. The rate of polymerisation was greatly dependent on the concentration of the catalyst, although the concentration of catalyst used was too high to investigate the effects on the CuAAC reaction. Polymerisation could be accelerated through the increase of the copper catalyst, but the CuAAC reaction was always faster. In DMSO, the two reactions occurred concurrently (Path 3 in Scheme 1.18), with the rate of the click reaction significantly slower and the rate of the polymerisation slightly higher when compared to toluene. The catalyst concentration was found to only affect the CuAAC reaction rate. The reactions in DMF were also simultaneous, with the rate of the click reaction faster than in DMSO, while the rate of polymerisation was similar as in toluene.

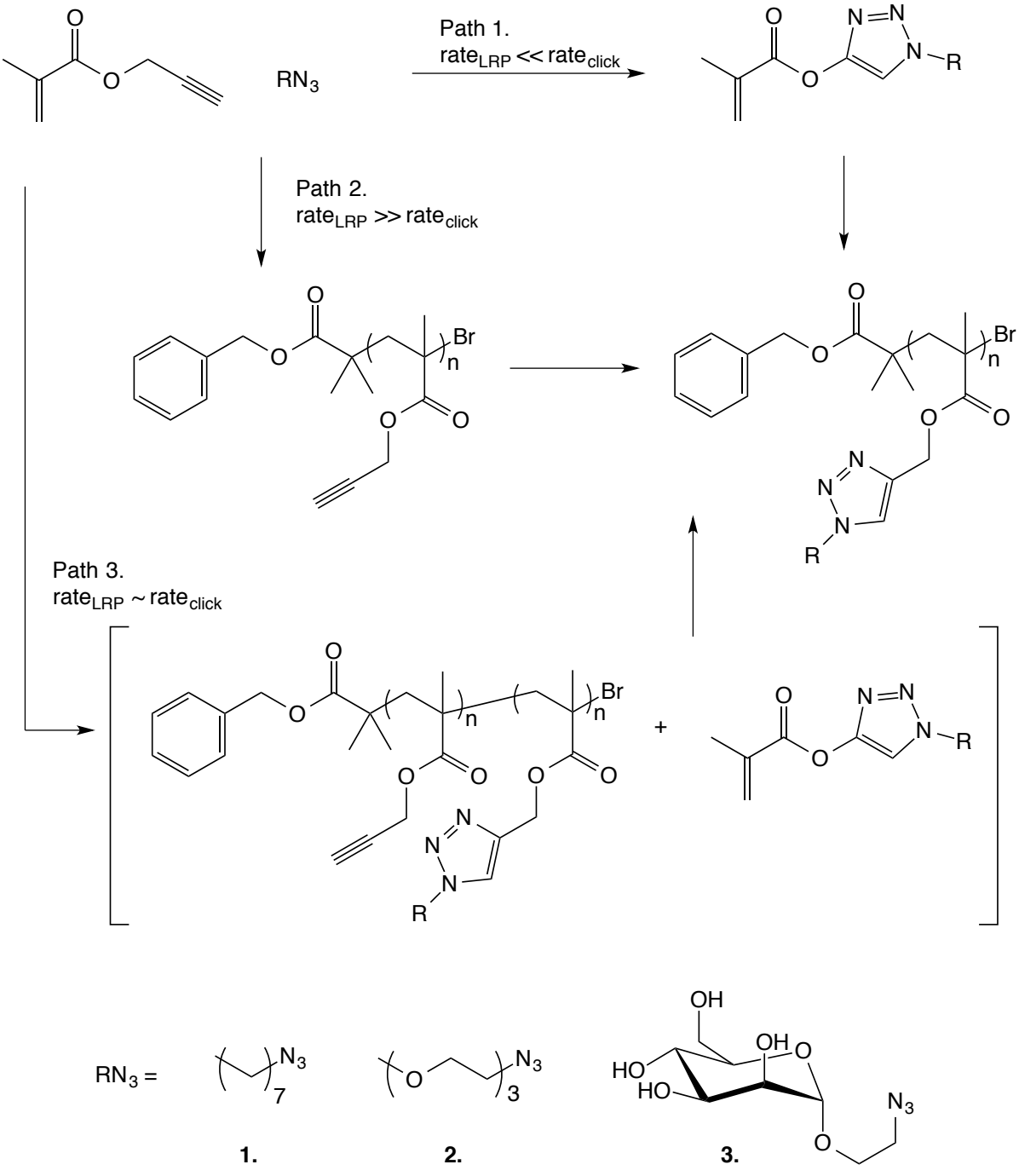

Scheme 1.18. One-pot CuAAC/LRP process: possible pathways (benzyl 2-bromoisobutyrate was employed as the polymerisation initiator). Reproduced from reference 107.

Damiron *et al.* utilised complementary click chemistry/ATRP for the synthesis of functionalised random copolymers.[108] MMA and propargyl methacrylate were copolymerised while the propargyl methacrylate was simultaneously clicked to a monofunctional azide. A CuBr/bipyridine complex catalysed the reactions.

Grignard *et al.* demonstrated the one-pot process with the synthesis of PMMA microspheres.[109] Ethynylpyrene was used as the alkyne, while (3-Azidoethyl) bromoisobutyrate was used as the azide source. In a reaction medium of supercritical carbon dioxide ($scCO_2$), using a Cu^I catalyst ligated to a perfluorinated polymeric amino-based macroligand, simultaneous ATRP of MMA from the azide source and clicking of the azide and alkyne was achieved (Scheme 1.19). The microspheres were characterised by size exclusion chromatography, UV detection, ^1H NMR and fluorescence microscopy.

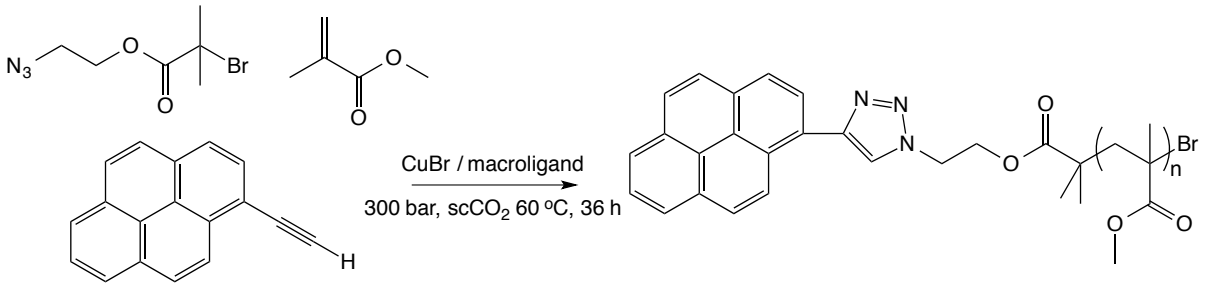

Scheme 1.19. Synthesis of functional PMMA chains by combination of click reaction and dispersion ATRP in $scCO_2$ in a "one-pot process. Reproduced from reference 109.

As with eATRP, a voltage can be applied to produce the catalytic Cu^I species. Rydzek *et al.* demonstrated simultaneous electropolymerisation and electro-click (SEEC) functionalisation for a one-pot self-construction of aniline- and naphthalene-based functional polymer film.[110] Cyclic voltammetry was applied for the concurrent oxidation and polymerisation of 4-azidoaniline, the reduction of Cu^{II} ions and the Cu^I catalysed azide/akyne cycloaddition. Ethynylferrocene incorporated into the polymer matrix allowed for characterisation through UV-visible and X-ray photoelectron spectroscopies.

Xu *et al.* combined SI-ATRP and click chemistry for the preparation of poly(5-ferrocene-triazolyl methacrylate) polymer brushes on a gold substrate.[111] Shown in Scheme 1.20, the gold surface was modified with a self-assembled monolayer of cystamine, followed by the attachment of an ATRP initiator. Simultaneous SI-ATRP and click chemistry of 2-azidoethyl

methacrylate (AzEMA) and ethynyl ferrocene allow the preparation of surface-grafted ferrocene functional polymer brushes.

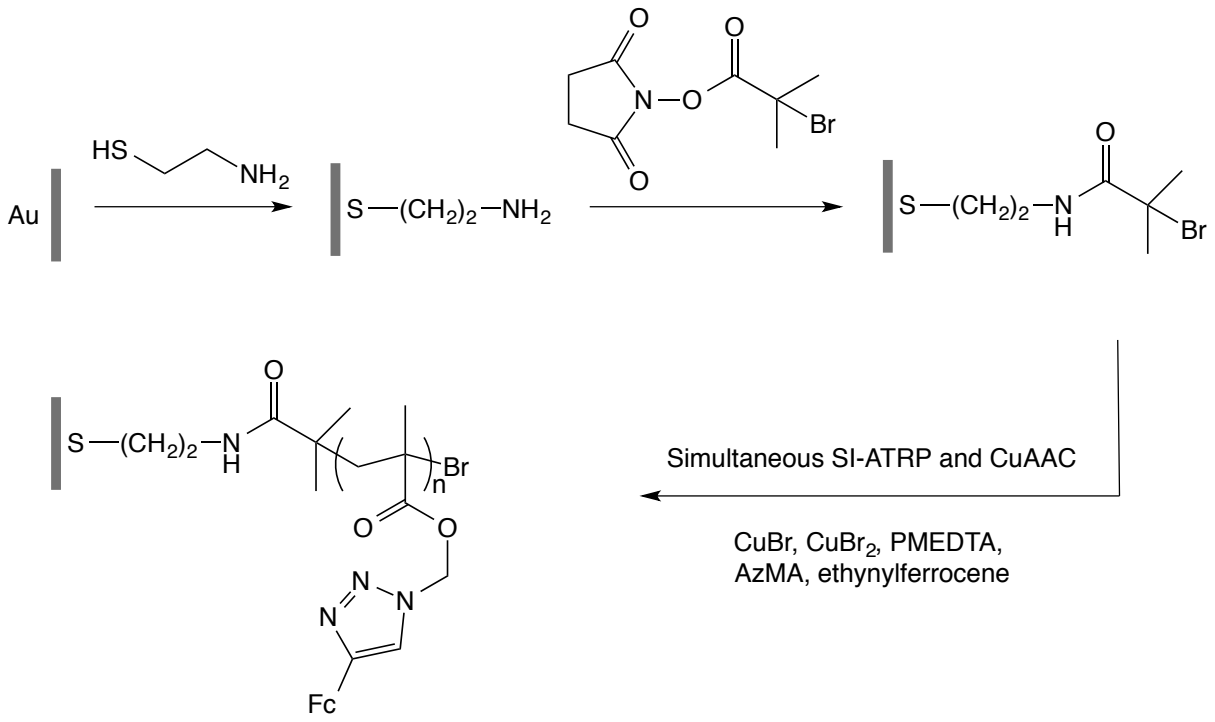

Scheme 1.20. Synthesis of ferrocene-functionalised polymer brushes on a gold substrate by simultaneous SI-ATRP and CuAAC. Reproduced from reference 111.

1.10. Aims

The aim of this work is to establish methods for preparation of systems for the growth of polymer brushes from surfaces, such that the number of attachment points is controllable and well defined. This will be achieved through the following specific objects. To:

1. prepare monolayer films of Ar-COOH and Ar-Eth on carbon surfaces through the electrochemical grafting and deprotection of aryl diazonium salts.
2. tether polymerisation initiators to the grafted monolayers.
3. modify carbon surfaces with a polymerisation initiator though direct reaction with the carbon substrate.
4. grow and identify polymer brushes of PMPDSAH by SI-ATRP from the tethered polymerisation initiators prepared by the grafting of aryl diazonium salts.
5. grow and identify polymer brushes of PMMA from the tethered polymerisation initiator derived from the Ar-Eth monolayer using SI-ATRP and eSI-ATRP, and from surfaces modified with a polymerisation initiator by direct reactions.
6. prepare polymer brushes of PMMA from the Ar-Eth monolayer by a one-pot simultaneous CuAAC/SI-ATRP reaction.

Chapter 2. Experimental

2.1. General Synthesis and Reagents

2.1.1. Reagents and Solvents

All solvents and chemicals were obtained from commercial sources and used as received unless otherwise stated. For electrochemistry, acetonitrile (ACN) and ethanol (EtOH) were HPLC grade. When anhydrous solvents were required, HPLC grade solvents were dried in an alumina column drying system. Milli-Q water (resistivity > 18 MΩ cm) was used to prepare all aqueous solutions and was used for all washing steps. Methyl methacrylate was passed through an alumina column prior to use to remove the inhibitor. Azidomethyl ferrocene ($FcMeN_3$) and 4-((triisopropylsilyl)ethynyl) benzenediazonium tetrafluoroborate (TIPS-Eth-Ar-N_2^+) were prepared by Lita Lee, Department of Chemistry, University of Canterbury, following literature procedures.[112,113]

2.1.2. Buffer Solutions

Phosphate buffer saline (PBS) solutions of pH 5.2 and 7 were prepared using NaH_2PO_4 and Na_2HPO_4. The combined concentration of NaH_2PO_4 and Na_2HPO_4 used in the pH 5.2 and 7 solutions were 0.01 and 0.1 M respectively. 0.1 M of KCl was added to each solution. The amount of each reagent was estimated using the Henderson-Hasselbach equation (Equation 2.1), where the pK_a is that of the acidic proton of the acid base pair in use, $[A^-]$ is the concentration of the base component, HPO_4^{2-}, and [HA] is the concentration of the acidic component, $H_2PO_4^-$. The pH was measured with a pH meter.

$$pH = pK_a + \log\left([A^-]/[HA]\right) \qquad (2.1)$$

2.1.3. Tetrabutylammonium tetrafluoroborate ($TBABF_4$)

Tetrabutylammonium tetrafluoroborate ($TBABF_4$) was prepared by diluting 20 mL of tetrabutylammonium hydroxide (40%) to 100 mL. To this, a 5 mL solution of (50%) fluoroboric acid diluted with 20 mL of H_2O was added with stirring. The white precipitate of $TBABF_4$ was collected, washed with water and dried overnight. The electrolyte was dried at 50°C for a further 3 day, then at 80°C for 3 days. The electrolyte was stored in a desiccator.

2.1.4. Synthesis of Aryl Diazonium Salts

4-Nitrobenzenediazonium tetrafluoroborate (NBD)

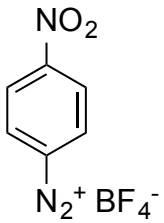

4-Nitrobenzenediazonium tetrafluoroborate (NBD) salt was prepared following a literature procedure.[114] p-Nitroaniline (0.70 g, 5 mmol) was dissolved in a 2 mL solution of mixture of HBF_4/H_2O (1:1), and cooled in an ice bath. Meanwhile, $NaNO_2$ (0.35 g, 5 mmol) was dissolved in the minimum amount of water and transferred dropwise to the chilled amine solution with gentle stirring. The diazonium salt precipitated out as a white solid, which was filtered and collected under suction, washed with methanol and ether, then recrystallised from an ACN/diethyl ether mixture. The p-nitrophenyl diazonium salt was filtered and dried under suction and stored in the freezer in the dark. Pale yellow solid (yield 65%). ^{1}H NMR (400 MHz, CD_3CN, ppm): δ = 8.36 (d, 2H, J = 8.8 Hz), 7.76 (d, 2H, J = 8.4 Hz), 2.64 (s, 3H).

Fm protected carboxybenzenediazonium salt

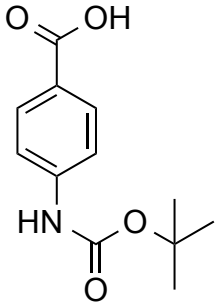

4-(((*tert*-butoxy)carbonyl)amino)benzoic acid (Boc-NH-Ar-COOH) was synthesised by following a literature method.[115] To a 75 mL solution of dioxane/water (2:1) mixture, 4-aminobenzoic acid (3.0 g, 22 mmol) was

dissolved. Triethylamine (4.5 mL, 32 mmol) was added, followed by di-*tert*-butyl dicarbonate (0.33 g, 1.5 mmol). The mixture was stirred at room temperature overnight. Excess solvent was removed under vacuum and 3 M HCl was added dropwise to the residue to obtain 4-(((*tert*-butoxy)carbonyl)amino) benzoic acid (Boc-NH-Ar-COOH) as a white precipitate. This was collected by filtration and washed with water (yield = 4.63 g, 90%). ^{1}H NMR (400 MHz, DMSO-d_6, ppm) δ: 9.69 (s, 1H), 7.81 (d, 2H, J = 9 Hz), 7.53 (d, 2H, J = 9 Hz), 1.48 (s, 9H).

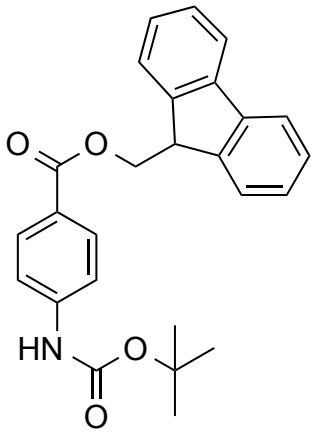

9-H-Fluoren-9-ylmethyl 4-(((*tert*-butoxy)carbonyl)amino) benzoate (Boc-NH-Ar-COO-Fm) was prepared by the following Steglich esterification method.[116] Boc-NH-Ar-COOH (4.0 g, 18 mmol) was dissolved in the minimum amount of DMF. To this solution, 4-dimethylaminopyridine (80 mg, 0.65 mmol) and 9-fluorenylmethanol (4.0 g, 20 mmol) were added and the solution was cooled in an ice bath. *N,N'*-dicyclohexylcarbodiimide (DCC) (0.27 g, 13 mmol) was added and stirred for 5 min. The solution was removed from the ice bath and stirred for further 3 h at room temperature. After the precipitated urea was removed by filtration, and the filtrate was evaporated under vacuum, the residue was taken up in dichloromethane (DCM). This solution was washed twice with 0.5 M HCl then with a saturated $NaHCO_3$ solution, and dried over $MgSO_4$. The solvent was removed under vacuum and the desired product was obtained by column chromatography on silica (eluent DCM). The product was a colourless oil (yield 2.63 g, 35%). ^{1}H NMR (400 MHz, $CDCl_3$, ppm) δ: 8.03 (d, 2H, J = 8.4 Hz), 7.79 (d, 2H, J = 7.2 Hz), 7.65 (d, 2H, J = 7.6 Hz), 7.47 (d, 2H, J = 8.8 Hz), 7.41 (t, 2H, J = 7.2 Hz), 7.32 (t, 2H, J = 7.2 Hz), 4.59 (d, 2H, J = 7.2 Hz), 4.38 (t, 1H, J = 7.6 Hz), 1.26 (s, 9H).

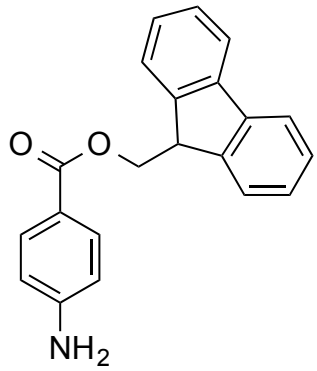

9-*H*-Fluoren-9-ylmethyl 4-aminobenzoate (NH_2-Ar-COO-Fm) was prepared by the removal of the Boc group of Boc-NH-Ar-COO-Fm by using trifluoroacetic acid (TFA).[117] Boc-NH-Ar-COO-Fm (2.5 g, 6 mmol) was dissolved in DCM (15 mL) followed by the addition of TFA (10 mL). The reaction mixture was stirred for 1 h at room temperature. Excess solvent was removed under vacuum and saturated $NaHCO_3$ was added dropwise to neutralise the solution. The white precipitate was collected by filtration and washed with hexane (yield = 1.6 g, 85%). ^{1}H NMR (400 MHz, $CDCl_3$, ppm) δ: 7.93 (d, 2H, *J* = 8.4 Hz), 7.79 (d, 2H, *J* = 7.2 Hz), 7.66 (d, 2H, *J* = 7.2 Hz), 7.41 (t, 2H, *J* = 7.2 Hz), 7.32 (t, 2H, *J* = 7.6 Hz), 6.70 (d, 2H, *J* = 8 Hz), 4.55 (d, 2H, *J* = 7.2 Hz), 4.37 (t, 1H, *J* = 7.2 Hz).

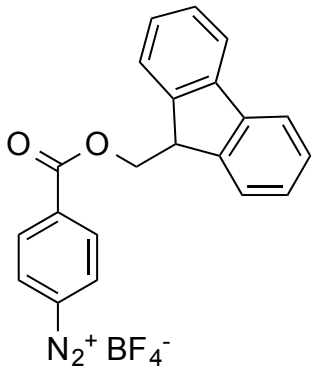

4((9-*H*-Fluoren-9-ylmethoxy)carbonyl)benzene-1-diazonium tetrafluoroborate (Fm-COO-Ar-N_2^+ BF_4^-) was synthesised by dissolving NH_2-Ar-COO-Fm (0.15 g, 0.45 mmol) in dry ACN and the solution was stirred at -40 °C, followed by the addition of $NOBF_4$ (65 mg, 0.55 mmol). The reaction was stirred for a further 2 h at -40 °C and the solvent was evaporated under vacuum. The residue was re-dissolved in a small amount of ACN and re-precipitated by the addition of cold diethyl ether. The yellow precipitate was collected under vacuum and stored in the freezer in the dark (yield = 0.18 g, 93%). ^{1}H NMR (400 MHz, CD_3CN, ppm) δ: 8.57 (d, 2H, *J* = 9 Hz), 8.34 (d, 2H, *J* = 9 Hz), 7.90 (d, 2H, *J* = 7.5 Hz), 7.73 (d, 2H, *J* = 7.5 Hz), 7.48 (t, 2H, *J* = 7.5 Hz), 7.40 (t, 2H, *J* = 7.5 Hz), 4.81 (d, 2H, *J* = 6.5 Hz), 4.48 (t, 1H, *J* = 6.5 Hz).

2.1.5. Synthesis of Polymerisation Initiators

(3-Azidopropyl)bromoisobutyrate (APBiB)

3-Azido-1-propanol was synthesised according to a literature procedure.[118] Sodium azide (8.15 g, 131 mmol) and a catalytic amount of potassium iodide were dissolved in 20 mL of water. To this, a solution of 3-chloro-1-propanol (2.75 mL, 32.8 mmol) in 80 mL of acetone was slowly added. The reaction was stirred at room temperature for 48 h, after which the mixture was extracted with 3 × 50 mL of diethyl ether, the organic layers combined, dried over K_2CO_3, and concentrated under reduced pressure to give 3-azido-propan-1-ol as a yellow oil (3.186 g, 31.5 mmol, 96%). ^{1}H-NMR (400 MHz, $CDCl_3$, ppm) δ: 3.69 (t, 2H, J = 6.1 Hz), 3.59 (t, 2H, J = 6.5 Hz), 1.92 (q, 2H, J = 6.3 Hz).

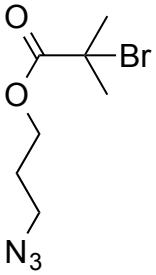

(3-Azidopropyl)bromoisobutyrate (APBiB) was synthesised according to a literature procedure.[119] Triethylamine (7.5 mL, 53.8 mmol) and 3-azido-1-propanol (2.72 g, 26.9 mmol) were added to 140 mL diethyl ether. α-Bromoisobutyryl bromide (ABiB, 7.31 mL, 59.18 mmol) was added dropwise over 1 h to the mixture that was stirred and kept at 0 °C. The mixture was then warmed to room temperature and stirred for 24 h. The solution was filtered and the organic phase was washed with 50 mL of saturated $NaHCO_3$, dried over Na_2SO_4 and filtered giving APBiB as a pale yellow oil (yield = 5.01 g, 74%). ^{1}H-NMR (400 MHz, $CDCl_3$, ppm) δ: 4.31 (t, J = 6.10 Hz, 2 H), 4.46 (q, J = 7.04 Hz, 2 H), 2.13 (m, J = 6.26 Hz, 2 H), 1.91 (s, 6 H).

α-Bromoisobutyric acid (ABiA)

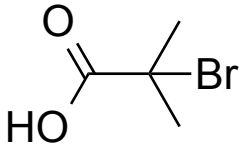

α-Bromoisobutyric acid (ABiA) was isolated from the $NaHCO_3$ washings during the purification of APBiB. ABiA was recrystallised from petroleum ether, forming large white crystals. ^{1}H-NMR (400 MHz,

$CDCl_3$, ppm) δ: 2.00 (6 H).

2.1.6. Synthesis of Triazole Compounds

Triazole compounds were synthesised through a Huisgen copper catalysed azide-alkyne cycloaddition (CuAAC)[51] using a modified literature procedure.[120] An azide derivative (2 mmol) was added to a solution of ethynylbenzene (204 mg, 2 mmol), $CuSO_4 \cdot 5H_2O$ (5 mg, 0.02 mmol), sodium ascorbate (7.9 mg, 0.04 mmol) and benzoic acid (24.4 mg, 0.2 mmol) in 3 mL of *tert*-butanol/water (1 : 2). The reaction mixture was stirred for 30 min and then 20 mL of DCM was added. The organic layer was washed with water, brine, and dried over anhydrous Na_2SO_4. The solvent was removed under vacuum and the product was isolated.

3-(4-Phenyl-1H-1,2,3-triazol-1-yl)propanol

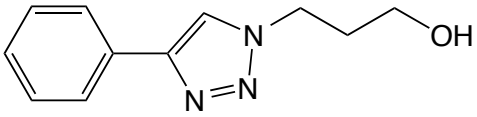

3-(4-Phenyl-1H-1,2,3-triazol-1-yl)propanol was synthesised using 3-azido-1-propanol as the azide source. Pale yellow solid (yield = 82%). ^{1}H-NMR (400 MHz, $CDCl_3$, ppm) δ: 8.12 (d, *J* = 7 Hz, 1 H), 7.62 (t, *J* = 7.4 Hz, 2 H), 3.83 (t, *J* = 6.1 Hz, 2 H), 3.69 (t, *J* = 6.3 Hz, 2 H), 3.50 (s, 1 H), 2.02 (quin, *J* = 6.3 Hz, 2 H), 7.3 (m, 3 H), ESI-MS calculated for $C_{11}H_{14}N_3O$ [$M+H^+$] = 204.1131; found = 204.1134.

3-(4-Phenyl-1H-1,2,3-triazol-1-yl)propyl 2-bromo-2-methylpropionate

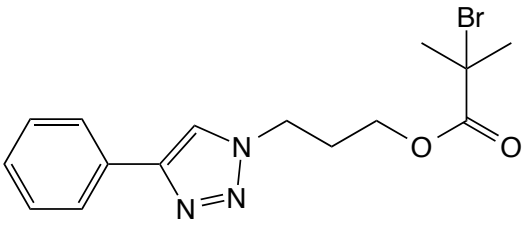

3-(4-Phenyl-1H-1,2,3-triazol-1-yl)propyl 2-bromo-2-methylpropionate was synthesised using APBiB as the azide source. Pale yellow solid (yield = 84%). ^{1}H-NMR (400 MHz, $CDCl_3$, ppm) δ: 8.09 (d, *J* = 7.8 Hz, 1 H), 7.66 (m, *J* = 7.66 Hz, 1 H), 7.51 (m, 1 H), 7.47 (dd, *J* = 7.6 Hz, 1.8, 2 H), 4.32 (t, *J* = 6.1 Hz, 3 H), 3.63 (t, *J* = 6.3 Hz, 3 H), 3.06 (s, 1H), 2.13 (q, *J* = 6.2 Hz,

2 H), 1.93 (m, 9 H). ESI-MS calculated for $C_{15}H_{19}N_3O_2Br$ [M+H$^+$] = 352.0655, 343.0635; found = 352.0660, 354.0641.

2.2. Surface Modification Procedures.

2.2.1. Electrochemical Modification

Electrochemical grafting of aryl diazonium salts was conducted on GC or PPF substrates as the working electrode. Platinum mesh was used as the auxiliary electrode, with a calomel electrode (CE) with 1 M LiCl as the reference electrode. Unless otherwise specified, grafting experiments were conducted using 1 mM aryl diazonium salt in ACN with 0.1 M $TBABF_4$ supporting electrolyte. Five cyclic voltammogram scans between 0.8 and -0.75 V at a scan rate of 50 mV s^{-1} were used for the grafting procedure. The experiment was performed under a N_2 atmosphere.

2.2.2. Non-electrochemical reactions on electrodes

Unless specified otherwise in the experimental section of each chapter, the reactions below were used to couple functional molecules to the bare or modified electrode surfaces.

2.2.2.1. Cleavage of Protecting Groups

Removal of Fm protecting group from Ar-COO-Fm film

The Fm protecting group was removed from the Ar-COO-Fm film by immersing the modified electrode in a stirred solution of 20% piperidine/dimethylformamide (DMF) for 3 h, giving the Ar-COOH film. The electrode was sonicated in DMF for 5 min, rinsed with acetone then sonicated in water for 5 min and dried with N_2 (g).

Removal of TIPS protecting group from Ar-Eth-TIPS film

The TIPS protecting group was removed from the Ar-Eth-TIPS film by immersing the modified electrode in a stirred solution of 0.05 M tetra-n-butylammonium fluoride (TBAF) in tetrahydrofuran (THF) for 40 min, giving the Ar-Eth film. The electrode was sonicated in THF for 5 min, rinsed with acetone then sonicated in water for 5 min and dried with N_2 (g).

2.2.2.2. Attachment of Polymerisation Initiators to Aryl Films

Attachment of ethanolamine to the Ar-COOH film

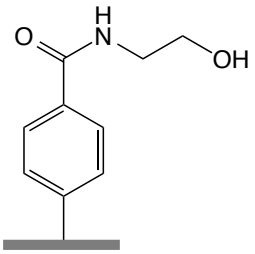

A GC plate modified with the Ar-COOH film was immersed in 5 mL of PBS (pH 5.2) solution containing 1-ethyl-3-(3-dimethylaminopropyl) carbodiimide (EDC) (0.27 g, 5 mmol), *N*-hydroxysuccinimide (NHS) (0.41 g, 3 mmol) and ethanolamine (53 μL, 0.87 mmol). The reaction was stirred for 2 h at room temperature. The film was sonicated in water for 5 min, rinsed with DCM then acetone and dried with N_2 (g). This film was used directly in the next step without further purification

Attachment of ABiB to the Ar-CONH-OH film

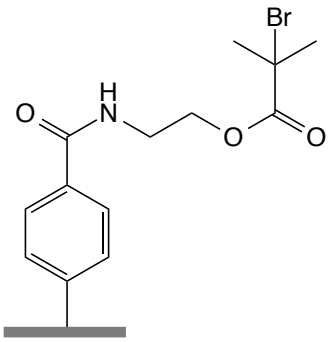

The GC electrode modified with the film prepared above, or the resultant film from the spontaneous attachment of ethanolamine to bare GC, was added to a solution of triethylamine (23 μL, 0.01 mmol), 4-(dimethylamino) pyridine (0.01g, 0.08 mmol), and 10 mL DCM. The vial was sealed and kept at 0 °C for 10 min. With stirring, ABiB (17 μL, 0.14 mmol) was slowly added by a syringe. The reaction was stirred for 12 h at room temperature. The modified substrate was sonicated for 5 min in DCM, rinsed with acetone then sonicated again in water and dried with N_2 (g).

Attachment of APBiB to the Ar-Eth film

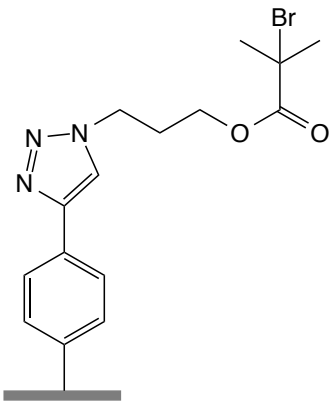

APBiB was coupled to the Ar-Eth layer by a CuAAC reaction.[51] The electrode modified with the Ar-Eth film was immersed in a stirred solution of APBiB (0.25 g, 1 mmol) in 5 mL THF, and 2.5 mL of an aqueous 0.01 M $CuSO_4$ solution was added. After 15 min, 2.5 mL of a solution containing L-Ascorbic acid (0.01 M) and 15 mg of $NaHCO_3$ was added dropwise. The mixture was stirred for 3 hr. A N_2 atmosphere was maintained throughout the reaction. The resulting modified electrode was rinsed with EDTA-Na_2 (0.01 M) for 10 min, sonicated in THF for 5 min, rinsed with acetone, sonicated in water for 5 min, and then dried with N_2 (g).

2.2.2.3. Click Reaction of $FcMeN_3$ with modified electrodes

Attachment of APBiB to the Ar-Eth film

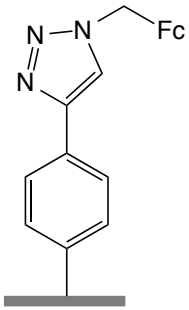

Three methods were explored for the coupling of $FcMeN_3$ to Ar-Eth modified electrodes.

Method 1.[50b]

The electrode modified with the Ar-Eth film was immersed in a stirred 5 mL solution of $FcMeN_3$ (1 mg, 4 μmol) in THF and 2.5 mL of an aqueous 0.01 M $CuSO_4$ solution. After 15 min, 2.5 mL of a solution containing L-ascorbic acid (0.01 M) and 15 mg of $NaHCO_3$ was added dropwise. The mixture was stirred for 3 h. A N_2 (g) atmosphere was maintained throughout the reaction. The modified electrode was sonicated in THF for 5 min, rinsed with acetone, sonicated in water for 5 min, and then dried with N_2 (g). $\Gamma_{Fc} = 2.8 \pm 0.3 \times 10^{-10}$ mol cm^{-2} (62% of maximum coverage).

Method 2.[120]

The electrode modified with the Ar-Eth film was immersed in a stirred 3 mL *tert*-butanol/water (1:2) solution containing $FcMeN_3$ (1 mg, 4 μmol), $CuSO_4$ (5 mg, 0.02 mmol), sodium ascorbate (7.9 mg, 0.04 mmol) and benzoic acid (24.4 mg, 0.2 mmol). The mixture was stirred for 1 h. The modified electrode was sonicated in DCM for 5 min, rinsed with acetone, sonicated in water for 5 min, and then dried with N_2 (g). $\Gamma_{Fc} = 1.8 \pm 0.3 \times 10^{-10}$ mol cm^{-2} (40% of maximum coverage).

Method 3.[121]

The electrode modified with the Ar-Eth film placed in an electrochemical cell holding a 10 mL ACN solution containing $TBABF_4$ (0.329 g, 0.1 M), CuBr (7.17 mg, 0.05 mmol), *N,N,N',N',N''*-pentamethyldiethylenetriamine (PMDTA) (20 μL, 1 mmol) and $FcMeN_3$ (1 mg, 4 μmol). A Pt mesh auxiliary electrode and CE (1 M LiCl) reference electrode were used. A fixed potential of -0.55 V vs CE (1 M LiCl) was applied to the electrode for 1 h. The modified electrode was sonicated in ACN for 5 min, rinsed with acetone, sonicated in water for 5 min, and then dried with N_2 (g). $\Gamma_{Fc} = 5.3 \pm 0.2 \times 10^{-11}$ mol cm^{-2} (12% of maximum coverage).

Method 3a.

A second electrode modified with an Ar-Eth film utilised the same reaction conditions as Method 3, but with no potential applied to the working electrode. $\Gamma_{Fc} = 7.0 \pm 0.2 \times 10^{-11}$ mol cm^{-2} (16% of maximum coverage).

2.2.2.4. Oxalyl Chloride Activation

Acid chloride coupling reactions were carried out based on a literature method.[122] Ferrocene monocarboxylic acid (FcCOOH) and α-Bromoisobutyric acid (ABiA) were the carboxylic acid derivatives used.

Activation of carboxylic acid derivatives and reactions with GC or ethanolamine-modified GC

The carboxylic acid derivative (10 mg) was placed in a sealed reaction vessel under a N_2 atmosphere. Anhydrous DCM (6 mL) was introduced followed by $(COCl)_2$ (25 μL, 0.3 mmol) and pyridine (8 μL, 0.1 mmol). After refluxing for 1 h, all volatile compounds were removed under vacuum. Freshly polished or modified GC electrodes were inserted into the reaction vessel followed by the addition of anhydrous DCM (6 mL) (to re-dissolve the activated compound) and triethylamine (50 μL, 0.36 mmol). The reaction was stirred in an ice-bath for 5 min and then at room temperature for 16 h. The modified electrode was sonicated in DCM for 5 min, rinsed with acetone, sonicated in water for 5 min, and then dried with N_2 (g).

Activation of GC and reaction with carboxylic acid derivatives

A freshly polished GC electrode was placed in a sealed reaction vessel under a N_2 atmosphere. Anhydrous DCM (6 mL) was introduced followed by $(COCl)_2$ (25 μL, 0.3 mmol) and pyridine (8 μL, 0.1 mmol). After refluxing for 1 h, all volatile compounds were removed under vacuum. The carboxylic acid derivative (10 mg) was dissolved in anhydrous DCM (6 mL) and introduced into the reaction vessel, along with triethylamine (50 μL, 0.36 mmol). The reaction was stirred in an ice-bath for 5 min and then at room temperature for 16 h. The

modified electrode was sonicated in DCM for 5 min, rinsed with acetone, sonicated in water for 5 min, and then dried with N_2 (g).

2.2.2.5. Spontaneous amine-surface reaction for coupling reactions

The Michael-like addition of ethanolamine to GC followed a modified literature procedure.[14] A freshly polished GC electrode was immersed in a stirred solution of ethanolamine (600 μL, 10 mmol) and ACN (10 mL). The reaction mixture was stirred for 17 h at room temperature. The modified electrode was sonicated in ACN for 5 min, rinsed with acetone, sonicated in water for 5 min, and then dried with N_2 (g). The modified electrode was used for the esterification reaction with ABiB as described in section 2.3.2.2, or for the FcCOOH coupling reaction described in section 2.3.2.4.

2.3. Surface Initiated Polymerisation Reactions

All the polymerisation reactions used in this work are examples of surface initiated atom transfer radical polymerisation (SI-ATRP).

PMPDSAH polymer brush growth by SI-ATRP

Polymer brushes of poly(3-(methacryloylamino)propyl)-*N,N*'-dimethyl(3-sulfopropyl)-ammonium hydroxide) (PMPDSAH) were grown according to a literature procedure.[81] A 20 mL water/DMF (4:6) solution containing (3-(methacryloylamino)propyl)dimethyl(3-sulfopropyl) ammonium hydroxide inner salt (MPDSAH) (2 g, 6.8 mmol), 2,2'-bipyridyl (0.16g, 1 mmol), CuBr (7.17 mg, 0.05 mmol) and $CuBr_2$ (1 mg, 4.5 μmol) was degassed by three freeze-pump-thaw cycles and transferred by syringe to a separate vessel containing the electrode modified with a polymerisation initiator. The tube was sealed in an N_2 atmosphere and the reaction mixture was slowly stirred at room temperature overnight. The modified

electrode was sonicated in DCM for 5 min, rinsed with acetone, sonicated in water for 5 min, and then dried with N_2 (g).

PMMA polymer brush growth by SI-ATRP

Polymer brushes of poly(methyl methacrylate) (PMMA) were grown according to a literature procedure.[99] A solution of 8 mL methyl methacrylate (MMA), 8 mL ACN, PMDTA (20 μL, 1 mmol), CuBr (7.17 mg, 0.05 mmol) and $CuBr_2$ (1 mg, 4.5 μmol) was degassed through three freeze-pump-thaw cycles. The solution was heated to 50 °C to solubilise the copper catalyst. An electrode modified with a polymerisation initiator was immersed into the solution and stirred for 17 h while under a N_2 atmosphere. The modified electrode was sonicated in ACN for 5 min, rinsed with acetone, sonicated in water for 5 min, and then dried with N_2 (g).

PMMA polymer brush growth by Electrochemically Induced SI-ATRP

Electrochemically induced SI-ATRP (eSI-ATRP) reactions were done in a pear-shaped electrochemical cell for GC disk electrodes, and a pear-shaped electrochemical cell with a hole in the bottom for GC plate and PPF electrodes. An electrode modified with a polymerisation initiator was placed in the electrochemical cell with a Pt mesh auxiliary electrode and a CE (1 M LiCl) reference electrode. A solution of MMA (8 mL, 75 mmol), ACN (8 mL), 0.1 M $TBABF_4$, CuBr (7.17 mg, 0.05 mmol) and *N*,*N*,*N*′,*N*′,*N*′′-pentamethyldiethylenetriamine (10.4 μL, 5 mmol) was added to the cell and degassed with N_2 for 30 min. A potential of -0.55 V was applied throughout the experiment. The modified electrode was sonicated in ACN for 5 min, rinsed with acetone, sonicated in water for 5 min, and then dried with N_2 (g).

PMMA polymer brush growth by One-pot CuAAC/eATRP

The one-pot CuAAC/eATRP reaction on an electrode modified with an Ar-Eth film followed the method for e-SI-ATRP as above, with the inclusion of APBiB (0.25 g, 1 mmol) in the reaction mixture. After polymerisation, the modified electrode was sonicated in ACN for 5 min, rinsed with acetone, sonicated in water for 5 min, and then dried with N_2 (g).

2.4. Electrochemical Methods

2.4.1. Electrodes

Glassy carbon (GC)

GC disk electrodes are 3 mm diameter disks of GC, imbedded in a Teflon tube with one end flush with the tube, the other in contact with a brass rod. GC plate electrodes were cut from a GC slab to 15 mm × 15 mm squares. GC disk or plate electrodes were cleaned before any electrochemistry or modification was carried out. The electrodes were hand polished successively with 1.0 and 0.05 μm alumina slurry made from dry alumina powder and water on a piece of micro-fabric cloth. The electrode was then ultrasonicated (Elmasonic S 30 H sonicator) in water for 10 min (in two sets of 5 min, changing the water between sets) to remove any alumina from the surface. This method was then repeated with 0.05 μm alumina. The electrode was dried under a stream of N_2 (g). This procedure was repeated after each set of experiments.

Pyrolysed Photoresist Film (PPF)

Pyrolysed photoresist film (PPF) chip electrodes were prepared by following a literature procedure.[7] A 15 mm × 15 mm Si (100) wafer substrate was twice spin-coated with photoresist (AZ7908 MIF (Clariant)) and then heated in a tube furnace under a forming gas

atmosphere. The temperature was increased to 1100 °C at 5 °C/min and maintained at 1100 °C for 1 h. After cooling to room temperature, the PPF samples were removed from the furnace and stored under vacuum. Prior to use, they were briefly sonicated (3 s) in successive baths of acetone, methanol, and isopropyl alcohol and were dried with N_2 (g). This process removed small loosely bound surface debris features.

2.4.2. Cell Setup

Electrochemical cells were washed in a 10% HNO_3 acid bath after each set of experiments. The cells were rinsed with MQ water prior to use. A conventional three-electrode cell was used for experiments comprising of a GC electrode as the working electrode, an auxiliary electrode and reference electrode (see 2.2.3). A pear shaped glass electrochemical cell was used for electrochemical experiments with GC disk electrodes. GC disk electrodes have a working area of 0.071 cm^2. For electrochemical experiments using GC plate and PPF electrodes, a pear shaped glass electrochemical cell with a hole in the base was used. The electrode was positioned between the metal base holder and the glass cell. Two Kalrez O-rings were placed between the GC surface and the glass cell to provide a seal to avoid leakage of solution and defined the working area. A strip of copper was placed between the GC plate and a rubber strip on the metal base holder to maintain electrical contact, and the setup was then secured by four metal springs attached to the four corners of the cell. The auxiliary electrode, reference electrode and gas inlet were introduced from the top of the cell.

2.4.3. Reference Electrodes

A saturated calomel reference electrode (SCE) was used for all aqueous solutions and a calomel electrode (CE) with 1 M LiCl was used for non-aqueous solutions.

2.5. Methods and Instruments

Atomic Force Microscopy

Atomic force microscopy (AFM) measurements were performed using a Nanoscope® DimensionTM 3100 microscope (Digital Instruments) integrated with a Nanoscope® IIIa scanning probe microscope controller (Digital Instruments, Veeco). All measurements were performed in ambient conditions in noncontact tapping mode. Budget Sensors Tap300Al-G series cantilevers were used for topographical imaging. Images were analysed using the Nanoscope Analysis Version 1.50 software. Average film roughness (R_q) was calculated using a tool in the software.

Atomic Force Microscopy Depth Profiling Technique

Film thickness measurements by depth profiling were performed on modified PPF surfaces. The general method involved using an AFM tip to mechanically remove a section of film from the modified PPF surface, followed by measuring the depth of the trench created by scanning across the scratch with an AFM tip. The method of scratching away a section of film utilized a chip configuration that has three silicon cantilever tips (MikroMasch CSC37/AIBS) of different lengths. Two of the three tips, the longest and the shortest, were utilised. The laser on the AFM was focused on the shortest tip, in resonance. As the shortest tip approaches the surface to begin a tapping mode scan, the longer tip embeds into the surface film and effectively scratches the film from the PPF surface. The size of the scratch is 10 μm × 2.5 μm. After scratching, the tip was withdrawn from the PPF surface and replaced with a new cantilever (Budget Sensors Tap300Al-G) and rescanned orthogonal to the scratch direction in tapping mode. The depth of the scratch was determined from the AFM images using Nanoscope Analysis Version 1.50 software. An analysis “box” was positioned over the AFM

images using the step height calculation tool to give an average line profile. The box size was selected to include the maximum amount of the scratch area while avoiding the inclusion of large amount of scratching debris or defects. For each surface, 3 scratches were made and at least 8 transverse cross sections were made on each scratch. The reported thickness for each film is the mean of at least 24 values, and the uncertainty is the standard deviation of the mean.

Contact Angle Measurements

Contact angle measurements were made by delivering a 2 μL drop of solution from a microsyringe onto the surface of the sample mounted on an illuminated horizontal stage. The image of the static droplet was captured by an Edmund Scientific video camera using Matrox Intellicam DCF2 8.0 Build 1230 software. Images were analysed using ImageJ Version 1.47 software with the Low Bond Axisymmetric Drop Shape Analysis plug-in. The contact angle was measured for 8 drops on each sample, and the mean contact angle was calculated. The uncertainty is the standard deviation of the mean.

Electrochemistry

Electrochemical measurements were preformed using an Ecochemie Autolab PGSTAT302 potentiostat/galvanostat interfaced to a PC computer system and controlled by Autolab General Purpose Electrochemical System (GPES) Version 4.9 software.

Electrochemical Characterisation of Modified Electrodes

The properties of modified GC surfaces were investigated using redox probe voltammetry. Cyclic voltammograms (CVs) were recorded using a ferricyanide redox probe solution prepared using 1 mM $K_3Fe(CN)_6$ in a PBS solution (pH 7), or 0.1 M HCl (pH 1) at a scan rate

of 100 mV s^{-1}. CV of immobilised ferrocene groups were obtained in a solution of 0.1 M $LiClO_4$ in ethanol at a scan rate of 200 mV s^{-1}.

Estimation of Molecular Dimensions (Avogadro)

Avogadro 1.1.1 freeware[123] was used to calculate the dimension of molecules. The molecular structures were drawn in the lowest energy conformation and the dimensions were measured using the tools in the software.

Integration of Voltammetric Peak Area (Linkfit)

Voltammetric peak areas were determined by correcting the baseline using a third order polynomial and integrating the area under the peak using Linkfit 4.1 software (John S. Loring, Copyright 1996-200).[124] Lorentzian, Gaussian, or a mixture of Lorentzian-Gaussian peaks was fitted to the voltammetric peak via the Levenberg-Marquardt algorithm. Surface concentration, (Γ, mol cm^{-2}), of the electroactive species was calculated using equation 2.2, where Q is the charge obtained from the voltammetric peak area (V × A), divided by the scan rate (ν, V s^{-1}) (equation 2.3.), n is the number or electrons involved in the redox process, F is Faraday's constant (96485 C mol^{-1}) and A is the geometric area of the electrode (cm^2).

$$\Gamma = \frac{Q}{nFA} \qquad (2.2)$$

$$Q = \frac{peak\ area}{v} \qquad (2.3)$$

When more than one sample was analysed, the reported surface coverage is the average based on the number of samples, n, indicated in the text. When two surface coverages were averaged, the uncertainties indicate the range of values. When three or more surface coverages were averaged, the reported uncertainties are standard deviations of the average.

Mass Spectroscopy

Mass spectra were recorded by Dr Marie Squire on a Bruker MaXis 4G spectrometer, operated in high resolution positive ion electrospray mode. Samples were dissolved and diluted to the required concentration in HPLC grade ACN or methanol.

Nuclear Magnetic Resonance Spectroscopy (NMR)

^{1}H NMR studies were performed on an Agilent 400-MR NMR Spectrometer operating at 400 MHz. All samples were dissolved in commercially available deuterated solvents. Spectra were referenced to $CDCl_3$: 7.26 ppm, CD_3CN: 2.0 ppm or DMSO-d_6: 2.6 ppm. Spectra were analysed using the ACD/NMR Processor Academic Edition Version 12.01 software.

X-Ray Photoelectron Spectroscopy (XPS)

X-ray photoelectron spectroscopy (XPS) spectra were recorded by Dr Colin Doyle, Department of Chemical and Materials Engineering, The University of Auckland. XPS data were obtained on GC plates using a Kratos Axis Ultra DLD spectrometer with a monochromatic Al Kα source (1486.7 eV). Data were analysed using Casa XPS Version 2.3.15 software.

Chapter 3. Preparation and Characterisation of Aryl Diazonium Derived Monolayer Films for the Attachment of Polymerisation Initiators

3.1. Introduction

As described in Chapter 1, electrochemical modification of carbon surfaces using an aryl diazonium salt produces an aryl radical that reacts with the surface, resulting in the formation of a bond between the surface and the modifier.[125] The electrochemical reduction of diazonium salts usually produces a disorganised multilayer. Monolayers are sought after to preserve the underlying topography and for producing a well-organised layer for further surface chemistry. By limiting film thickness, micro- and nano-scale surface features can be retained in the final film.

In this chapter, the modification of glassy carbon (GC) electrodes by three aryl diazonium ions is investigated: N_2^+-Ar-NO_2, N_2^+-Ar-COO-Fm and N_2^+-Ar-Eth-TIPS. The grafting of nitrobenzene diazonium ions and the resulting nitrophenyl films have been thoroughly investigated.[10, 23,18,126] This diazonium ion is initially studied here to establish techniques and provide familiarity with the general methodology. The main focus of this chapter is on the films derived from the two protected aryl diazonium salts. As described in Chapter 1, the formation of a multilayer is followed by the selective cleavage of protecting groups giving a well-defined monolayer.[50b,39,50a,35,38] The electrochemical grafting of N_2^+-Ar-COO-Fm followed by the selective cleavage of the Fm protecting group revealing a reactive Ar-COOH monolayer has been demonstrated by Lee *et al*.[35] Similarly, Ar-Eth monolayers have been

produced by the electrochemical grafting of N_2^+-Ar-Eth-TIPS, followed by the removal of the TIPS protecting group by Leroux and co-workers.[50b]

In the present work, these monolayers have been characterised by redox probe voltammetry, contact angle measurements and X-ray photoelectron spectroscopy and have been used in chemical reactions, both with model compounds and for the attachment of the polymerisation initiators, ABiB and APBiB.

3.2. Experimental

3.2.1 Preparation of Aryl Diazonium Salts

The p-nitrophenyl diazonium tetrafluoroborate ($BF_4^-N_2^+$-Ar-NO_2) and 4-((9-H-Fluoren-9-ylmethoxy)carbonyl)-benzene-1-diazonium tetrafluoroborate ($BF_4^-N_2^+$-Ar-COO-Fm) were synthesised according to literature procedures,[35,43] as described in Chapter 2. $BF_4^-N_2^+$-Ar-Eth-TIPS was prepared by Lita Lee, Department of Chemistry, University of Canterbury, according to a modified literature procedure.[113]

3.2.2. Electrochemistry

Electrochemical grafting of aryl diazonium salts

Electrochemical grafting experiments were conducted according to the procedures described in Chapter 2.3.1. GC and pyrolysed photoresist film (PPF) electrodes were modified by the electrochemical grafting of aryl diazonium salts following the experimental details given in Chapter 2.3.1. GC disk electrodes (surface area = 0.071 cm^2) were used for surfaces prepared for electrochemical studies. GC plate electrodes (surface area = 0.709 cm^2) were used for surfaces prepared for contact angle studies, while PPF electrodes (surface area = 0.709 cm^2) were used when AFM imaging was required.

Electrochemical analysis of Fc coupled electrodes

CVs of immobilised Fc groups were obtained in a solution of 0.1 M $LiClO_4$ in ethanol at a scan rate of 200 mV s^{-1}. The modified GC electrode was used as the working electrode. A Pt mesh auxiliary electrode and a calomel reference electrode (1 M LiCl) were used for all immobilised Fc electrochemistry experiments. Surface concentrations of immobilised Fc (Γ_{Fc}) were calculated from these CVs (details in Chapter 2.5).

Electrochemical analysis of modified surfaces by redox probe voltammetry

All redox probe voltammetry experiments were conducted in a pear-shaped electrochemistry cell using a PBS (pH 7) solution containing 1 mM $K_3Fe(CN)_6$ with a Pt mesh auxiliary electrode and a SCE reference electrode unless specified.

3.2.3. Chemical Reactions on Modified Surfaces

The details of grafting, deprotection and coupling reactions are given in Chapter 2.

3.2.4. Atomic Force Microscopy and Depth Profiling Measurements

Atomic force microscopy (AFM) imaging and depth profiling measurement details are given in Chapter 2.5.

3.3. Results and Discussion

3.3.1. Nitrophenyl Film

As an introduction to surface modification of carbon electrodes by the electrochemical grafting of aryl diazonium salts, GC disk electrodes were modified by grafting nitrophenyl films. Scheme 3.1 (also Scheme 1.5, but repeated for convenience) shows the proposed build up of a disorganised nitrophenyl multilayer through attack of aryl radicals on the grafted layer.

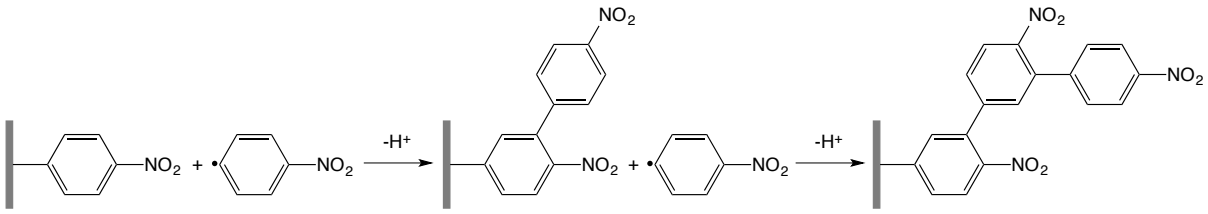

Scheme 3.1. Proposed grafting scheme for the formation of a nitrophenyl multilayer. Reproduced from reference 23.[23]

3.3.1.1. Electrochemical Grafting of Nitrophenyl Film on GC

Nitrobenzene diazonium salt (NBD) was electrochemically grafted to GC disk electrodes by recording cyclic voltammetry scans in the presence of 1 mM NBD salt and 0.1 M $TBABF_4$ in acetonitrile (ACN). Three cyclic voltammetry scans between 0.6 V and -0.2 V were used for the grafting procedure (Scan 1, Figure 3.1). The irreversible reduction peaks at $E_{p,c} \approx 0.27$ and -0.16 V (vs CE 1 M LiCl) are assigned to the reduction of the diazonium group. Two peaks are frequently observed for the reduction of aryl diazonium ions but their origin remains unexplained.[36] The disappearance of the reduction peaks in subsequent scans is consistent with the formation of a film on the electrode surface, which restricts further electrochemical reduction of nitrobenzene diazonium ions by inhibiting electron transfer from the electrode surface to the nitrobenzene diazonium ions in solution.

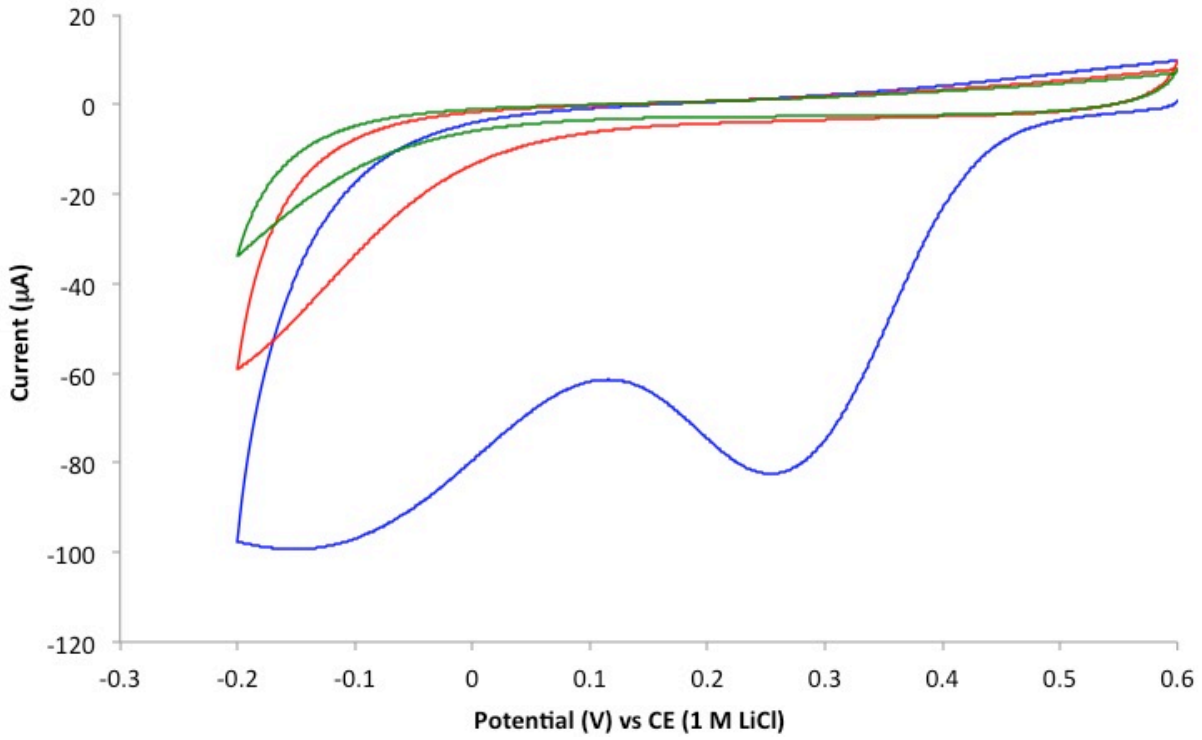

Figure 3.1. Three consecutive scans at a bare GC disk electrode in a solution of 1 mM N_2^+-Ar-NO_2 in 0.1 M $TBABF_4$-ACN. Scan rate = 50 m Vs^{-1}. The blue line represents the 1st scan, red the 2nd scan and green the 3rd scan.

3.3.1.2. Characterisation of Nitrophenyl Film

The GC electrode surface electrochemically modified by the reduction of NBD was characterised by its blocking properties and through its electrochemical reduction.

3.3.1.2.1. Effect of Nitrophenyl Modification on Redox Probe Voltammetry

Redox probe voltammetry can be used to confirm the presence of a blocking film on the electrode surface.[127] The presence of an insulating film will increase the distance for electron transfer and will therefore decrease the rate of electron transfer between the electrode and the redox probe species. This will give rise to an increase in the CV peak-to-peak separation (ΔE_p) and a decrease in the peak current.[128] As a film becomes more blocking of the electron transfer, the ΔE_p increases until no peaks are observed. Hence, thicker films will give larger

ΔE_p values for CVs compared to thin films. Figure 3.2 shows CVs obtained of potassium ferricyanide ($K_3Fe(CN)_6$) in a phosphate buffer solution (PBS) (pH 7). The CV recorded at the surface of bare GC (blue line) shows the quasi-reversible $Fe(CN)_6^{3-/4-}$ redox couple with a peak separation ΔE_p = 110 mV. After modification, the $Fe(CN)_6^{3-/4-}$ redox peaks are widely separated (~ 700 mV) as electron transfer from the electrode surface to the redox couple is inhibited. The changes in the CVs are clearly consistent with the presence of an insulating film on the modified electrode.

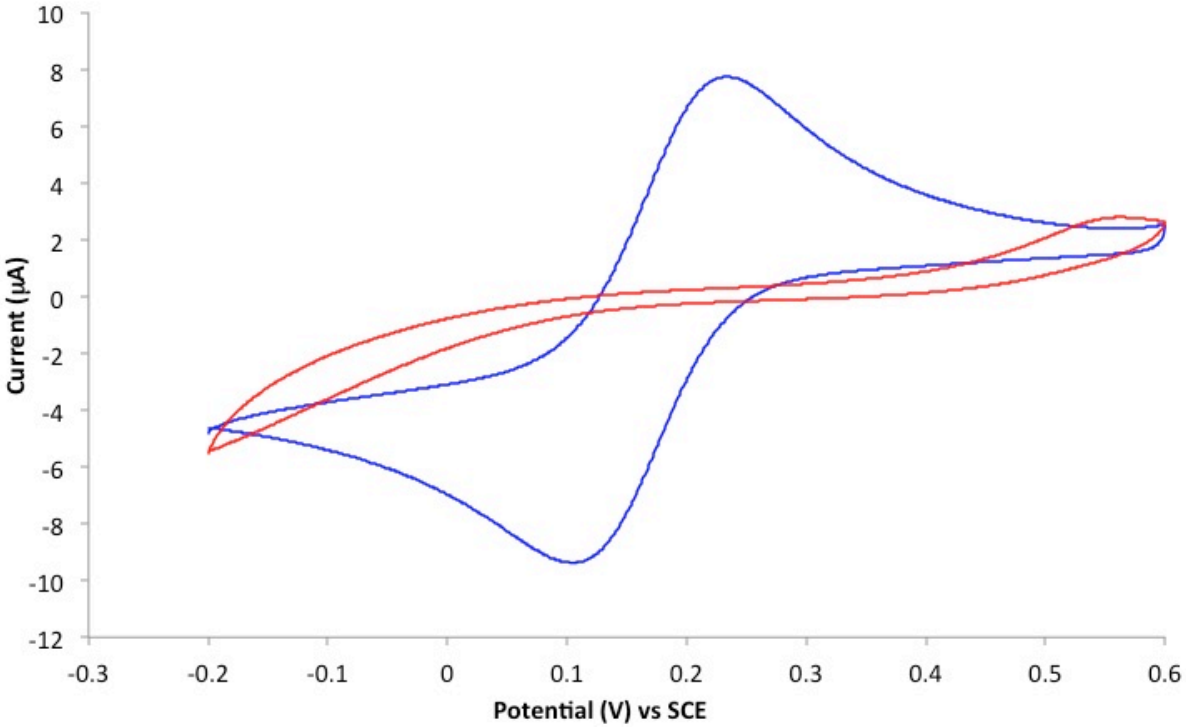

Figure 3.2. CVs of 1 mM $K_3Fe(CN)_6$ in PBS (pH 7) showing the blocking effect of nitrophenyl film grafting of GC. Scan rate = 100 mV s^{-1}. The blue line is a scan taken before grafting and the red line is a scan taken after grafting of the film.

3.3.1.2.2. Electrochemistry of Nitrophenyl Modified GC

Surface grafted nitrophenyl (Ar-NO_2) groups are electroactive in aqueous and non-aqueous electrolytes. Therefore, the film formation can be monitored using voltammetry of the modified surface. In aqueous acid, the nitrophenyl group is irreversibly reduced in a multi-

electron and multi-proton reduction to the amine or hydroxyaminophenyl group (Figure 3.3). The large, irreversible reduction peak at E_{pc} = -0.74 V (vs SCE) is assigned to the reduction of Ar-NO_2 groups according to the reactions in Equations 1 and 2.

$$(1)\ \mathrm{Ar-NO_2 + 4H^+ + 4e^- \rightarrow Ar-NHOH + H_2O}$$

$$(2)\ \mathrm{Ar-NHOH + 2H^+ + 2e^- \rightarrow Ar-NH_2 + H_2O}$$

$$(3)\ \mathrm{Ar-NHOH \rightarrow Ar-NO + 2H^+ + 2e^-}$$

The disappearance of the reduction peak on the second scan indicates that nearly all the electroactive Ar-NO_2 groups are reduced in the first scan. The reversible couple that appears in the second scan at $E_{1/2}$ = 0.26 V after the Ar-NO_2 reduction is assigned as the reversible Ar-NHOH / Ar-NO couple shown in Equation 3. The origin of the small couple at more positive potentials is unknown, but is frequently observed.[126]

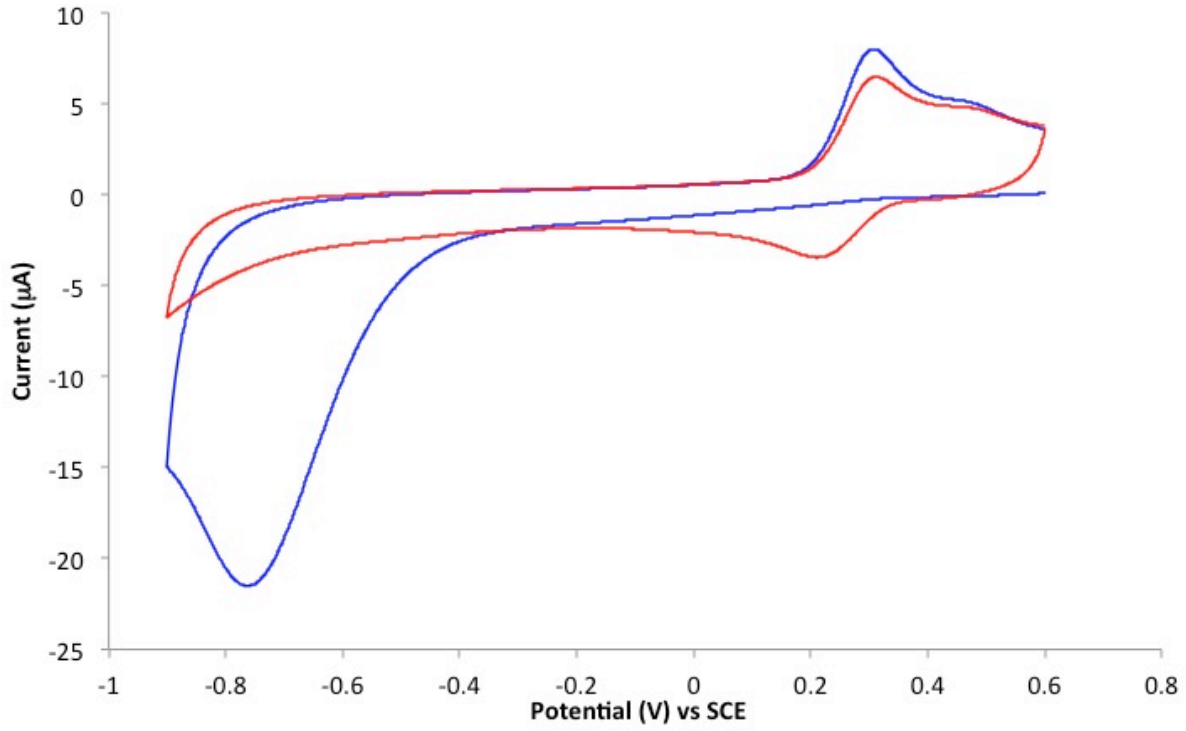

Figure 3.3. CVs recorded in aqueous 0.1 M H_2SO_4 of a nitrophenyl film. Scan rate = 100 mV s^{-1}. The blue line represents the first scan and the red line the second scan.

3.3.2. Carboxyphenyl Film

GC electrodes have been modified with carboxyphenyl (Ar-COOH) monolayers by the electrochemical grafting of N_2^+-Ar-COO-Fm.[35] After grafting, the Fm protecting group can be selectively cleaved from the surface by treating the surface with a 20% solution of piperidine in DMF (Scheme 3.2), repeated from Scheme 1.10 for convenience, yielding an Ar-COOH monolayer. This treatment effectively removes the protecting group and any additional groups that have attached to the Fm moiety during grafting.

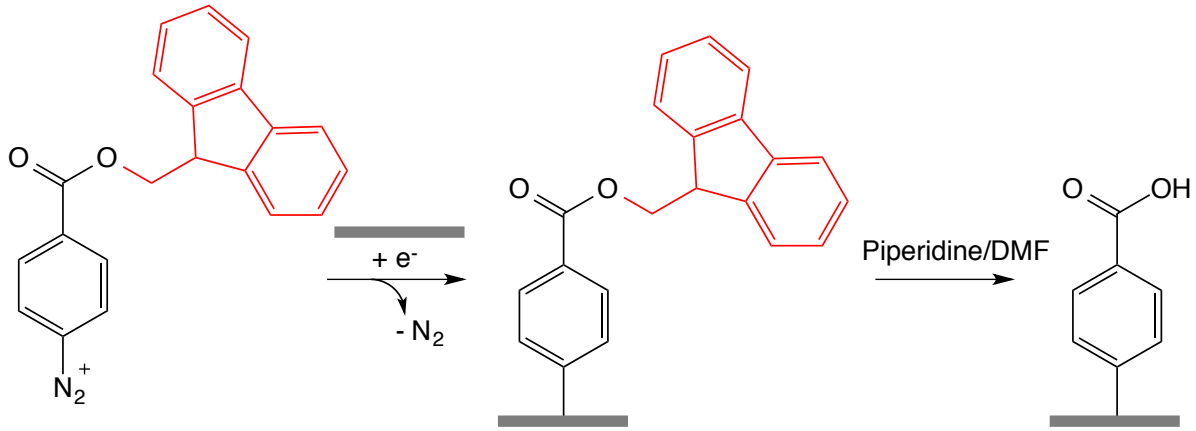

Scheme 3.2. Electrochemical grafting of N_2^+-Ar-COO-Fm to a carbon electrode followed by the deprotection of the Fm protecting group.

In this work, the grafted and deprotected layers were characterised through redox probe voltammetry and water contact angles. Additionally, X-ray photoelectron spectroscopy (XPS) was used to analyse the Ar-COOH monolayer.

The Ar-COOH layer was reacted in a two-step procedure to attach the ATRP initiator, ABiB (Scheme 3.3). Firstly, the film underwent an amide coupling reaction with ethanolamine to introduce a terminal alcohol functional group. Secondly, ABiB was coupled to the film through the newly introduced alcohol functionality *via* an esterification reaction. This layer

was prepared for use in surface initiated atom transfer radical polymerisation in Chapter 5. These films were characterised using redox probe voltammetry and XPS analysis.

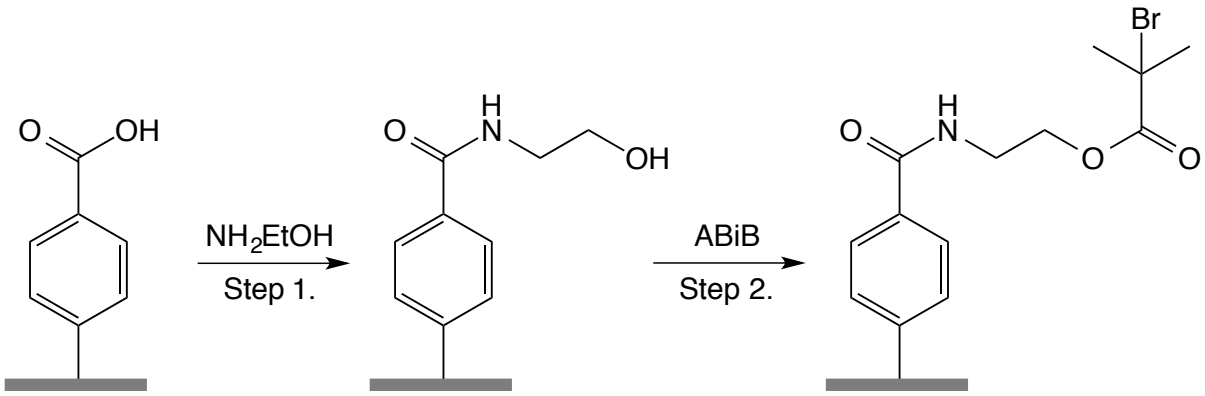

Scheme 3.3. Two step immobilisation of ABiB groups to the Ar-COOH monolayer.

3.3.2.1. Electrochemical Grafting of Ar-COO-Fm Film on GC Electrode

N_2^+-Ar-COO-Fm was electrochemically grafted to GC electrodes by recording cyclic voltammetry scans in the presence of 1 mM N_2^+-Ar-COO-Fm and 0.1 M $TBABF_4$ in ACN. Figure 3.4 shows the 5 cyclic voltammetry scans between 0.8 V and -0.75 V at a scan rate of 50 m Vs^{-1} that were used for the grafting procedure. The blue line shows the irreversible reduction peaks ($E_{p,c} \approx 0$ and 0.3 V vs CE (1 M LiCl)) of the aryl diazonium ions. The disappearance of the reduction peaks on subsequent scans (2-5) is consistent with the formation of a grafted layer. The grafted layer hinders further electrochemical reduction of the aryl diazonium ions by inhibiting electron transfer from the electrode surface to the aryl diazonium ions in solution.

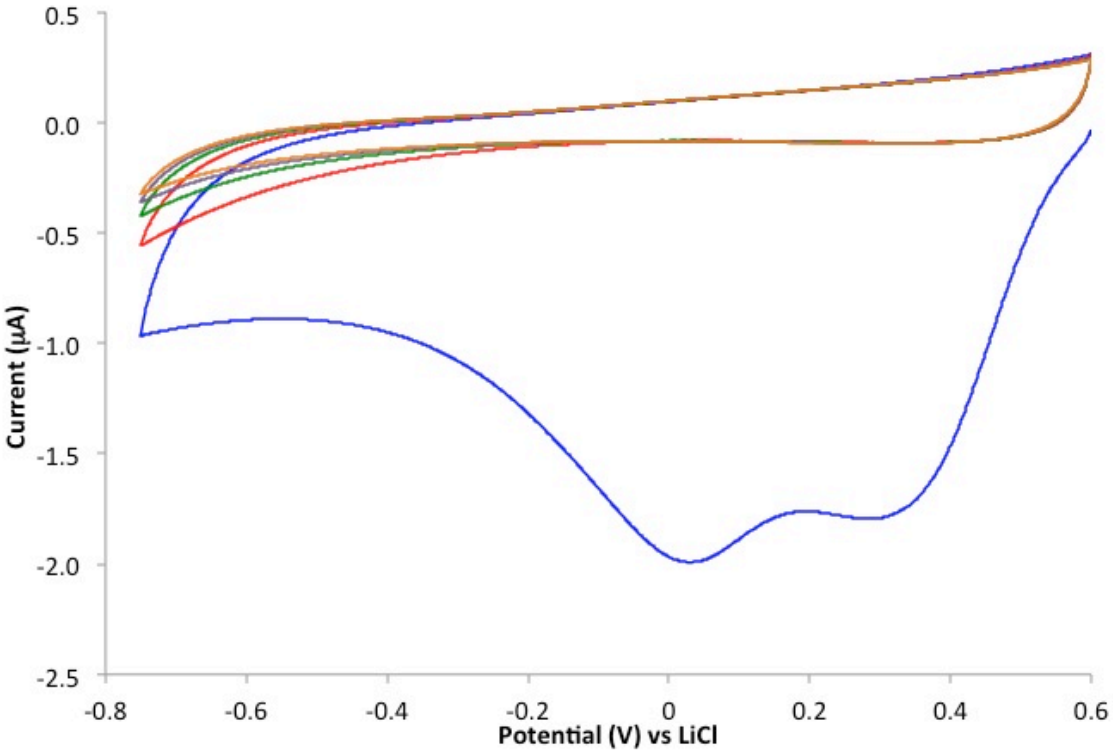

Figure 3.4. Five consecutive scans at a bare GC disk electrode in a solution of 1 mM N_2^+-Ar-COO-Fm in 0.1 M $TBABF_4$-ACN. Scan rate = 50 mVs^{-1}. The blue line represents the 1st scan, red the 2nd scan, green the 3rd scan, purple the 4th scan and orange the 5th scan.

3.3.2.2. Characterisation of Modified Layers

3.3.2.2.1. Effect of Modification on Redox Probe Voltammetry

The presence of the Ar-COO-Fm film on the GC electrode surface was studied using redox probe voltammetry. A solution $K_3Fe(CN)_6$ in PBS (pH 7) was used as the redox probe. Scanning of the redox probe at bare GC (blue line, Figure 3.5) gave a peak separation, ΔE_p, of 70 mV. The scan of the redox probe at the modified surface shows no observable peaks (red line, Figure 3.5). This indicates that the film is sufficiently thick to inhibit electron transfer between the electrode surface and the redox species in solution.

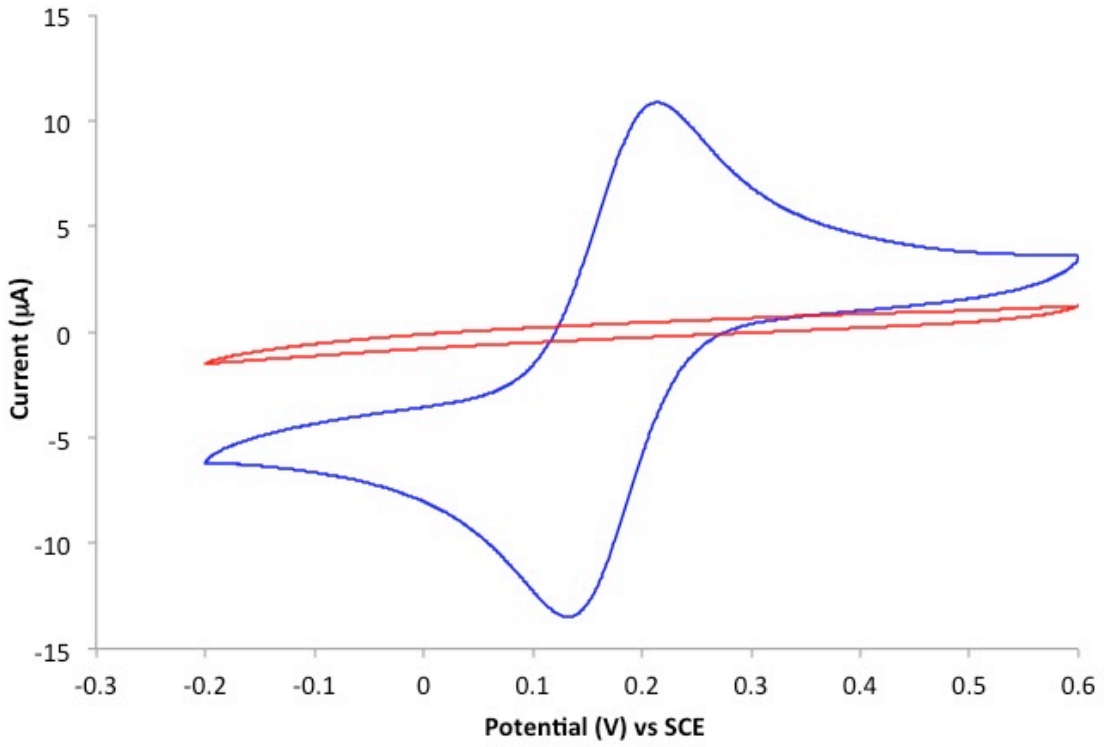

Figure 3.5. CVs showing the blocking effect of the Ar-COO-Fm film at GC in a solution of 1 mM $K_3Fe(CN)_6$ in PBS pH 7. Scan rate = 100 mV s^{-1}. The blue line is a scan taken before grafting and the red line is a scan taken after grafting of a film.

The electrochemically grafted Ar-COO-Fm film can be selectively cleaved to yield a carboxylic acid terminated monolayer.[35,129] The Fm protecting group was removed by immersing the surface in a solution of 20% piperidine in DMF for 40 min. The removal of the protecting group from the film was investigated again through redox probe voltammetry. After deprotection, a partial restoration of the redox probe voltammetry was observed (green line, Figure 3.6). This is similar behavior to previously reported.[35]

After deprotection, the Ar-COOH film is expected to have a negative surface charge in pH 7 medium. The pKa of Ar-COOH multilayer is within the range of 2.8-3.3,[130] therefore the Ar-COOH film is deprotonated (negatively charged) at pH 7. This will lead to electrostatic repulsion with the anionic redox probe. Hence even though the deprotected film is only a

monolayer with a reported thickness of 0.4 ± 0.3 nm,[35] the $Fe(CN)_6^{3-}$ electrochemistry is significantly retarded.

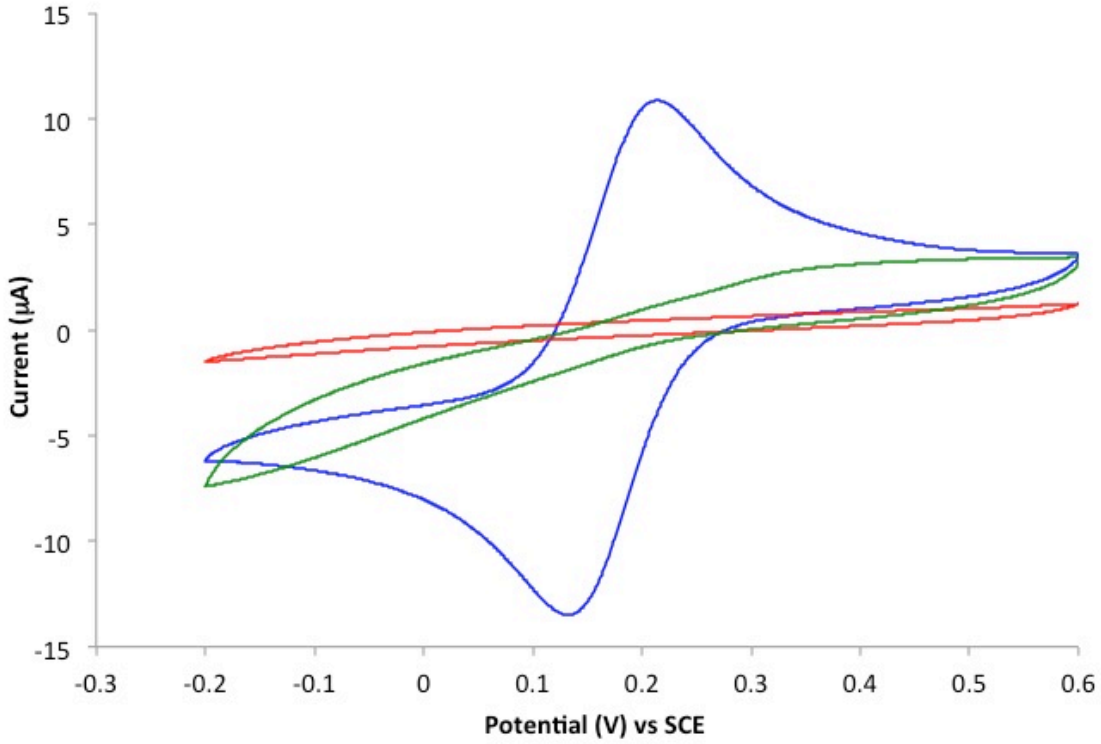

Figure 3.6. CV showing the partial restoration of the redox probe voltammetry of the Ar-COOH film obtained in 1 mM $K_3Fe(CN)_6$ in PBS pH 7. Scan rate = 100 mV s^{-1}. The blue line is a scan taken before grafting and the red line is a scan taken after grafting of the Ar-COO-Fm film and the green line is a scan taken after deprotection of the carboxylic acid groups.

The attachment of ABiB through the procedure described above (Scheme 3.3) and in Chapter 2 yields the Ar-CONH-ABiB film. After this modification procedure, the surface was once more investigated by redox probe voltammetry. The purple line in Figure 3.7 represents the scan taken in the presence of this film. There is only a minor change compared with the Ar-COOH film. Based on these results, it is not possible to establish whether the ABiB coupling reaction has proceeded as expected. After coupling the ABiB group, the film thickness will increase but the negative charge will decrease. These two changes have the opposite effect on

the electron transfer rate of $Fe(CN)_6^{3-/4-}$ and hence the nature of the surface after reaction with ABiB cannot be deduced.

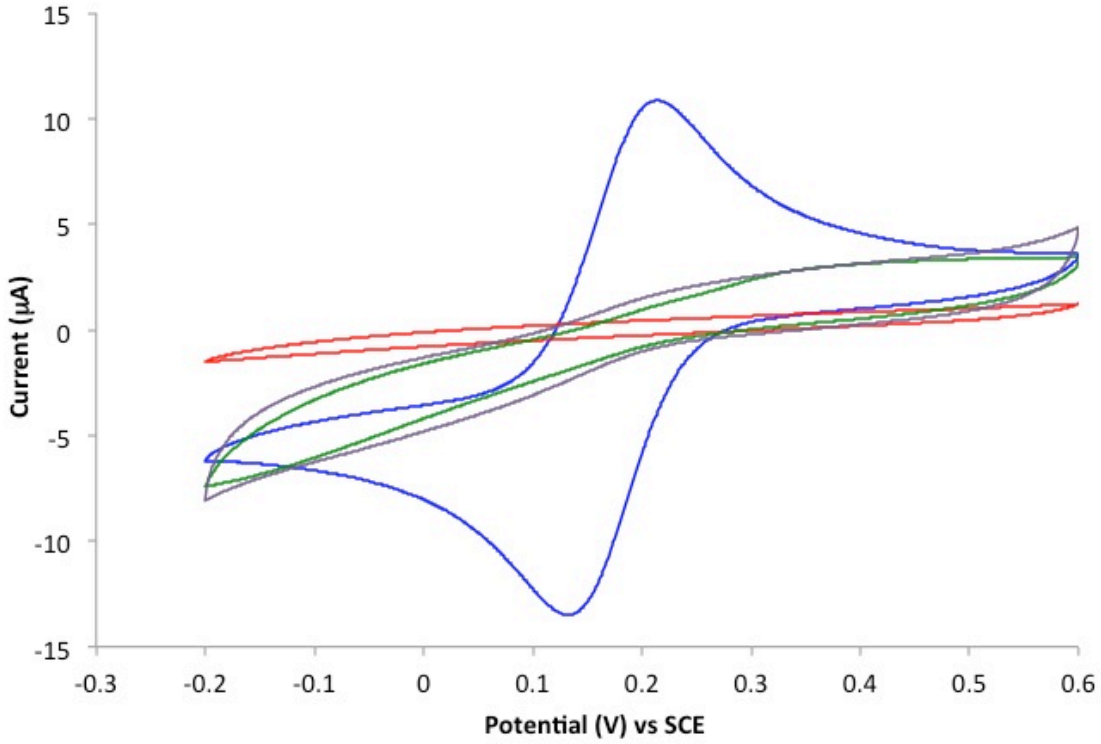

Figure 3.7. CVs obtained in a solution of 1 mM $K_3Fe(CN)_6$ in PBS pH 7 showing the effects of the reaction of the modified electrode with ABiB. Scan rate = 100 mV s^{-1}. The blue line is a scan taken before grafting, the red line is a scan taken after grafting of the Ar-COO-Fm film, the green line is a scan taken after deprotection of the carboxylic acid groups and the purple line is a scan taken after the coupling of ABiB to the film.

3.3.2.2.2. Effect of Modification on Immobilised Fc Coupling

To monitor the surface modification, ferrocene (Fc) groups were coupled to the surface after selected steps. Before modification, a bare GC surface was reacted with ferrocenoyl chloride (FcCOCl) (see Chapter 2 for the synthesis of FcCOCl and coupling to GC). A CV of the Fc modified surface was taken in a $LiClO_4$-Ethanol (EtOH) solution at a scan rate = 200 mV s^{-1} is shown in Figure 3.8. The CV shows the typical reversible redox peaks of immobilised Fc/Fc^+ couple.[128] The surface concentration of immobilised Fc groups, Γ_{Fc}, calculated from the peak area (determined by methods detailed in Chapter 2.5), was estimated to be 9.7 ± 0.1

$\times 10^{-11}$ mol cm^{-2} (n = 4). This value is lower than that obtained by Lee and Downard[15] (1.6 ± 0.2 $\times 10^{-10}$ mol cm^{-2}), but may be attributed to variation in the GC manufacturing process and surface condition. An ideal close-packed monolayer of Fc on a flat surface has a calculated surface coverage of 4.5 $\times 10^{-10}$ mol cm^{-2}.[131] Hence it is assumed that 9.7 ± 0.1 $\times 10^{-11}$ mol cm^{-2}, which equates to 22% of a maximum coverage, approximately represents the surface concentration of groups on the GC surface that can be reacted with acid chlorides.

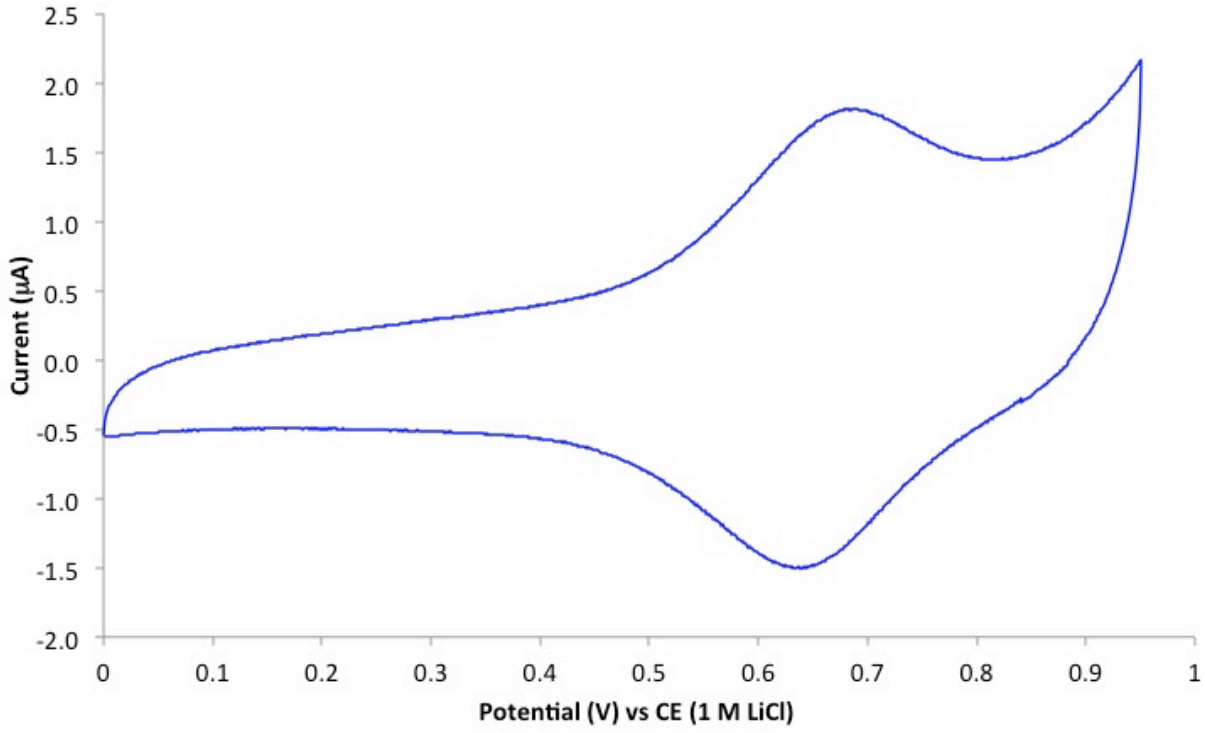

Figure 3.8. Second scan of a CV in 0.1 M $LiClO_4$ –EtOH of a GC electrode after reaction with FcCOCl. Scan rate = 200 mV s^{-1}.

Figure 3.9 shows a CV taken after modification of the GC surface by grafting an Ar-COOH film and reaction with FcCOCl. Again, the reversible redox peaks of immobilised Fc/Fc^{+} couple are seen. As expected, ΔE_p is close to zero for a surface immobilised species.[128] Γ_{Fc} was calculated to be 5.5 ± 0.9 $\times 10^{-10}$ mol cm^{-2} (n = 2). This corresponds to roughly a 5-fold increase in the number of immobilised Fc molecules compared to the reaction of FcCOCl with polished GC. The calculated Γ_{Fc} for the Ar-COOH film (5.5 ± 0.9 $\times 10^{-10}$ mol cm^{-2})

corresponds to 122% coverage of Fc molecules. It is to be noted, that Fc groups may attach directly to the GC surface through the same linkers as when immobilised on a bare GC surface, hence the increased surface concentration of Fc.

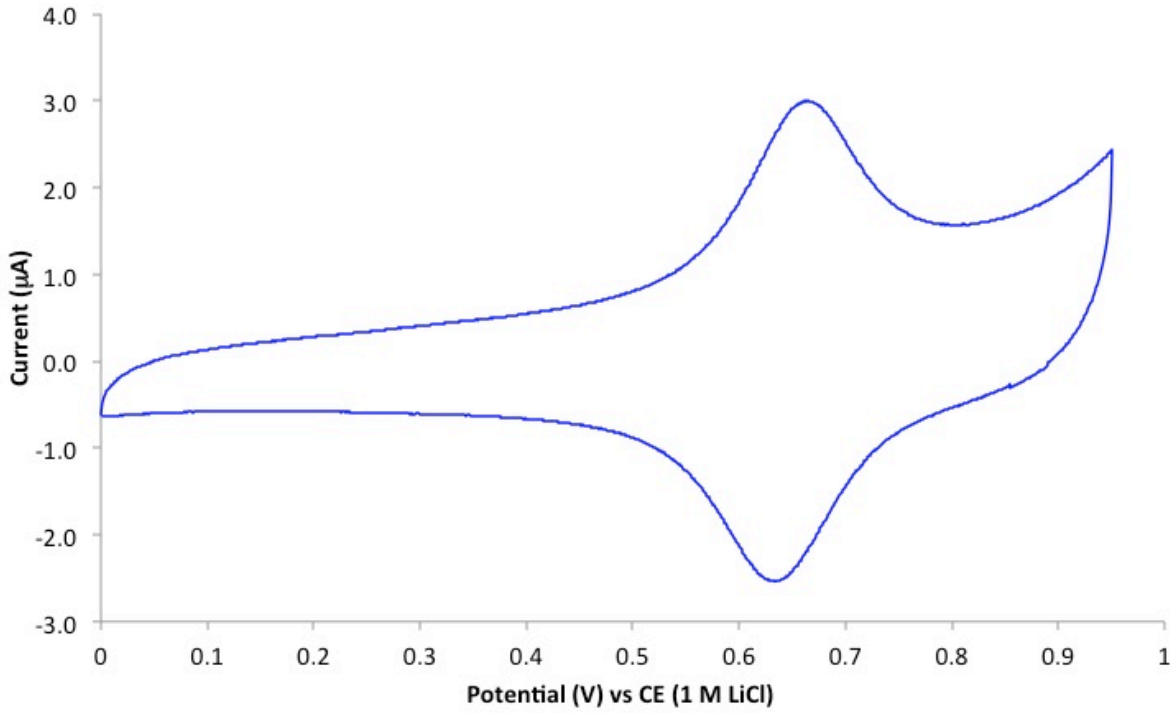

Figure 3.9. Second scan of a CV in 0.1 M $LiClO_4$ –EtOH of an Ar-COOH modified GC electrode after reaction with FcCOCl. Scan rate = 200 mV s^{-1}.

The red line in Figure 3.10 shows a CV taken after activated FcCOOH was reacted with an Ar-CONH-ABiB film. Compared to the blue line, the same CV shown in Figure 3.9, the CV shows a significant decrease in peak current and an increase in ΔE_p, indicating a lower concentration of immobilised Fc molecules. Γ_{Fc} for the Ar-CONH-ABiB surface was calculated to be $6.6 \pm 1.1 \times 10^{-11}$ mol cm^{-2} ($n = 2$). This is a significant decrease compare to the Ar-COOH film, which is to be expected as the potential binding sites for the Fc molecules have been reacted. The Γ_{Fc} value calculated corresponds to 15% of the maximum surface coverage of Fc molecules. A summary of the calculated Γ_{Fc} values for the polished GC surface, Ar-COOH and Ar-CONH-ABiB modified films is included in Table 3.1.

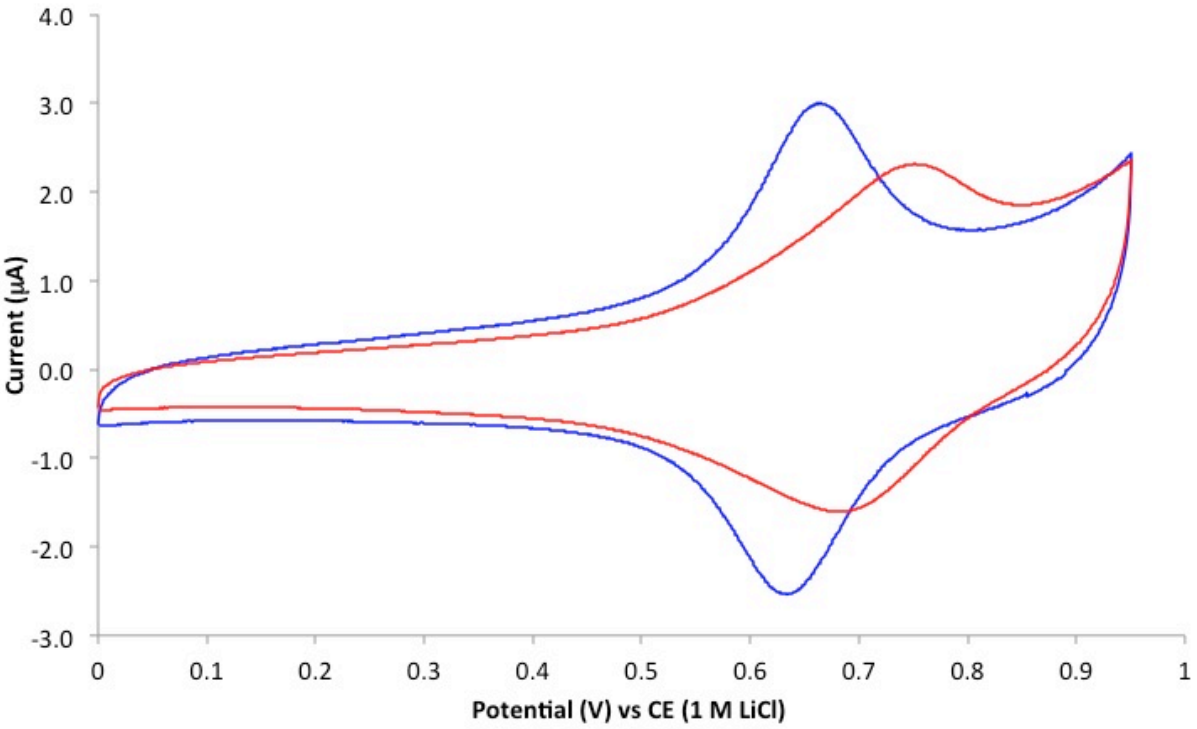

Figure 3.10. Second scan of a CV in 0.1 M $LiClO_4$ –EtOH of an Ar-COOH modified GC electrode after reaction (blue line) with FcCOCl and (red line) after reacting FcCOCl to an Ar-CONH-ABiB modified GC electrode. Scan rate = 200 mV s^{-1}.

Table 3.1. Surface concentration of immobilised Fc (Γ_{Fc}) throughout the modification procedure.

Surface	Γ_{Fc}	% of maximum coverage	n[a]
Bare GC	$9.7 \pm 0.1 \times 10^{-11}$ mol cm^{-2}	22%	4
Ar-COOH	$5.5 \pm 0.9 \times 10^{-10}$ mol cm^{-2}	122%	2
Ar-CONH-OH-ABiB	$6.6 \pm 1.1 \times 10^{-11}$ mol cm^{-2}	15%	2

[a] n is the number of samples analysed.

3.3.2.2.3. Effect of Modification on Contact Angle Measurements

Water contact angles on the modified surfaces were used to monitor the sequence of grafting and deprotection steps. A 2 μL droplet of solution (MQ water, 0.1 M HCl (pH 1) or

$NaOH/NaHCO_3$ buffer (pH 10)) was placed on top of the modified area then photographed after a 10 second equilibration time. Table 3.2 lists the average contact angle for the three solutions at polished and modified GC surfaces. Bare GC has an average water contact angle of 72 ± 1 °, while the average contact angles for pH 1 and pH 10 solutions were 66 ± 2 ° and 65 ± 2 ° respectively. After grafting of the Ar-COO-Fm film, the average contact angles showed no significant changes, which is not unexpected considering the structure of the protected modifier. After deprotection of the film, the Ar-COOH film has an average water contact angle of 50 ± 3 °. This decrease is attributed to the increased hydrophilicity of the film, caused by the carboxylic acid groups. The average contact angle for the pH 1 solution is 51 ± 3 °, while the pH 10 buffer solution gave an average contact angle of 36 ± 3 °. At low pH the carboxylic acid groups are expected to be protonated, but at high pH the carboxylic acid groups are deprotonated, creating a charged film. This increases the hydrophilicity of the film, lowering the surface contact angle. The similarities between the water and acid contact angle measurements suggest that at the pH of the water (~6.4), the film is protonated. These findings are in agreement with the pH dependency found in the voltammetry experiments. After the amide coupling reaction between the Ar-COOH film and ethanolamine (Step 1, Scheme 3.3), the surface lost the pH dependency exhibited before modification. After the coupling of ABiB to the film, there was only a noticeable change in contact angle for the pH 1 solution. The reason for this is unknown at this stage.

Table 3.2. Average contact angle measurements for polished and modified GC surfaces. Error is the standard deviation.

	Bare GC	Ar-COO-Fm	Ar-COOH	Ar-CONH-OH	Ar-CONH-ABiB
MQ Water	72 ± 1 °	65 ± 1 °	50 ± 3 °	53 ± 2 °	57 ± 3 °
0.1 M HCl (pH 1)	66 ± 2 °	68 ± 2 °	51 ± 3 °	53 ± 3 °	65 ± 2 °
Buffer (pH 10)	65 ± 2 °	61 ± 2 °	36 ± 3 °	52 ± 4 °	53 ± 2 °

3.3.2.2.4. X-ray Photoelectron Spectroscopy Analysis

XPS analysis was used to confirm the amide coupling of ethanolamine to the Ar-COOH monolayer and the esterification of ABiB to the Ar-CONH-OH film (Scheme 3.3). XPS measurements were made on GC surfaces. An unmodified, polished GC plate was used as a blank.

Atomic compositions at each surface were obtained from survey spectra, giving the data shown in Table 3.3. The blank GC surface shows the atomic percentage of nitrogen to be 0.7%. This is occasionally seen in GC surfaces and is most likely caused by contamination in the manufacturing process.[132] The 6.3% oxygen content is typical for GC.[15] After the formation of the Ar-COOH layer (Scheme 3.2) and after the amide coupling between ethanolamine and the Ar-COOH monolayer (Step 1, Scheme 3.3), the atomic percentage of nitrogen in the film increased to 2.1%. After esterification of ABiB to the Ar-CONH-OH film, producing the Ar-CONH-ABiB surface, 0.5% of the atomic composition of the surface was detected to be bromine. This is compelling evidence for coupling of ABiB to the film. In similar films, low bromine content has also been seen, with Iruthayaraj *et al* reporting values ranging from 0.04 to 2.95% atomic bromine.[100]

Table 3.3. XPS survey data for the polished and modified GC plates.

Sample	Atomic%			
	C	**N**	**O**	**Br**
Polished GC	93.0	0.7	6.3	
Ar-CONH-OH	82.2	2.1	15.7	
Ar-CONH-ABiB	86.3	3.0	10.2	0.5

Narrow scan spectra of carbon (C1s), nitrogen (N1s) and oxygen (O1s) were taken for each sample. A narrow scan spectrum of bromine (Br3d) was taken for the Ar-CONH-ABiB film.

Figure 3.11 (a) shows a wide scan spectrum and (b-d) shows the narrow scan spectra for the C1s, N1s and O1s regions for polished GC surface. The binding energies, assignments and atomic percentages for peaks fitted to the C1s, N1s and O1s signals obtained at the polished GC surface are listed in Table 3.4.

Table 3.4. Binding energies, assignments and atomic% for the C1s, N1s and O1s XPS narrow scan spectra for bare GC.

	Binding Energy (eV)	Atomic%	Assignment	Ref
C1s	284.5	41.0	Graphitic C	[133,134]
	284.8	39.86	C-C, C-C (sp^2), C-C (sp^3)	[133]
	286.5	14.91	C-OH, ester	[135,134]
	289.2	4.21	COOH, ester	[133,134, 135]
N1s	399.7	100	Reduced N	
O1s	531.4	23.3	>C=O, -C-O-C-	[135]
	532.8	76.7	>C-OH, adsorbed CO, adsorbed O_2, bound H_2O	[135]

The C1s narrow scan spectrum was fitted with four peaks, with the prominent aromatic carbon peak centred at 284.5 eV. The other contributing peaks are a mixture of oxidised C bonding modes. The percentage of graphitic carbon is 41%, similar to that observed by Ilangovan *et al*.[135] These bonding modes are often quite similar in binding energy, making assignments of the peaks difficult. The N1s narrow scan spectrum was fitted with a single peak at 399.7 eV, consistent with reduced N. The O1s spectrum was fitted with two peaks, at 531.4 and 532.8 eV respectively. The broadness of the O1s narrow scan peak can be attributed to the variety of oxide functionalities and adsorbed oxygen molecules that can be present on the polished GC surface.

(a) (b)

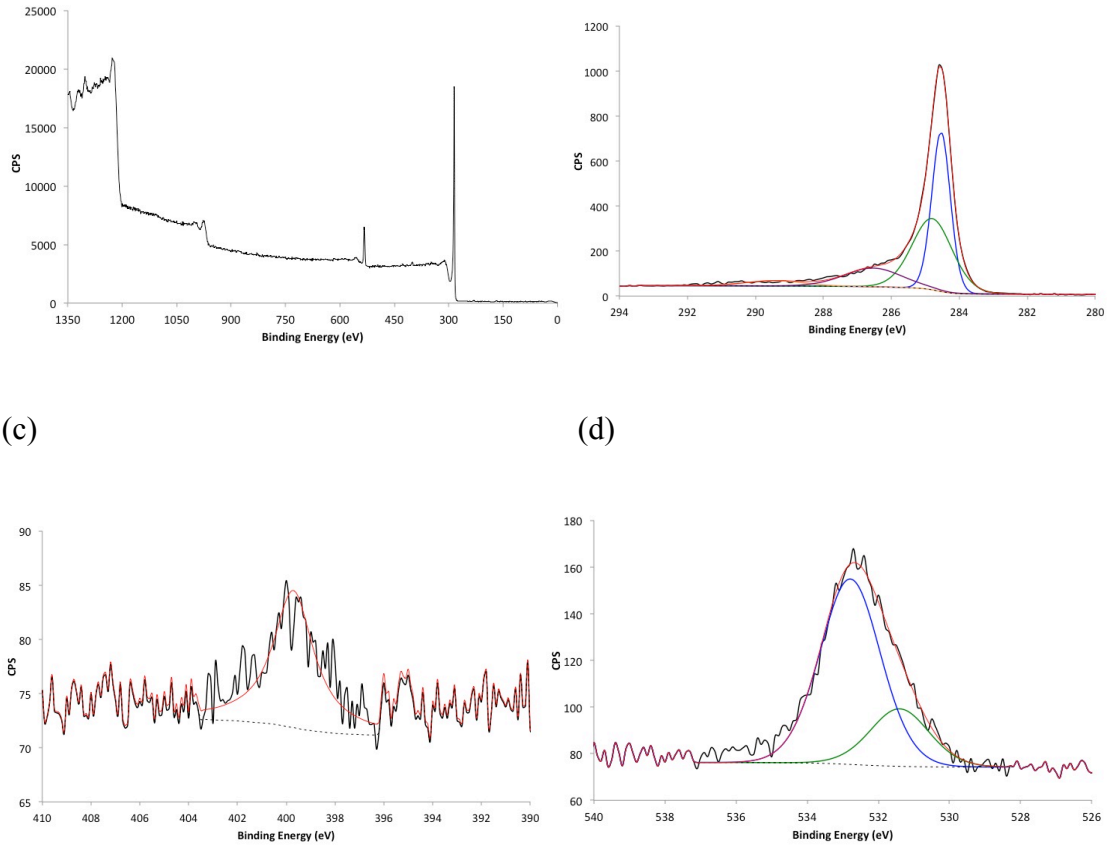

Figure 3.11. XPS spectra of a bare GC surface: wide scan (a) and narrow scan spectra for C1s (b), N1s (c) and O1s (d) regions. The black lines are the experimental spectra recorded and the coloured lines represent those used for peak fitting.

The wide scan spectra for the Ar-CONH-OH-modified GC surface is shown in Figure 3.12 (a). The COOH peak in the C1s narrow scan spectra (Figure 3.14 (b)) at 288.9 eV is still present, indicating that amide coupling was not complete. The N1s narrow scan spectra (Figure 3.12 (c)) shows two peaks, at 400.4 and 402.6 eV. The peak at 402.6 eV has been assigned to the azo and amide functional groups. The O1s narrow scan spectra (Figure 3.12 (d)) has been fitted with two peaks, at 532.2 and 533.5 eV. The majority peak at 532.2 eV is assigned to the carbonyl peak while the peak at 533.5 eV has been assigned to C-O.

The binding energies, assignment and atomic percentage for the C1s, N1s and O1s narrow scan spectra for the Ar-CONH-OH modified GC surface are listed in Table 3.5.

Table 3.5. Binding energies, assignments and atomic% for the C1s, N1s and O1s XPS narrow scan spectra for the Ar-CONH-OH film on GC.

	Binding Energy (eV)	Atomic%	Assignment	Ref.
C1s	284.7	31.2	Graphitic C	[133,134]
	285.3	43.9	C-C, C-C (sp^2), C-C (sp^3)	[133]
	286.5	18.8	C-OH, C=O	[134]
	288.9	5.95	COOH	[133]
N1s	400.4	75.9	Reduced N	
	402.6	24.1	Azo, Amide	
O1s	532.2	73.4	>C=O, -C-O-C-, chemisorbed water	[135]
	533.5	26.6	>C-OH, adsorbed CO, adsorbed O_2, bound H_2O	[135]

(a) (b)

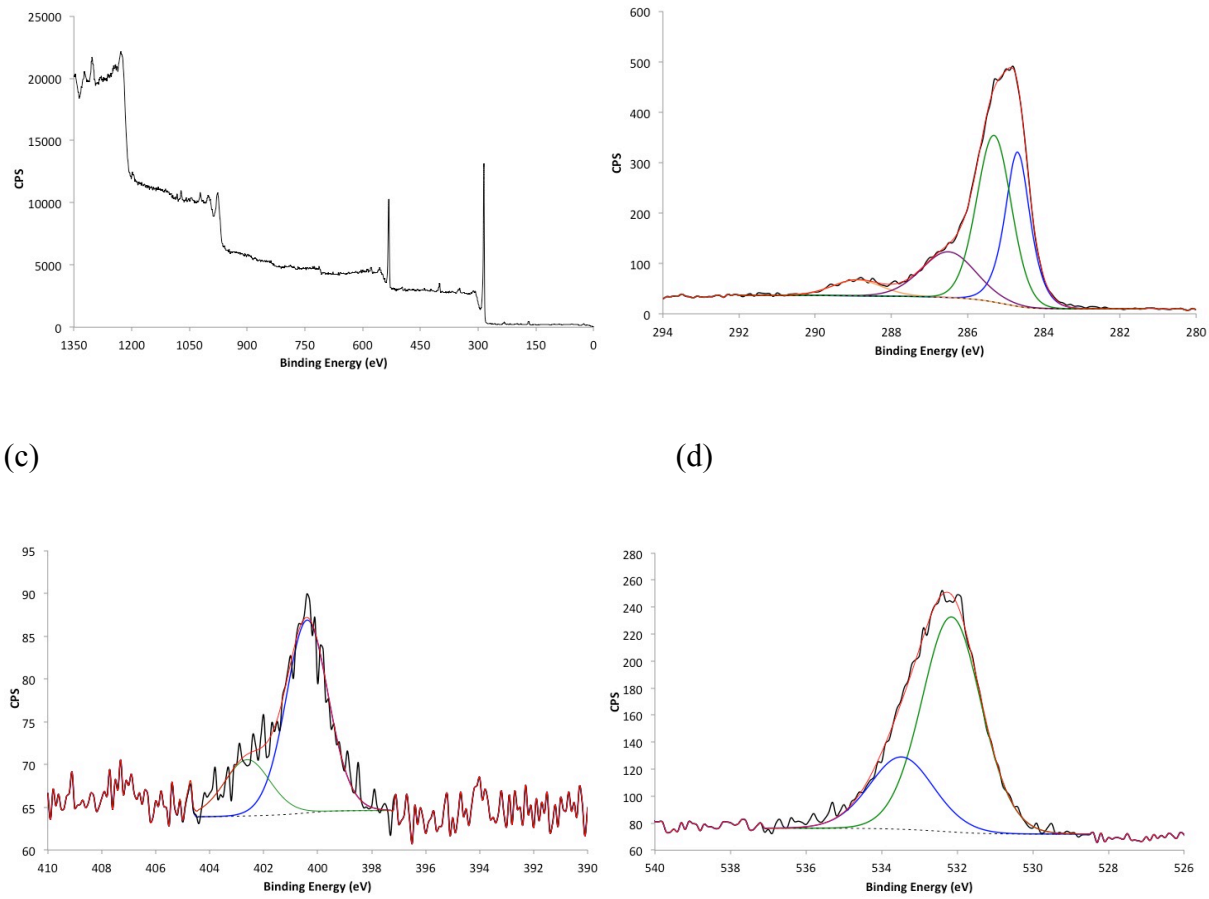

Figure 3.12. XPS spectra of the Ar-CONH-OH surface: wide scan (a) and narrow scan spectra for C1s (b), N1s (c) and O1s (d) regions. The black lines are the experimental spectra recorded and the coloured lines represent those used for peak fitting.

The wide scan spectra for the Ar-CONH-ABiB is shown in Figure 3.13 (a). The C1s (b), N1s (c) and O1s (d) narrow scan spectra of the Ar-CONH-ABiB film shows no significant changes from the Ar-CONH-OH film. The presence of two peaks in the Br3d narrow scan spectrum is evidence for the coupling of ABiB to the Ar-CONH-OH-modified surface. The two peaks located at 68.2 and 70.8 eV, arise from the 3d 5/2 and 3d peaks respectively.

The binding energies, assignment and atomic percentage for the C1s, N1s, O1s and Br3d narrow scan spectra for the Ar-CONH-ABiB-modified GC surface are listed in Table 3.6.

Table 3.6. Binding energies, assignments and atomic% for the C1s, N1s, O1s and Br3p XPS narrow scan spectra for the Ar-CONH-ABiB film on GC.

	Binding Energy (eV)	Atomic%	Assignment	Ref
C1s	284.7	22.2	Graphitic C	[133,134]
	285.0	51.2	C-C, C-C (sp^2), C-C (sp^3)	[133]
	286.4	23.3	C-OH, C=O	[134]
	289.0	5.33	COOH	[133]
N1s	400.3	85.4	Surface N	
	402.3	14.6	Azo, Amide	
O1s	532.1	64.5	>C=O, -C-O-C-, chemisorbed water	[135]
	533.6	35.5	>C-OH, adsorbed CO, adsorbed O_2, bound H_2O	[135]
Br3d	68.2	23.9	Br (3d 5/2)	
	70.8	76.1	Br (3d)	

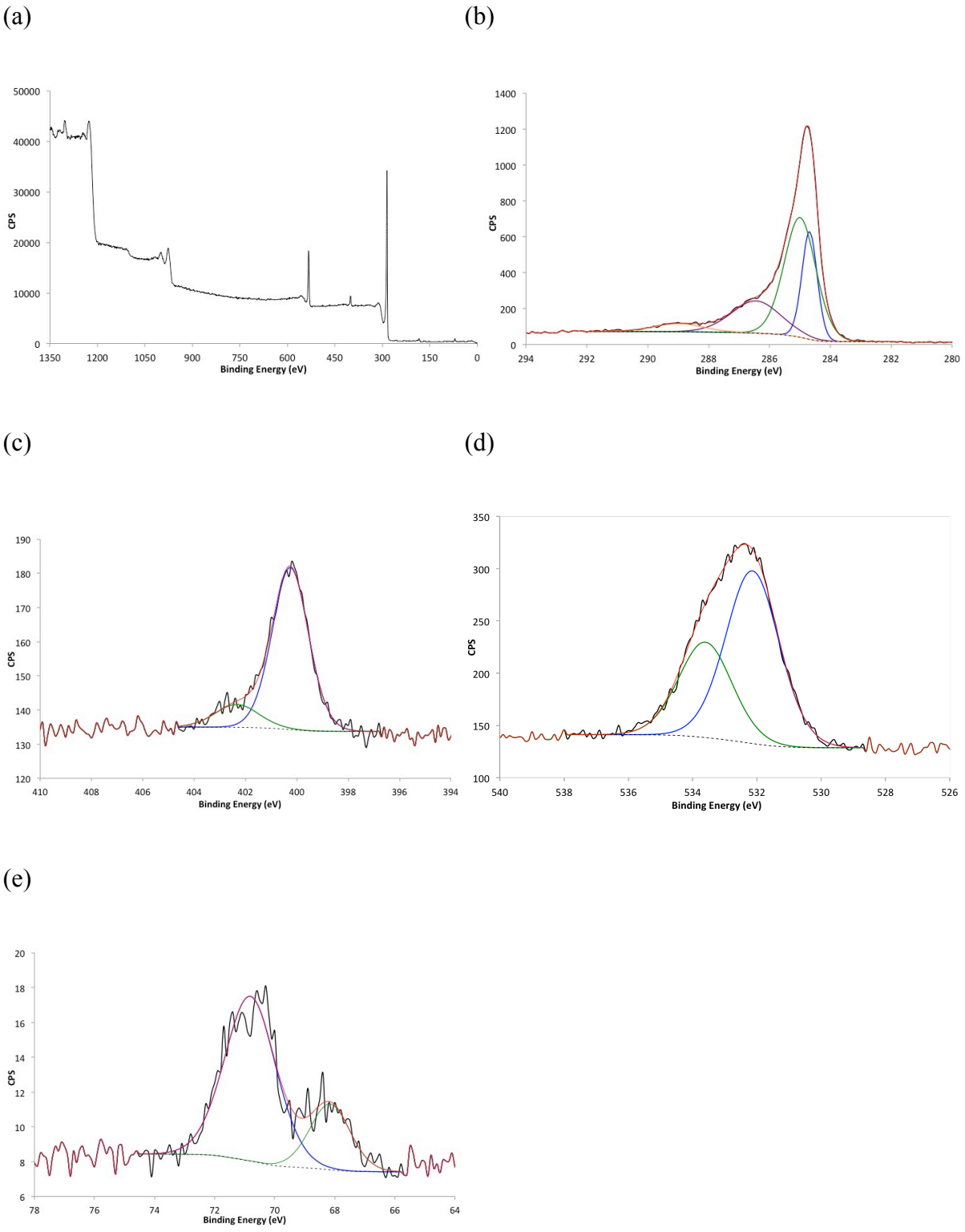

Figure 3.13. XPS spectra of the Ar-CONH-ABiB surface: wide scan (a) and narrow scan spectra for C1s (b), N1s (c), O1s (d) and Br3d (e) regions. The black lines are the experimental spectra recorded and the coloured lines represent those used for peak fitting.

3.3.3. Ethynylaryl Film

Carbon electrode surfaces (GC and PPF) were modified by the electrochemical grafting of N_2^+-Ar-Eth-TIPS. The protecting TIPS group was selectively cleaved from the surface by immersing the modified surface in a solution of 0.05 M tetra-n-butylammonium fluoride (TBAF) in tetrahydrofuran (THF) for 40 min (Scheme 3.4), revealing the ethynylaryl (Ar-Eth) monolayer.[35,129] This treatment removes the TIPS group and any additional Ar-Eth-TIPS groups that may have grafted to the protecting group during grafting resulting in a multilayer.

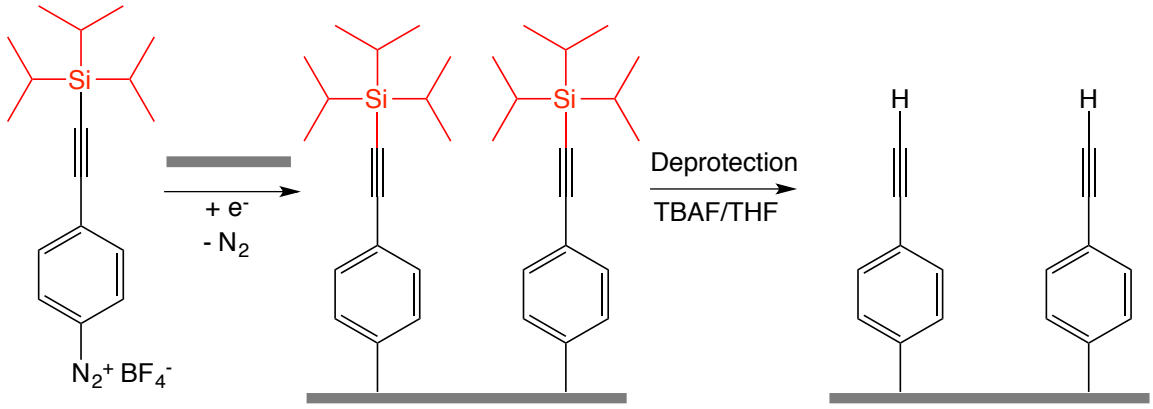

Scheme 3.4. Electrochemical grafting of N_2^+-Ar-Eth-TIPS to a carbon electrode followed by the deprotection of the TIPS protecting group.

The reactivity of the Ar-Eth monolayer was tested through immobilising azidomethylferrocene via 'click' chemistry (Scheme 3.5). The detection of redox active Fc groups through electrochemistry allows for the quantification of surface concentration of immobilised Fc molecules, and thus the determination of the amount of Ar-Eth groups. Various reaction conditions were used to click the Fc groups to the surface: that of Leroux and coworkers,[50b] a modified literature method,[120] and an electrochemically mediated method.[121] The efficacy of these three methods were assessed and compared by the number of calculated Fc groups attached to the surface for a given period of time.

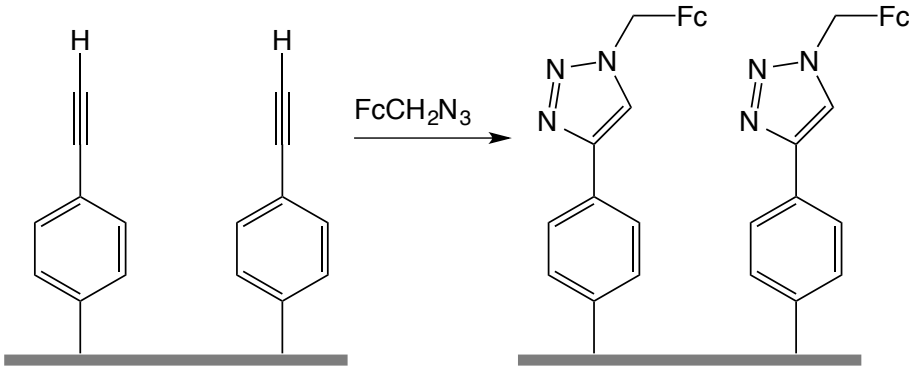

Scheme 3.5. Immobilisation of Fc groups to the ethynylaryl monolayer through click chemistry.

The azide functionalised ATRP initiator, (3-azidopropyl)bromoisobutyrate (APBiB), was coupled to the Ar-Eth monolayer through the same click chemistry (Scheme 3.6). This layer was used as a tethered initiation group for surface induced atom transfer radical polymerisation (Chapter 5).

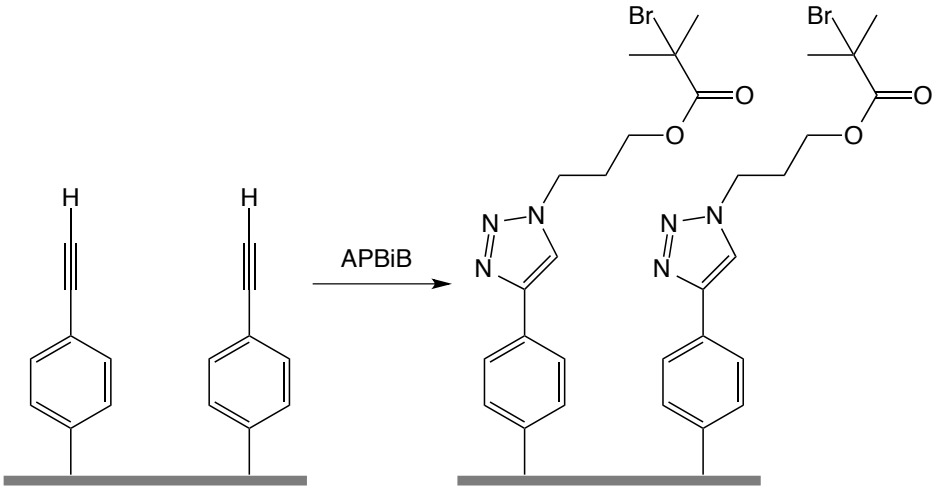

Scheme 3.6. Immobilisation of APBiB groups to the ethynylaryl monolayer through click chemistry.

3.3.3.1. Electrochemical Grafting of Ar-Eth-TIPS Film on Carbon Electrodes

N_2^+-Ar-Eth-TIPS was electrochemically grafted to GC electrodes by recording cyclic voltammetry scans in the presence of 1 mM [N_2^+-Ar-Eth-TIPS] BF_4^- and 0.1 M $TBABF_4$ in ACN. Figure 3.14 shows the 5 cyclic voltammetry scans between 0.8 V and -0.75 V at a scan rate of 50 mV s^{-1} used for the grafting procedure. The blue line representing the first scan

shows the irreversible reduction peaks of the aryl diazonium ions. The disappearance of the reduction peak on the subsequent scans (2-5) is consistent with the formation of a grafted layer, which hinders further electrochemical reduction of the aryl diazonium ions by inhibiting electron transfer from the electrode surface to the aryl diazonium ions in solution.

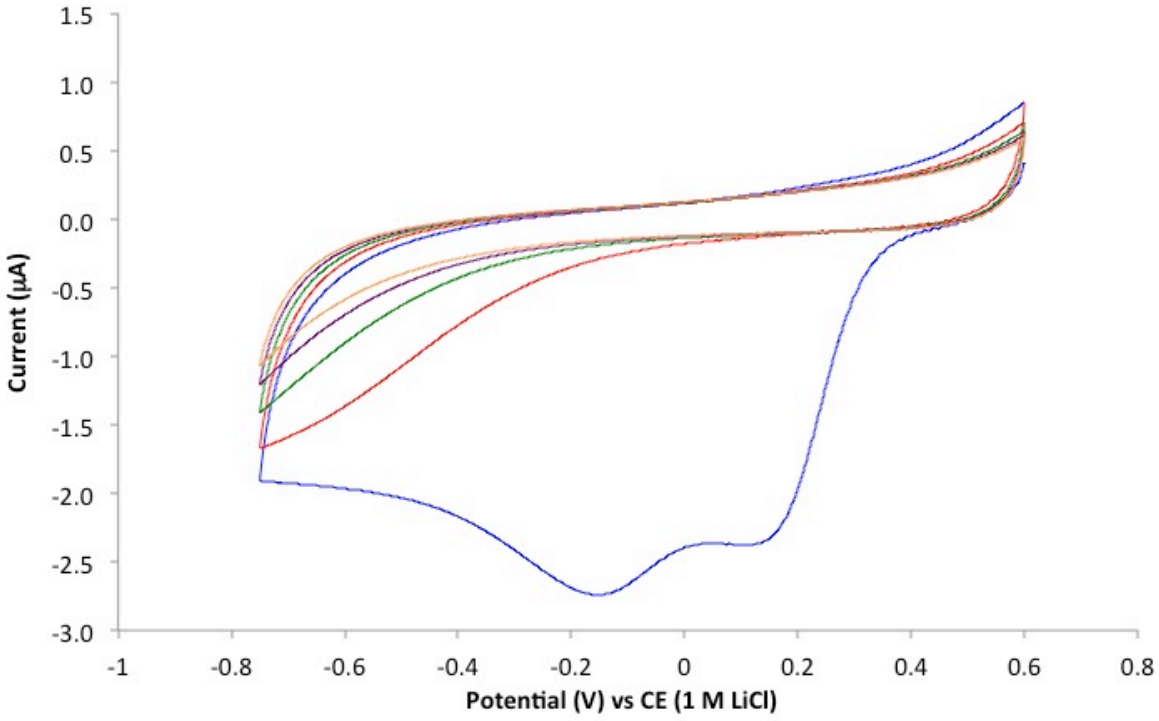

Figure 3.14. Five consecutive scans at a bare GC disk electrode in a solution of 1 mM N_2^+-Ar-Eth-TIPS in 0.1 M $TBABF_4$-ACN. Scan rate = 50 mV s^{-1}. The blue line represents the 1st scan, red the 2nd scan, green the 3rd scan, purple the 4th scan and orange the 5th scan.

3.3.3.2. Characterisation of Modified Layers

The films described above were characterised by electrochemistry, water contact angle measurements, atomic force microscopy and X-ray photoelectron spectroscopy.

3.3.3.2.1. Effect of Modification on Redox Probe Voltammetry

The presence of the Ar-Eth-TIPS and Ar-Eth films on the GC electrode surface was studied using redox probe voltammetry. A solution of $K_3Fe(CN)_6$ in PBS (pH 7) was used as the

redox probe. The bare GC surface was scanned in the redox probe solution prior to grafting of the layer (Figure 3.15, blue line). The bare GC surface shows the characteristic chemically reversible peak (ΔE_p = 65 mV) that can be associated with moderately fast electron transfer from the surface to the redox species in solution.

The same GC electrode modified with an Ar-Eth-TIPS film was scanned in the same redox probe solution. The featureless CV scan (Figure 3.15, red line) indicates that the grafted film is sufficiently thick to inhibit electron transfer between the electrode surface and the redox species in solution.

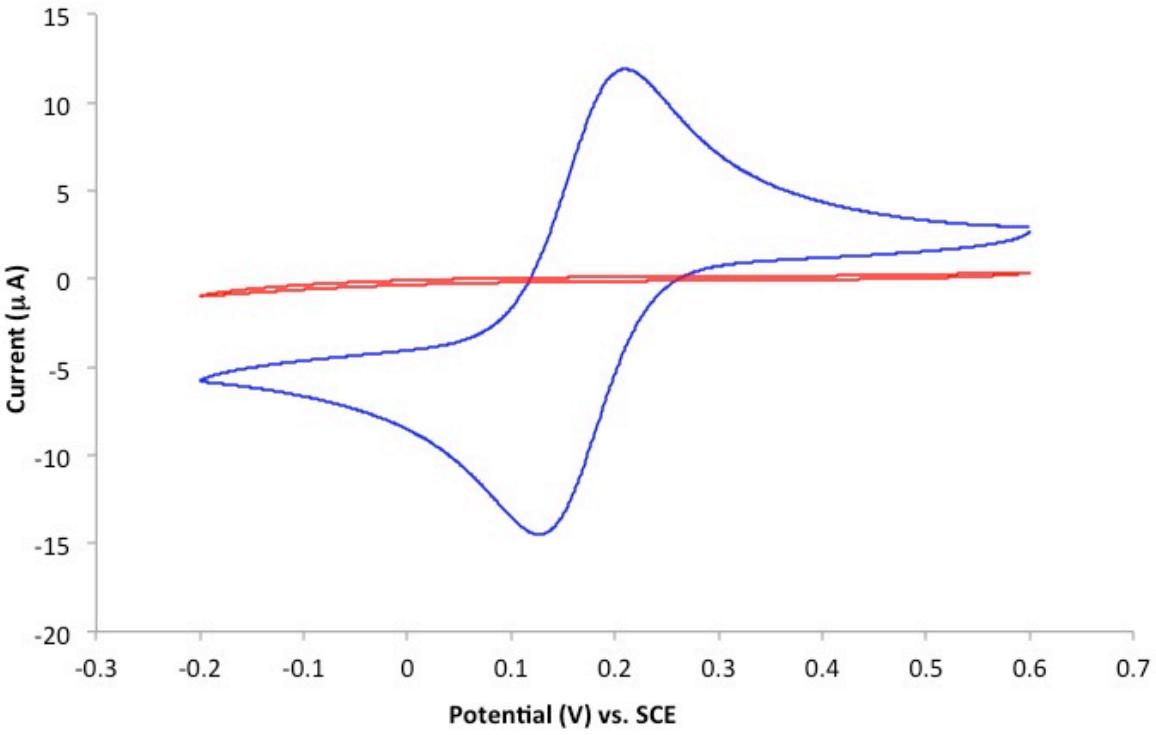

Figure 3.15. CV showing the blocking effect of the Ar-Eth-TIPS film at GC in a solution of 1 mM $K_3Fe(CN)_6$ in PBS pH 7. The blue line is a scan taken before grafting and the red line is a scan taken after grafting of a film.

After treating the Ar-Eth-TIPS film with a solution of 0.05 M TBAF in THF for 20 min to remove the TIPS protecting group, the surface was once again scanned in the redox probe solution. The restoration of a peak in the CV (Figure 3.16, green line) is observed. The

response does not return to that of the fully reversible bare GC response, indicating that electron transfer is still being inhibited somewhat. This is in agreement with the CVs obtained by Leroux *et al*. for the same system.[39]

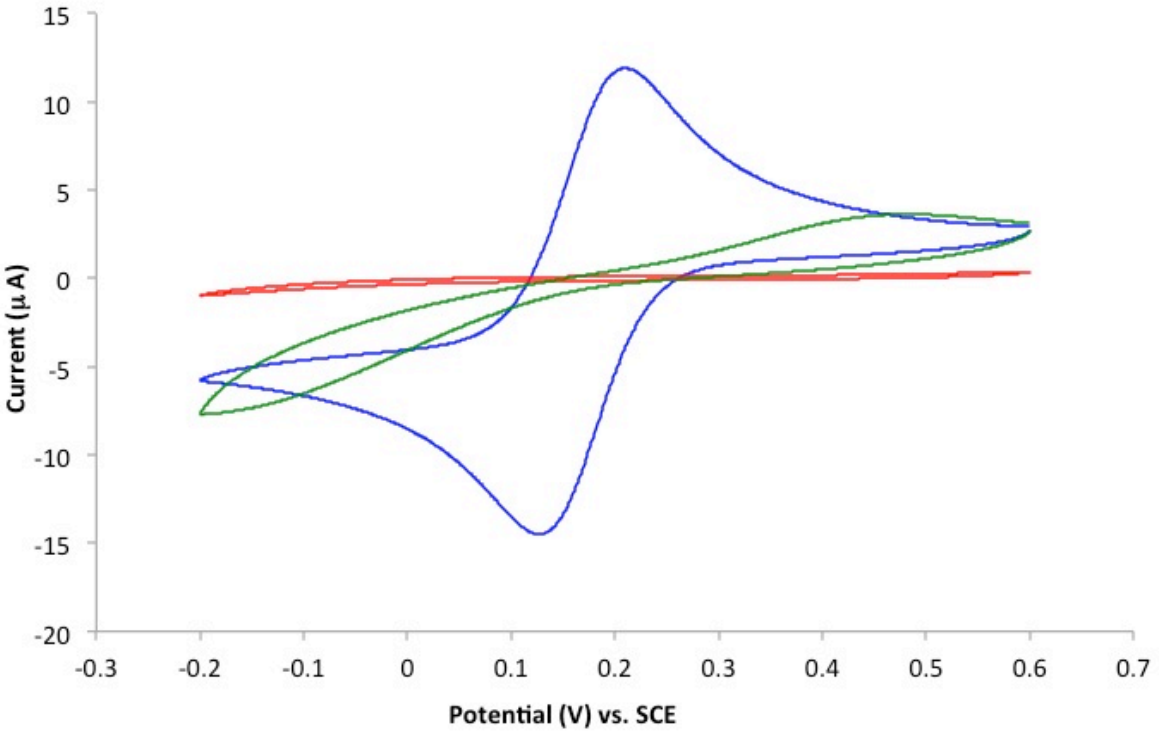

Figure 3.16. CV showing the partial restoration of the redox probe from the Ar-Eth film at GC in a solution of 1 mM $K_3Fe(CN)_6$ in PBS pH 7. The blue line is a scan taken of the bare GC surface before grafting, the red line is a scan taken after grafting of the Ar-Eth-TIPS film and the green line is a scan taken after removal of the TIPS groups.

3.3.3.2.2. Effect of Modification on Water Contact Angle Measurements

Wettability of the surface was determined through experiments conducted using a contact angle apparatus. A 2 μL droplet of solution (MQ water, 0.1 M HCl (pH 1) or $NaOH/NaHCO_3$ buffer (pH 10) was placed on top of the modified area. Averages are from 16 droplets comprised of 8 individual droplets on 2 samples. The error is the standard deviation in the measurements. Table 3.6 lists the average contact angle measurements for the bare and modified surfaces.

Modification of GC with Ar-Eth-TIPS groups had an insignificant effect on the hydrophobicity of the surface. After removal of the TIPS protecting group by treatment of the surface with TBAF/THF solution, there was a decrease in water contact angle, from 77 ± 3 ° to 54 ± 2 °. After coupling of APBiB, the average water contact angle slightly decreased to 50 ± 3 °. As to be expected, there were insignificant differences in the contact angle measurements between acidic and basic droplets. It is clear from the data in Table 3.9 that immersion in the deprotection solution causes a major change in the film, consistent with the expected deprotection. However, the evidence for successful coupling of APBiB is less conclusive.

Table 3.6. Average contact angle measurements for polished and modified GC surface. Error is the standard deviation.

	Bare GC	**Ar-Eth-TIPS**	**Ar-Eth**	**Ar-Tri-APBiB**
MQ	71 ± 1 °	77 ± 3 °	54 ± 2 °	50 ± 3 °
0.1 M HCl (pH 1)	67 ± 2 °	76 ± 2 °	54 ± 3 °	52 ± 2 °
Buffer (pH 10)	63 ± 1 °	77 ± 2 °	54 ± 3 °	47 ± 1 °

3.3.3.2.3. Model Reactions for Ethynylaryl Film

The coupling of ferrocene groups to the Ar-Eth film through click chemistry has been used as a model reaction for the ethynylaryl film. Azidomethylferrocene (N_3MeFc) was used as a quantifiable azide derivative for the future azide-alkyne click reactions. Immobilised Fc molecules are electrochemically active through the ferrocene/ferrocenium (Fc/Fc^+) redox

couple. The surface concentrations of immobilised Fc molecules (Γ_{Fc}) can be calculated from cyclic voltammetry scans of the modified surface.

Three reaction methods were investigated for the coupling of N_3MeFc to the Ar-Eth layer. All three reactions explored are examples of Cu^I catalysed azide-alkyne click (CuAAC) reactions (all reaction details are given in Chapter 2). Method 1 is an established method in the literature[50b,38] This method uses $_L$-ascorbic acid to reduce Cu^{II} to Cu^I and requires an inert atmosphere. Method 2 is a carboxylic acid promoted reaction, adapted from a literature procedure.[120] No atmospheric control is required for this reaction. Method 3 is an electrochemically mediated click reaction, adapted from a literature procedure.[121] A fixed potential is applied to the modified working electrode. The applied potential is such that Cu^{II} at the electrode surface is reduced to Cu^I, the species needed to catalyse the click reaction. Method 3a was included as a blank for Method 3. It utilised the same reaction conditions as Method 3, but with no potential applied to the working electrode. An inert atmosphere was not required for Method 3 and 3a.

The potential to be applied in Method 3 was found by scanning an unmodified GC electrode in a solution of 0.05 mmol $CuBr_2$, 1 mmol *N,N,N',N'',N''*-pentamethyl-diethylenetriamine (PMDTA), 0.1 M $TBABF_4$ in ACN. Figure 3.17 shows the CV obtained. The reduction peak at $E_{p,c} \approx$ -0.32 V vs CE (1 M LiCl) is assigned to the reduction of Cu^{II} to Cu^I. Therefore, at an applied potential negative of -0.32 V, Cu^I is the dominant species. An applied potential of -0.55 V vs CE (1 M LiCl) was used for all subsequent electrochemical CuAAC reactions.

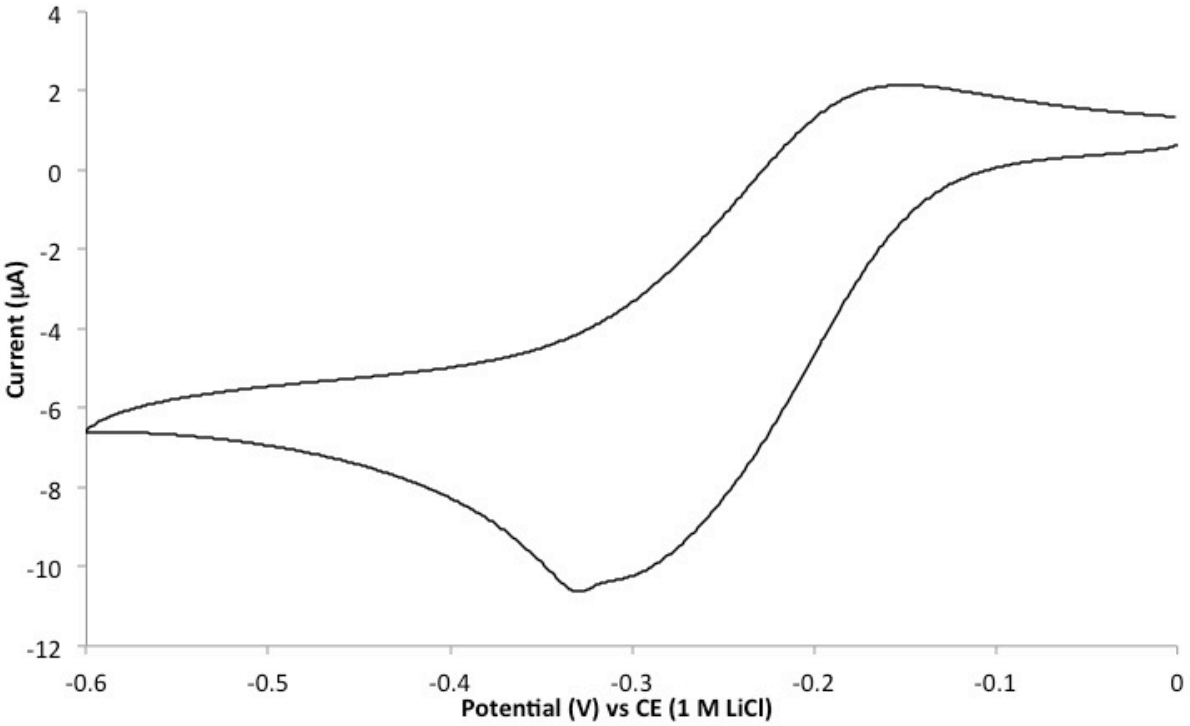

Figure 3.17. CV recorded in a solution of 1 mM $CuBr_2$, 1 mM PMDTA, 0.1 M $TBABF_4$ in ACN showing the reduction peak of Cu^{II} to Cu^{I}.

CVs were recorded in a 0.1 M $LiClO_4$ –EtOH solution for the four GC electrodes modified using clicking Methods 1-3 and 3a. The typical reversible redox peaks of the immobilised Fc/Fc^+ couple can be seen in the CV of Figure 3.18. This CV was obtained after reaction of N_3MeFc with an Ar-Eth modified GC electrode using Method 1. As expected for a surface immobilised species, ΔE_p is close to zero.[128]

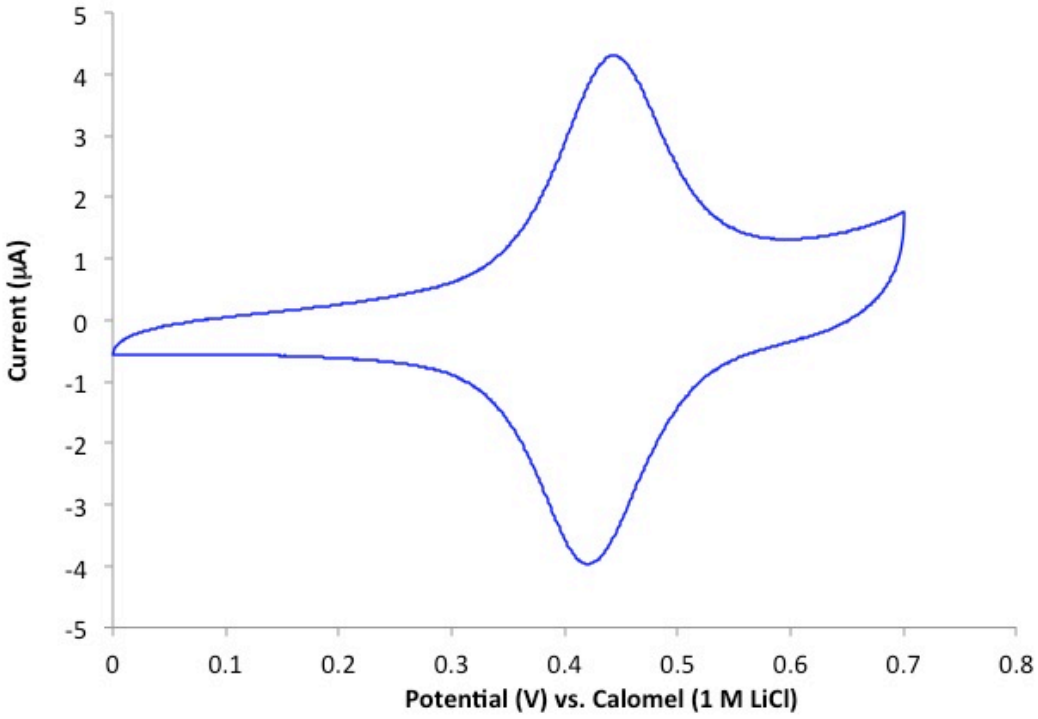

Figure 3.18. Second scan of a CV in 0.1 M $LiClO_4$ –EtOH of a GC electrode after clicking of N_3MeFc to an Ar-Eth monolayer through Method 1.

The calculated average Γ_{Fc} for the four reactions is listed in Table 3.7. The Γ_{Fc} value was calculated from the integrated oxidation and reduction peak currents then by applying Equations 2 and 3 in Chapter 2. Two electrodes were modified through each method, giving four values (one for the integrated oxidation peak and one for the reduction peak) for each method.

Although Method 1 requires an inert atmosphere, it results in the highest Γ_{Fc} out of the three methods with a $\Gamma_{Fc} = 2.8 \pm 0.3 \times 10^{-10}$ mol cm^{-2}. This value is close to that reported by Lee *et al*. using the same system ($2.0 \pm 0.2 \times 10^{-10}$ mol cm^{-2}).[38]

Table 3.7. Γ_{Fc} values for the Ar-Tri-Fc film produced by different methods.

Method	Γ_{Fc}	% of maximum coverage
1.	$2.8 \pm 0.3 \times 10^{-10}$ mol cm^{-2}	62%
2.	$1.8 \pm 0.3 \times 10^{-10}$ mol cm^{-2}	40%
3.	$5.3 \pm 0.2 \times 10^{-11}$ mol cm^{-2}	12%
3a.	$7.0 \pm 0.2 \times 10^{-11}$ mol cm^{-2}	15%

Method 2 produces lower surface concentrations compared to Method 1 but does not require an inert atmosphere. Applying an inert atmosphere to Method 2 may result in Γ_{Fc} values closer to Method 1. Surprisingly, the Γ_{Fc} value for Method 3a ($5.3 \pm 0.2 \times 10^{-11}$ mol cm^{-2}) was higher than Method 3, where a fixed potential was applied. Method 3 yielded the lowest in Γ_{Fc} value for all of the methods explored. This method was included in the study as an investigation into electrochemically mediated reactions, which will be explored more thoroughly in Chapter 5.

3.3.3.2.4. Atomic Force Microscopy and Depth Profiling of Modified PPF Surfaces

Atomic force microscopy (AFM) topography images and film thickness measurements confirmed the presence and deprotection of the grafted layers on a pyrolysed photoresist film (PPF) surface. Topography images of an unmodified PPF surface are shown in Figure 3.19. The average surface roughness (R_q) value is taken from the topography image is calculated to be 0.7 ± 0.1 nm. (R_q values represent the surface roughness of the film excluding the high protrusions observed in the topography images). This roughness value is typical for PPF.[43]

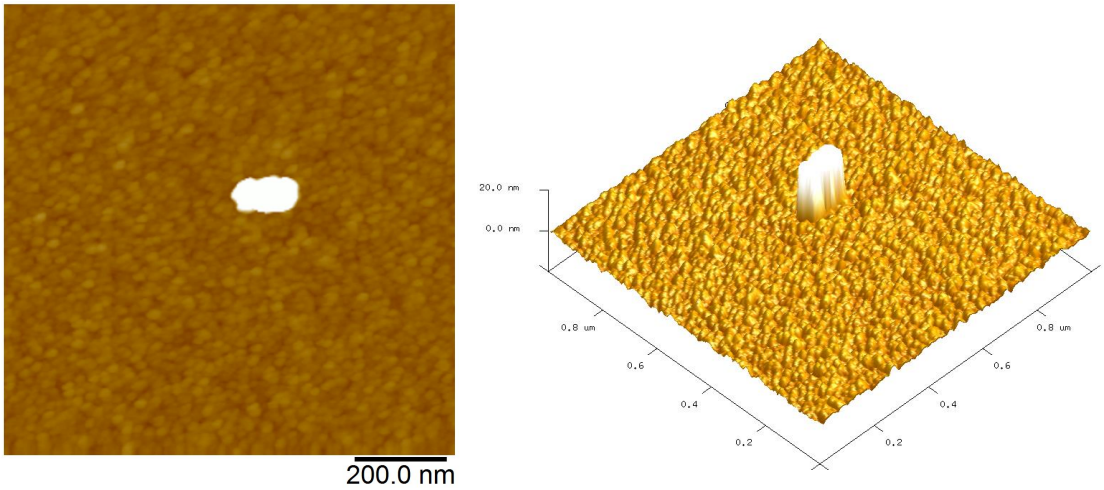

Figure 3.19. AFM topographical images of unmodified PPF. Scan size = 1 × 1 μm.

After electrochemical grafting of an Ar-Eth-TIPS film to the surface (Step 1, Scheme 3.5), the modified surface was re-imaged (Figure 3.20), with R_q increasing to 0.9 ± 0.1 nm. The very small increase in roughness after the grafting of the Ar-Eth-TIPS layer shows how uniform the film growth through this method is. The average film thickness of the Ar-Eth-TIPS film was measured by scratching a 2.5 μm × 10 μm channel through the layer with an AFM tip and profiling perpendicularly across the scratch to measure its depth (Figure 3.21) (details of the profiling technique are given in Chapter 2.5). Average thickness was estimated from 24 values obtained from three individual scratches made in different positions on the modified film, with each scratch contributing eight individual depth measurements.

The average film thickness for the Ar-Eth-TIPS modified surface was estimated to be 3.1 ± 0.4 nm, corresponding to roughly 3 layers when 1.1 nm is used as the calculated molecular dimensions for the Ar-Eth-TIPS groups (Figure 3.22 (a)). Leroux *et al.* estimated the thickness of the Ar-Eth-TIPS film they electrodeposited to be 2.06 ± 0.5 nm,[50b] corresponding to two layers when a molecular dimension of 1.01 nm was used (the discrepancy in the molecular dimensions can be attributed to the inclusion of the bond between the aryl modifier and the surface). The cause in the difference in film thickness is

uncertain but may be attributed to differences in the concentration of aryl diazonium salt used during grafting (10 mM used by Leroux and co-workers, 1 mM used in this work) or in AFM scratching, imaging or processing.

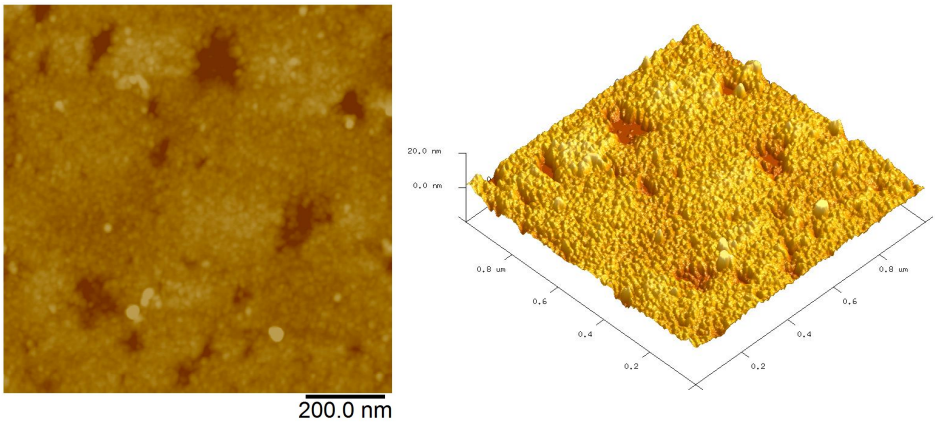

Figure 3.20. AFM topographical images of Ar-Eth-TIPS film on PPF. Scan size = 1 × 1 µm.

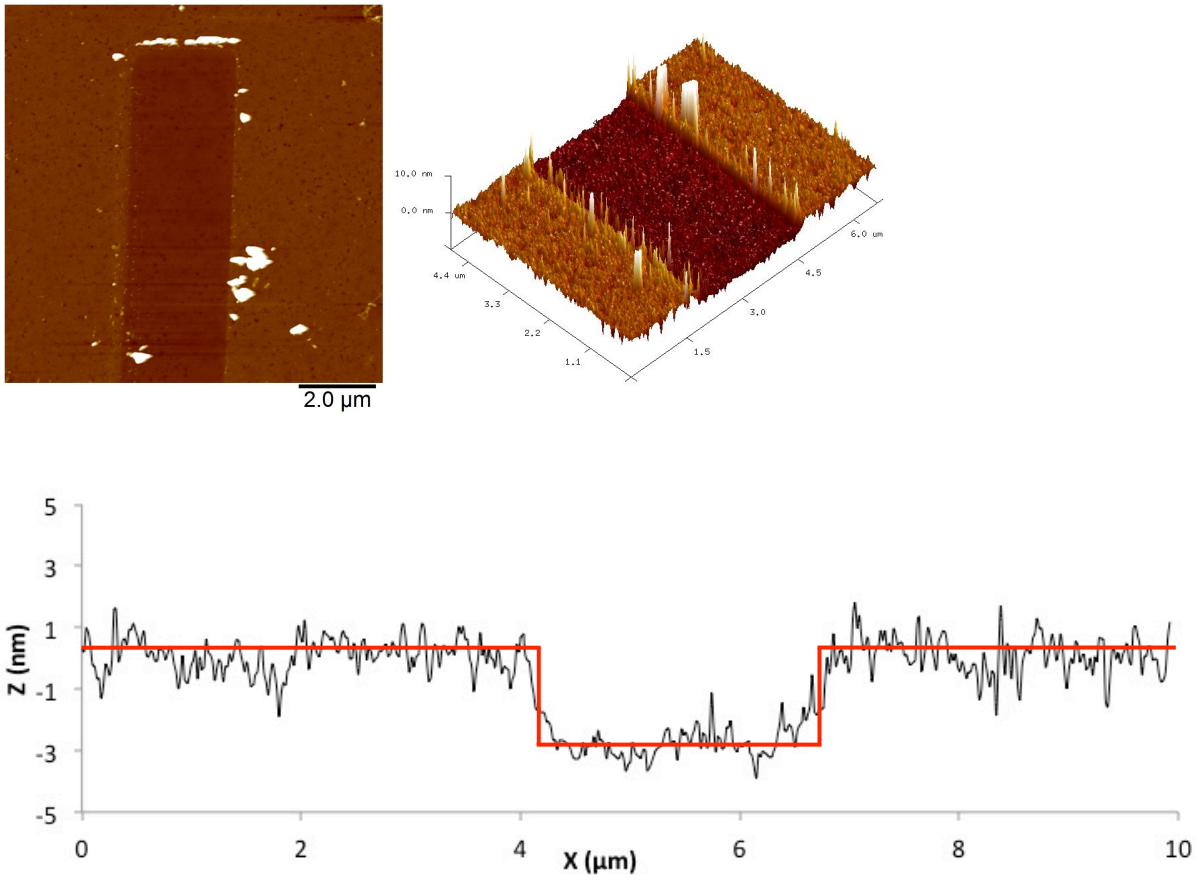

Figure 3.21. AFM topographical image of PPF substrate modified with an Ar-Eth-TIPS film showing a 2.5 × 10 µm scratch (top) and a line profile (black) with a fitted line (red) orthogonal to the scratch.

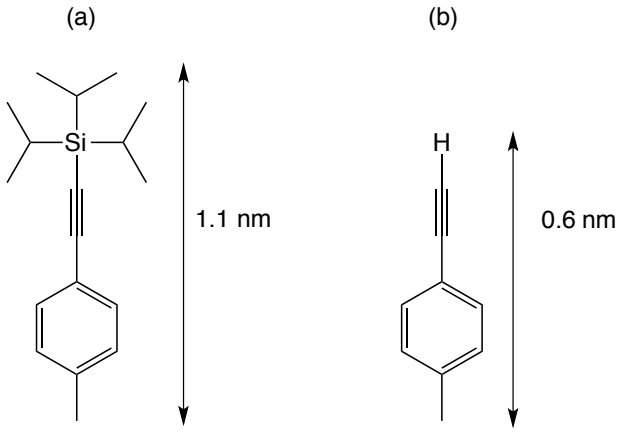

Figure 3.22. Molecule constituting the grafted Ar-Eth-TIPS (a) and Ar-Eth (b) layers on PPF substrate and their average lengths calculated with *Avogadro freeware*.

After the removal of the TIPS protecting group (Step 2, Scheme 3.4), the modified surface was once again imaged (Figure 3.23). The R_q value for the Ar-Eth modified PPF surface is essentially unchanged from the Ar-Eth-TIPS modified surface (0.9 ± 0.1 nm) with $R_q = 0.8 \pm 0.1$ nm. The same depth profiling technique used for the calculation of the average film thickness for Ar-Eth-TIPS film was applied to the Ar-Eth film. The scratch images and line profile can be seen in Figure 3.24. The average film thickness is estimated to be 0.7 ± 0.1 nm. This value is in good agreement with the Ar-Eth film depth estimated by Leroux *et al.* of 0.65 ± 0.18 nm. Both these values correspond to a monolayer when using the dimensions calculated for the Ar-Eth molecule (Figure 3.22). The reduction in film thickness after treating the Ar-Eth-TIPS surface with tetra-n-butylammonium fluoride (TBF)/THF (Scheme 3.4) is good evidence for the removal of the TIPS protecting group.

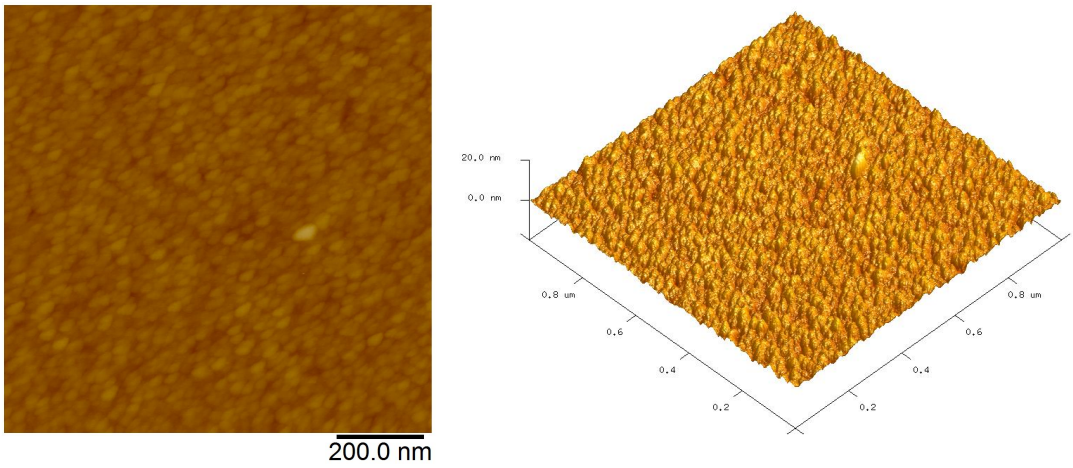

Figure 3.23. AFM topographical images of Ar-Eth film on PPF. Scan size = 1 µm × 1 µm.

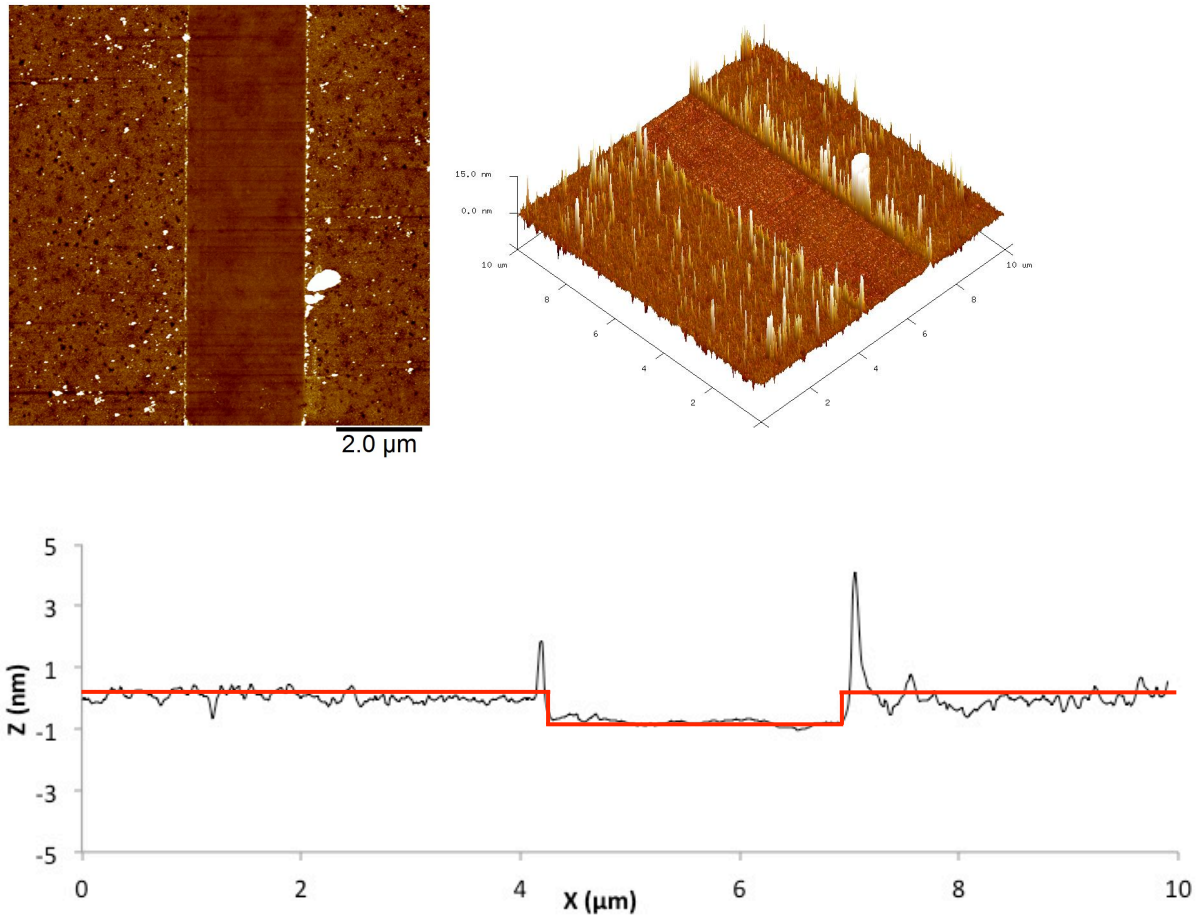

Figure 3.24. AFM topographical image of a PPF surface modified with an Ar-Eth film showing a 2.5 × 10 µm scratch (top) and a line profile (black) with a fitted line (red) orthogonal to the scratch.

The average surface roughness R_q values for the unmodified and modified PPF surfaces are listed in Table 3.8, along with the estimated film thickness for the modified surfaces.

Table 3.8. Average surface roughness, R_q, and film thickness for films on PPF.

	Bare PPF	Ar-Eth-TIPS	Ar-Eth
R_q (nm)	0.7 ± 0.1	0.9 ± 0.1	0.8 ± 0.1
Film thickness (nm)		3.1 ± 0.4	0.7 ± 0.1

The average film thicknesses for the modified layers are shown in Table 3.10. Average thickness was calculated from 24 values obtained from three individual scratches made in different positions on the modified film, with each scratch contributing eight individual depth measurements.

3.3.3.2.5. X-ray Photoelectron Spectroscopy Analysis

The surface resulting from the CuAAC reaction between APBiB and the Ar-Eth monolayer was analysed by XPS and compared with data obtained from an unmodified, polished GC plate.

Survey spectra were obtained for polished GC and the Ar-Tri-APBiB modified surface giving the data shown in Table 3.9. After the coupling of APBiB to the Ar-Eth monolayer (Scheme 3.7), 0.7% of the surface was identified as bromine. This is strong evidence for the successful coupling of APBiB to the Ar-Eth layer. The bromine percentage is similar to that detected in the Ar-CONH-ABiB film (0.5%) and that observed by Iruthayarj *et al*. (0.04 – 2.94%).[100]

Table 3.9 XPS survey data for the polished and modified GC plates.

Sample	Atomic%			
	C	**N**	**O**	**Br**
Polished GC	93.0	0.7	6.3	
Ar-Tri-APBiB	84.3	3.9	11.1	0.7

XPS data and analysis for the unmodified GC surface can be found earlier in the chapter. The wide scan spectrum for the Ar-Tri-APBiB modified GC surface is shown in Figure 3.25a.

The C1s narrow scan spectrum (Figure 3.25 (b)) was fitted with four peaks, with the peak at 289.2 eV increasing in size compared to the unpolished GC surface (Figure 3.11 (b)). The narrow scan of the N1s region (Figure 3.25 (c)) shows a broad peak fitted with two peaks at 400.4 and 401.8 eV. This broad nitrogen peak can be indicative of a triazole formation as observed by Ciampi *et al.*[136] No traces of adsorbed azide species at high energy (>404.0 eV) were observed. The narrow scan spectrum in the O1s region (Figure 3.25 (d)) was fitted with two peaks at 532.4 and 533.7 eV. The increase in atomic percentage of the lower energy peak is thought to be due to the carbonyl and ester groups from APBiB. Perhaps the strongest evidence for the successful click reaction of APBiB to the Ar-Eth monolayer comes from the observance of bromine in the survey scan and in the narrow scan of the Br3d region (Figure 3.25 (e)). The shoulder peak at 68.3 eV is attributed to Br (3d5/2) and was also observed for the Ar-CONH-ABiB modified GC surface. The narrow scan XPS data for the Ar-Tri-APBiB modified surface is tabulated in Table 3.10.

Table 3.10. Binding energies, assignments and atomic% for the C1s, N1s and O1s XPS narrow scan spectra for the Ar-Tri-APBiB film on GC.

	Binding Energy (eV)	Atomic%	Assignment	Ref.
C1s	284.7	45.5	Aromatic C	[133]
	285.4	24.5	C-C, C-C (sp^2), C-C (sp^3)	[133,134]
	286.5	23.5	C-N, C-O, C-COOR	[133,134]
	289.2	6.5	CO-C=O, C=O	[133,134]
N1s	400.4	69.3	C-N, N=N, surface N	[136]
	401.8	30.7	C-N, N=N, surface N	[136]
O1s	532.4	63.1	>C=O, -C-O-C-	[135]
	533.7	36.9	Surface >C-OH, adsorbed CO, adsorbed O_2, bound H_2O	[135]
Br3d	68.3	12.8	Br (3d 5/2)	
	70.9	87.2	Br (3d)	

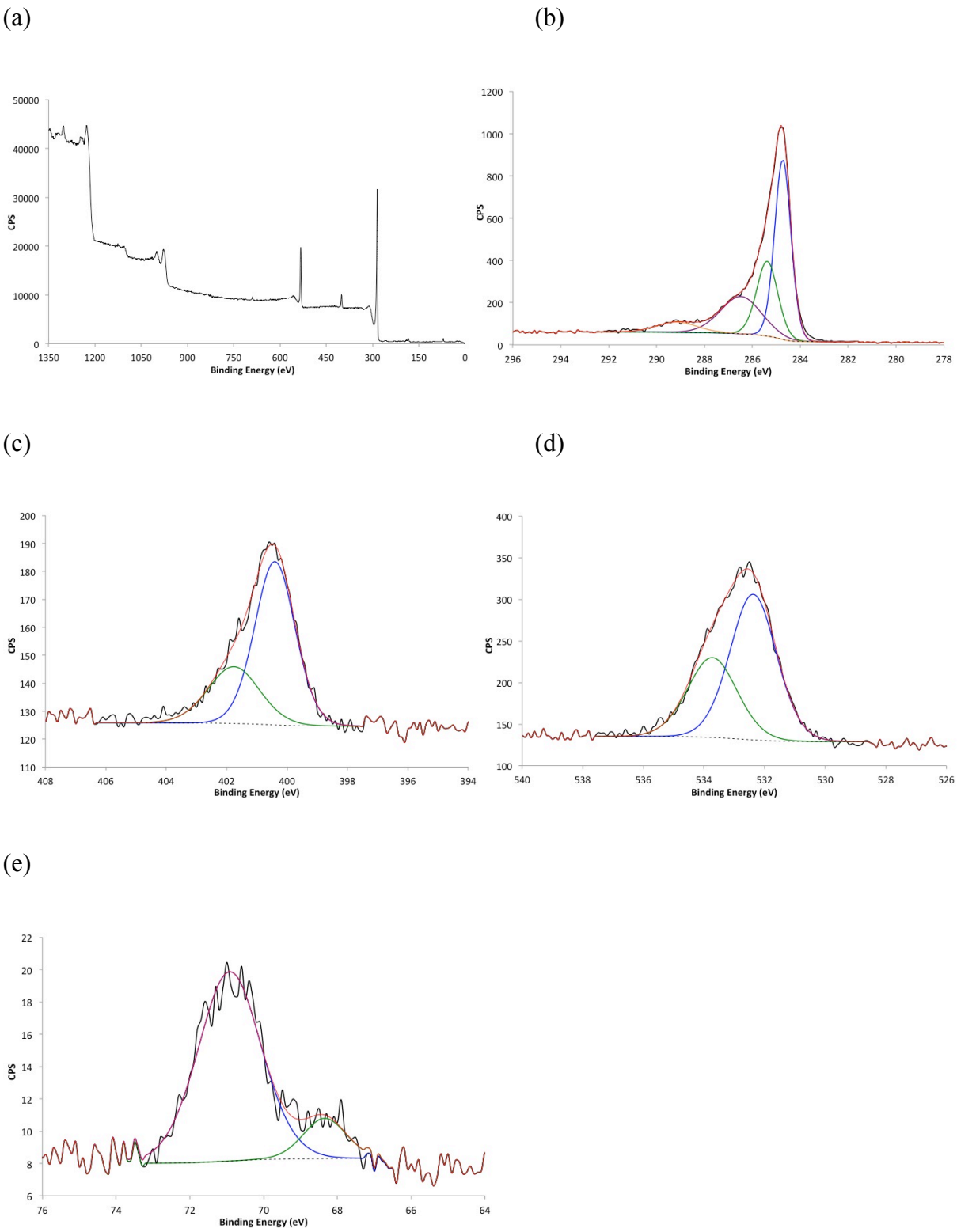

Figure 3.25. XPS spectra obtained from Ar-Tri-APBiB film on GC: wide scan (a) and narrow scan spectra for C1s (b), N1s (c), O1s (d) and Br3d (e) regions. The black lines are the experimental spectra recorded and the coloured lines represent those used for peak fitting.

3.4. Conclusion

Polymerisation initiators were coupled to monolayers derived from the electrochemical grafting of aryl diazonium salts. Monolayers were sought after to retain the substrates bulk properties and topography, and to provide a well-organised layer for polymer brush growth.

Ar-COO-Fm and subsequent films were characterised by redox probe voltammetry and water contact angle measurements. After the removal of the Fm protecting group, the resulting Ar-COOH film was identified as a monolayer by the redox probe voltammetry response and the films pH dependency. Evidence for the successful coupling of the polymerisation initiator, ABiB, was provided by XPS analysis. The procedure for preparing the Ar-CONH-ABiB film has multiple surface modification steps, and while successful, the coupling reactions appear to have low efficiency.

Ar-Eth-TIPS and subsequent films were characterised by redox probe voltammetry, water contact angle measurements, AFM imaging and depth profiling, and XPS analysis. Depth profiling through AFM scratching indicated an Ar-Eth monolayer after removal of the TIPS protecting group. An azide functionalised ATRP initiator, APBiB, was coupled to the Ar-Eth monolayer *via* click chemistry. Evidence for the successful coupling was given by XPS analysis.

Both the Ar-CONH-ABiB and Ar-Tri-APBiB monolayers are covalently tethered to the substrate. These polymerisation initiators are excellent candidates for surface-initiated atom transfer radical polymerisation, and hence will be used in Chapter 5 for growth of polymer brushes.

Chapter 4. Direct Reactions with Glassy Carbon for the Attachment of a Polymerisation Initiator

4.1. Introduction

The previous chapter describes strategies for attachment of polymerisation initiators to GC, based on the electrochemical grafting of aryl diazonium salts. This chapter explores the attachment of polymerisation initiators through reactions of amines, carboxylic acids, and acid chlorides with GC. Using specific modifiers and reaction conditions can promote exclusive, single step reactions with the surface but not with grafted groups, producing monolayer films on carbon substrates.[15] A monolayer film is desired for a well-defined layer from which further surface chemistry can take place. However, as these reactions rely on oxygen functionalities on the substrate surface, there is a lack of control over the spacing of the attached groups.

As discussed in Chapter 1, in earlier studies undertaken in the 1970s and 1980s, deliberate oxidation of carbon substrates was used to increase the surface oxide or carboxylic acid concentrations for the reaction with amines in the presence of activating agents to give amide-coupled modifiers.[22,137,12] However, the oxidation of carbon substrates can lead to undesirable larger capacitances and unknown surface area.[15] More recently, Gallardo *et al.* described the spontaneous attachment of primary amines to carbon surfaces.[14] The proposed reaction mechanism is through a Michael-like addition (Scheme 1.1, Chapter 1), with the amine derivative attacking a double bond of GC and electron delocalisation across the aromatic GC framework. Lee and Downard coupled ferrocene (Fc) derivatives to GC through direct reactions.[15] The attachment of an amine derivative of Fc was consistent with the work by Gallardo *et al*. In another approach, Lee and Downard activated GC surfaces by the

conversion of carboxylic acid groups to acid chlorides, followed by the reaction with various functionalised Fc derivatives (Scheme 1.2, Chapter 1). Finally, acid chloride derivatives of Fc, ferrocenoyl chloride (FcCOCl), were reacted with hydroxyl groups on the GC surface, producing an ester linker.[15]

In the present work, use of these pathways for covalently attaching polymerisation initiators is investigated. For method development, Fc derivatives have been used in place of polymerisation initiators. The immobilisation of Fc derivatives is easy to monitor electrochemically whereas detection and quantification of surface immobilised polymerisation initiators is much more challenging.

The polymerisation initiator derivatives used in this work are shown in Figure 4.1: (a) α-bromoisobutyryl bromide (ABiB), (b) α-bromoisobutyric acid (ABiA) and (c) α-bromoisobutyric chloride (ABiC). The synthesis of ABiA and ABiC can be found in Chapter 2.

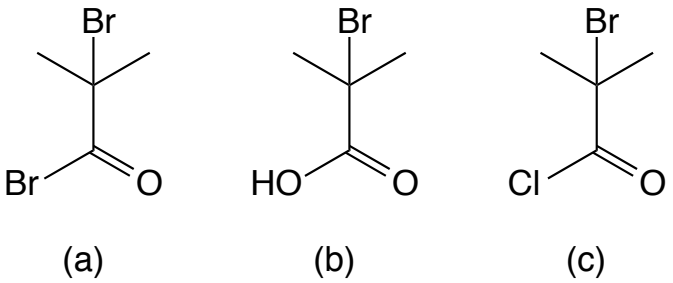

Figure 4.1. Polymerisation initiators used in this work: (a) ABiB, (b) ABiA and (c) ABiC.

4.2. Experimental

4.2.1. Conversion of Carboxylic Acids to Acid Chlorides

Carboxylic acid derivatives were converted to acid chlorides through the procedure described in Chapter 2.3.2.4. This method was applied to ABiA, FcCOOH, and GC electrodes, which were assumed to have surface carboxylic acid groups.

4.2.2. Reactions with Glassy Carbon Surfaces

The details for the modification of GC surfaces by direct reaction with modifiers or Fc derivatives are given in Chapter 2. All modifications were conducted on GC disk electrodes (surface area = 0.071 cm^2), except for the samples analysed by XPS, which were conducted on GC plate electrodes (surface area = 0.709 cm^2).

4.2.3. Cyclic Voltammetry

Electrochemical analysis of Fc coupled electrodes

CVs of immobilised Fc groups were obtained in a solution of 0.1 M $LiClO_4$ in ethanol at a scan rate of 200 mV s^{-1}. The modified GC electrode was used as the working electrode. A Pt mesh auxiliary electrode and a calomel reference electrode (1 M LiCl) were used for all immobilised Fc electrochemistry experiments. Surface concentrations of immobilised Fc (Γ_{Fc}) were calculated from these CVs (details in Chapter 2.5).

Redox probe voltammetry

All redox probe voltammetry experiments were conducted in a pear-shaped electrochemistry cell using a PBS (pH 7) solution containing 1 mM $K_3Fe(CN)_6$ with a Pt mesh auxiliary electrode and a SCE reference electrode.

4.3. Results and Discussion

4.3.1. Modification of GC with activated FcCOOH

The reaction of acid chloride derivatives with polished GC was tested using FcCOCl. The proposed reaction mechanism for the attachment of Fc is given in Scheme 4.1 (repeated from Chapter 1 for convenience). FcCOCl is expected to react with surface hydroxyl groups, forming an ester linkage.[15] Surface carboxylic acid groups may also react, forming anhydride linkers, however the majority of the oxygen functionalities on GC are reported to be hydroxyl groups.[138,139,140]

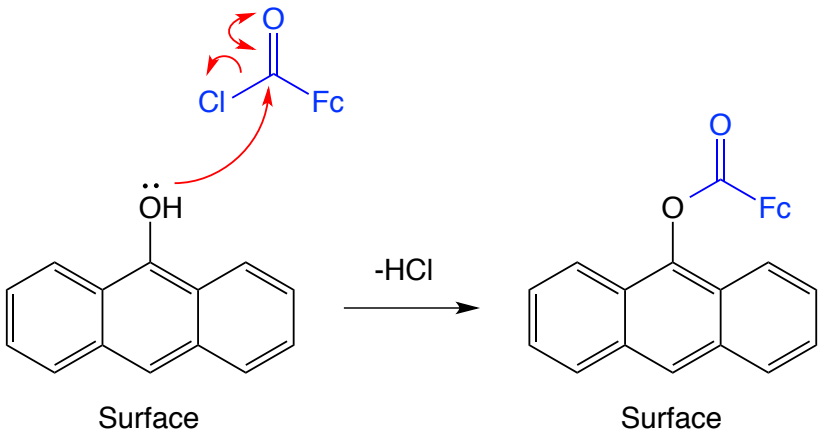

Scheme 4.1. Proposed mechanism for the reaction of GC with FcCOCl.

As Fc groups are electroactive through the Fc/Fc^+ couple, electrochemistry is a powerful tool for the analysis of the immobilised molecules. The reversible redox peaks of the immobilised Fc/Fc^+ couple can be seen in the CV of Figure 4.2, confirming the successful immobilisation of the modifier. The CV obtained is consistent with those observed by Lee and Downard using the same system.[15] From this CV, Γ_{Fc} was calculated to be $9.7 \pm 0.1 \times 10^{-11}$ mol cm^{-2} (n (number of replicate samples) = 4). This value is lower than that of Lee and Downard ($1.6 \pm 0.2 \times 10^{-10}$ mol cm^{-2}),[15] which may be attributed to variation in the GC sample and surface condition. It is also significantly lower than the theoretical amount of Fc that can be

close-packed on a planar surface (4.5×10^{-10} mol cm^{-2}).[131] Hence it is assumed that $9.7 \pm 0.1 \times 10^{-11}$ mol cm^{-2} approximately represents the surface concentration of groups on the GC surface that can be reacted with acid chlorides.

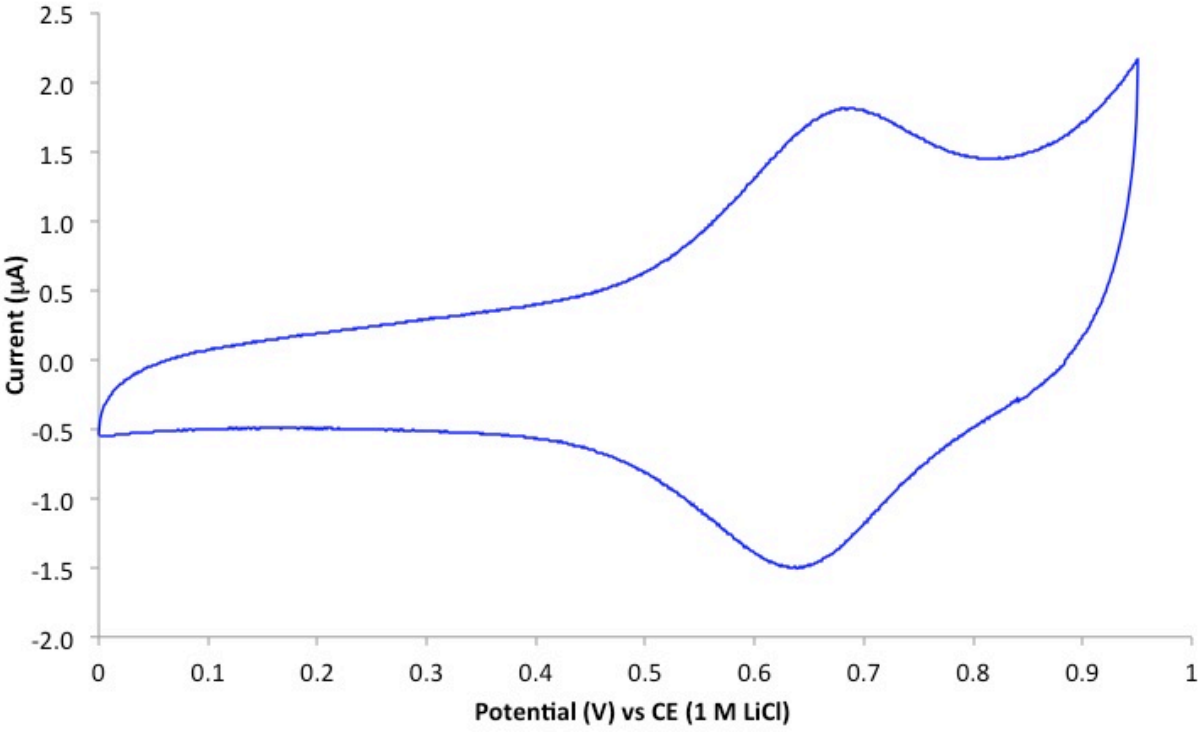

Figure 4.2. Second scan CV in 0.1 M $LiClO_4$ –EtOH of a GC electrode after modification with FcCOCl. Scan rate = 200 mV s^{-1}.

4.3.2. Modification of GC with α-Bromoisobutyric Chloride (ABiC)

The strategy for the reaction of carboxylic acid derivatives with GC was applied to couple the polymerisation initiator, α-bromoisobutyryl chloride (ABiC) to GC. The ABiC was formed in-situ through the reaction of ABiA with oxalyl chloride ($(COCl)_2$) (Scheme 4.2), then was reacted with a freshly polished GC electrode; the reaction details are given in Chapter 2.3.2.4. A proposed mechanism for the reaction between the surface hydroxide groups of GC and ABiC to give the ester-tethered groups, α-bromoisobutyryl ester (ABiE), is shown in

Scheme 4.3. Note, as there are many oxygen functional groups on the surface of GC, this is only one possible method of attachment.

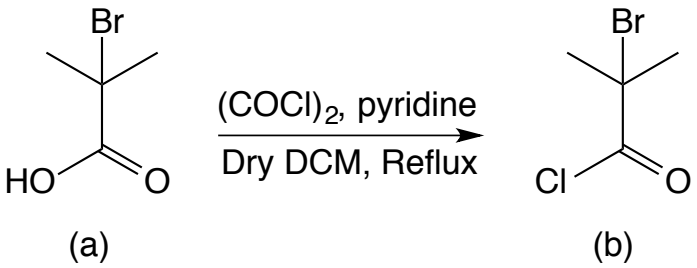

Scheme 4.2. Synthesis of ABiC (b) by treatment of ABiA (a) with $(COCl)_2$.

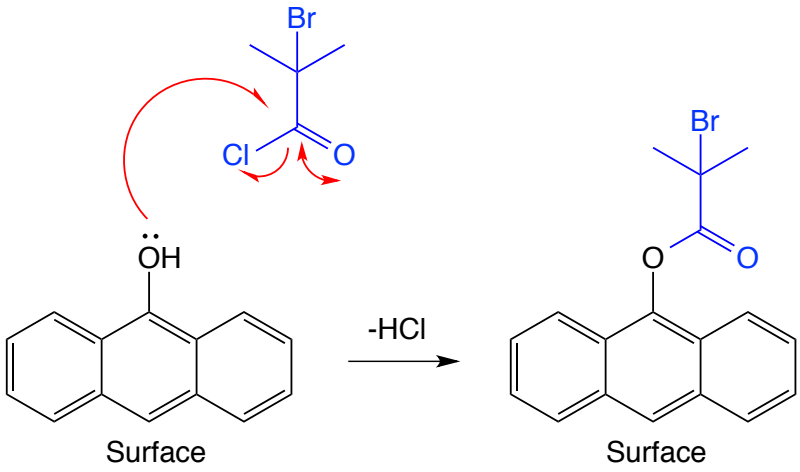

Scheme 4.3. Proposed mechanism for reaction of GC with ABiC giving the ester ABiE**.**

4.3.2.1. Characterisation of the ABiE layer though Fc coupling

As the immobilised polymerisation initiator is not electroactive, the film cannot be directly characterised through electrochemistry. Hence, an indirect method was used to estimate the amount of ABiE attached to the surface. It was assumed that after reaction with ABiC, residual acid chloride-reactive groups on GC would react with FcCOCl

After reacting the ABiE-modified surface with FcCOCl, the CV (red line) shown in Figure 4.3 was obtained. The reversible redox peak of the immobilised Fc/Fc^+ couple can be seen and the amount of immobilised Fc is clearly significantly less than at polished GC (blue line).

The Γ_{Fc} of the ABiC modified surface was calculated to be $2.0 \pm 0.8 \times 10^{-11}$ mol cm^{-2} ($n = 4$). Assuming ABiC and FcCOCl react with the same surface functionalities, subtraction of $\Gamma_{Fc(ABiC)}$ from $\Gamma_{Fc(polished\ GC)}$ ($9.7 \pm 0.1 \times 10^{-11}$ mol cm^{-2}) gives an estimated surface concentration of polymerisation initiator molecules $\Gamma_{initiator} = 7.7 \pm 0.9 \times 10^{-11}$ mol cm^{-2}.

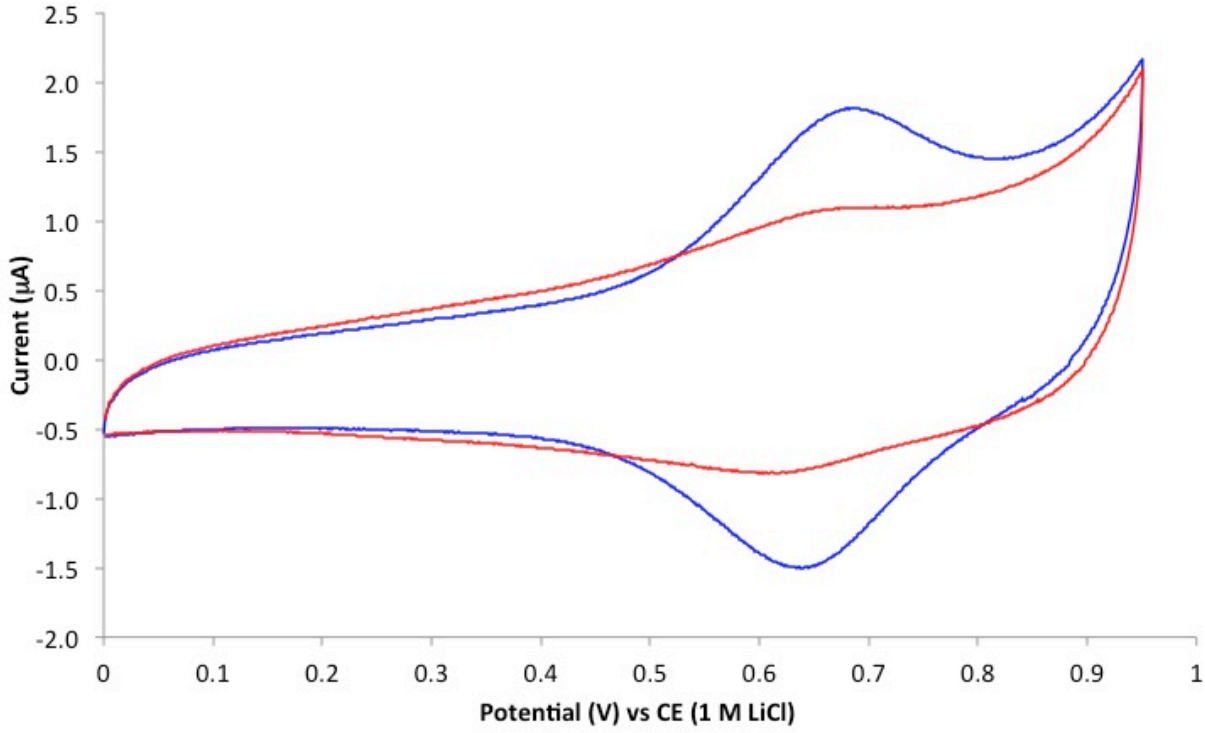

Figure 4.3. Second scan CV in 0.1 M $LiClO_4$ –EtOH of a GC electrode after modification with FcCOCl (blue line) and after modification with ABiC followed by FcCOCl (red line). Scan rate = 200 mV s^{-1}.

4.3.3. Modification of Activated GC with α-Bromoisobutyric acid (ABiA)

In a similar but reversed approach to that described in section 4.3.1, a polymerisation initiator was reacted directly with an activated GC surface. The GC surface was activated by treatment with $(COCl)_2$, converting surface carboxylic acid groups to acid chlorides, and increasing the reactivity of the surface (Step 1 in Scheme 4.4). The second step in this modification procedure was the reaction between the surface acid chloride groups and the carboxylic acid

derivative of the polymerisation initiator, ABiA (Step 2 in Scheme 4.4). The proposed mechanism involves the formation of an anhydride linker.

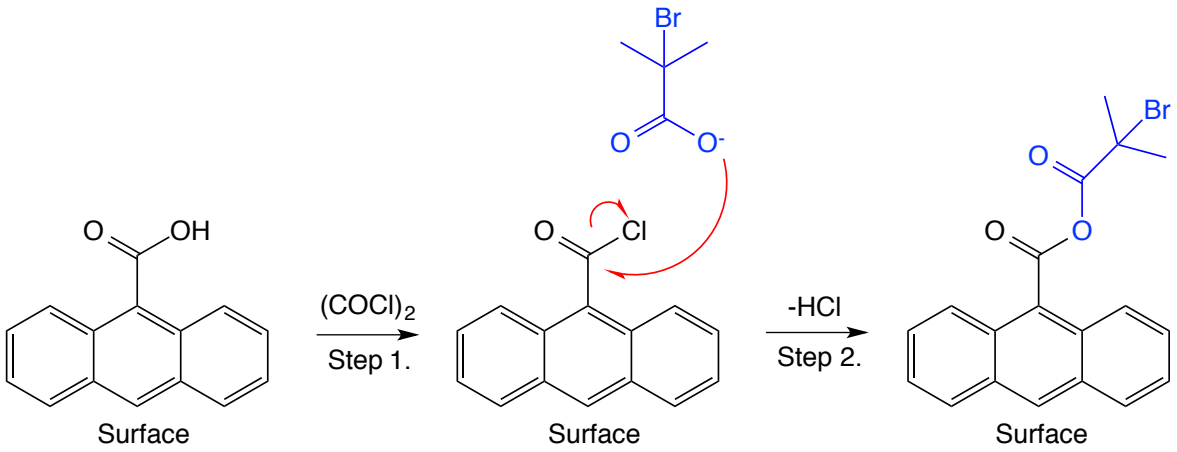

Scheme 4.4. Proposed pathway for activation of GC with $(COCl)_2$ and the reaction with ABiA.

4.3.3.1. Characterisation of the ABiE layer through Fc coupling

After reacting activated GC with ABiA, the modified surface was reacted with FcCOCl to assess the success of the ABiA modification procedure (note, after reaction of the activated surface with ABiA, the modified electrode was subjected to a series of cleaning steps that include sonication in water. This step would convert any activated surface oxides to their original form). A CV of the modified electrode obtained after the described reactions is shown in Figure 4.4. The CV (red line) shows a greatly reduced Fc/Fc^+ signal in comparison to that obtained when a polished electrode is reacted with FcCOCl (Figure 4.4, blue line). Γ_{Fc} was calculated to be $2.9 \pm 1.0 \times 10^{-11}$ mol cm^{-2} (n = 4). This is a three-fold decrease in Γ_{Fc} when compared to the polished GC ($9.7 \pm 0.1 \times 10^{-11}$ mol cm^{-2}), indicating the previously reacted ABiA groups have coupled to the reactive sites. This gives an estimated $\Gamma_{initiator} = 6.9 \pm 1.1 \times 10^{-11}$ mol cm^{-2}.

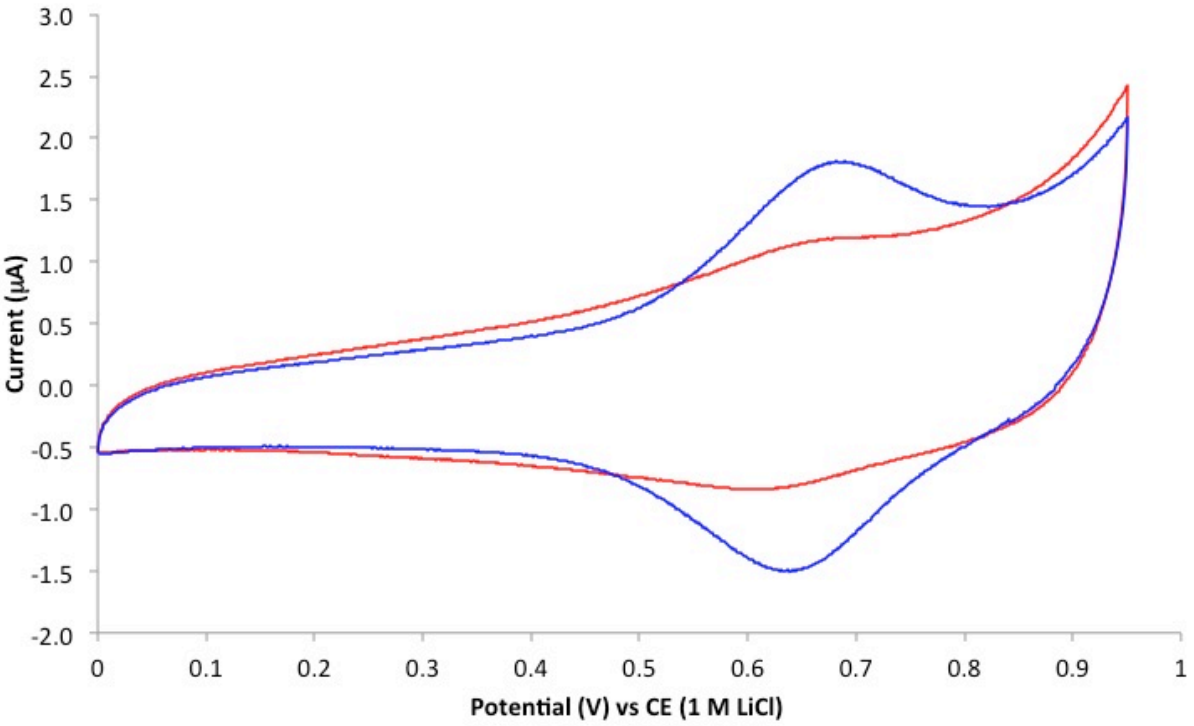

Figure 4.4. Second scan CV in 0.1 M $LiClO_4$ –EtOH of a GC electrode after modification with FcCOCl (blue line) and after modification of activated GC with ABiA followed by FcCOCl (red line). Scan rate = 200 mV s^{-1}.

4.3.3.2. XPS Analysis

XPS analysis was used to investigate the coupling of ABiA to the GC surface by the method shown in Scheme 4.4. The atomic composition of polished GC (2 samples) and modified GC was obtained from survey spectra; the data is shown in Table 4.1. Surprisingly, the survey data indicated that no bromine was present in the modified sample, raising the possibility that the proposed modification reaction had not occurred. However, the change in the O/C ratio after reaction suggests that the surface has been modified. The average O/C ratio for the polished GC surface was 0.075, while after modification with ABiA, the O/C ratio of the sample was 0.15. The ABiA modifier has an O/C ratio of 0.25, and although the ratio observed for the modified GC sample was significantly lower than this, the sampling depth for the XPS will lead to the inclusion of a significant proportion of bulk C, lowering the O/C ratio. This increased O/C ratio suggests that the surface has been modified with the

polymerisation initiator, even if no Br was identified on the surface. The lack of bromine may be due to its lability under the XPS conditions. The small amount of N detected for the modified sample is assumed to come from the GC underlying substrate and adventitious impurities.

Table 4.1. XPS survey data for polished GC and an ABiA-modified GC sample.

Sample	**Atomic%**			
	C	**N**	**O**	**O/C**
Polished GC	93.0	0.7	6.3	0.07
	91.7	0.8	7.5	0.08
ABiA-modified	85.5	1.3	13.2	0.15

4.3.4. Spontaneous Modification of GC with Ethanolamine

Alkylamines have been shown to spontaneously react with GC surfaces.[14] The reaction is proposed to proceed through a Michael-like addition reaction, shown in Scheme 4.5 (repeated from Scheme 1.1 for convenience), with the amine attacking the double bonds of GC with electron delocalization across the aromatic GC network. The addition of a primary amine to a GC substrate has the potential to introduce new functionalities to the surface.

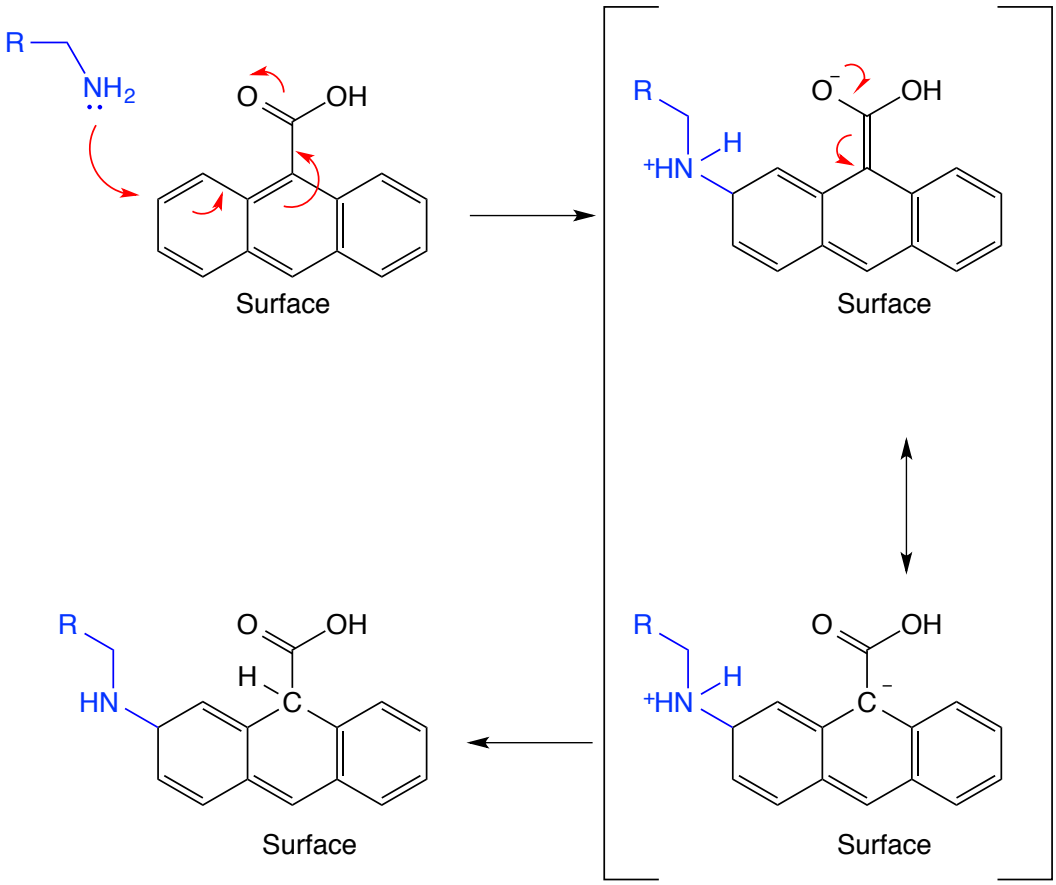

Scheme 4.5. Proposed mechanism for the reaction of an amine with GC surface via a Michael-like addition. Reproduced from reference 15.[15]

In this work, ethanolamine has been reacted with GC to increase the surface concentration of hydroxyl groups (Step 1, Scheme 4.6). The hydroxyl groups can then be reacted with ABiB (Step 2, Scheme 4.6). After each modification step, the surface was characterised by investigating the effect of the modification on the amount of Fc that could be coupled to the surface, and by redox probe voltammetry to confirm the presence of a blocking film.

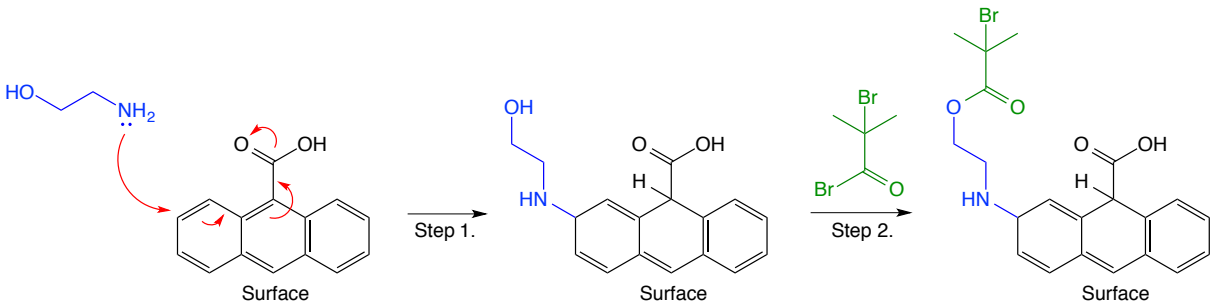

Scheme 4.6. Proposed mechanism for the reaction of ethanolamine with GC surface via Michael-like addition and the esterification between the resulting surface and ABiB.

4.3.4.1. Effect of Modification with Ethanolamine on Redox Probe Voltammetry

The presence of the ethanolamine film on the GC electrode was studied using redox probe voltammetry. Figure 4.5 shows two CV scans obtained in $K_3Fe(CN)_6$ in a PBS (pH 7) solution: the blue line is the unmodified GC electrode, while the red line is the GC electrode modified with ethanolamine. Interestingly, the ethanolamine modified surface shows an increase in peak current and a decrease in ΔE_p. This suggests that the coupling of ethanolamine to the GC surface does not produce a blocking film that would inhibit electron transfer from the electrode surface to the redox species in solution. The increased peak current can be attributed to the electrostatic contributions caused by protonation of the secondary amine at pH 7 (pKa diethylamine = 10.7).[141] The anionic $Fe(CN)^{3-}$ is expected to be accumulated at the modified surface leading to increased peak currents. This provides good evidence for the successful coupling of ethanolamine to the GC surface.

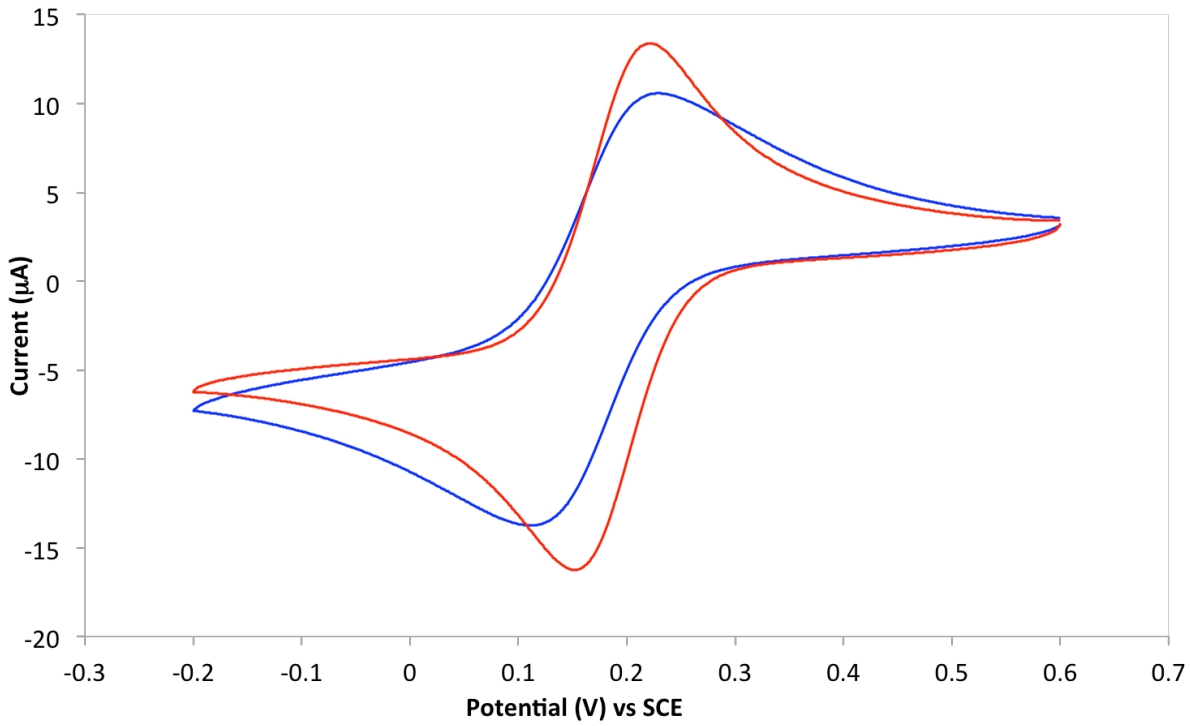

Figure 4.5. CV of 1 mM $K_3Fe(CN)_6$ in PBS (pH 7) showing the effect of ethanolamine modification of GC. Scan rate = 100 mV s^{-1}. The blue line is a scan taken before the reaction with ethanolamine and the red line is a scan taken after reaction with ethanolamine.

4.3.4.2. Effect of Modification with Ethanolamine on Fc Coupling

The effect of the modification of GC electrode with ethanolamine was tested through the coupling of FcCOCl. The reaction is expected to occur analogously to that in Scheme 4.1, but with the reaction of tethered hydroxyl groups in addition to those on the GC surface. Figure 4.6 (red line) shows a CV of the surface modified with ethanolamine and reacted with FcCOCl, and of a polished GC surface reacted with FcCOCl (blue line). The CV of the ethanolamine-modified electrode shows the reversible redox couple of Fc/Fc^+ and an increase in peak current compared to the polished GC modified with FcCOCl, confirming the successful coupling of Fc to the surface.

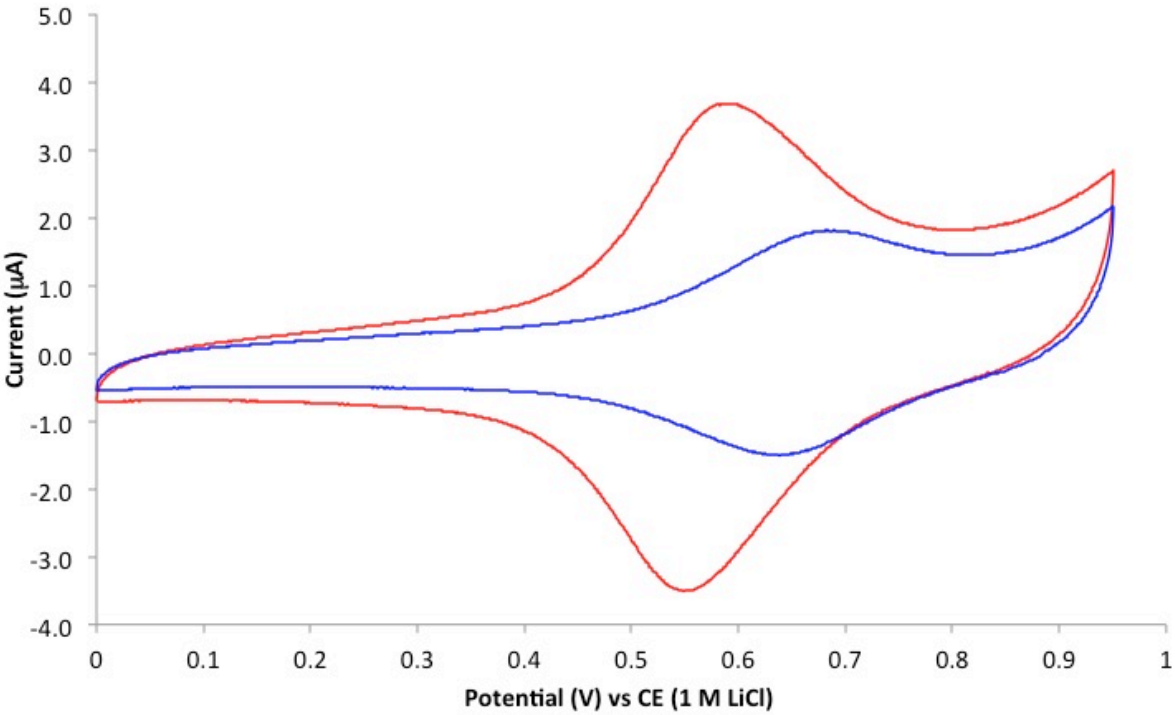

Figure 4.6. Second scans of CVs in 0.1 M $LiClO_4$ –EtOH of a polished GC electrode after modification with FcCOCl (blue line) and a GC surface after modification with ethanolamine and FcCOCl (red line). Scan rate = 200 mV s^{-1}.

With an increase in the number of terminal hydroxyl groups which can react with the activated Fc derivative forming ester linkers, Γ_{Fc} is expected to increase compared to the same reaction with an unmodified GC surface. The calculated value for Γ_{Fc} after modification with ethanolamine was $2.5 \pm 0.5 \times 10^{-10}$ mol cm^{-2} (n = 3). This corresponds to more than twice as many surface immobilised Fc molecules when compared to the reaction with polished GC ($\Gamma_{Fc} = 9.7 \pm 0.1 \times 10^{-11}$ mol cm^{-2}), indicating that the ethanolamine reaction with GC reaction was successful. Figure 4.6 shows that $E_{1/2}$ for the Fc/Fc^+ couple at the ethanolamine-modified electrode is less positive than that of the polished electrode. When coupled to ethanolamine the electron donating ethylene group will make the oxidation of Fc thermodynamically easier, accounting for the negative shift in $E_{1/2}$. Taking this into account, it is clear from the CV of the ethanolamine modified electrode in Figure 4.6 that the majority of the Fc groups are

coupled to ethanolamine. However, the asymmetric shape of the peaks suggests that there may also be a contribution from Fc coupled directly to surface hydroxyl groups This contribution has not been quantified but appears to be small.

4.3.4.3. Effect of Modification with Ethanolamine and ABiB on Redox Probe Voltammetry

The coupling of ABiB to the ethanolamine-modified surface was studied using redox probe voltammetry. Figure 4.7 shows three CV scans obtained in $K_3Fe(CN)_6$: the blue line is a scan of the unmodified GC electrode, the red line is a scan of the GC electrode modified with ethanolamine and the green line is a scan of the electrode after modification with ethanolamine and ABiB. Only a slight decrease in peak current between the ethanolamine/ABiB modified surfaces was observed. This indicates that after coupling ABiB, the film does not hinder electron transfer significantly more than the ethanolamine film. This suggests that the surface concentration of ABiB molecules is likely to be low. As with the ethanolamine-modified surface, the peak currents are greater than at the unmodified electrode due to the electrostatic attractions between the protonated amine modified and the anionic redox probe.

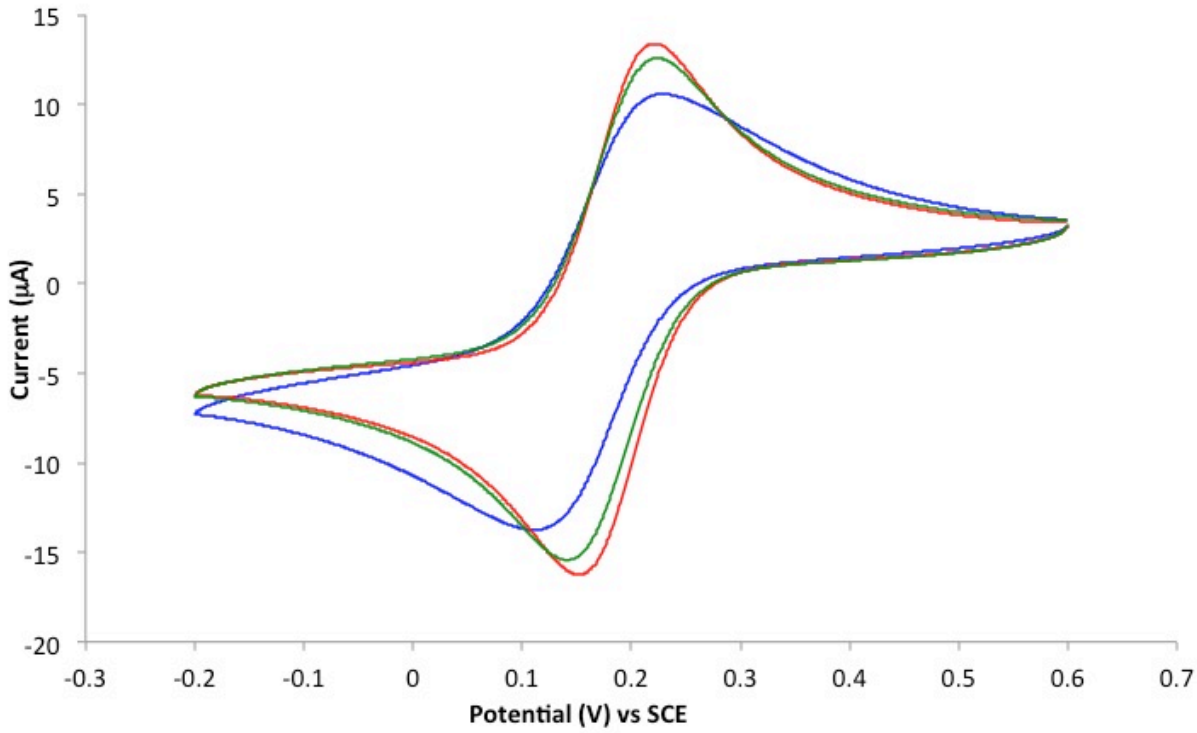

Figure 4.7. CVs of 1 mM $K_3Fe(CN)_6$ in PBS (pH 7) showing the effect of ABiB modification of ethanolamine-modified GC. Scan rate = 100 mV s^{-1}. The blue line is a scan taken before reaction with ethanolamine, the red line is a scan taken after reaction with ethanolamine and the green line is a scan after ABiB was coupled to the ethanolamine modified surface.

4.3.4.4. Characterisation of Ethanolamine and ABiB Modified Layer Through Fc Coupling

The extent of ABiB coupling to the ethanolamine-modified surface was tested through the reaction of FcCOCl at the ethanolamine/ABiB surface. Assuming ABiB and FcCOCl react with the same functional groups, FcCOCl should only react with those not coupled to ABiB. Figure 4.8 (green line) shows a CV of the surface after ethanolamine-modification, ABiB coupling and reaction with FcCOCl, along with the FcCOCl treated polished GC (blue line) and the ethanolamine-modified surface reacted with FcCOCl (red line). There is a clear decrease in peak current for the ABiB coupled surface in comparison to the ethanolamine-modified surface. The shift of $E_{1/2}$ of the Fc/Fc^+ redox peak to a more positive potential for FcCOCl reacted at the ethanolamine/ABiB modified surface compared to the ethanolamine-

modified surface is thought to be caused by the influence of the organic groups surrounding the Fc molecules. Rowe *et al*. reported a positive shift in redox potential values for Fc functionalised self assembled monolayers when the Fc groups became more buried in alkanethiol diluents.[142] The positive shift is explained by the progressively more alkane-like environment created by the co-adsorbed alkanethiols, which destabilises ferrocenium relative to Fc. Therefore, by the same reasoning, the presence of ABiE groups in close proximity to the Fc groups are the likely cause of the more positive $E_{1/2}$ potential observed for the Fc/Fc^+ couple of the ethanolamine/ABiB modified surface.

From the CV of Fc at the ethanolamine/ABiB-modified surface (Figure 4.8, green line), Γ_{Fc} was calculated to be $1.1 \pm 0.1 \times 10^{-10}$ mol cm^{-2} ($n = 2$). The increase in Γ_{Fc} compared to bare GC ($9.7 \pm 0.1 \times 10^{-11}$ mol cm^{-2}) is attributed to FcCOCl reacting with both the unreacted terminal alcohol groups and directly with the GC substrate. From the difference between Fc groups coupled to the surface before ($2.5 \pm 1.1 \times 10^{-10}$ mol cm^{-2}) and after ($1.1 \pm 0.1 \times 10^{-10}$ mol cm^{-2}) reaction with ABiB, the surface concentration of coupled ABiB is estimated to be $1.3 \pm 1.1 \times 10^{-10}$ mol cm^{-2}.

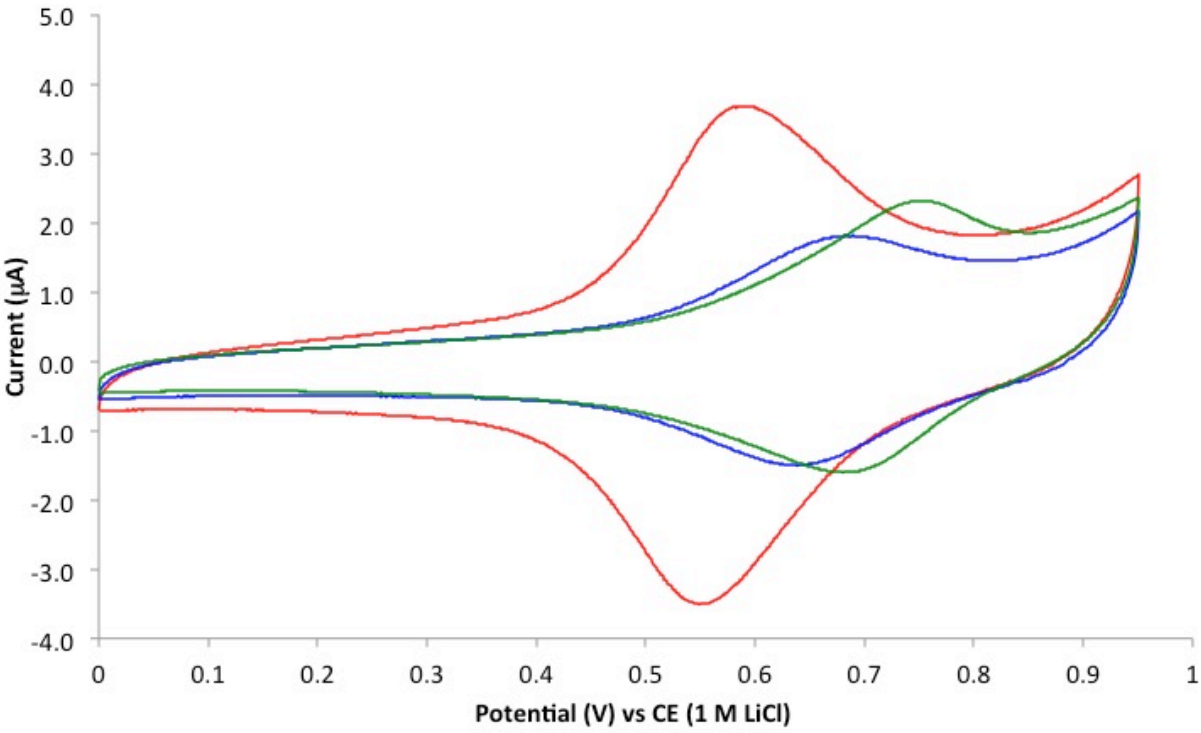

Figure 4.8. Second scan CVs in 0.1 M $LiClO_4$ –EtOH of a polished GC electrode after modification with FcCOCl (blue line), after modification with ethanolamine and FcCOCl (red line), and after modification with ethanolamine/ABiB and FcCOCl (green line). Scan rate = 200 mV s^{-1}.

4.3.4.5. Characterisation of Ethanolamine and ABiC Modified Layer Through Fc Coupling

The ethanolamine-modified surface was reacted in a similar fashion to that shown in Scheme 4.6, with ABiC used as the polymerisation initiator derivative instead of ABiB. After modification, the ethanolamine/ABiC surface was reacted with FcCOCl. It is assumed that ABiC and FcCOCl will react with the same functional groups, so FcCOCl should only react with those not coupled to ABiC. Figure 4.9 (red line) shows a CV of the surface after ethanolamine modification and reaction with FcCOCl (black line), and the surface after the ethanolamine/ABiC modification and reaction with FcCOCl (black line). There is a clear decrease in peak current for the ABiC coupled surface in comparison to the ethanolamine-modified surface. As there is no clear oxidation peak for the Fc/Fc^+ redox couple, the $E_{1/2}$ for the ethanolamine/ABiC surface reacted with FcCOCl cannot be determined. The broadness

and lack of distinct oxidation peak of the Fc/Fc^+ redox couple suggests that the observed response (black line, Figure 4.9) is a combination of two peaks resulting from the Fc groups coupling to the surface in two ways: through the hydroxyl groups of ethanolamine and directly to the surface. The observable reduction peak current is at a similar potential to that of the ethanolamine-FcCOCl modified surface (red line, Figure 4.9), which suggests that a significant portion of the tether Fc groups reacted with the hydroxyl groups of ethanolamine.

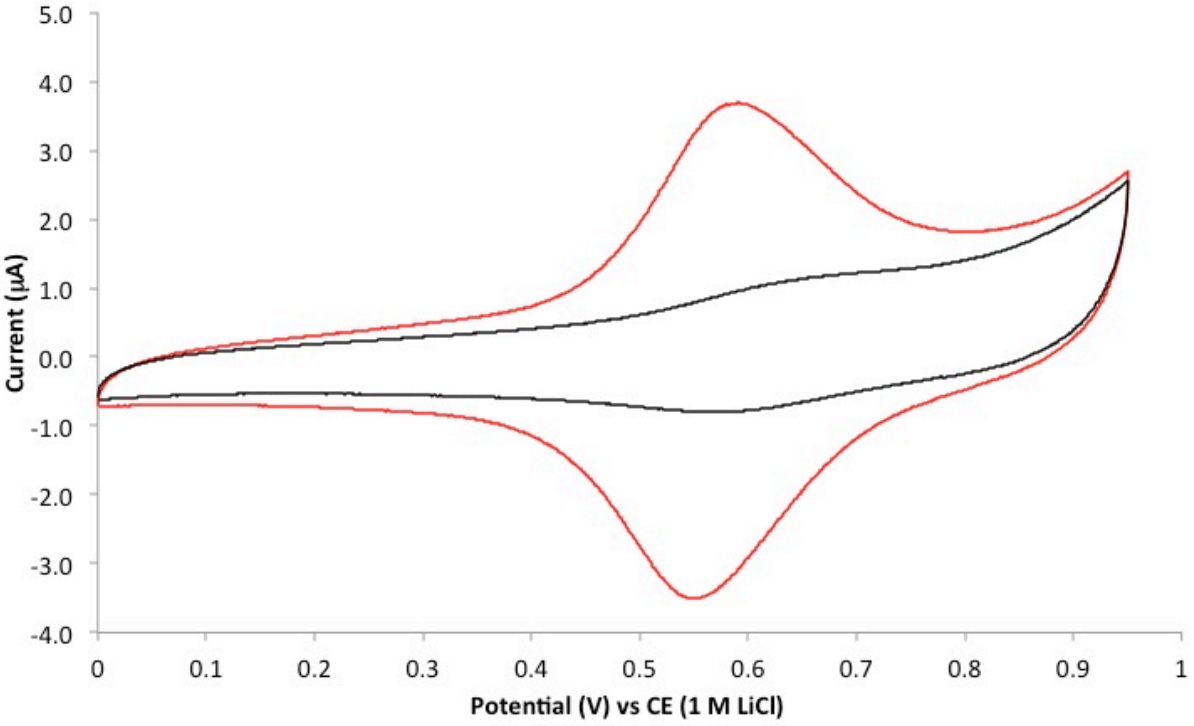

Figure 4.9. Second scan CVs in 0.1 M $LiClO_4$ –EtOH of a polished GC electrode after modification with ethanolamine and FcCOCl (red line), and after modification with ethanolamine/ABiC and FcCOCl (black line). Scan rate = 200 mV s^{-1}.

From the CV of Fc at the ethanolamine/ABiC-modified surface (Figure 4.9, black line), Γ_{Fc} was calculated to be $2.9 \pm 0.4 \times 10^{-11}$ mol cm^{-2} (n = 2). This is a significant decrease in Γ_{Fc} compared to the ethanolamine-modified surface ($2.5 \pm 0.5 \times 10^{-10}$ mol cm^{-2}) and gives an estimated $\Gamma_{Initiator}$ for the ethanolamine/ABiC-modified surface of $2.2 \pm 0.9 \times 10^{-10}$ mol cm^{-2}.

4.3.5. Comparison of Methods

The Γ_{Fc} values for modification strategies explored in this chapter are given in Table 4.2. From comparison of these values, it is clear that modifying the GC surface with ethanolamine increases the surface reactivity towards FcCOCl compared with that of polished GC. There is roughly a three fold increase in Γ_{Fc} from $9.7 \pm 0.1 \times 10^{-11}$ mol cm^{-2} for polished GC to $2.5 \pm 0.5 \times 10^{-10}$ mol cm^{-2} for ethanolamine modified GC. After reaction of the ethanolamine-modified with a polymerisation initiator derivative (ABiB or ABiC), there was a significant decrease in Γ_{Fc}. A significant decrease in Γ_{Fc} was also observed after treating a polished GC surface with ABiC or ABiA.

Table 4.2. Γ_{Fc} values for the modified surfaces after reaction with FcCOCl.

Film	Γ_{Fc}	n[a]
Polished GC	$9.7 \pm 0.1 \times 10^{-11}$ mol cm^{-2}	4
Ethanolamine	$2.5 \pm 0.5 \times 10^{-10}$ mol cm^{-2}	3
Ethanolamine/ABiB	$1.1 \pm 0.1 \times 10^{-10}$ mol cm^{-2}	2
Ethanolamine/ABiC	$2.9 \pm 0.4 \times 10^{-11}$ mol cm^{-2}	2
ABiC	$2.0 \pm 0.8 \times 10^{-11}$ mol cm^{-2}	4
ABiA	$2.9 \pm 1.0 \times 10^{-11}$ mol cm^{-2}	4

[a] n is the number of samples analysed.

Estimations of $\Gamma_{Initiator}$ for the ABiC and ABIA modified surfaces were made by the subtraction of Γ_{Fc} of the polymerisation initiator and FcCOCl modified surface from the Γ_{Fc}

value obtained from the reaction of FcCOCl before modification with the polymerisation initiator. Estimations of $\Gamma_{\text{Initiator}}$ for the ethanolamine/polymerisation initiator modified surfaces were made by subtracting the Γ_{Fc} of the polymerisation initiator and FcCOCl modified surface from the Γ_{Fc} value obtained from the reaction of FcCOCl with the ethanolamine-modified surface. The resulting $\Gamma_{\text{Initiator}}$ values are shown in Table 4.3.

Table 4.3. Estimated $\Gamma_{\text{initiator}}$ for each modification strategy.

Film	**Estimated $\Gamma_{\text{initiator}}$**
ABiC	$7.7 \pm 0.9 \times 10^{-11}$ mol cm^{-2}
ABiA	$6.8 \pm 1.1 \times 10^{-11}$ mol cm^{-2}
Ethanolamine/ABiB	$1.4 \pm 1.1 \times 10^{-10}$ mol cm^{-2}
Ethanolamine/ABiC	$2.2 \pm 0.9 \times 10^{-10}$ mol cm^{-2}

Table 4.3 shows that both the ABiC and ABiA strategies give similar estimated $\Gamma_{\text{initiator}}$ values ($7.7 \pm 0.9 \times 10^{-11}$ mol cm^{-2} and $6.8 \pm 1.1 \times 10^{-11}$ mol cm^{-2}, respectively). The two-step ethanolamine/ABiB and ethanolamine/ABiC modification methods gave the highest values of coupled polymerisation initiator ($1.4 \pm 1.1 \times 10^{-10}$ mol cm^{-2} and $2.2 \pm 0.9 \times 10^{-10}$ mol cm^{-2}, respectively). These estimated values are similar to the surface bromine density for substrates modified by the electrochemical grafting of 4-(2-hydroxylethyl)benzene diazonium ions followed by the reaction with ABiB (3.6×10^{-10} mol cm^{-2}), approximated by Iruthayaraj *et al.*[100] The value for the ethanolamine/ABiB and FcCOCl-modified surface is consistent with the shift in $E_{1/2}$ of Fc that suggests there must be a significant amount of the organic groups on the surface. The $E_{1/2}$ of the ethanolamine/ABiC and FcCOCl-modified surface could not be

calculated due to the lack of definition in the Fc/Fc^+ redox couple peaks. It is thought that the surrounding organic groups may also be influencing this.

It should be emphasised that the values for $\Gamma_{initiator}$ are indirect estimates and the uncertainties reported are extrapolated from the uncertainties in Γ_{Fc} and the actual uncertainties may be higher.

4.4. Conclusion

Reactions between polymerisation initiators and GC have been explored. The conversion of carboxylic acids to acid chlorides has been used to increase the reactivity of the modifier and the GC surface. The modified surfaces were indirectly characterised by the coupling of Fc groups onto the surface. After coupling the polymerisation initiator to the GC substrate, activated FcCOOH was reacted with the surface to assess the change in the amount of immobilised Fc.

Large uncertainties in $\Gamma_{initiator}$ makes it impossible to assess the relative success of the two one-step modification methods and similarly the two two-step (ethanolamine) modification methods. For work described in the next chapter involving the formation of polymer brushes, only the single-step ABiC method was used to immobilise the initiator.

Chapter 5. Growth of Polymer Brushes from Surface Tethered Polymerisation Initiators

5.1. Introduction

Chapters 3 and 4 described the modification of carbon surfaces by the covalent attachment of polymerisation initiators through the grafting of aryl diazonium salts (Chapter 3) and through direct reactions with the carbon surface (Chapter 4). This chapter investigates the growth of polymer brushes from modified surfaces selected from the preceding chapters. Surface initiated atom transfer radical polymerisation (SI-ATRP) was the chosen polymerisation technique used for the preparation of polymer brushes in this work.

In contrast to other studies describing growth of polymer brushes from tether layers, the tether layers used in this work are monolayers. This lays the groundwork for preparing interfaces with better control of polymer chain density, particularly when starting with tether layers prepared from grafting protected diazonium salts.

The growth of two polymers from the tethered layers was investigated in this work. Polymer brushes of poly(3-(methacryloylamino)propyl)-*N,N*'-dimethyl(3-sulfopropyl)-ammonium hydroxide) (PMPDSAH) are of interest because of its switchable properties. Polymer brushes of PMPDSAH have been grown previously by Pei *et al.* on a conducting polymer film.[81] PMPDSAH is a zwitterionic polymer containing a quaternary amine (R_4N^+) and sulfonate ($-SO_3^-$) functional groups. These polymer brushes displayed reversible conformational switching triggered by the oxidation state of the conducting polymer, with secondary effects due to the ionic strength of the solution and the temperature. In the present work, polymer brushes of PMPDSAH were grown by SI-ATRP from Ar-CONH-ABiB and Ar-Tri-APBiB

modified GC surfaces (surface modification described in Chapter 3). The proposed polymer brush growth is shown in Scheme 5.1.

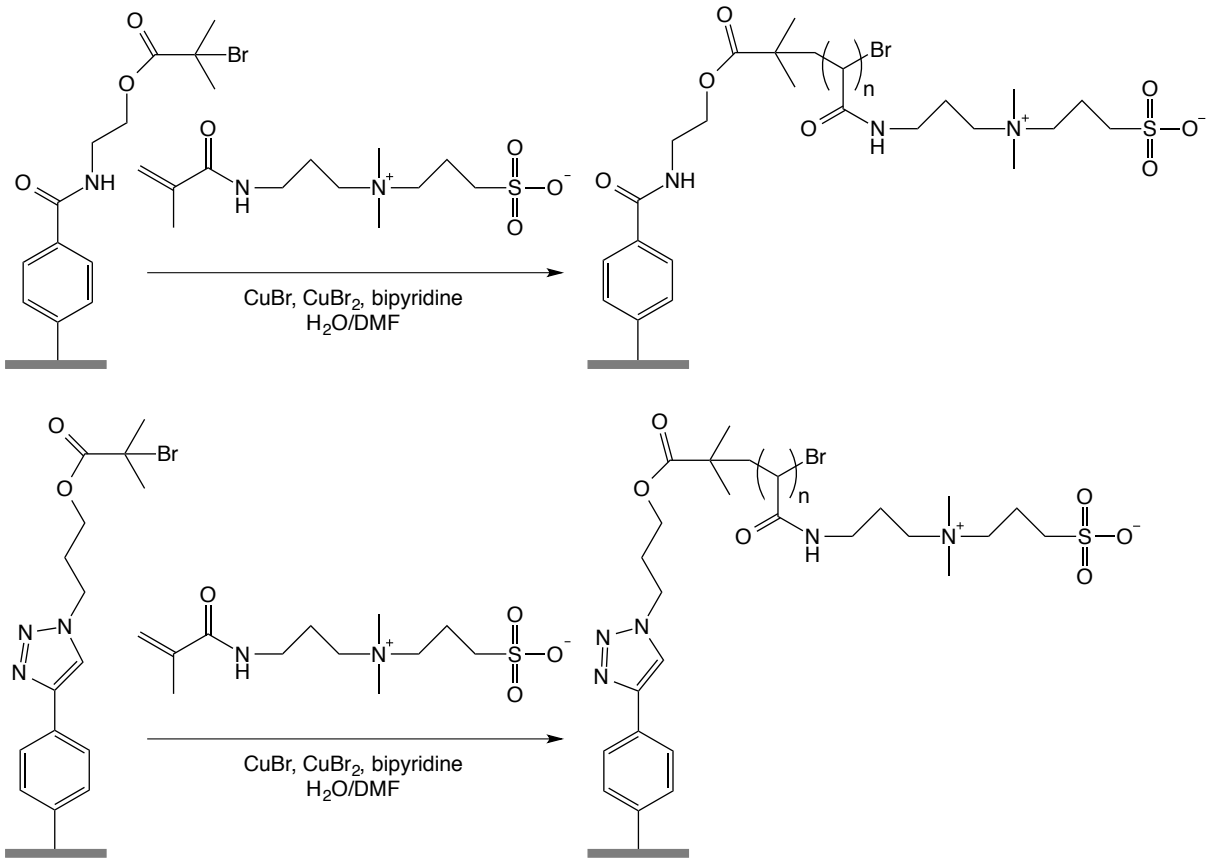

Scheme 5.1. Proposed growth of PMPDSAH polymer brush from an Ar-CONH-ABiB (top) or Ar-Tri-APBiB (bottom) modified GC electrode.

Matrab *et al.* have reported polymer brushes of poly(methyl methacrylate) (PMMA) grown from GC electrodes and metallic surfaces modified by the electrochemical grafting of a brominated aryl multilayer from an aryl diazonium salt.[99,143] They used the polymer brush surface for protein adsorption studies. In this work, polymer brushes of PMMA were grown from Ar-Tri-APBiB (Scheme 5.2) and ABiC (Scheme 5.3) modified GC surfaces (modified as described in Chapter 3 and 4). Three SI-ATRP methods were used for the growth of PMMA brushes: SI-ATRP,[88] electrochemically mediated SI-ATRP (eSI-ATRP) and a one-pot simultaneous copper catalysed azide-alkyne click reaction/SI-ATRP (CuAAC/SI-ATRP) from

the Ar-Eth modified surface (Scheme 5.4). In eSI-ATRP, the application of an electrochemical potential to the working electrode aims to maintain the Cu^1 oxidation state of the catalyst in close proximity to the electrode surface, thus catalysing the ATRP reaction. The combined CuAAC/SI-ATRP approach was designed as a new and elegant method for growth of polymer brushes, reducing the number of surface modification steps required.

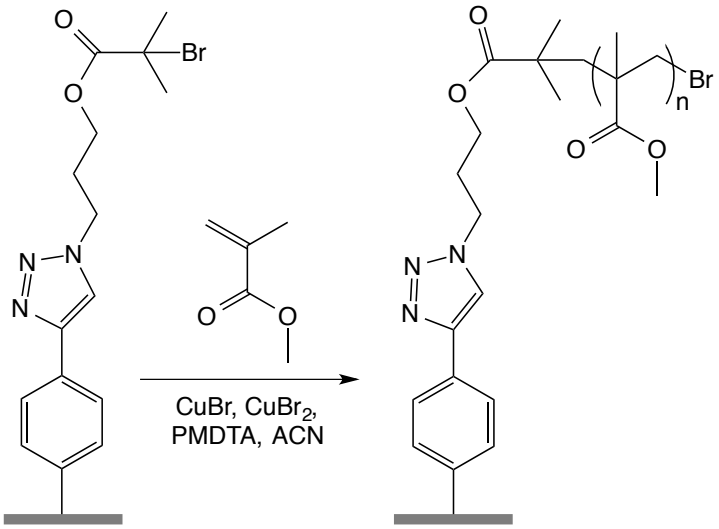

Scheme 5.2. Proposed growth of PMMA polymer brush from an Ar-Tri-APBiB modified GC electrode by SI-ATRP and eSI-ATRP.

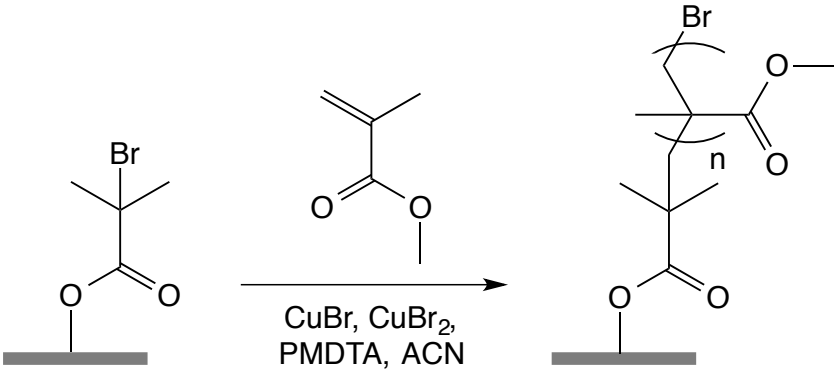

Scheme 5.3. Proposed growth of PMMA polymer brush from an ABiC modified electrode by SI-ATRP.

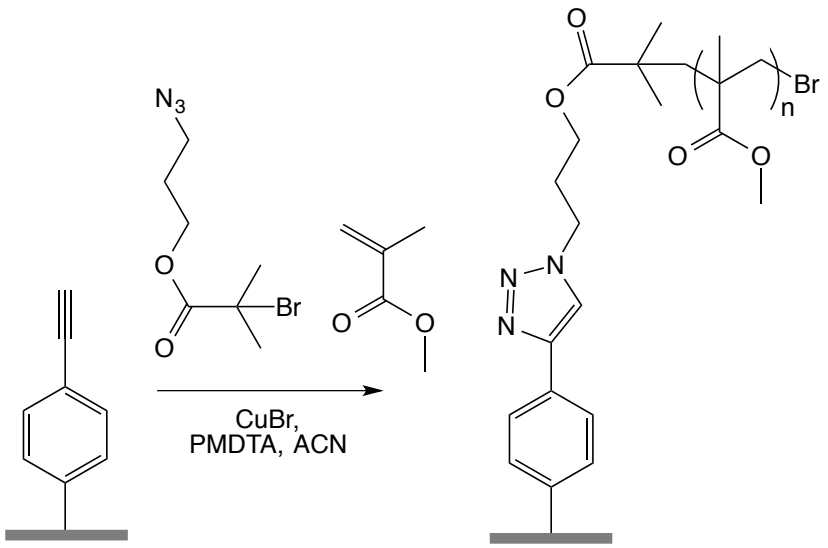

Scheme 5.4. Proposed one-pot CuAAC/SI-ATRP for the simultaneous reaction of APBiB with the ethynylaryl monolayer and the polymerisation of methyl methacrylate.

The main goal of the work in this chapter was to establish whether polymer brushes were grown from the prepared monolayer surfaces under the conditions used. To investigate this, the resulting surfaces were analysed by redox probe voltammetry, contact angle measurements, X-ray photoelectron spectroscopy (XPS), atomic force microscopy (AFM) and depth profiling through AFM scratching.

5.2. Experimental

5.2.1. Polymer Brush Synthesis

Polymer brushes of PMPDSAH were synthesised by SI-ATRP from Ar-CONH-ABiB and Ar-Tri-APBiB modified GC surfaces. Polymer brushes of PMMA were synthesised from Ar-Tri-APBiB modified surfaces through three methods: SI-ATRP, eSI-ATRP, and the one-pot CuAAC/SI-ATRP (from the Ar-Eth modified surface). PMMA polymer brushes were also grown from ABiC modified surface. Reaction details for the polymerisation procedures are given in Chapter 2.4.

GC disk electrodes were modified for experiments involving electrochemical analysis. GC plate electrodes were modified when contact angle and XPS analyses were required. PPF electrodes where modified for AFM imaging.

5.2.2. Cyclic Voltammetry

All redox probe voltammetry experiments were conducted using GC disk electrodes in a pear-shaped electrochemistry cell using a PBS (pH 7) solution containing 1 mM $K_3Fe(CN)_6$ with a Pt mesh auxiliary electrode and a SCE reference electrode.

5.2.3. Atomic Force Microscopy and Depth Profiling

Atomic force microscopy (AFM) imaging and depth profiling details are given in Chapter 2.5.

5.3. Results and Discussion

5.3.1. PMPDSAH Polymer Brushes from Ar-CONH-ABiB Modified Surface

The strategy for the growth of PMPDSAH polymer brushes from the Ar-CONH-ABiB prepared surface is shown in Scheme 5.1 The resulting surface after reaction was characterised by redox probe voltammetry, contact angle measurements, and XPS analysis.

5.3.1.1. Redox Probe Voltammetry

Redox probe voltammetry was used to monitor changes of the GC surface as a result of the polymer brush reactions. The blue line in Figure 5.1 shows the CV obtained in a solution of $K_3Fe(CN)_6$ at the Ar-CONH-ABiB modified surface. The red line in Figure 5.1 shows the CV obtained in the same solution after reaction with the polymerisation solution. There is a significant difference in the shape of the CVs before and after the reaction. The change in

peak currents and shape of the voltammogram clearly indicate that the electrode surface coating has changed, however the processes leading to the observed responses are not understood. After the polymerisation reaction, it appears that the forward scan is dominated by linear diffusion of $Fe(CN)_6^{3-}$ while on the reverse scan there is a contribution from radial diffusion leading to the observed flattening of the peak.[128] However, why this behaviour would be exhibited at the polymer modified electrode is unclear.

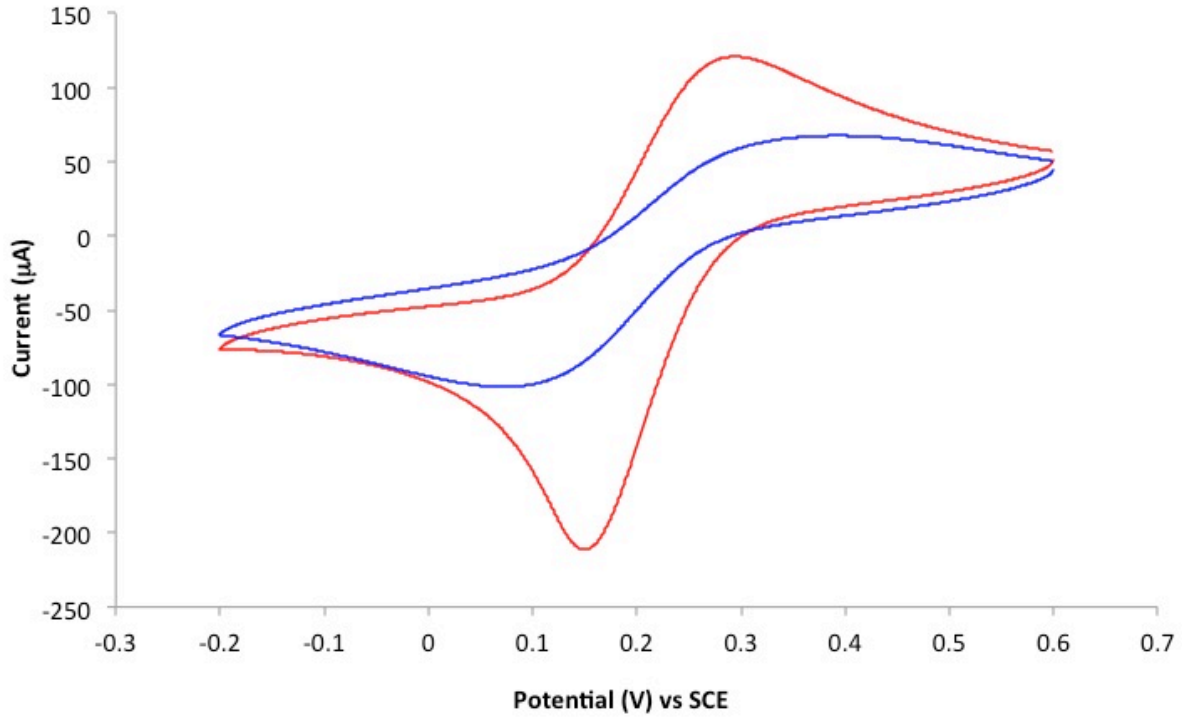

Figure 5.1. CV of 1 mM $K_3Fe(CN)_6$ in PBS pH 7 showing the effect of polymerisation of MPDSAH. Scan rate = 100 mV s^{-1}. The blue line is a scan taken of the Ar-CONH-ABiB modified surface and the red line is a scan taken after the growth of the PMPDSAH polymer brushes.

5.3.1.2. Contact Angle Measurements

Water contact angle measurements on the modified surface were used to investigate the PMPDSAH polymer brush film. A 2 μL droplet of solution (MQ water, 0.1 M HCl (pH 1) or $NaOH/NaHCO_3$ buffer (pH 10)) was placed on top of the modified area then photographed after a 10 s equilibration time. Table 5.1 lists the average contact angles for the polished, Ar-CONH-ABiB modified GC surfaces and the surface after the polymerisation reaction. As

stated in Chapter 3.3.2.2.3, the basis of the difference in contact angles of the acidic and basic solution droplets on the Ar-CONH-ABiB modified surface is unknown. After the polymerisation reaction, the water contact angle decreased from 57 ± 3 ° to 43 ± 2 °, indicating that the surface has changed and become more hydrophilic. At pH 10, the contact angle increased after modification from 53 ± 2 ° to 60 ± 1 °, while at pH 1, the contact angle decreased from 65 ± 1 ° to 59 ± 2 °. The significant changes in contact angles after the polymerisation reaction confirms that changes have occurred on the surface, however the origin of each angle is not clear. In addition to chemical composition, surface roughness influences contact angle and the observed contact angle changes may be due to changes in both properties.

Table 5.1. Average contact angle measurements for polished and modified GC surfaces. Error is the standard deviation.

	Bare GC	**Ar-CONH-ABiB**	**Ar-CONH-ABiB-PMPDSAH**
MQ Water	72 ± 1 °	57 ± 3 °	43 ± 2 °
0.1 M HCl (pH 1)	66 ± 2 °	65 ± 1 °	59 ± 2 °
Buffer (pH 10)	65 ± 2 °	53 ± 2 °	60 ± 1 °

In this work, an investigation of the effect of the salt concentration of the droplet solution on the contact angle of the PMPDSAH polymer brushes revealed no significant change in contact angle with salt concentrations of 0, 0.01 M, 0.1 M and 1 M NaCl. Altering the salt concentration of the droplet alone is evidently not sufficient to induce a change in the polymer brush conformational state.

5.3.1.3. XPS Analysis

XPS analysis was used to confirm the presence of PMPDSAH polymer brushes grown from the Ar-CONH-ABiB surface. XPS measurements were made on modified GC surfaces. An unmodified, polished GC plate was used as a blank. Data obtained from the Ar-CONH-ABiB modified GC is repeated from Chapter 3 for convenience and comparison.

Atomic compositions at each surface were obtained from survey spectra, giving the data shown in Table 5.2. The atomic percentages for C, N and O are essentially the same before and after the growth of PMPDSAH polymer brushes on the Ar-CONH-ABiB surface. The N:O atomic percentage ratio for the Ar-CONH-ABiB-modified GC surface was found to be close to the expected value of 1:3 (without taking into consideration any N contributions from any azo linkages or O from the GC substrate), while after the polymerisation the N:O ratio expected is 1:2 (providing that the number or monomer units significantly outnumbers the number of tethered groups). However, no significant change in the N:O ratio was observed.

After modification of the Ar-CONH-ABiB surface, the atomic percentage of bromine decreases by an order of magnitude. This decrease in the bromine atomic percentage has been observed by Iruthayaraj *et al*. after the growth of PMMA polymer brushes by a similar method.[100]

The detection of 0.9% sulfur content on the surface is strong evidence for the successful growth of PMPDSAH polymer brushes from the modified surface and is more than the content reported by Pei (0.18%) for the same PMPDSAH polymer brushes.[74] The amount of sulfur detected on the surface is a third of that of nitrogen. Considering the expected S/N ratio in the MPDSAH monomer is 1:3, this supports the successful growth of PMPDSAH polymer brushes.

Table 5.2. XPS survey scan data for Ar-CONH-ABiB modified GC and PMPDSAH polymer brush-modified Ar-CONH-ABiB surface.

Sample	**Atomic %**				
	C	**N**	**O**	**Br**	**S**
Polished GC	93.0	0.7	6.3		
Ar-CONH-ABiB	86.3	3.0	10.2	0.5	
Ar-CONH-ABiB-PMPDSAH	84.5	3.0	11.5	0.06	0.9

Narrow scan spectra of the carbon (C1s), nitrogen (N1s), oxygen (O1s), bromine (Br3d) and sulfur (S2p) regions were obtained for the Ar-CONH-ABiB-PMPDSAH surface. The peak binding energies, atomic percentages and assignments from the narrow scans are listed in Table 5.3.

There were no observable changes in the C1s and O1s narrow scan spectra (Figure 5.2(b) and (d), respectively) from the Ar-CONH-ABiB sample (Figure 3.13) to the PMPDSAH polymer brush sample. A notable change in the N1s narrow scan spectrum (Figure 5.2 (c)) after PMPDSAH polymer brush growth is the presence of an additional N1s peak located at 403.0 eV. This peak was also observed in the work by Pei and can be assigned to the quaternary amine present in the PMPDSAH structure,[74] and was similarly assigned in polysulfobetaine films prepared by Stach *et al*.[144] The S2p narrow scan spectrum (Figure 5.2 (f)) was fitted with two peaks located 164.2 and 168.7 eV and are assigned to the S2p 3/2 and S2p 1/2 peaks.[145]

Considering the change in the redox probe voltammetry response and contact angles after polymerisation at the Ar-CONH-ABiB surface, along with the XPS data providing evidence of quaternary amine and sulfonate functionalities, it appears that the SI-ATRP polymerisation for the growth of PMPDSAH polymer brushes from the Ar-CONH-ABiB surface has been successful, although the yield of the polymerisation reaction is not known.

Table 5.3. Binding energies, assignments and atomic% for the C1s, N1s, O1s, Br3d and S2p XPS narrow scan spectra for the Ar-CONH-ABiB-PMPDSAH film on GC.

	Binding Energy (eV)	**Atomic %**	**Assignment**	**Ref.**
C1s	284.7	18.4	Graphitic C	[133,134]
	285.1	50.0	C-C, C-C (sp^2), C-C (sp^3)	[133,134]
	286.4	26.0	C-OH, ester, amide	[133,134]
	289.0	5.6	COOH	[133]
N1s	400.4	76.3	Reduced N, C-N	[144]
	403.0	23.7	Quaternary amine	[144]
O1s	532.0	57.2	>C=O, -C-O-C-,	[133,134]
	533.4	42.8	>C-OH, adsorbed CO, adsorbed O_2, bound H_2O	[133,134]
Br3d	70.7	100	C-Br	
S2p	164.2	17.0	S 2p 3/2	[145]
	168.7	83.0	S 2p 1/2	[145]

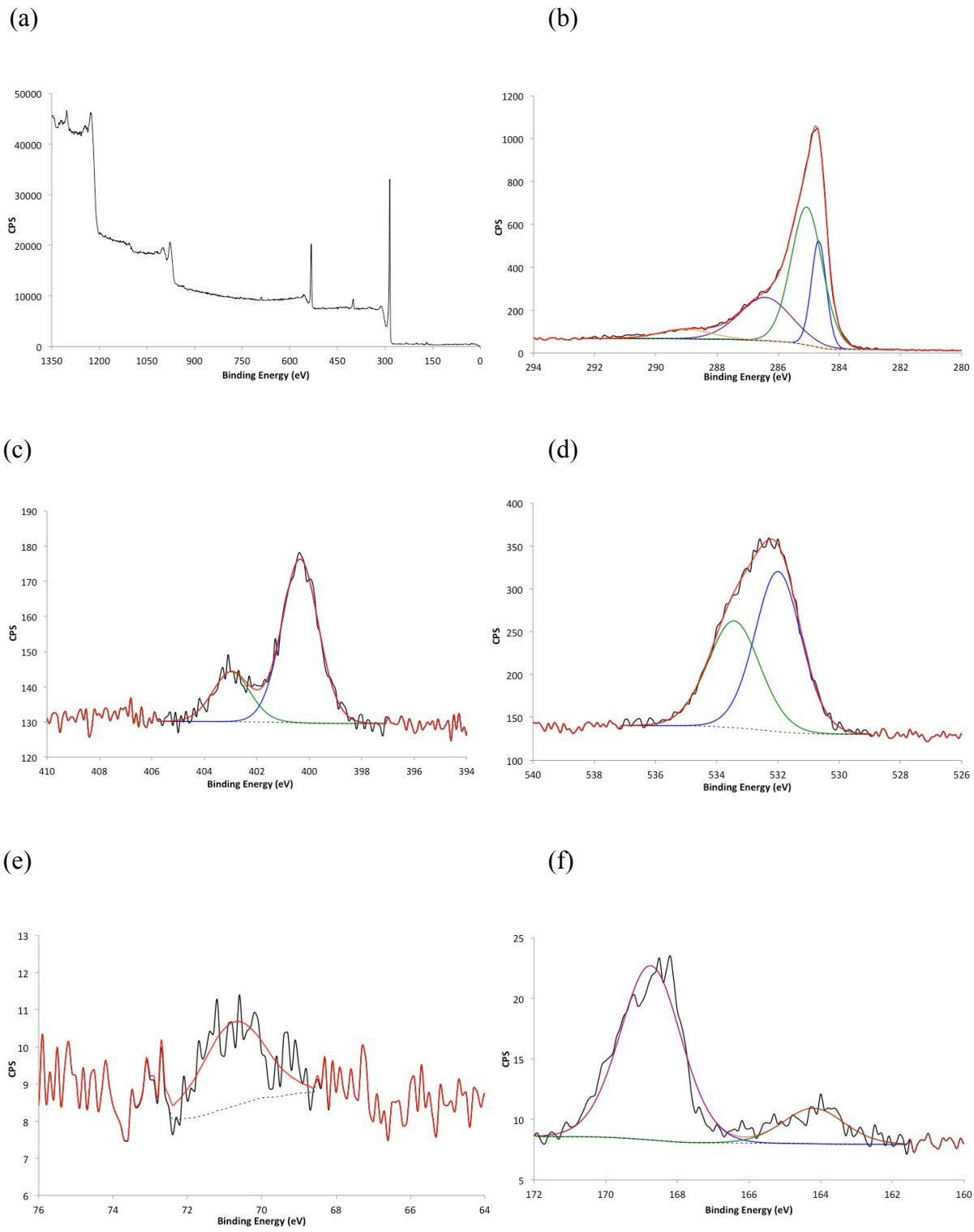

Figure 5.2. XPS spectra of PMPDSAH polymer brush grown from the Ar-CONH-ABiB modified GC: wide survey scan (a) and narrow scan spectra for C1s (b), N1s (c), O1s (d), Br3p (e) and S2p (f) regions. The black lines are the experimental spectra recorded and the coloured lines represent those used for peak fitting.

5.3.2. PMPDSAH Brushes Grown from Ar-Tri-APBiB Modified Surface

The modification strategy used for the growth of PMPDSAH polymer brushes from Ar-CONH-ABiB surface was applied to the Ar-Tri-APBiB modified GC surface (Scheme 5.1, bottom). Again, the modified surface was characterised by redox probe voltammetry, contact angle measurements, and XPS analysis.

5.3.2.1. Redox Probe Voltammetry

Redox probe voltammetry was used to confirm the presence of PMPDSAH polymer brushes grown from the Ar-Tri-APBiB modified film. An aqueous solution of $K_3Fe(CN)_6$ was used as the redox probe. Scanning of the redox probe at the Ar-Tri-APBiB modified GC gave the blue line CV in Figure 5.3. After the growth of PMPDSAH polymer brush from the Ar-Tri-APBiB modified surface, the surface was once again scanned in the redox probe solution. The CV observed (red line, Figure 5.3) shows a distinctive asymmetric peak that was also observed for the Ar-CONH-ABiB-PMPDSAH surface (red line, Figure 5.3). Although the reason for the asymmetric response is unknown, it is clear that the surface has been changed after reaction with MPDSAH.

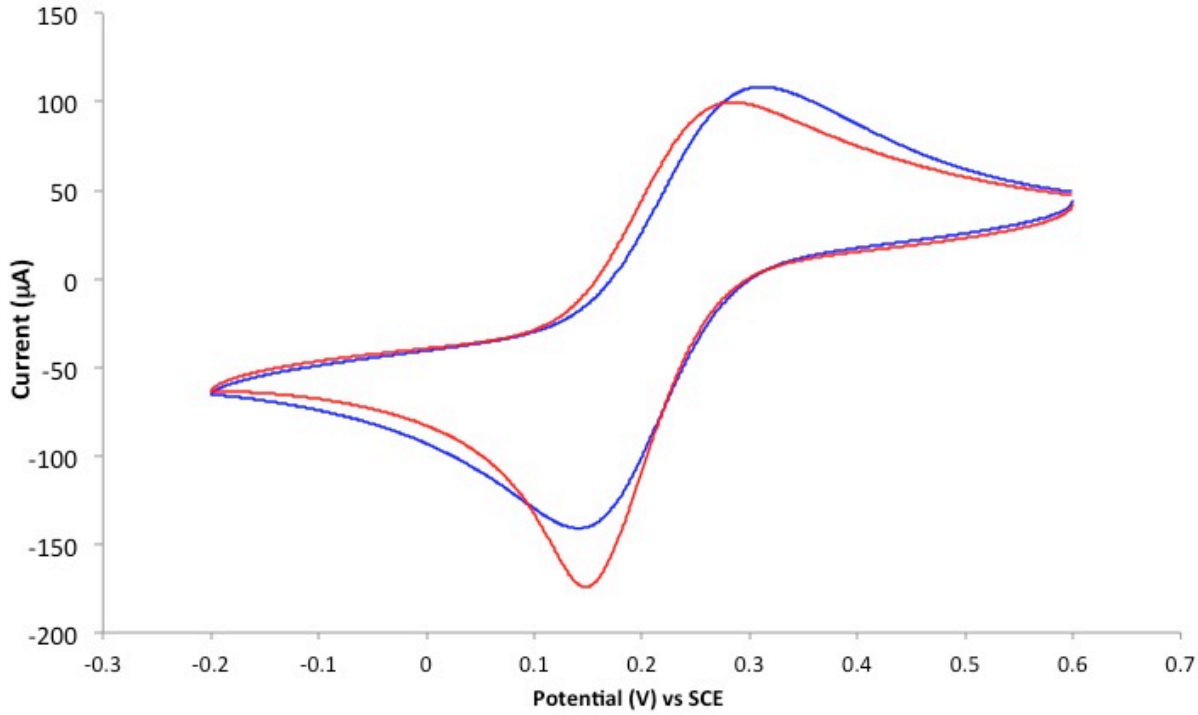

Figure 5.3. CV of 1 mM $K_3Fe(CN)_6$ in PBS pH 7 showing the effect of PMPDSAH polymer brush. Scan rate = 100 mV s^{-1}. The blue line is a scan taken of the Ar-Tri-APBiB modified surface, and the red line is a scan taken after the growth of the PMPDSAH polymer brushes.

5.3.2.2. Contact Angle Measurements

Contact angle measurements were used to investigate the PMPDSAH polymer brush grown from the Ar-Tri-APBiB modified GC surface. Table 5.4 lists the average contact angles for a polished GC surface, the Ar-Tri-APBiB modified GC surface, and the PMPDSAH polymer brush. From the water contact angle measurements of the Ar-Tri-APBiB-PMPDSAH sample (44 ± 2 °), it is clear that the Ar-Tri-APBiB surface (water contact angle = 50 ± 3 °) has been modified by the polymerisation of MPDSAH. The water contact angle for the Ar-Tri-APBiB-PMPDSAH surface is consistent with that of the Ar-CONH-ABiB-PMDSAH surface (43 ± 2 °). The reason behind the difference in contact angles of droplets of 0.1 M HCl and buffer (pH 10) for the polymer brushes grown from the Ar-Tri-APBiB modified surface in comparison those grown from the Ar-CONH-ABiB modified surface is uncertain at this point.

Table 5.4. Average contact angle measurements for polished and modified GC surfaces. Error is the standard deviation.

	Bare GC	Ar-Tri-APBiB	Ar-Tri-APBiB-PMPDSAH
MQ Water	71 ± 1 °	50 ± 3 °	44 ± 2 °
0.1 M HCl (pH 1)	66 ± 2 °	52 ±2 °	46 ± 2 °
Buffer (pH 10)	65 ± 2 °	54 ± 3 °	46 ± 1 °

5.3.2.3. XPS Analysis

The Ar-Tri-APBiB-PMPDSAH modified GC surface was analysed by XPS and compared with data obtained from an unmodified, polished GC plate and an Ar-Tri-APBiB modified GC surface (data repeated from Chapter 3 for the blank and Ar-Tri-APBiB modified GC surfaces).

Atomic compositions at each surface were obtained from survey spectra, giving the data shown in Table 5.5. There were insignificant changes in the atomic percentages of C, N and O after the growth of PMPDSAH polymer brushes. Importantly, as with the Ar-CONH-ABiB modified surfaces, the atomic percentage of bromine decreases by an order of magnitude after the polymerisation. The detection of 0.8% sulfur content is comparable to that for Ar-CONH-ABiB-PMPDSAH surface and to the content reported by Pei and is strong evidence for the successful growth of PMPDSAH polymer brushes.[74]

Table 5.5. XPS survey scan data for the Ar-Tri-APBiB modified GC and the PMPDSAH polymer brush-modified Ar-Tri-APBiB surface.

Sample	**Atomic%**				
	C	**N**	**O**	**Br**	**S**
Polished GC	93.0	0.7	6.3		
Ar-Tri-APBiB	84.3	3.9	11.1	0.65	
Ar-Tri-APBiB-PMPDSAH	84.0	3.9	11.2	0.07	0.8

The C1s and O1s narrow scan spectra (Figure 5.4 (b) and (d), respectively) showed no notable changes from the unmodified GC or Ar-Tri-APBiB modified surfaces (Figure 3.11 (b) and Figure 3.25 (b), respectively). The N1s narrow scan spectrum (Figure 5.4 (c)) was fitted with two peaks, located at 400.4 and 402.5 eV respectively. As there is no distinct peak at 402.5 eV in the modified surfaces prior to the growth of the PMPDAH polymer brush, this peak can been assigned to the quaternary N found in the PMPDSAH structure. The atomic percentage for the quaternary N is 27.3%, this is similar to that found for the Ar-CONH-ABiB-PMPDSAH modified surface (23.7%). Further evidence for the successful polymerisation is from the peaks detected in the S2p narrow scan spectrum (Figure 5.4 (f)).

Considering the change in the redox probe voltammetry response and contact angles after polymerisation at the Ar-Tri-APBiB surface, along with the XPS data providing evidence of quaternary amine and sulfonate functionalities, it appears that the SI-ATRP polymerisation for the growth of PMPDSAH polymer brushes from the Ar-Tri-APBiB surface has been successful, although the yield of the polymerisation reaction is not known.

Table 5.6. Binding energies, assignments and atomic% for the C1s, N1s, O1s, Br3d and S2p XPS narrow scan spectra for the Ar-Tri-APBiB-PMPDSAH film on GC.

	Binding Energy (eV)	Atomic%	Assignment	Ref.
C1s	284.7	16.5	Aromatic C	[133]
	285.0	49.4	C-C, C-C (sp^2), C-C (sp^3)	[133,134]
	286.3	28.4	C-N, C-O, C-COOR	[133,134]
	288.9	5.7	CO-C=O, C=O	[133,134]
N1s	400.4	72.7	C-N, N=N, surface N	[136]
	402.5	27.3	C-N, N=N, surface N, N^+	[136]
O1s	532.1	62.2	>C=O, -C-O-C-	[135]
	533.4	37.8	Surface >C-OH, adsorbed CO, adsorbed O_2, bound H_2O	[135]
Br3d	70.2	100	Br	
S2p	164.3	12.2	S 2p 3/2	[145]
	168.7	87.8	S 2p	[145]

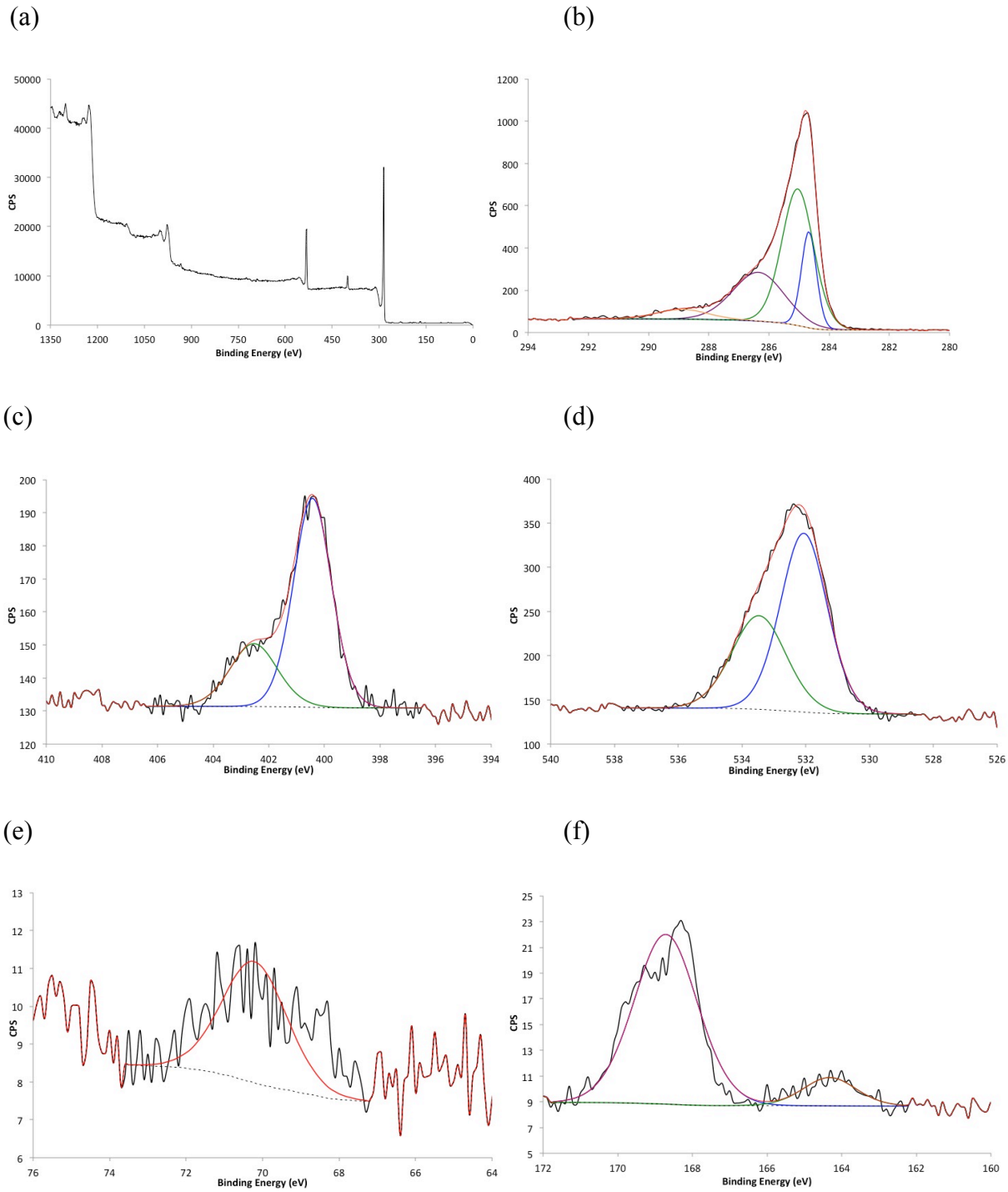

Figure 5.4. XPS spectra of PMPDSAH polymer brush grown from Ar-Tri-APBiB modified GC: wide survey scan (a) and narrow scan spectra for C1s (b), N1s (c), O1s (d), Br3p (e), and S2p (f) regions. The black lines are the experimental spectra recorded and the coloured lines represent those used for peak fitting.

5.3.3. PMMA Brushes from Ar-Tri-APBiB modified Surface

Polymer brushes of PMMA were grown from the Ar-Tri-APBiB modified surface through two procedures: surface initiated atom transfer radical polymerisation (SI-ATRP) and electrochemically induced SI-ATRP (eSI-ATRP). A proposed scheme for PMMA polymer brush growth from the Ar-Tri-APBiB surface is shown in Scheme 5.2. PMMA brushes were also grown simultaneously with the clicking of APBiB to an Ar-Eth modified surface (proposed polymer brush growth shown in Scheme 5.4).

5.3.3.1. PMMA Brushes from Ar-Tri-APBiB Modified Surface by SI-ATRP

5.3.3.1.1. Redox Probe Voltammetry

Redox probe voltammetry was used to confirm the presence of PMMA polymer brushes grown from the Ar-Tri-APBiB modified film. An aqueous solution of $K_3Fe(CN)_6$ was used as the redox probe. Scanning of the redox probe at the Ar-Eth modified surface gave the red line CV in Figure 5.5. After coupling APBiB to the Ar-Eth modified surface, rescanning of the redox probe gave the green line in Figure 5.5. It is clear that the surface has been modified after the coupling step, with the surface significantly hindering electron transfer from the electrode surface to the redox species. The CV taken after the growth of the PMMA polymer brush (purple line, Figure 5.5) shows an increase in current and a decrease in ΔE_p for the redox couple, indicating that the surface has been further changed.

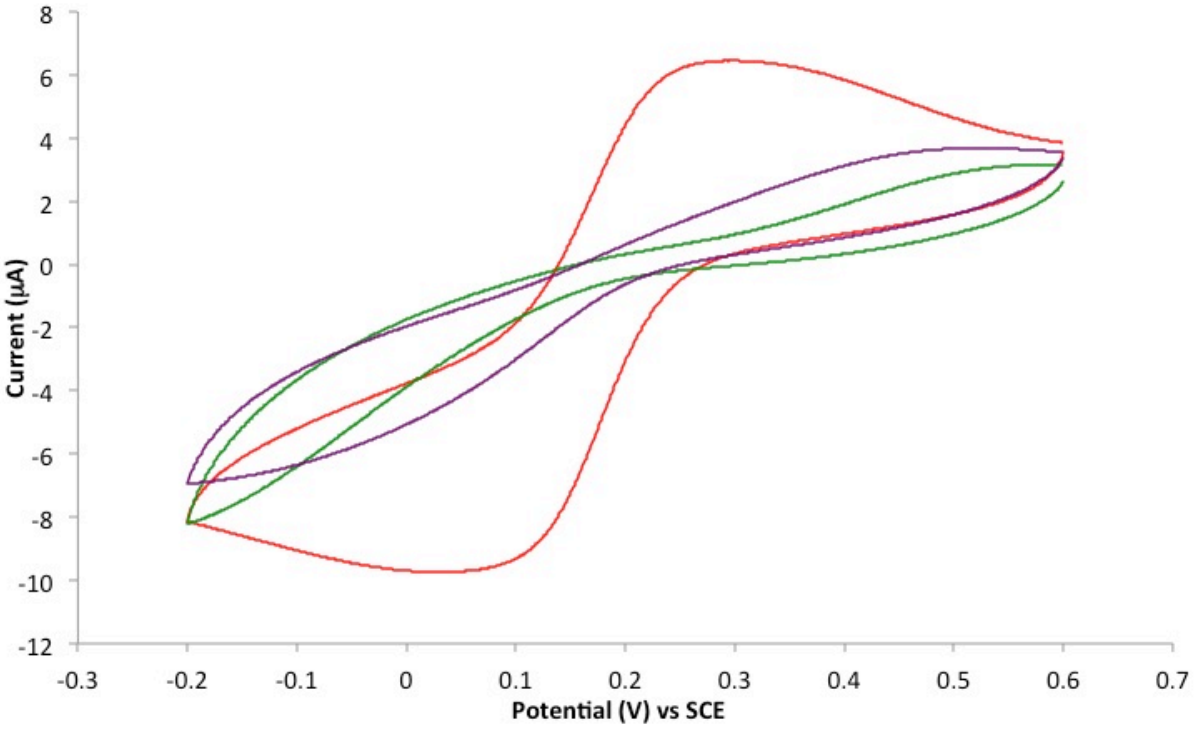

Figure 5.5. CVs of 1 mM $K_3Fe(CN)_6$ in PBS pH 7 showing the effect of PMMA polymer brush growth on a Ar-Tri-APBiB modified GC surface. Scan rate = 100 mV s^{-1}. The red line is a scan taken at the Ar-Eth modified surface, the green line at the Ar-Tri-APBiB modified surface and the purple line is taken after the growth of PMMA polymer brushes.

5.3.3.1.2. Contact Angle Measurements

Water contact angle measurements were used to assess the success of the polymerisation of PMMA. Table 5.7 shows the average contact angles for a droplet of water on polished GC, Ar-Tri-APBiB modified GC and the polymerised sample. There is a significant decrease in the contact angles from 62 ± 2 ° for the Ar-Tri-APBiB modified surface to 56 ± 1 ° after the polymerisation of PMMA. The average water contact angle value measured for the PMMA polymer brush is lower than that measured for a similar system by Matrab and co-workers (83.5 ± 1.4 °)[143] and that of solid sheet PMMA (64.3 ± 1.8 °).[146] The change in contact angle gives good evidence for the growth of polymer brushes, although the altered surface roughness may have an effect.

Table 5.7. Average contact angle measurements for polished GC, Ar-Tri-APBiB and PMMA polymer brushes grown by SI-ATRP. Error is the standard deviation.

	Bare GC	**Ar-Tri-APBiB**	**Ar-Tri-APBiB-PMMA**
MQ Water	88 ± 1 °	62 ± 2 °	56 ± 2 °

5.3.3.1.3. XPS Analysis

PMMA polymers grown from an Ar-Tri-APBiB modified surface by SI-ATRP were analysed by XPS and compared with data obtained from an unmodified, polished GC plate and an Ar-Tri-APBiB modified GC surface (data repeated from Chapter 3 for the blank and Ar-Tri-APBiB modified GC surfaces).

Atomic compositions of the modified surfaces were obtained by survey spectra, giving the data in Table 5.8. After the growth of PMMA polymer brushes from the Ar-Tri-APBiB modified surface, there were only small changes in the atomic composition. Most notably, a reduction in the atomic percentage of bromine is seen after the polymerisation of PMMA, as seen for the previous surfaces modified with PMPDSAH using the same SI-ATRP procedure.

Table 5.8. XPS survey scan data for the Ar-Tri-APBiB modified GC and the PMMA polymer brush-modified Ar-Tri-APBiB surface.

Sample	**Atomic%**			
	C	**N**	**O**	**Br**
Polished GC	93.0	0.7	6.3	
Ar-Tri-APBiB	84.3	3.9	11.1	0.7
Ar-Tri-APBiB-PMMA	87.1	2.5	10.0	0.4

The wide scan spectrum, narrow scan spectra for C1s, N1s, O1s and Br3d, and analysis for the Ar-Tri-APBiB modified surface can be found in Chapter 3. The wide scan spectrum for the Ar-Tri-APBiB-PMMA modified surface is shown in Figure 5.6 (a). Figure 5.6 also shows the narrow scan spectra for the C1s (b), N1s (c), O1s (d) and Br3d (e) regions for Ar-Tri-APBiB-PMMA modified GC surface. Table 5.9 lists the binding energies, assignments and atomic percentages from the narrow scan spectra. The C1s, N1s, O1s and Br3d narrow scan spectra (Figure 5.6 (b-e)) show no significant changes from the Ar-Tri-APBiB modified surface (Figure 3.25, Table 3.17). The lack of change between the surfaces may be due to the sampling depth for XPS analysis and the relative similarities between PMMA and the GC surface.

Table 5.9. Binding energies, assignments and atomic% for the C1s, N1s, O1s, Br3p and Br3d XPS narrow scan spectra for the Ar-Tri-ABiB-PMMA film on GC.

	Binding Energy (eV)	Atomic%	Assignment	Ref.
C1s	284.7	25.7%	Graphitic C	[133,134]
	285.0	46.6%	C-C, C-C (sp^2), C-C (sp^3)	[133]
	286.4	23.3%	C-OH, C=O	[134]
	288.9	4.4%	COOH	[133]
N1s	400.2	71.3%	C-N, N=N, surface N	
	401.7	28.7%	C-N, N=N, surface N	
O1s	532.2	62.2%	>C=O, -C-O-C-	[135]
	533.6	37.8%	Surface >C-OH, adsorbed CO, adsorbed O_2, bound H_2O	[135]
Br3d	68.7	14.0%	C-Br (3d 5/2)	
	70.8	86.0%	C-Br (3d)	

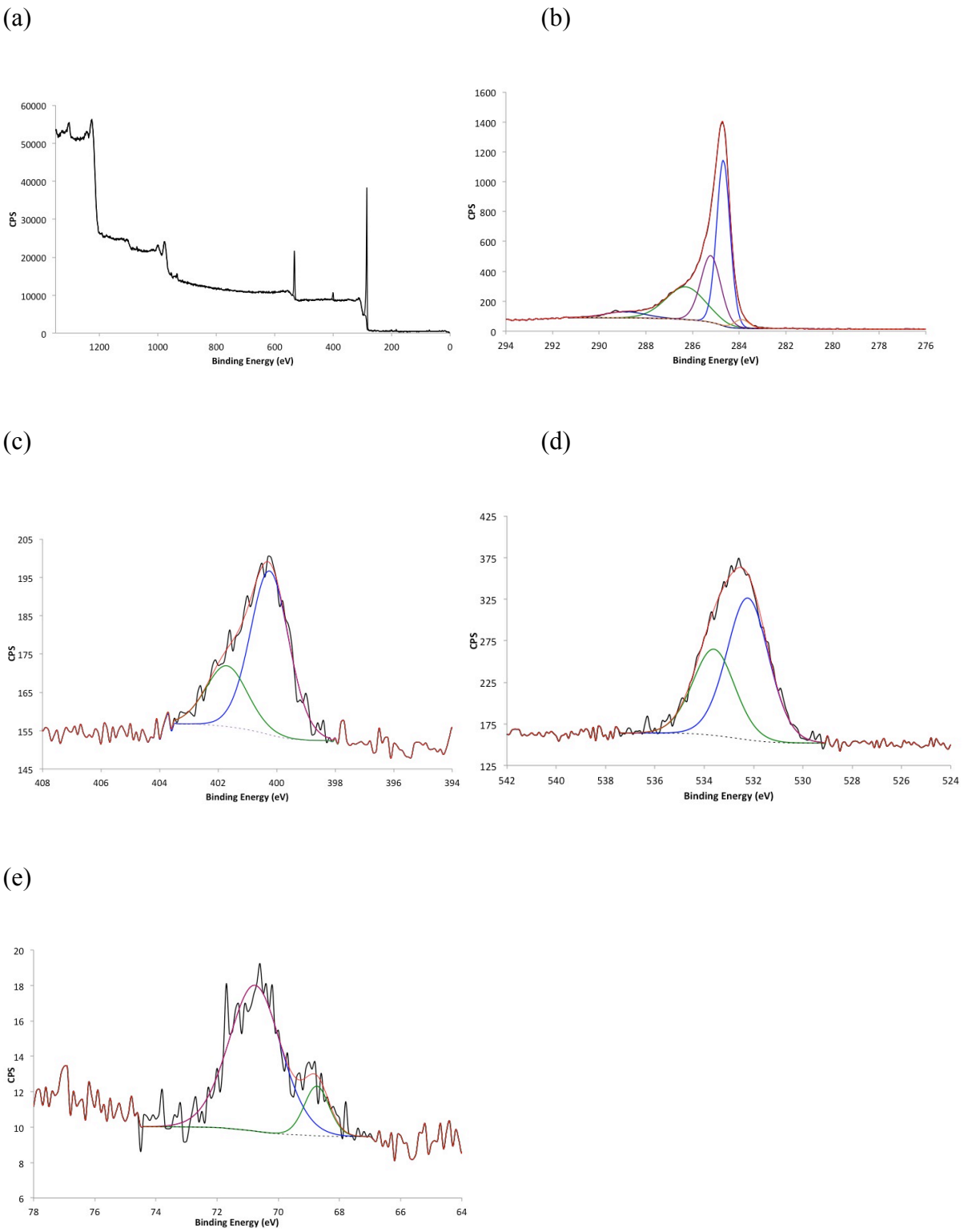

Figure 5.6. XPS spectra of PMMA brushes grown from an Ar-Tri-APBiB modified GC plate: wide scan (a) and narrow scan spectra for C1s (b), N1s (c), O1s (d) and Br (3d) regions. The black lines are the experimental spectra recorded and the coloured lines represent those used for peak fitting.

5.3.3.1.4. Atomic Force Microscopy

Atomic force microscopy (AFM) images were used to confirm the presence of PMMA polymer brushes grown from an Ar-Tri-APBiB modified pyrolysed photoresist film (PPF) surface by SI-ATRP. PPF, a GC-like material, was used for these measurements because it has a lower surface roughness than GC. [7] AFM images and a line profile (from the red line) of an unmodified PPF surface are shown in Figure 5.7. The unmodified surface has low roughness (as shown in the line profile), with the depressions in the film caused by imperfections in the PPF surface.

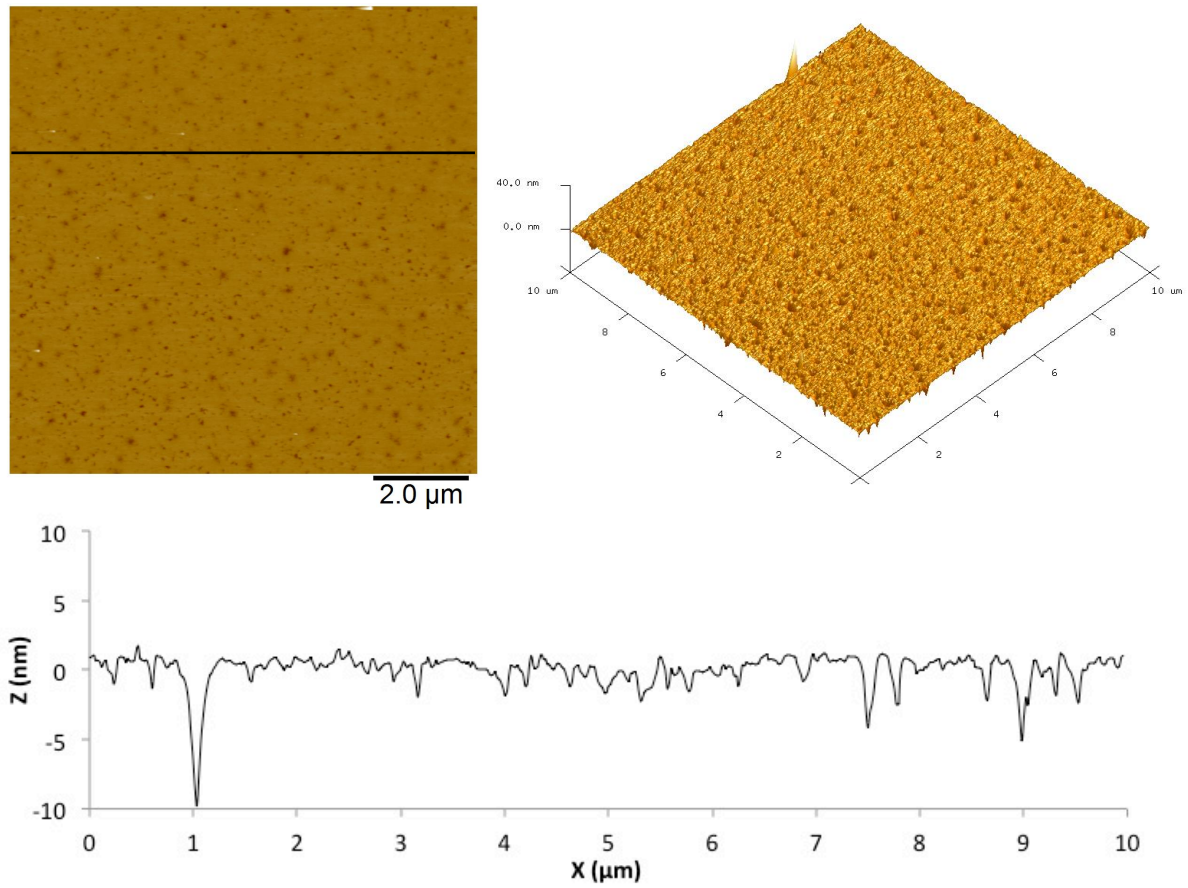

Figure 5.7. AFM topographical images of unmodified PPF and line profile. Scan size = 10 × 10 µm.

The topography images and line profiles of the Ar-Tri-APBiB-PMMA surface are shown in Figure 5.8. From these images, it is clear the surface has changed. The line profiles highlight two of the clusters of features, where it appears there is a higher density of polymer chains.

The features at the top left hand side approach 75 nm in height (as shown by the red line profile in Figure 5.8). Another cluster located near the centre of the image shows features approaching 30 nm in height. From the AFM images and line profiles, it appears that there is a significant amount of unmodified or sparsely modified regions. The relative flatness of the red line profile indicates a low density of features.

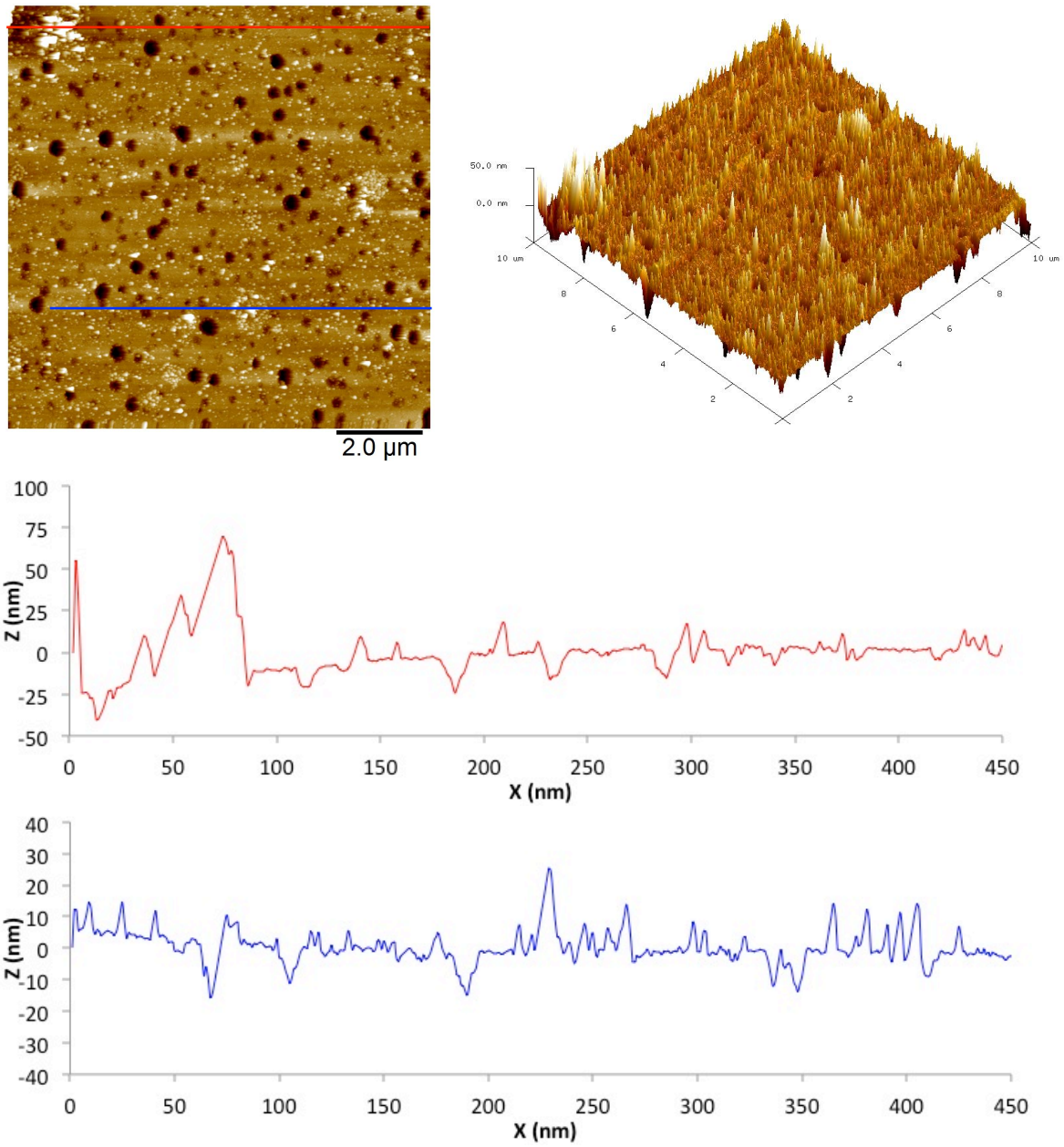

Figure 5.8. AFM topographical images and line profiles of PMMA polymer brushes grown from the Ar-Tri-APBiB modified PPF surface by SI-ATRP. Scan size = 10 × 10 µm.

Modification of the Ar-Tri-APBiB film on carbon electrodes by the polymerisation of PMMA appears to be successful. From the changes in the redox probe voltammetry CVs and water contact angles, it is clear the surface has been further modified. AFM imaging shows the appearance of surface features not previously observed on unmodified or Ar-Eth modified PPF surfaces; these are thought to be polymer chains. However, the surface appears to be non-uniformly modified, with clusters of features and areas of little modification being observed.

5.3.3.2. PMMA Brushes from Ar-Tri-APBiB Modified Surface by eSI-ATRP

PMMA polymer brushes were grown from an Ar-Tri-APBiB modified GC electrode by electrochemically mediated SI-ATRP (eSI-ATRP). The experimental procedure for polymerisation is described in Chapter 2.4. The modified surfaces were analysed by redox probe voltammetry, water contact angle measurements and AFM imaging.

5.3.3.2.1. Redox Probe Voltammetry

The polymerisation of methyl methacrylate from the Ar-Tri-APBiB modified surface by eSI-ATRP was followed by redox probe voltammetry. Figure 5.9 (red line) shows a CV scan obtained in $K_3Fe(CN)_6$ at the Ar-Tri-APBiB modified GC electrode. At 30 min intervals, the electrode was removed from the reaction vessel, sonicated in acetone for 5 min, then sonicated in water for 5 min, dried with N_2 (g) and scanned in the redox probe solution. After polymerisation time = 0.5 h (blue line), there was a significant change in the CV shape. After 1 h of reaction time (green line), there was little further change in the redox probe response. The CV obtained after 1.5 h of polymerisation (purple line) showed the greatest change, with the quasi-reversible $Fe(CN)_6^{3-/4-}$ redox peaks appearing (ΔE_p = 360 mV). After a further 0.5 h of polymerisation time (orange line), ΔE_p increased to 384 mV. The reason for the appearance of the redox peak for a film that is expected to be increasing in thickness is unknown.

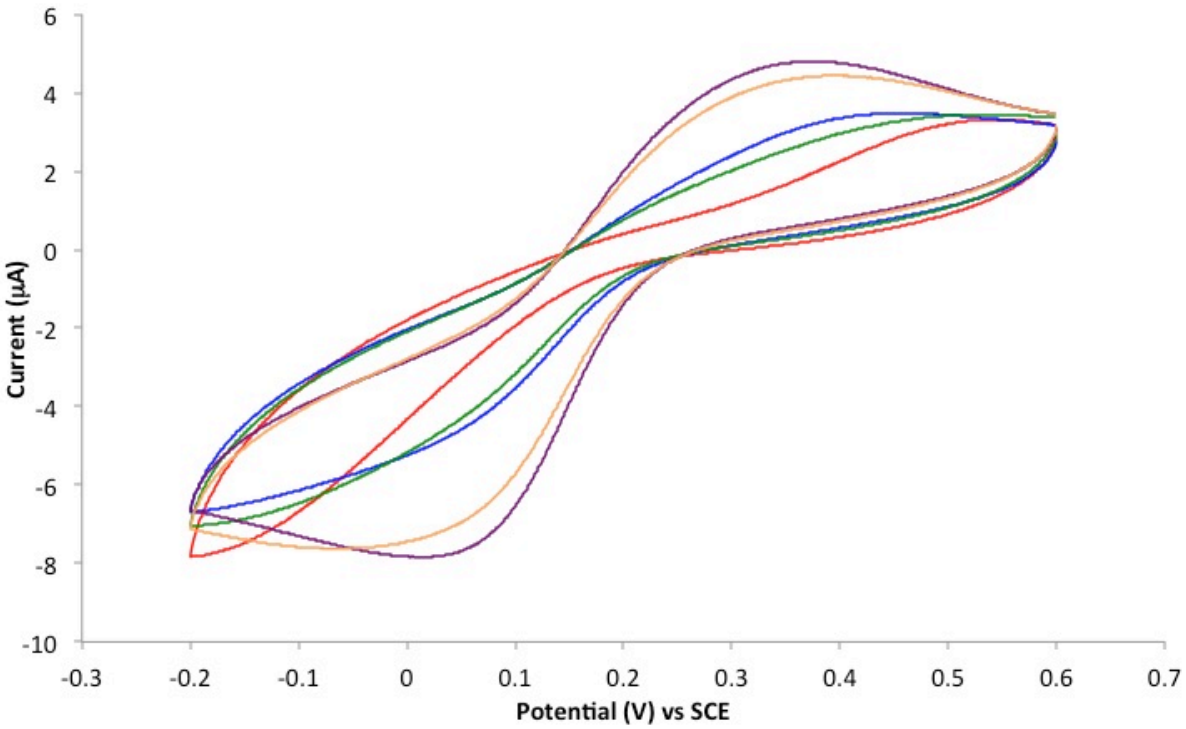

Figure 5.9. CV of 1 mM $K_3Fe(CN)_6$ in PBS (pH 7) showing the effect of PMMA polymer brush growth by eSI-ATRP from an Ar-Tri-APBiB modified surface over time. Scan rate = 100 mV s^{-1}. Scans taken at the Ar-Tri-APBiB surface (red line), after polymerisation time = 0.5 h (blue line), 1 h (green line), 1.5 h (purple line), and 2 h (orange line).

5.3.3.2.2. Contact Angle Measurements

Contact angle measurements of the PMMA polymer brushes grown from an Ar-Tri-APBiB modified GC surface by eSI-ATRP were used to assess the success of the polymerisation reaction. Table 5.10 lists the water contact angle measurements for a polished GC surface, a GC surface modified with an Ar-Tri-APBiB film, and the PMMA polymer brushes grown from the Ar-Tri-APBiB surface by eSI-ATRP over a period of 2 h.

The average water contact angle measured for the PMMA polymer brushes grown by eSI-ATRP (58 ± 1 °) is not significantly different to the value measured for the PMMA polymer brushes grown by SI-ATRP (56 ± 2). As mentioner earlier, the Ar-Tri-APBiB-PMMA surface

is hydrophilic compared to the values measured for PMMA brushes grown from GC by Matrab and co-workers (83.5 ± 1.4 °).[143]

Table 5.10. Average contact angle measurements for polished GC, Ar-Tri-APBiB and PMMA polymer brushes grown by eSI-ATRP over 2 h. Error is the standard deviation.

	Bare GC	**Ar-Tri-APBiB**	**Ar-Tri-APBiB-PMMA**
MQ Water	88 ± 1 °	62 ± 2 °	58 ± 1 °

5.3.3.2.3. Atomic Force Microscopy

AFM imaging of the Ar-Tri-APBiB surface after polymerisation of MMA by eSI-ATRP gave the images and line profile shown in Figure 5.10. The resulting surface has similar features to the surface polymerised by SI-ATRP. The eSI-ATRP prepared surface has clusters of features along with regions that appear to be less densely modified. The features in the AFM image reach a maximum of ~30 nm in height (as shown by the line profile in Figure 5.10).

As for the Ar-Tri-APBiB surface modified by SI-ATRP, the polymerisation of PMMA by eSI-ATRP appears to be successful. Changes in the redox probe voltammetry response and in water contact angle measurements indicate a change in the surface composition. AFM imaging shows an increase it the surface roughness (as seen in the line profile of Figure 5.10) compared to the unmodified PPF surface (Figure 5.7). The surface modification appears to be non-uniform, with clusters of features and regions of little modification, similar to that observed for the SI-ATRP modified surface.

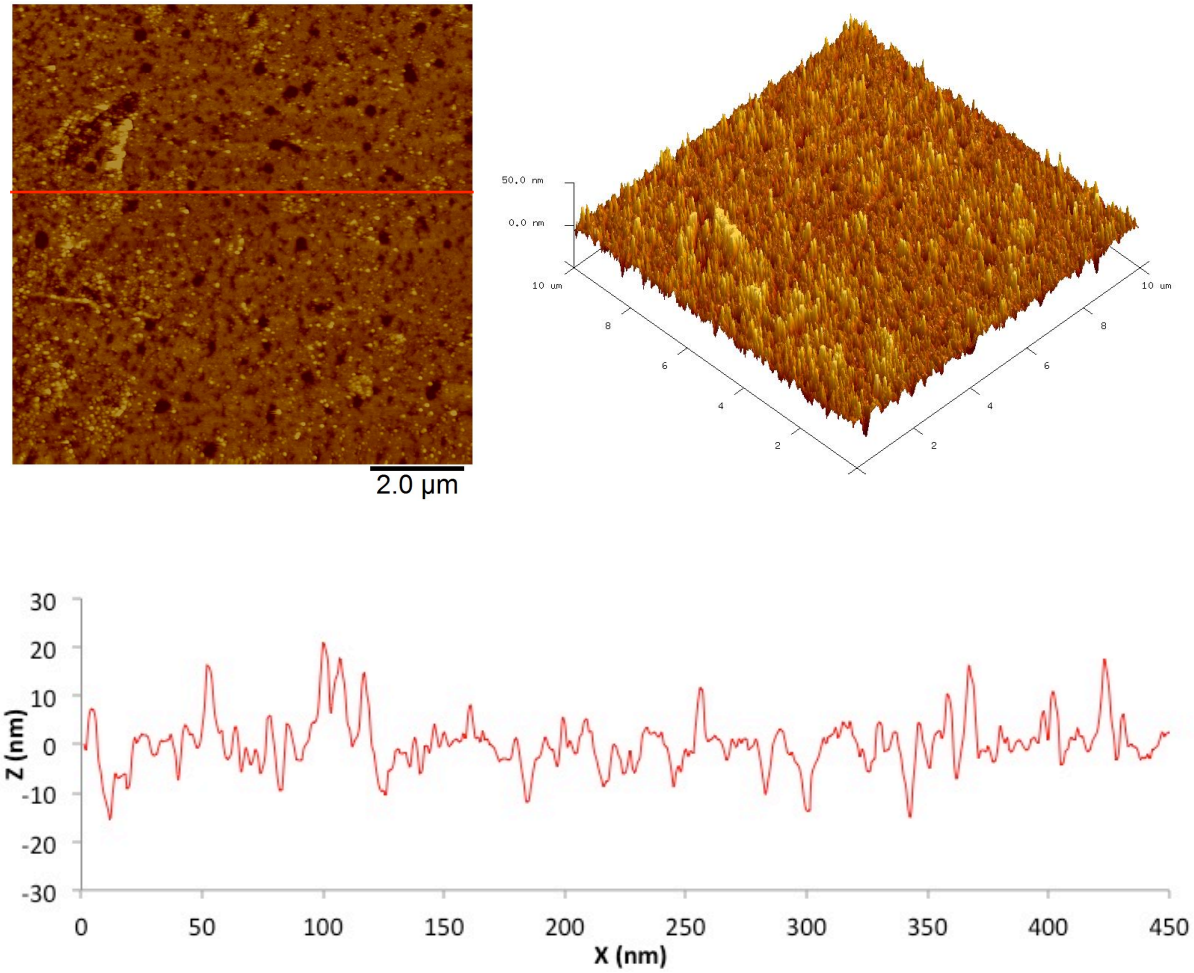

Figure 5.10. AFM topographical images of PMMA polymer brushes grown from the Ar-Tri-APBiB modified PPF surface by eSI-ATRP. Scan size = 10 × 10 µm.

5.3.3.3. PMMA Brushes from Ar-Eth Modified Surface by One-Pot CuAAC/SI-ATRP

PMMA polymer brushes were grown from an Ar-Eth modified carbon electrode using a simultaneous one-pot copper catalysed azide-alkyne click reaction / SI-ATRP reaction (Scheme 5.4). No reports could be found describing a similar strategy involving the simultaneous attachment of an initiator and polymerisation. The details of the reaction are in Chapter 2. The PMMA polymer brushes were analysed by redox probe voltammetry, water contact angle measurements and AFM imaging.

5.3.3.3.1. Redox Probe Voltammetry

Redox probe voltammetry was used to confirm the presence of PMMA polymer brushes on the surface. An aqueous solution of $K_3Fe(CN)_6$ was used as the redox probe. Scanning of the redox probe at the Ar-Eth modified surface gave the blue line CV in Figure 5.11. Rescanning of the redox probe solution after the one-pot CuAAC/SI-ATRP modification gave the red line in Figure 5.10. It is clear that the surface has been modified after the reaction, with the surface significantly hindering electron transfer from the electrode surface to the redox species. This is good evidence for the successful clicking of APBiB to the Ar-Eth surface and simultaneous growth of PMMA polymer brushes.

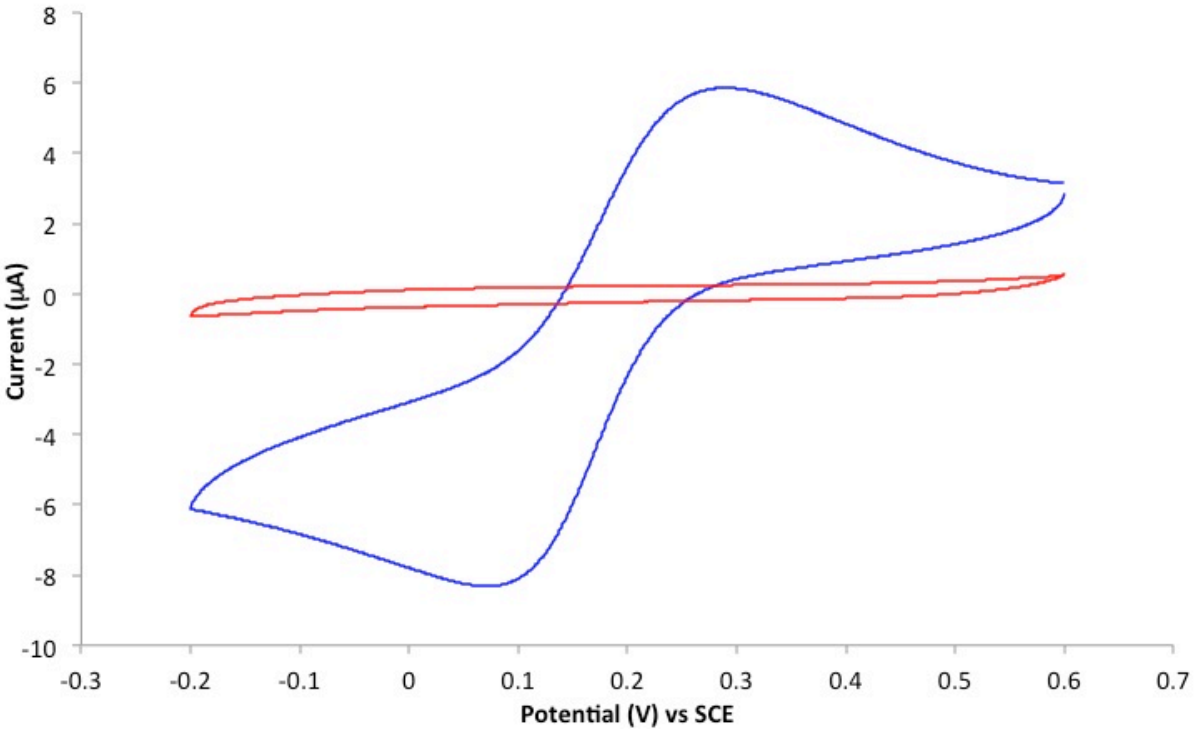

Figure 5.11. CV of 1 mM $K_3Fe(CN)_6$ in PBS (pH 7) showing the effect of the one-pot CuAAC/SI-ATRP modification for PMMA polymer brush growth from an Ar-Eth modified surface. Scan rate = 100 mV s^{-1}. The blue line is the scan taken at the Ar-Eth modified surface, and the red line is the scan taken after the polymerisation procedure.

5.3.3.3.2. Contact Angle Measurements

Water contact angle measurements were taken before and after the one-pot modification of an Ar-Eth film to determine the wettability of the surface. A polished GC plate (average water contact angle = 88 ± 1 °) was modified with an Ar-Eth film (details of Ar-Eth modification are given in Chapter 3) which gave an average water contact angle = 66 ± 2 °. Following the one-pot CuAAC/SI-ATRP reaction for the simultaneous click coupling of APBiB to the Ar-Eth modified surface and the polymerisation of PMMA, the average water contact angle reduced to 61 ± 1 ° (Table 5.11). While the change in contact angle from the Ar-Eth surface to the polymer brush surface was small, the published water contact angle for solid sheets of PMMA is 64.3 ± 1.8 ° and so the contact angle obtained after polymerisation is not inconsistent with the presence of PMMA.[146] The PMMA polymer brushes grown from GC surface by Matrab and co-workers (contact angle = 83.5 ± 1.4 °)[143] is still considerably more hydrophobic that the polymer brushes produced by this method.

Table 5.11. Average water contact angle measurements for polished and modified GC surfaces. Error is the standard deviation.

	Bare GC	**Ar-Eth**	**Ar-Tri-APBiB-PMMA**
MQ Water	88 ± 1 °	66 ± 2 °	62 ± 1 °

5.3.3.3.3. Atomic Force Microscopy and Depth Profiling

AFM images and a line profile taken of the Ar-Eth modified PPF are shown in Figure 5.12 (repeated from Figure 3.24 for comparison).

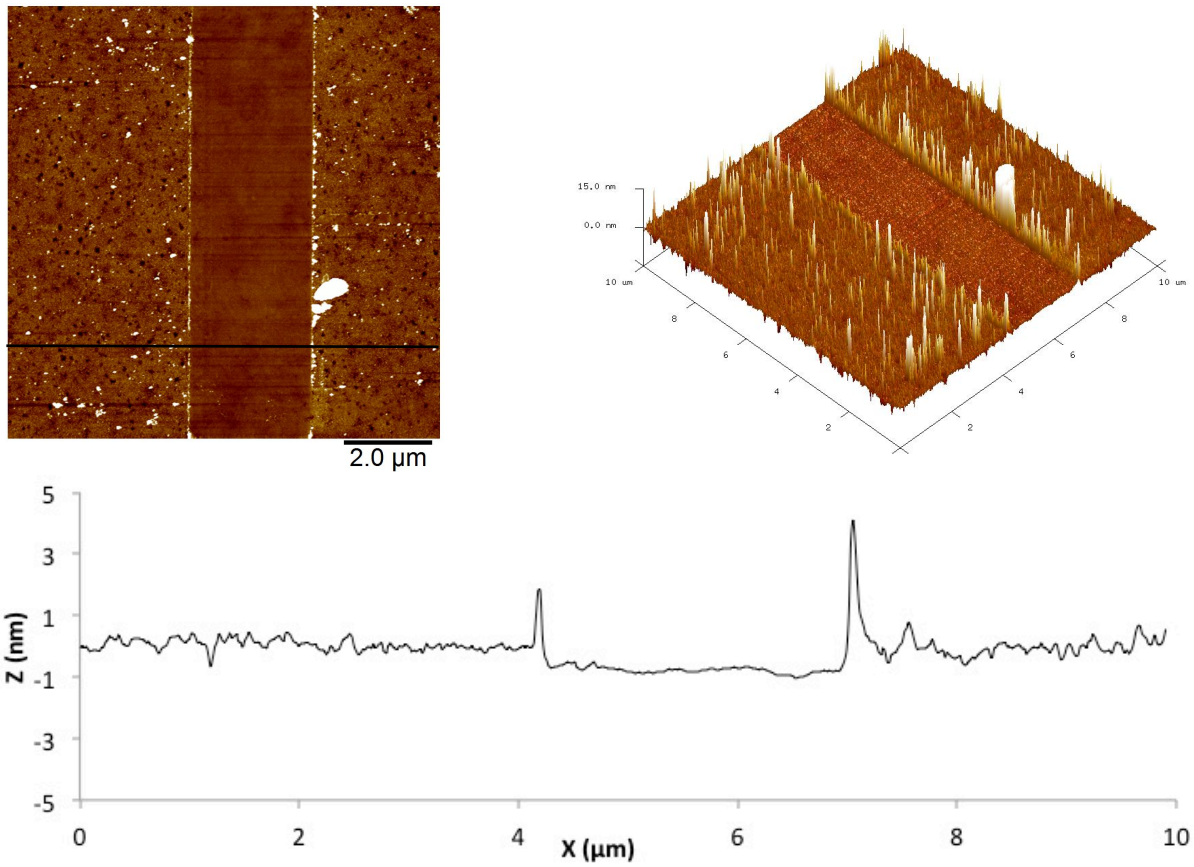

Figure 5.12. AFM topographical images and a line profile of an Ar-Eth modified PPF surface showing a 2.5 × 10 µm scratch. Scan size = 10 × 10 µm.

After the one-pot CuAAC/SI-ATRP modification, AFM images of the resultant surface (Figure 5.13) show a large number of features on the surface. Depth profiling of the film through AFM scratching (details for the depth profiling technique are given in Chapter 2.5) gives an estimated film thickness of 10 nm. A line profile taken across the scratch shows the extent of modification on either side of the scratch, when compared to the line profile of the scratch on the Ar-Eth surface (Figure 5.12). The one-pot modified surface appears to be more uniformly modified in comparison to the PMMA polymer brushes grown by SI-ATRP and eSI-ATRP, with less unmodified regions and clustering of features.

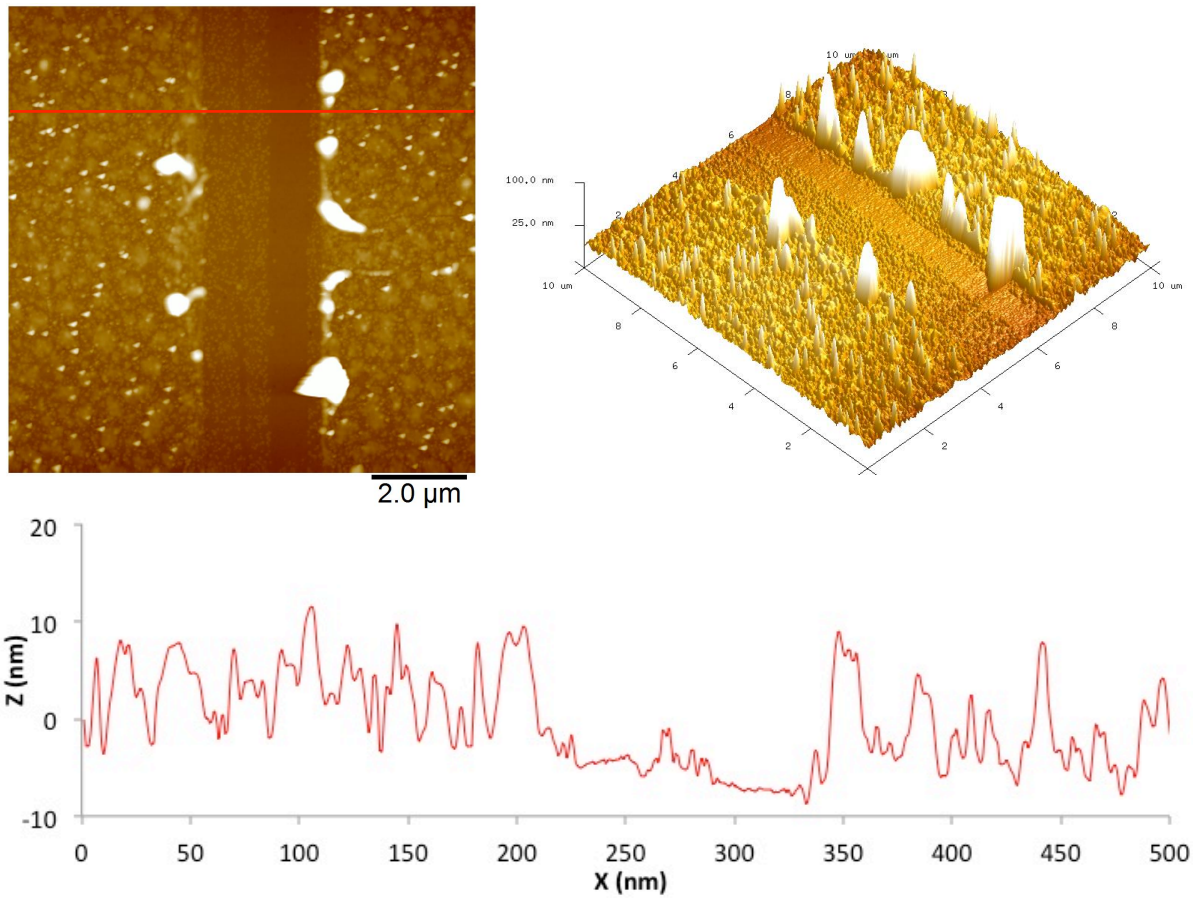

Figure 5.13. AFM topographical images of PMMA brush grown from Ar-Tri-APBiB modified PPF surface by the one-pot CuAAC/SI-ATRP method showing a 2.5 × 10 µm scratch. Scan size = 10 × 10 µm.

The further modification of an Ar-Eth carbon electrode by a one-pot CuAAC/SI-ATRP reaction for the simultaneous coupling of APBiB to the surface tethered Ar-Eth molecules and the polymerisation of PMMA (Scheme 5.4) appears to be successful. Redox probe voltammetry indicates the presence of a thick film, while water contact angles agreement with literature values for a solid PMMA sheet. AFM imaging of the reacted surface shows uniform modification (in comparison to the surface modified by SI-ATRP and eSI-ATRP), while depth profiling gave an estimated film thickness of 10 nm. It can be concluded that the one-pot CuAAC/SI-ATRP reaction was successful.

5.3.3.4. PMMA Brushes from ABiC Modified Surface

PMMA polymer brushes were grown from ABiC modified PPF surfaces using the SI-ATRP polymerisation method described in Chapter 2 (Scheme 5.3). An AFM image of the ABiC modified PPF surface is shown in Figure 5.14. The accompanying line profile shows a relatively feature-free film with low surface roughness. After polymerisation of PMMA by SI-ATRP, the surface appears to have been modified (Figure 5.15). From the line profile of the AFM image, it is clear that the number of features on the surface has increased and the surface roughness has increased. The features on the polymerised surface appear to reach greater than 20 nm in height. The surface modification appears to be uniform in comparison to the samples prepared using SI-ATRP and eSI-ATRP from the Ar-Tri-APBiB prepared surface.

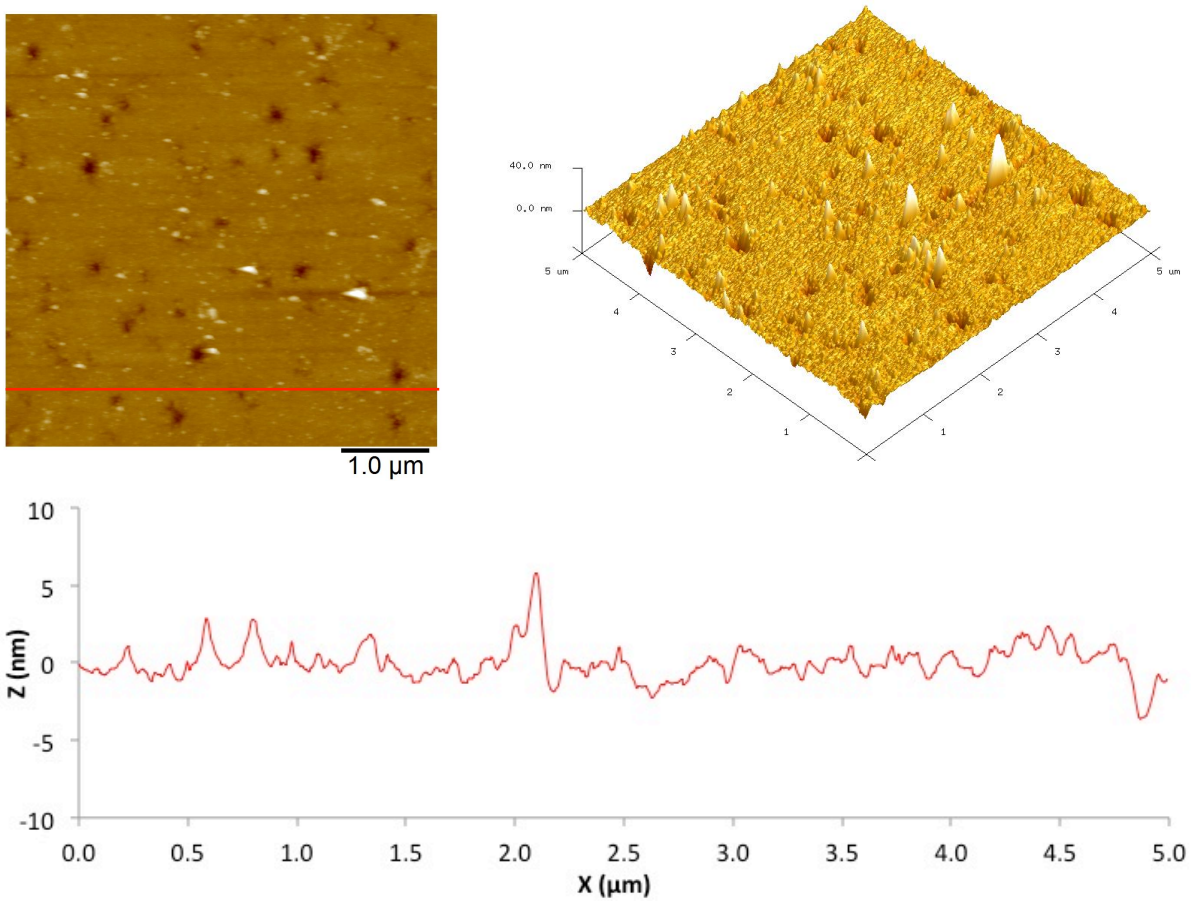

Figure 5.14 AFM topographical images and line profile of ABiC modified PPF.

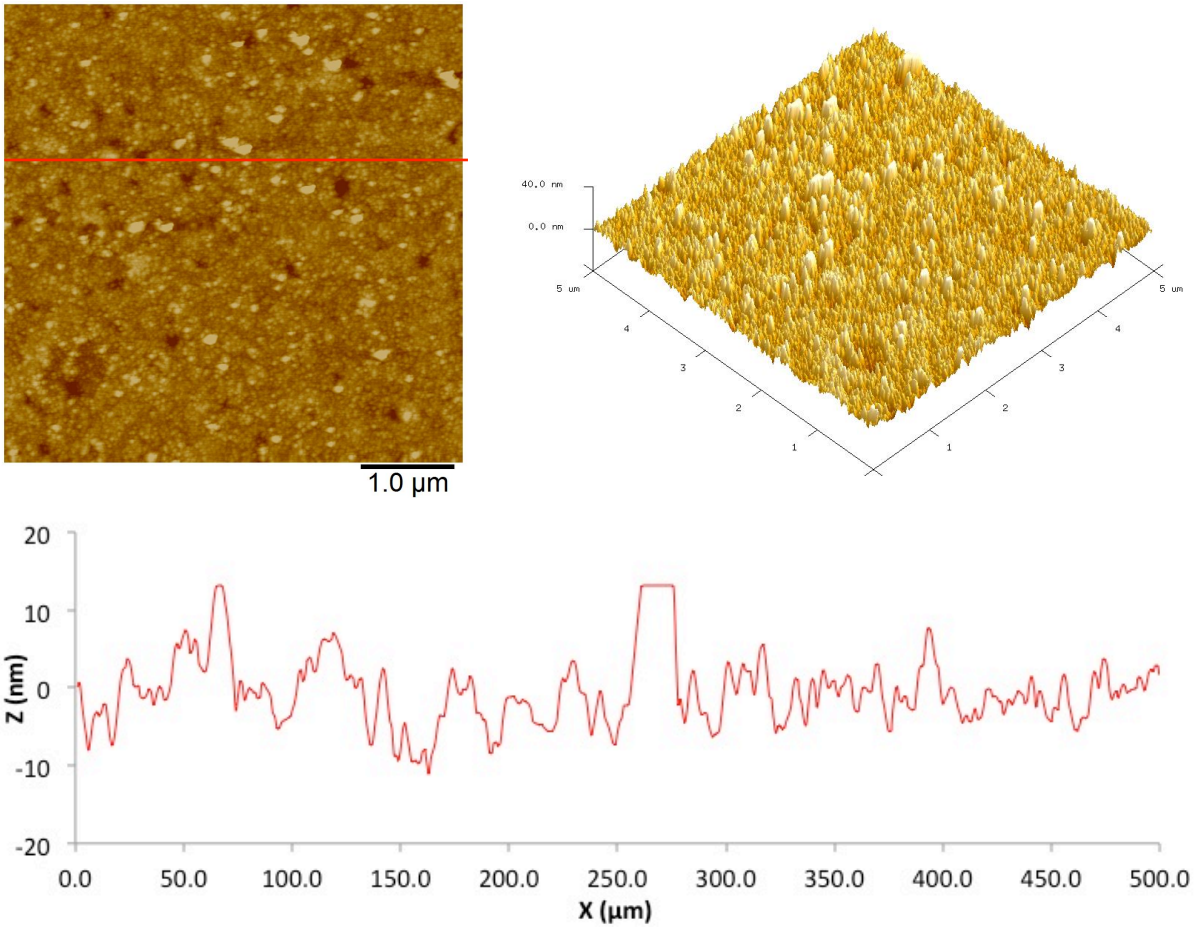

Figure 5.15 AFM topographical images of PMMA polymer brushes grown by SI-ATRP from the ABiC modified PPF.

5.3.2. Comparison of Methods

The growth of PMMA polymer chains from the surface by all three methods of SI-ATRP (SI-ATRP, eSI-ATRP and one-pot CuAAC/SI-ATRP) has been successful. However, the degree to which the polymer chains have polymerised varies significantly.

Cyclic voltammetry scans of an aqueous solution of ferricyanide ($K_3Fe(CN)_6$) in PBS (pH 7) was used as a redox probe. Scanning the redox probe at the surface modified by SI-ATRP gave the red line CV (Figure 5.16), by eSI-ATRP (blue CV, Figure 5.16) and by the one-pot CuAAC/SI-ATRP method (green CV, Figure 5.16). It is clear to see that the surface modified

by the one-pot method inhibits electron transport between the surface and the redox species significantly more than the surfaces modified by the other two methods.

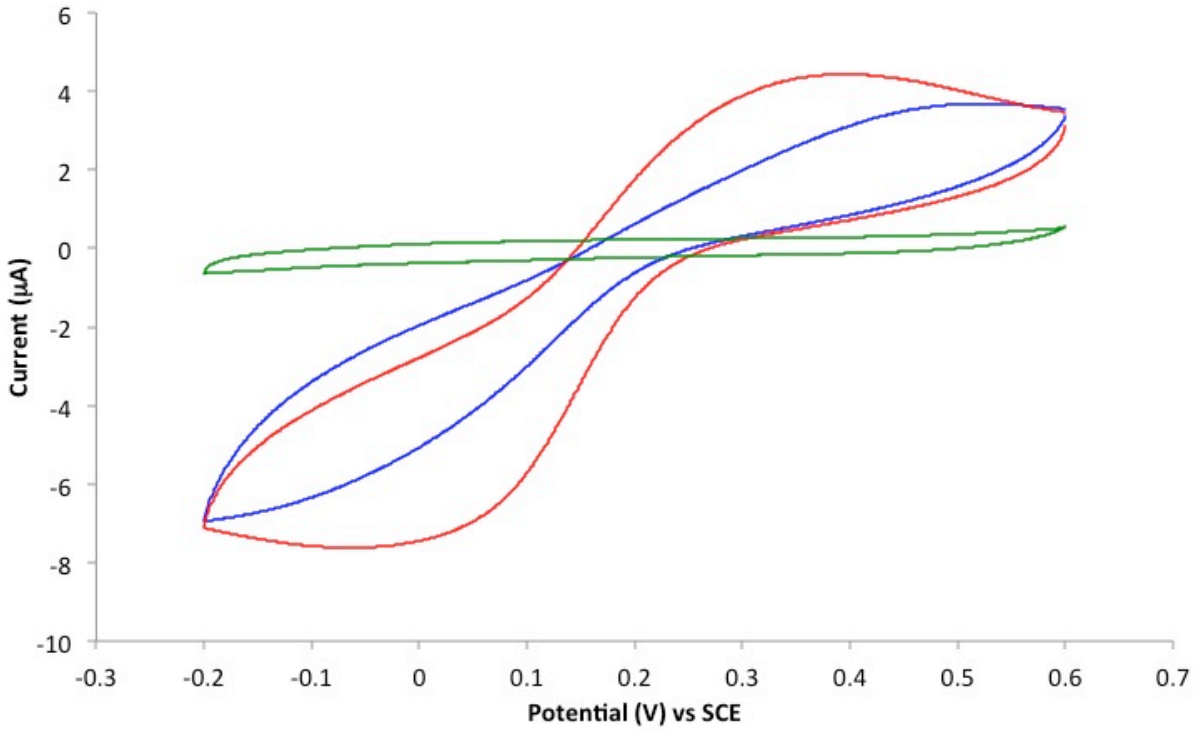

Figure 5.16. CV of 1 mM K3Fe(CN)6 in PBS (pH 7) showing the difference in blocking properties of three PMMA polymer brush surfaces. Scan rate = 100 mV s-1. The scans are taken at the PMMA polymer brush surface grown by (red line) SI-ATRP, (blue line) eSI-ATRP, and (green line) one-pot CuAAC/SI-ATRP.

The AFM images of the PMMA polymer brush modified surfaces show different degrees of modification (Figure 5.17). The PMMA polymer brushes grown by the SI-ATRP and eSI-ATRP method (Figure 5.17 (a) and (b), respectively) appear to have the least number of features on the surface, with regions of sparse modification. The surface modified by the one-pot CuAAC/SI-ATRP method (Figure 5.17 (c)) appears to be more uniformly modified compared to the other methods. The polymer brushes grown from the ABiC modified surface by SI-ATRP (Figure 5.17 (d)) also appears to have a high polymer brush density.

Water contact angles are similar at all surfaces and do not differentiate between the polymerisation methods.

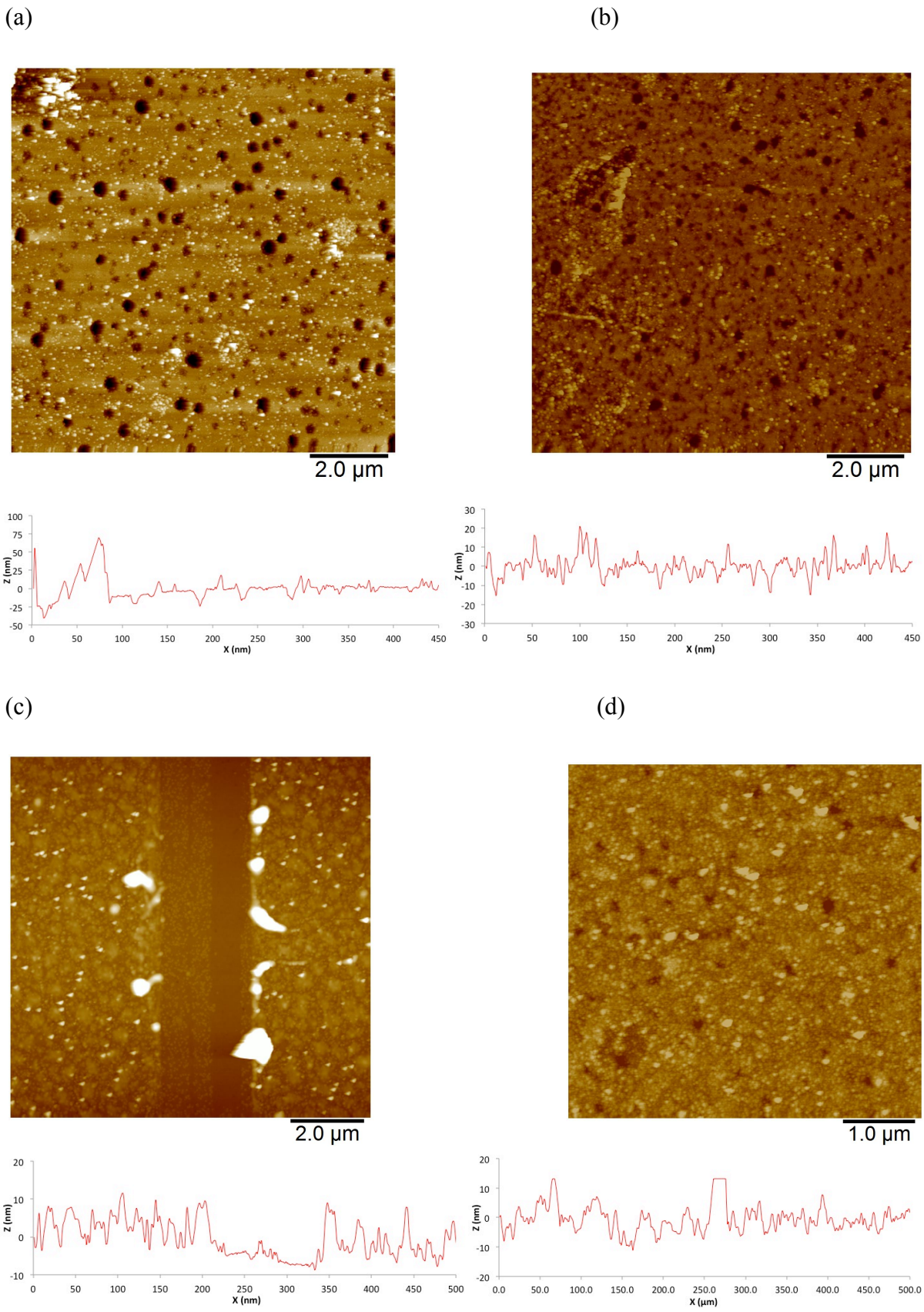

Figure 5.17. AFM images and line profiles for PPF surfaces modified with PMMA polymer brushes by: (a) SI-ATRP, (b) eSI-ATRP, (c) one-pot CuAAC/SI-ATRP, and (d) (ABiC modified) SI-ATRP

5.4. Conclusion

This preliminary work was aimed at identifying the best route for grafting polymers from monolayer tethers. Polymer brushes of PMPDSAH were grown from Ar-CONH-ABiB and Ar-Tri-APBiB modified GC surfaces. These polymer brushes were characterised through redox probe voltammetry, contact angle measurements and XPS analysis. The detection of quaternary amines and sulfonate groups by XPS analysis are good evidence for the successful polymerisation of PMPDSAH. Attempts at switching the conformational state of the polymer brushes through increased salt content in a droplet of solution places upon the modified surface were unsuccessful, and it is thought that altering oxidation state of the underlying surface is necessary in controlling the polymer brush conformation.

Polymer brushes of PMMA were grown from Ar-Tri-APBiB modified surfaces by two methods, SI-ATRP and electrochemically mediated SI-ATRP. Both these methods appear to have been successful, evidenced through redox probe voltammetry, contact angle measurements and AFM imaging.

PMMA brushes were also grown from an Ar-Eth modified surface by a simultaneous one-pot CuAAC/SI-ATRP reaction. Redox probe voltammetry of the polymerised surface exhibited greatly reduced electron transfer from the surface to the redox species, indicating that a blocking film was present on the surface. AFM images of the surface after polymerisation showed a greatly increased number of features on the surface and increased surface roughness, consistent with polymer brush growth.

AFM imaging of PMMA polymer brushes grown from an ABiC modified PPF surface indicated successful polymerisation initiation.

Consideration of all the data suggests that the one-pot CuAAC/SI-ATRP approach is the method of choice for growing uniform polymer chains of PMMA from a surface.

Chapter 6. Conclusions and Future Work

The modification of a surface with a monolayer is important as topographical features and bulk substrate properties are retained. Aryl diazonium chemistry and selected coupling reactions are excellent candidates for the covalent attachment of organic molecules to a surface, offering high attachment yields and selective bonding with the surface. Accordingly, the aim of this thesis work was to investigate the covalent attachment of polymerisation initiators to carbon substrates.

Carboxyphenyl (Ar-COOH) and ethynylaryl (Ar-Eth) monolayers were obtained from the electrochemical grafting of the corresponding protected (Ar-COO-Fm and Ar-Eth-TIPS, respectively) aryl diazonium salts. Selective cleavage of protecting groups after electrochemical grafting yielded the reactive monolayer films, as characterised by ferricyanide redox probe voltammetry, contact angle measurements and depth profiling by atomic force microscopy (AFM) (for the Ar-Eth modified surface). Before removal of the protecting groups, the film inhibits electron transfer from the surface to the redox species in solution, indicating a thick film. After deprotection, electron transfer is partially restored, indicating the reduction of the film thickness. The Ar-COOH monolayer displayed pH dependency during contact angle measurements. The reactivity of the Ar-Eth monolayer was explored by a model reaction with azidomethylferrocene ($FcMeN_3$). The copper azide-alkyne click reaction (CuAAC) was successful at coupling ferrocene to the surface, as shown by cyclic voltammetry after the reaction.

Polymerisation initiators were attached the grafted monolayers. The attachment of α-bromoisobutyryl bromide (ABiB) to the Ar-COOH layer was accomplished through a two-step modification, where ethanolamine was first reacted with the carboxylic acid groups in an amide coupling reaction, followed by the esterification of ABiB with the terminal alcohol

groups. XPS analysis indicated the presence of bromine on the surface, albeit at a relatively low atomic percentage. A synthesised azide derivate of the polymerisation initiator, (3-azidopropyl) bromoisobutyrate (APBiB), was coupled to the ethynylaryl surface using the same CuAAC reaction as for the coupling of $FcMeN_3$. XPS analysis showed that the reaction was successful.

The single step CuAAC reaction for the attachment of molecules to the Ar-Eth monolayer is an elegant method coupling. In comparison, the two-step approach required for attaching the polymerisation initiator to the Ar-COOH film was difficult to characterise and has unknown yield. Further investigation on the coupling of molecules to the Ar-COOH monolayer may be able to optimise the surface concentration of coupled molecules, either through better selection of amide/ester coupling agents or through altering the polymerisation initiator molecule to react directly with the tethered carboxylic acid groups, reducing the number of surface modification steps required.

The attachment of polymerisation initiators by direct reactions with the carbon surface was explored. The conversion of carboxylic acids to acid chlorides to increase reactivity was utilised. Characterisation of the coupled initiator molecules is difficult, so an indirect method for estimating the amount of tethered initiator was used. Ferrocenoyl chloride (FcCOCl) is expected to react with the same functional groups as the polymerisation initiator derivatives. Thus, if FcCOCl is reacted with the modified surface, there should be a decreased amount of Fc immobilised on the surface compared to when FcCOCl is reacted with an unmodified surface. The accuracy of this method of quantification of the surface concentration of polymerisation initiator molecules was not established, but it was adopted as a practical approach because the polymerisation initiators are not electrochemically active and do not produce very thick films. XPS analysis and infrared spectroscopy could be used in the future to help further characterise these modified surfaces.

A two-step method of tethering a polymerisation initiator was investigated. Primary amines have been shown in the literature to spontaneously react with GC through a proposed Michael-like addition. In this work, ethanolamine was attached to the surface, increasing the surface concentration of alcohol functional groups. These groups were reacted with ABiB and with α-bromoisobutyryl chloride (ABiC) in esterification reactions. Both reactions showed potential, with greatly reduced amount of Fc being coupled to the surface after reaction with the polymerisation initiator. Future work could involve the full characterisation of these modified surfaces and the growth of polymer brushes from the tethered initiators.

Polymer brushes of PMPDSAH were grown by SI-ATRP from the Ar-CONH-ABiB and Ar-Tri-APBiB prepared surfaces. The zwitterionic polymer brushes were analysed through redox probe voltammetry, where an unusual asymmetric response was observed for the ferricyanide redox peak. XPS analysis provided evidence for the successful polymerisation of PMPDSAH by the detection of quaternary amine and sulfonate groups. PMPDSAH has been shown to exhibit switchable behaviour when grafted to ECPs. Further investigation into methods for switching the conformation of polymers grafted in the present work would be interesting.

Polymer brushes of PMMA were grown Ar-Tri-APBiB and ABiC modified electrode surfaces. Surface initiated atom transfer radical polymerisation (ATRP) and electrochemically mediated SI-ATRP (eSI-ATRP) were used to polymerise methyl methacrylate from the Ar-Tri-APBiB. AFM imaging of the modified surface shows features resulting from the polymerisation reaction. These features are well distributed across the surface, with clusters of higher density forming in some areas, but the overall polymer coverage appears to be quite low.

The polymer brushes grown from the ABiC modified PPF surface was an interesting result. =. Although further characterisation of the surface is needed, the AFM image shows a clear change in the surface consistent with the presence of polymer brushes.

Perhaps the most successful piece of work in this thesis was the simultaneous clicking of APBiB to the well-defined Ar-Eth modified surface and polymerisation of PMMA. This is an elegant method for producing polymer brushes as the number of surface modification steps is greatly reduced. AFM images taken of the polymer brushes grown from this method appear to show a higher brush density than those produced by SI-ATRP and eSI-ATRP. Redox probe voltammetry was consistent with a significant change in the thickness of the film on the electrode after the one-pot procedure. To the best of the author's knowledge, this is the first example of modifying a carbon electrode simultaneously by clicking an ATRP initiator and polymerising PMMA from said initiator. Further characterisation of this method is needed, as the one-pot reaction rates are not known at this time. It would be valuable to explore the scope of the method for the formation of other polymer brushes with the possibility of establishing a new general method for one-pot CuAAC/SI-ATRP. Another direction for future research is to use protected Ar-Eth diazonium salts with different size protecting groups. These would generate monolayers with different densities of tether groups and hence leas to different densities of grafted polymer chains. These would offer useful systems for fundamental studies of polymer interactions, especially in the context of switchable behaviour.

References

1. Jenkins, G. M.; Kawamura, K. Structure of Glassy Carbon. *Nature* **1971,** *231* (5299), 175-176.

2. Pesin, L. A. Review Structure and properties of glass-like carbon. *J. Mater. Sci.* **2002,** *37* (1), 1-28.

3. Pesin, L. A.; Baitinger, E. M. A new structural model of glass-like carbon. *Carbon* **2002,** *40* (3), 295-306.

4. Heiduschka, P.; Munz, A. W.; Göpel, W. Impedance spectroscopy and scanning tunneling microscopy of polished and electrochemically pretreated glassy carbon. *Electrochim. Acta* **1994,** *39* (14), 2207-2223.

5. Collier, W. G.; Tougas, T. P. Determination of surface hydroxyl groups on glassy carbon with x-ray photoelectron spectroscopy preceded by chemical derivatization. *Anal. Chem.* **1987,** *59* (3), 396-399.

6. Kim, J.; Song, X.; Kinoshita, K.; Madou, M.; White, R. Electrochemical Studies of Carbon Films from Pyrolyzed Photoresist. *J. Electrochem. Soc.* **1998,** *145* (7), 2314-2319.

7. Ranganathan, S.; McCreery, R. L. Electroanalytical Performance of Carbon Films with Near-Atomic Flatness. *Anal. Chem.* **2001,** *73* (5), 893-900.

8. Brooksby, P. A.; Downard, A. J.; Yu, S. S. C. Effect of Applied Potential on Arylmethyl Films Oxidatively Grafted to Carbon Surfaces. *Langmuir* **2005,** *21* (24), 11304-11311.

9. Pinson, J. Attachment of Organic Layers to Materials Surfaces by Reduction of Diazonium Salts. In *Aryl Diazonium Salts*, Chehimi, M. M., Ed. Wiley-VCH Verlag GmbH & Co. KGaA: 2012; pp 1-35.

10. Allongue, P.; Delamar, M.; Desbat, B.; Fagebaume, O.; Hitmi, R.; Pinson, J.; Savéant, J.-M. Covalent Modification of Carbon Surfaces by Aryl Radicals Generated from the Electrochemical Reduction of Diazonium Salts. *J. Am. Chem. Soc.* **1997,** *119* (1), 201-207.

11. Yacynych, A. M.; Kuwana, T. Cyanuric chloride as a general linking agent for modified electrodes: attachment of redox groups to pyrolytic graphite. *Anal. Chem.* **1978,** *50* (4), 640-645.

12. Ianniello, R. M.; Yacynych, A. M. Immobilized enzyme chemically modified electrode as an amperometric sensor. *Anal. Chem.* **1981,** *53* (13), 2090-2095.

13. Elliott, C. M.; Murray, R. W. Chemically modified carbon electrodes. *Anal. Chem.* **1976,** *48* (8), 1247-1254.

14. Gallardo, I.; Pinson, J.; Vilà, N. Spontaneous Attachment of Amines to Carbon and Metallic Surfaces. *J. Phys. Chem. B* **2006,** *110* (39), 19521-19529.

15. Lee, L.; Downard, A. Preparation of ferrocene-terminated layers by direct reaction with glassy carbon: a comparison of methods. *J. Solid State Electrochem.* **2014**, 1-10.

16. Liu, Y.-C.; McCreery, R. L. Reactions of Organic Monolayers on Carbon Surfaces Observed with Unenhanced Raman Spectroscopy. *J. Am. Chem. Soc.* **1995,** *117* (45), 11254-11259.

17. Barbier, B.; Pinson, J.; Desarmot, G.; Sanchez, M. Electrochemical Bonding of Amines to Carbon Fiber Surfaces Toward Improved Carbon‐Epoxy Composites. *J. Electrochem. Soc.* **1990,** *137* (6), 1757-1764.

18. Delamar, M.; Hitmi, R.; Pinson, J.; Saveant, J. M. Covalent Modification Of Carbon Surfaces By Grafting Of Functionalized Aryl Radicals Produced From Electrochemical Reduction Of Diazonium Salts. *J. Am. Chem. Soc.* **1992,** *114* (14), 5883-5884.

19. Downard, A. J. Electrochemically Assisted Covalent Modification of Carbon Electrodes. *Electroanalysis* **2000,** *12* (14), 1085-1096.

20. Kuo, T. C.; McCreery, R. L.; Swain, G. M. Electrochemical Modification of Boron‐Doped Chemical Vapor Deposited Diamond Surfaces with Covalently Bonded Monolayers. *Electrochem. Solid-State Lett.* **1999,** *2* (6), 288-290.

21. Uetsuka, H.; Shin, D.; Tokuda, N.; Saeki, K.; Nebel, C. E. Electrochemical Grafting of Boron-Doped Single-Crystalline Chemical Vapor Deposition Diamond with Nitrophenyl Molecules. *Langmuir* **2007,** *23* (6), 3466-3472.

22. Firth, B. E.; Miller, L. L.; Mitani, M.; Rogers, T.; Lennox, J.; Murray, R. W. Anodic and cathodic reactions on a chemically modified edge surface of graphite. *J. Am. Chem. Soc.* **1976,** *98* (25), 8271-8272.

23. Kariuki, J. K.; McDermott, M. T. Nucleation and Growth of Functionalized Aryl Films on Graphite Electrodes. *Langmuir* **1999,** *15* (19), 6534-6540.

24. Ray, K.; McCreery, R. L. Spatially Resolved Raman Spectroscopy of Carbon Electrode Surfaces: Observations of Structural and Chemical Heterogeneity. *Anal. Chem.* **1997,** *69* (22), 4680-4687.

25. Adenier, A.; Bernard, M.-C.; Chehimi, M. M.; Cabet-Deliry, E.; Desbat, B.; Fagebaume, O.; Pinson, J.; Podvorica, F. Covalent Modification of Iron Surfaces by

Electrochemical Reduction of Aryldiazonium Salts. *J. Am. Chem. Soc.* **2001,** *123* (19), 4541-4549.

26. Adenier, A.; Barré, N.; Cabet-Deliry, E.; Chaussé, A.; Griveau, S.; Mercier, F.; Pinson, J.; Vautrin-Ul, C. Study of the spontaneous formation of organic layers on carbon and metal surfaces from diazonium salts. *Surf. Sci.* **2006,** *600* (21), 4801-4812.

27. Mesnage, A.; Lefèvre, X.; Jégou, P.; Deniau, G.; Palacin, S. Spontaneous Grafting of Diazonium Salts: Chemical Mechanism on Metallic Surfaces. *Langmuir* **2012,** *28* (32), 11767-11778.

28. Doppelt, P.; Hallais, G.; Pinson, J.; Podvorica, F.; Verneyre, S. Surface Modification of Conducting Substrates. Existence of Azo Bonds in the Structure of Organic Layers Obtained from Diazonium Salts. *Chem. Mater.* **2007,** *19* (18), 4570-4575.

29. Pandurangappa, M.; Lawrence, N. S.; Compton, R. G. Homogeneous chemical derivatisation of carbon particles: a novel method for funtionalising carbon surfaces. *Analyst* **2002,** *127* (12), 1568-1571.

30. Mévellec, V.; Roussel, S.; Tessier, L.; Chancolon, J.; Mayne-L'Hermite, M.; Deniau, G.; Viel, P.; Palacin, S. Grafting Polymers on Surfaces: A New Powerful and Versatile Diazonium Salt-Based One-Step Process in Aqueous Media. *Chem. Mater.* **2007,** *19* (25), 6323-6330.

31. Allongue, P.; de Villeneuve, C. H.; Pinson, J.; Ozanam, F.; Chazalviel, J. N.; Wallart, X. Organic monolayers on Si(111) by electrochemical method. *Electrochim. Acta* **1998,** *43* (19–20), 2791-2798.

32. Toupin, M.; Bélanger, D. Thermal Stability Study of Aryl Modified Carbon Black by in Situ Generated Diazonium Salt. *J. Phys. Chem. C* **2007,** *111* (14), 5394-5401.

33. Haque, A.-M. J.; Kim, K. Reusable bio-functionalized surfaces based on electrochemical desorption of benzenediazonium-grafted organic layers. *Chem. Commun.* **2011,** *47* (24), 6855-6857.

34. D'Amour, M.; Bélanger, D. Stability of Substituted Phenyl Groups Electrochemically Grafted at Carbon Electrode Surface. *J. Phys. Chem. B* **2003,** *107* (20), 4811-4817.

35. Lee, L.; Ma, H.; Brooksby, P. A.; Brown, S. A.; Leroux, Y. R.; Hapiot, P.; Downard, A. J. Covalently Anchored Carboxyphenyl Monolayer via Aryldiazonium Ion Grafting: A Well-Defined Reactive Tether Layer for On-Surface Chemistry. *Langmuir* **2014,** *30* (24), 7104-7111.

36. Lee, L.; Brooksby, P. A.; Downard, A. J. The stability of diazonium ion terminated films on glassy carbon and gold electrodes. *Electrochem. Commun.* **2012,** *19* (0), 67-69.

37. Lyskawa, J.; Bélanger, D. Direct Modification of a Gold Electrode with Aminophenyl Groups by Electrochemical Reduction of in Situ Generated Aminophenyl Monodiazonium Cations. *Chem. Mater.* **2006,** *18* (20), 4755-4763.

38. Lee, L.; Brooksby, P. A.; Leroux, Y. R.; Hapiot, P.; Downard, A. J. Mixed Monolayer Organic Films via Sequential Electrografting from Aryldiazonium Ion and Arylhydrazine Solutions. *Langmuir* **2013,** *29* (9), 3133-3139.

39. Leroux, Y. R.; Hapiot, P. Nanostructured Monolayers on Carbon Substrates Prepared by Electrografting of Protected Aryldiazonium Salts. *Chem. Mater.* **2013,** *25* (3), 489-495.

40. Saby, C.; Ortiz, B.; Champagne, G. Y.; Bélanger, D. Electrochemical Modification of Glassy Carbon Electrode Using Aromatic Diazonium Salts. 1. Blocking Effect of 4-Nitrophenyl and 4-Carboxyphenyl Groups. *Langmuir* **1997,** *13* (25), 6805-6813.

41. Doppelt, P.; Hallais, G.; Pinson, J.; Podvorica, F.; Verneyre, S. Surface Modification of Conducting Substrates. Existence of Azo Bonds in the Structure of Organic Layers Obtained from Diazonium Salts. *Chem. Mater.* **2007,** *19* (18), 4570-4575.

42. Downard, A. J. Potential-Dependence of Self-Limited Films Formed by Reduction of Aryldiazonium Salts at Glassy Carbon Electrodes. *Langmuir* **2000,** *16* (24), 9680-9682.

43. Brooksby, P. A.; Downard, A. J. Nanoscale Patterning of Flat Carbon Surfaces by Scanning Probe Lithography and Electrochemistry. *Langmuir* **2005,** *21* (5), 1672-1675.

44. Allongue, P.; Henry de Villeneuve, C.; Cherouvrier, G.; Cortès, R.; Bernard, M. C. Phenyl layers on H–Si(111) by electrochemical reduction of diazonium salts: monolayer versus multilayer formation. *J. Electroanal. Chem.* **2003,** *550–551* (0), 161-174.

45. Podvorica, F. I.; Kanoufi, F.; Pinson, J.; Combellas, C. Spontaneous grafting of diazoates on metals. *Electrochim. Acta* **2009,** *54* (8), 2164-2170.

46. Combellas, C.; Kanoufi, F.; Pinson, J.; Podvorica, F. I. Sterically Hindered Diazonium Salts for the Grafting of a Monolayer on Metals. *J. Am. Chem. Soc.* **2008,** *130* (27), 8576-8577.

47. Combellas, C.; Jiang, D.-e.; Kanoufi, F.; Pinson, J.; Podvorica, F. I. Steric Effects in the Reaction of Aryl Radicals on Surfaces. *Langmuir* **2008,** *25* (1), 286-293.

48. Mattiuzzi, A. J., I; Mangeney, C; Roux, C; Reinaud, O; Santos, L; Bergamini, J-F; Hapiot, P; Lagrost, C. Electrografting of calix[4]arenediazonium salts to form versatile robust platforms for spatially controlled surface functionalization. *Nature Communications* **2012,** *3*.

49. Nielsen, L. T.; Vase, K. H.; Dong, M.; Besenbacher, F.; Pedersen, S. U.; Daasbjerg, K. Electrochemical Approach for Constructing a Monolayer of Thiophenolates from Grafted Multilayers of Diaryl Disulfides. *J. Am. Chem. Soc.* **2007,** *129* (7), 1888-1889.

50. (a) Leroux, Y. R.; Hui, F.; Hapiot, P. A protecting-deprotecting strategy for structuring robust functional films using aryldiazonium electroreduction. *J. Electroanal. Chem.* **2013,** *688* (0), 298-303; (b) Leroux, Y. R.; Fei, H.; Noël, J.-M.; Roux, C.; Hapiot, P. Efficient Covalent Modification of a Carbon Surface: Use of a Silyl Protecting Group To Form an Active Monolayer. *J. Am. Chem. Soc.* **2010,** *132* (40), 14039-14041.

51. Kolb, H. C.; Finn, M. G.; Sharpless, K. B. Click Chemistry: Diverse Chemical Function from a Few Good Reactions. *Angew. Chem. Int. Ed.* **2001,** *40* (11), 2004-2021.

52. Rostovtsev, V. V.; Green, L. G.; Fokin, V. V.; Sharpless, K. B. A Stepwise Huisgen Cycloaddition Process: Copper(I)-Catalyzed Regioselective "Ligation" of Azides and Terminal Alkynes. *Angew. Chem. Int. Ed.* **2002,** *41* (14), 2596-2599.

53. Tornøe, C. W.; Christensen, C.; Meldal, M. Peptidotriazoles on Solid Phase: [1,2,3]-Triazoles by Regiospecific Copper(I)-Catalyzed 1,3-Dipolar Cycloadditions of Terminal Alkynes to Azides. *J. Org. Chem.* **2002,** *67* (9), 3057-3064.

54. Evans, R. A. The Rise of Azide–Alkyne 1,3-Dipolar 'Click' Cycloaddition and its Application to Polymer Science and Surface Modification. *Aust. J. Chem.* **2007,** *60* (6), 384-395.

55. Baldwin, M. G.; Johnson, K. E.; Lovinger, J. A.; Parker, C. O. 1,3-Dipolar cycloaddition polymerization of compounds containing both azido and acetylene groups. *J. Polym. Sci., Polym Lett. Ed.* **1967,** *5* (9), 803-806.

56. van Steenis, D. J. V. C.; David, O. R. P.; van Strijdonck, G. P. F.; van Maarseveen, J. H.; Reek, J. N. H. Click-chemistry as an efficient synthetic tool for the preparation of novel conjugated polymers. *Chem. Commun.* **2005,** (34), 4333-4335.

57. Laurent, B. A.; Grayson, S. M. An Efficient Route to Well-Defined Macrocyclic Polymers via "Click" Cyclization. *J. Am. Chem. Soc.* **2006,** *128* (13), 4238-4239.

58. Binder, W. H.; Sachsenhofer, R. 'Click' Chemistry in Polymer and Material Science: An Update. *Macromol. Rapid Commun.* **2008,** *29* (12-13), 952-981.

59. Gooding, J. J.; Liu, G.; Gui, A. L. The Use of Aryl Diazonium Salts in the Fabrication of Biosensors and Chemical Sensors. In *Aryl Diazonium Salts*, Chehimi, M. M., Ed. Wiley-VCH Verlag GmbH & Co. KGaA: 2012; pp 197-218.

60. Radi, A.-E.; Montornés, J. M.; O'Sullivan, C. K. Reagentless detection of alkaline phosphatase using electrochemically grafted films of aromatic diazonium salts. *J. Electroanal. Chem.* **2006,** *587* (1), 140-147.

61. Liu, G.; Böcking, T.; Gooding, J. J. Diazonium salts: Stable monolayers on gold electrodes for sensing applications. *J. Electroanal. Chem.* **2007,** *600* (2), 335-344.

62. Liu, G.; Nguyen, Q. T.; Chow, E.; Böcking, T.; Hibbert, D. B.; Gooding, J. J. Study of Factors Affecting the Performance of Voltammetric Copper Sensors Based on Gly-Gly-His Modified Glassy Carbon and Gold Electrodes. *Electroanalysis* **2006,** *18* (12), 1141-1151.

63. Ruffien, A.; Dequaire, M.; Brossier, P. Covalent immobilization of oligonucleotides on p-aminophenyl-modified carbon screen-printed electrodes for viral DNA sensing. *Chem. Commun.* **2003,** *0* (7), 912-913.

64. Joyeux, X.; Mangiagalli, P.; Pinson, J. Localized Attachment of Carbon Nanotubes in Microelectronic Structures. *Adv. Mater.* **2009,** *21* (43), 4404-4408.

65. Ranganathan, S.; Steidel, I.; Anariba, F.; McCreery, R. L. Covalently Bonded Organic Monolayers on a Carbon Substrate: A New Paradigm for Molecular Electronics. *Nano Lett.* **2001,** *1* (9), 491-494.

66. McCreery, R. L. Molecular Electronic Junctions. *Chem. Mater.* **2004,** *16* (23), 4477-4496.

67. Levesque, L.; Lawrence, M. F.; Bourguignon, B.; Leclerc, G. Drug Eluting Device For Treating Vascular Diseases. PCT Patent Application WO 02066092, 2002.

68. Zhou, F.; Huck, W. T. S. Surface grafted polymer brushes as ideal building blocks for "smart" surfaces. *PCCP* **2006,** *8* (33), 3815-3823.

69. Halperin, A.; Tirrell, M.; Lodge, T. P. Tethered chains in polymer microstructures. In *Macromolecules: Synthesis, Order and Advanced Properties*, Springer Berlin Heidelberg: 1992; Vol. 100/1, pp 31-71.

70. Zhao, B.; Brittain, W. J. Polymer brushes: surface-immobilized macromolecules. *Prog. Polym. Sci.* **2000,** *25* (5), 677-710.

71. Milner, S. T. Polymer Brushes. *Science* **1991,** *251* (4996), 905-914.

72. De Gennes, P. G. Scaling theory of polymer adsorption. *J. Phys. France* **1976,** *37* (12), 1445-1452.

73. Weir, M. P.; Parnell, A. J. Water Soluble Responsive Polymer Brushes. *Polymers* **2011,** *3* (4), 2107-2132.

74. Pei, Y. PhD Thesis.Synthesis and Characterization of Poymer Brush-Grafted Conducting Polymers and Their Applications in Electrochemical Control of Surface Wettability. University of Auckland, 2012.

75. Liu, Y.; Mu, L.; Liu, B.; Kong, J. Controlled Switchable Surface. *Chem. Eur. J.* **2005,** *11* (9), 2622-2631.

76. Farhan, T.; Azzaroni, O.; Huck, W. T. S. AFM study of cationically charged polymer brushes: switching between soft and hard matter. *Soft Matter* **2005,** *1* (1), 66-68.

77. Zhou, F.; Hu, H.; Yu, B.; Osborne, V. L.; Huck, W. T. S.; Liu, W. Probing the Responsive Behavior of Polyelectrolyte Brushes Using Electrochemical Impedance Spectroscopy. *Anal. Chem.* **2006,** *79* (1), 176-182.

78. Fujishige, S.; Kubota, K.; Ando, I. Phase transition of aqueous solutions of poly(N-isopropylacrylamide) and poly(N-isopropylmethacrylamide). *J. Phys. Chem.* **1989,** *93* (8), 3311-3313.

79. Jones, D. M.; Smith, J. R.; Huck, W. T. S.; Alexander, C. Variable Adhesion of Micropatterned Thermoresponsive Polymer Brushes: AFM Investigations of Poly(N-isopropylacrylamide) Brushes Prepared by Surface-Initiated Polymerizations. *Adv. Mater.* **2002,** *14* (16), 1130-1134.

80. Sun, T.; Wang, G.; Feng, L.; Liu, B.; Ma, Y.; Jiang, L.; Zhu, D. Reversible Switching between Superhydrophilicity and Superhydrophobicity. *Angew. Chem. Int. Ed.* **2004,** *43* (3), 357-360.

81. Pei, Y.; Travas-Sejdic, J.; Williams, D. E. Reversible Electrochemical Switching of Polymer Brushes Grafted onto Conducting Polymer Films. *Langmuir* **2012,** *28* (21), 8072-8083.

82. Xia, F.; Ge, H.; Hou, Y.; Sun, T.; Chen, L.; Zhang, G.; Jiang, L. Multiresponsive Surfaces Change Between Superhydrophilicity and Superhydrophobicity. *Adv. Mater.* **2007,** *19* (18), 2520-2524.

83. Kato, M.; Kamigaito, M.; Sawamoto, M.; Higashimura, T. Polymerization of Methyl Methacrylate with the Carbon Tetrachloride/Dichlorotris-(triphenylphosphine)ruthenium(II)/Methylaluminum Bis(2,6-di-tert-butylphenoxide) Initiating System: Possibility of Living Radical Polymerization. *Macromolecules* **1995,** *28* (5), 1721-1723.

84. Wang, J.-S.; Matyjaszewski, K. Controlled/"Living" Radical Polymerization. Halogen Atom Transfer Radical Polymerization Promoted by a Cu(I)/Cu(II) Redox Process. *Macromolecules* **1995,** *28* (23), 7901-7910.

85. Wang, J.-S.; Matyjaszewski, K. Controlled/"living" radical polymerization. atom transfer radical polymerization in the presence of transition-metal complexes. *J. Am. Chem. Soc.* **1995,** *117* (20), 5614-5615.

86. Edmondson, S.; Osborne, V. L.; Huck, W. T. S. Polymer brushes via surface-initiated polymerizations. *Chem. Soc. Rev.* **2004,** *33* (1), 14-22.

87. Gam-Derouich, S.; Mahouche-Chergui, S.; Romdhane, H. B.; Chehimi, M. M. Polymer Grafting to Aryl Diazonium-Modified Materials: Methods and Applications. In *Aryl*

Diazonium Salts, Chehimi, M. M., Ed. Wiley-VCH Verlag GmbH & Co. KGaA: 2012; pp 103-120.

88. Matyjaszewski, K.; Xia, J. Atom Transfer Radical Polymerization. *Chem. Rev.* **2001,** *101* (9), 2921-2990.

89. Li, B.; Yu, B.; Huck, W. T. S.; Zhou, F.; Liu, W. Electrochemically Induced Surface-Initiated Atom-Transfer Radical Polymerization. *Angew. Chem. Int. Ed.* **2012,** *51* (21), 5092-5095.

90. Matyjaszewski, K.; Dong, H.; Jakubowski, W.; Pietrasik, J.; Kusumo, A. Grafting from Surfaces for "Everyone": ARGET ATRP in the Presence of Air. *Langmuir* **2007,** *23* (8), 4528-4531.

91. Magenau, A. J. D.; Strandwitz, N. C.; Gennaro, A.; Matyjaszewski, K. Electrochemically Mediated Atom Transfer Radical Polymerization. *Science* **2011,** *332* (6025), 81-84.

92. Koutsos, V.; van der Vegte, E. W.; Pelletier, E.; Stamouli, A.; Hadziioannou, G. Structure of Chemically End-Grafted Polymer Chains Studied by Scanning Force Microscopy in Bad-Solvent Conditions. *Macromolecules* **1997,** *30* (16), 4719-4726.

93. Koutsos, V.; van der Vegte, E. W.; Hadziioannou, G. Direct View of Structural Regimes of End-Grafted Polymer Monolayers: A Scanning Force Microscopy Study. *Macromolecules* **1999,** *32* (4), 1233-1236.

94. Yang, X.; Shi, J.; Johnson, S.; Swanson, B. Growth of Ultrathin Covalently Attached Polymer Films: Uniform Thin Films for Chemical Microsensors. *Langmuir* **1998,** *14* (7), 1505-1507.

95. Mansky, P. L. Y. Controlling polymer-surface interactions with random copolymer brushes. *Science* **1997,** *275* (5305), 1458.

96. Bergbreiter, D. E.; Franchina, J. G.; Kabza, K. Hyperbranched Grafting on Oxidized Polyethylene Surfaces. *Macromolecules* **1999,** *32* (15), 4993-4998.

97. Davis, K.; O'Malley, J.; Paik, H.-J.; Matyjaszewski, K. Effect of the counteranion in atom transfer radical polymerization using alkyl (pseudo)halide initiators. *Polym. Prepr. (Am. Chem. Soc., Div Polym. Chem)* **1997,** *38* (1), 687-688.

98. Edmondson, S.; Vo, C.-D.; Armes, S. P.; Unali, G.-F. Surface Polymerization from Planar Surfaces by Atom Transfer Radical Polymerization Using Polyelectrolytic Macroinitiators. *Macromolecules* **2007,** *40* (15), 5271-5278.

99. Matrab, T.; Chehimi, M. M.; Perruchot, C.; Adenier, A.; Guillez, A.; Save, M.; Charleux, B.; Cabet-Deliry, E.; Pinson, J. Novel Approach for Metallic Surface-Initiated

Atom Transfer Radical Polymerization Using Electrografted Initiators Based on Aryl Diazonium Salts. *Langmuir* **2005,** *21* (10), 4686-4694.

100. Iruthayaraj, J.; Chernyy, S.; Lillethorup, M.; Ceccato, M.; Røn, T.; Hinge, M.; Kingshott, P.; Besenbacher, F.; Pedersen, S. U.; Daasbjerg, K. On Surface-Initiated Atom Transfer Radical Polymerization Using Diazonium Chemistry To Introduce the Initiator Layer. *Langmuir* **2010,** *27* (3), 1070-1078.

101. Li, C.; Hu, J.; Yin, J.; Liu, S. Click Coupling Fullerene onto Thermoresponsive Water-Soluble Diblock Copolymer and Homopolymer Chains at Defined Positions. *Macromolecules* **2009,** *42* (14), 5007-5016.

102. Jiang, X.; Lok, M. C.; Hennink, W. E. Degradable-Brushed pHEMA–pDMAEMA Synthesized via ATRP and Click Chemistry for Gene Delivery. *Bioconjugate Chem.* **2007,** *18* (6), 2077-2084.

103. He, H.; Averick, S.; Roth, E.; Luebke, D.; Nulwala, H.; Matyjaszewski, K. Clickable poly(ionic liquid)s for modification of glass and silicon surfaces. *Polymer* **2014,** *55* (16), 3330-3338.

104. Chen, G.; Tao, L.; Mantovani, G.; Ladmiral, V.; Burt, D. P.; Macpherson, J. V.; Haddleton, D. M. Synthesis of azide/alkyne-terminal polymers and application for surface functionalisation through a [2 + 3] Huisgen cycloaddition process, "click chemistry". *Soft Matter* **2007,** *3* (6), 732-739.

105. Urien, M.; Erothu, H.; Cloutet, E.; Hiorns, R. C.; Vignau, L.; Cramail, H. Poly(3-hexylthiophene) Based Block Copolymers Prepared by “Click” Chemistry. *Macromolecules* **2008,** *41* (19), 7033-7040.

106. Mantovani, G.; Ladmiral, V.; Tao, L.; Haddleton, D. M. One-pot tandem living radical polymerisation-Huisgens cycloaddition process ("click") catalysed by N-alkyl-2-pyridylmethanimine/Cu(i)Br complexes. *Chem. Commun.* **2005,** (16), 2089-2091.

107. Geng, J.; Lindqvist, J.; Mantovani, G.; Haddleton, D. M. Simultaneous Copper(I)-Catalyzed Azide–Alkyne Cycloaddition (CuAAC) and Living Radical Polymerization. *Angew. Chem. Int. Ed.* **2008,** *47* (22), 4180-4183.

108. Damiron, D.; Desorme, M.; Ostaci, R.-V.; Al Akhrass, S.; Hamaide, T.; Drockenmuller, E. Functionalized random copolymers from versatile one-pot click chemistry/ATRP tandems approaches. *J. Polym. Sci., Part A: Polym. Chem.* **2009,** *47* (15), 3803-3813.

109. Grignard, B.; Calberg, C.; Jerome, C.; Detrembleur, C. “One-pot” dispersion ATRP and alkyne-azide Huisgen's 1,3-dipolar cycloaddition in supercritical carbon dioxide:

Towards the formation of functional microspheres. *The Journal of Supercritical Fluids* **2010,** *53* (1–3), 151-155.

110. Rydzek, G.; Terentyeva, T. G.; Pakdel, A.; Golberg, D.; Hill, J. P.; Ariga, K. Simultaneous Electropolymerization and Electro-Click Functionalization for Highly Versatile Surface Platforms. *ACS Nano* **2014,** *8* (5), 5240-5248.

111. Xu, L. Q.; Wan, D.; Gong, H. F.; Neoh, K.-G.; Kang, E.-T.; Fu, G. D. One-Pot Preparation of Ferrocene-Functionalized Polymer Brushes on Gold Substrates by Combined Surface-Initiated Atom Transfer Radical Polymerization and "Click Chemistry". *Langmuir* **2010,** *26* (19), 15376-15382.

112. Casas-Solvas, J. M.; Ortiz-Salmerón, E.; Giménez-Martínez, J. J.; García-Fuentes, L.; Capitán-Vallvey, L. F.; Santoyo-González, F.; Vargas-Berenguel, A. Ferrocene–Carbohydrate Conjugates as Electrochemical Probes for Molecular Recognition Studies. *Chemistry – A European Journal* **2009,** *15* (3), 710-725.

113. Anderson, S. Phenylene Ethynylene Pentamers for Organic Electroluminescence. *Chemistry – A European Journal* **2001,** *7* (21), 4706-4714.

114. Saunders, K. H.; Allen, R. L. M. *Aromatic Diazo Compounds*. Edward Arnold: London: 1985.

115. Mu, F.; Coffing, S. L.; Riese, D. J.; Geahlen, R. L.; Verdier-Pinard, P.; Hamel, E.; Johnson, J.; Cushman, M. Design, Synthesis, and Biological Evaluation of a Series of Lavendustin A Analogues That Inhibit EGFR and Syk Tyrosine Kinases, as Well as Tubulin Polymerization. *J. Med. Chem.* **2001,** *44* (3), 441-452.

116. Neises, B.; Steglich, W. Simple Method for the Esterification of Carboxylic Acids. *Angewandte Chemie International Edition in English* **1978,** *17* (7), 522-524.

117. Shendage, D. M.; Fröhlich, R.; Haufe, G. Highly Efficient Stereoconservative Amidation and Deamidation of α-Amino Acids. *Organic Letters* **2004,** *6* (21), 3675-3678.

118. Gann, A. W.; Amoroso, J. W.; Einck, V. J.; Rice, W. P.; Chambers, J. J.; Schnarr, N. A. A Photoinduced, Benzyne Click Reaction. *Organic Letters* **2014,** *16* (7), 2003-2005.

119. Bertoldo, M.; Zampano, G.; Terra, F. L.; Villari, V.; Castelvetro, V. Amphiphilic Amylose-g-poly(meth)acrylate Copolymers through "Click" onto Grafting Method. *Biomacromolecules* **2010,** *12* (2), 388-398.

120. Shao, C.; Wang, X.; Xu, J.; Zhao, J.; Zhang, Q.; Hu, Y. Carboxylic Acid-Promoted Copper(I)-Catalyzed Azide−Alkyne Cycloaddition. *J. Org. Chem.* **2010,** *75* (20), 7002-7005.

121. Strover, L. T.; Malmström, J.; Laita, O.; Reynisson, J.; Aydemir, N.; Nieuwoudt, M. K.; Williams, D. E.; Dunbar, P. R.; Brimble, M. A.; Travas-Sejdic, J. A new precursor for

conducting polymer-based brush interfaces with electroactivity in aqueous solution. *Polymer* **2013,** *54* (4), 1305-1317.

122. Noël, J.-M.; Sjöberg, B.; Marsac, R.; Zigah, D.; Bergamini, J.-F.; Wang, A.; Rigaut, S.; Hapiot, P.; Lagrost, C. Flexible Strategy for Immobilizing Redox-Active Compounds Using in Situ Generation of Diazonium Salts. Investigations of the Blocking and Catalytic Properties of the Layers. *Langmuir* **2009,** *25* (21), 12742-12749.

123. Hanwell, M. D.; Curtis, D. E.; Lonie, D. C.; Vandermeersch, T.; Zurek, E.; Hutchison, G. R. Avogadro: an advanced semantic chemical editor, visualization, and analysis platform. *Journal of Cheminformatics* **2012,** *4* (1), 17-33.

124. Loring, J. S. Ph.D. Dissertation, University of California, Davis, 2000.

125. Delamar, M.; Hitmi, R.; Pinson, J.; Saveant, J. M. Covalent Modification of Carbon Surfaces by Grafting of Functionalized Aryl Radicals Produced from Electrochemical Reduction of Diazonium Salts. *J. Am. Chem. Soc.* **1992,** *114*, 5883-5884.

126. Brooksby, P. A.; Downard, A. J. Multilayer Nitroazobenzene Films Covalently Attached to Carbon. An AFM and Electrochemical Study. *J. Phys. Chem. B* **2005,** *109* (18), 8791-8798.

127. Banks, C. E.; Davies, T. J.; Wildgoose, G. G.; Compton, R. G. Electrocatalysis at graphite and carbon nanotube modified electrodes: edge-plane sites and tube ends are the reactive sites. *Chem. Commun.* **2005,** (7), 829-841.

128. Bard, A. J.; Faulkner, L. R. *Electrochemical Methods Fundamentals and Applications*. 2 ed.; John Wiley: New York, 2001.

129. Isidro-Llobet, A.; Álvarez, M.; Albericio, F. Amino Acid-Protecting Groups. *Chem. Rev.* **2009,** *109* (6), 2455-2504.

130. Abiman, P.; Crossley, A.; Wildgoose, G. G.; Jones, J. H.; Compton, R. G. Investigating the Thermodynamic Causes Behind the Anomalously Large Shifts in pKa Values of Benzoic Acid-Modified Graphite and Glassy Carbon Surfaces. *Langmuir* **2007,** *23* (14), 7847-7852.

131. Chidsey, C. E. D.; Bertozzi, C. R.; Putvinski, T. M.; Mujsce, A. M. Coadsorption of ferrocene-terminated and unsubstituted alkanethiols on gold: electroactive self-assembled monolayers. *J. Am. Chem. Soc.* **1990,** *112* (11), 4301-4306.

132. Menanteau, T.; Levillain, E.; Breton, T. Spontaneous Grafting of Nitrophenyl Groups on Carbon: Effect of Radical Scavenger on Organic Layer Formation. *Langmuir* **2014,** *30* (26), 7913-7918.

133. Pantea, D.; Darmstadt, H.; Kaliaguine, S.; Roy, C. Heat-treatment of carbon blacks obtained by pyrolysis of used tires. Effect on the surface chemistry, porosity and electrical conductivity. *J. Anal. Appl. Pyrolysis* **2003,** *67* (1), 55-76.

134. Biniak, S.; Szymański, G.; Siedlewski, J.; Świątkowski, A. The characterization of activated carbons with oxygen and nitrogen surface groups. *Carbon* **1997,** *35* (12), 1799-1810.

135. Ilangovan, G.; Chandrasekara Pillai, K. Electrochemical and XPS Characterization of Glassy Carbon Electrode Surface Effects on the Preparation of a Monomeric Molybdate(VI)-Modified Electrode. *Langmuir* **1997,** *13* (3), 566-575.

136. Ciampi, S.; Böcking, T.; Kilian, K. A.; James, M.; Harper, J. B.; Gooding, J. J. Functionalization of Acetylene-Terminated Monolayers on Si(100) Surfaces: A Click Chemistry Approach. *Langmuir* **2007,** *23* (18), 9320-9329.

137. Bourdillon, C.; Bourgeois, J. P.; Thomas, D. Covalent linkage of glucose oxidase on modified glassy carbon electrodes. Kinetic phenomena. *J. Am. Chem. Soc.* **1980,** *102* (12), 4231-4235.

138. Cabaniss, G. E.; Diamantis, A. A.; Murphy, W. R.; Linton, R. W.; Meyer, T. J. Electrocatalysis of proton-coupled electron-transfer reactions at glassy carbon electrodes. *J. Am. Chem. Soc.* **1985,** *107* (7), 1845-1853.

139. Kamau, G. N.; Willis, W. S.; Rusling, J. F. Electrochemical and Electron Spectroscopic Studies of Highly Polished Glassy Carbon Electrodes. *Anal. Chem.* **1985,** *57* (2), 545-551.

140. Sundberg, K. M.; Smyrl, W. H.; Atanasoska, L.; Atanasoski, R. Surface Modification and Oxygen Reduction on Glassy Carbon in Chloride Media. *J. Electrochem. Soc.* **1989,** *136* (2), 434-439.

141. Clayden, J.; Greeves, N.; Warren, S.; Wothers, P. *Organic Chemistry*. 3 ed.; Oxford University Press: 2009.

142. Rowe, G. K.; Creager, S. E. Redox and ion-pairing thermodynamics in self-assembled monolayers. *Langmuir* **1991,** *7* (10), 2307-2312.

143. Matrab, T.; Chehimi, M. M.; Pinson, J.; Slomkowski, S.; Basinska, T. Growth of polymer brushes by atom transfer radical polymerization on glassy carbon modified by electro-grafted initiators based on aryl diazonium salts. *Surf. Interface Anal.* **2006,** *38* (4), 565-568.

144. Stach, M.; Kroneková, Z.; Kasák, P.; Kollár, J.; Pentrák, M.; Mičušík, M.; Chorvát Jr, D.; Nunney, T. S.; Lacík, I. Polysulfobetaine films prepared by electrografting technique for

reduction of biofouling on electroconductive surfaces. *Appl. Surf. Sci.* **2011,** *257* (24), 10795-10801.

145. Naumkin, A. V.; Kraut-Vass, A.; Gaarenstroom, S. W.; Powell, C. J. NIST Standard Reference Databae 20, Version 4.1 (web version). (http:/srdata.nist.gov/xps/).

146. McCafferty, E.; Wightman, J. P. Determination of the acid-base properties of metal oxide films and the polymers by contact angle measurements. *Journal of Adhesion Science & Technology* **1999,** *13* (12), 1415.